

**THE ROLE AND PRODUCTION OF POLAR/SUBTROPICAL JET SUPERPOSITIONS
IN TWO HIGH-IMPACT WEATHER EVENTS OVER NORTH AMERICA**

By

Andrew C. Winters

A dissertation submitted in partial fulfillment of
the requirements for the degree of

Doctor of Philosophy

(Atmospheric and Oceanic Sciences)

at the

UNIVERSITY OF WISCONSIN-MADISON

2015

Date of final oral examination: 7/27/2015

This dissertation is approved by the following members of the Final Oral Committee:

Jonathan E. Martin, Professor, Atmospheric and Oceanic Sciences
Matthew H. Hitchman, Professor, Atmospheric and Oceanic Sciences
Michael C. Morgan, Professor, Atmospheric and Oceanic Sciences
Gregory J. Tripoli, Professor, Atmospheric and Oceanic Sciences
Samuel N. Stechmann, Associate Professor, Mathematics

**© Copyright by Andrew C. Winters
All Rights Reserved**

This dissertation is dedicated to the memory of
RUTH WINTERS and PATRICIA BARBIAN.

Two of the best teachers I ever had.

Acknowledgments

From a young age, the only thing I ever wanted to do with my life was study the weather. Surprisingly, this desire was born out of an intense fear I held for thunderstorms, which sent me cowering into my parents' arms at the first crack of thunder that reverberated through our neighborhood. At the same time, however, I became captivated by the same atmospheric phenomena that surrounded me. I strongly believed that one way to mitigate the fear I had of the weather was to harness a greater understanding of it. What followed were numerous hours spent watching "The Weather Channel", a rapid accumulation of books written about different atmospheric phenomena, the development of an imagination that desired to emulate broadcast meteorologists, and unrelenting aspiration to never throw away the winter glove that shook the hand of Mark Baden, a local broadcast meteorologist.

Eight years ago, I brought this passion to the University of Wisconsin campus to begin the formal academic preparation that has culminated with a doctorate in Atmospheric and Oceanic Sciences. While my academic journey has been characterized by considerable personal effort and an unwavering dedication, I strongly believe that I stand where I am today because of the network of individuals that I've had at my side the past 26 years. I am confident that I am a better scholar, a stronger friend, a more dedicated brother and son, and an overall better man because of my interactions with these individuals. This dissertation is as much of a testament to them as it is to my own personal effort. With this in mind, it is only fitting to dedicate some space to acknowledge the individuals who have been so transformative in helping me reach the summit of my formal education.

Over the past five years, I could not have dreamed of a better mentor than I've had in Jon Martin. I have not met another individual who has shown more compassion and support for his

students than Jon has. It's because of him that I have an unshaken confidence and ability to interrogate and to communicate about the atmosphere, an inquisitive mind that continually aspires to learn more about the surrounding environment, and the motivation to stand tall in the face of adversity. Not only has Jon served as a role model for me professionally, but also personally. I have come to consider him a great friend, and I will truly miss our morning conversations recapping various events from the night before, attending Badger basketball games together, and our attempts to 'landscape' the local golf course. I am forever grateful for the opportunity to work with him and I hope to live out my career and life with the same vigor that has characterized his own.

I am also incredibly grateful to Michael Morgan, who went from the professor who "made me stand" during an AOS 311 Lab Quiz, to someone I now consider a true friend. It is difficult for me to articulate how much I will miss our conversations on the bus, tossing the apple around, the ridiculously cheesy puns, and forwarding each other the gratuitous pictures of food and recipes that we stumble upon while browsing the web. I vow that someday I will be able to dethrone his Mac & Cheese as the champion at a future 'throwdown'. I am particularly appreciative of the unwavering support Michael has shown me over the past year as I've worked to finish up my degree. The research that is presented within this dissertation is undoubtedly enhanced as a result of our regular conversations and the encouragement that Michael has given me to think even more critically about my results and about the science as a whole.

In addition, this dissertation has greatly benefitted from the remaining members of my Ph.D. committee, Greg Tripoli, Matt Hitchman, and Sam Stechmann. I am grateful for all of the constructive comments and advice that you have given me over the past three years while I worked to produce this document. I know that I am a stronger scholar because of our

collaboration and look forward to continuing our professional relationships into the future. I have also been surrounded by an incredible array of faculty at Wisconsin, who have undoubtedly increased the breadth of knowledge that I have in the field and have allowed me to represent the department as a graduate student in various outreach, recruiting, and strategic planning exercises. These experiences have taught me the importance of a strong and functional departmental community and the roles we can all play to embody the Wisconsin Idea beyond the boundaries of the campus.

Over the course of my graduate career, performing outreach in the local community became my escape from the daily grind that characterized research and teaching. However, these outreach opportunities would have never occurred had it not been for the support and input from Galen McKinley, Margaret Mooney, Steve Ackerman, Don Gillian-Daniel, and the rest of the Delta Program staff. Not only am I inspired to continue science outreach in the future as a function of the opportunities that I've had, but I have also learned a great deal on how to become an effective educator inside the formal classroom. I greatly anticipate the day when I can implement the lessons I've learned from these outreach opportunities, and from the Delta Program as a whole, while communicating atmospheric science in formal and informal classroom settings as a part of my career.

It is impossible to underestimate the role that the AOS staff has played during my tenure in the department. Pete Pokrandt is an absolute wizard when it comes to technology and I am certain that I'd still be downloading my first GFS analysis for this dissertation if it wasn't for his guidance and assistance. I will miss our conversations concerning the latest developments from the Brewers rumor mill and, more generally, about sports and weather. Debbie Weber is the cornerstone of the entire AOS department. She addressed any logistical questions with

impeccable accuracy and it has been a joy to get to know her personally over the past four years. Kathy Kruger, Sue Foldy, Sonja Johnson, and Toni Sumner-Beebe also deserve a considerable amount of credit for their help with travel arrangements, scheduling seminars, and in formalizing the steps needed to obtain my degree. I can only hope that my future plans allow me to work with a similar group of individuals who truly are the underpinnings to a successful department.

Amidst the academic pursuits that have characterized my time at UW-Madison, I have had the pleasure to get to know and work with many AOS undergraduate and graduate students, including Darren Pilcher, Alexis Ritzer, Elise Kubicek, Alex Kubicek, Elena Willmot, and Bill Line, who have made life in the department and in the classroom considerably more vibrant. In particular, the Martin group has been characterized by a cohort of incredibly intelligent individuals, including Zak Handlos, Croix Christenson, Kyle Griffin, and Melissa Breeden, who have been a joy to work with both professionally and personally. Not only do I look forward to seeing you all become leaders within your respective fields, but also to continuing the strong friendships that we have developed over the years. It goes without saying that I will sorely miss the interactions with students in department that I have come to appreciate so immensely, including trips to Pizza Hut Buffet, GL+B, Vintage happy hour, and Concerts on the Square.

An acknowledgment should also be directed to Daphne LaDue and the members of the 2010 NWC-REU cohort. Without a doubt, this experience transformed my career aspirations as a junior undergraduate student. I am completely certain that I am pursuing a career in research today because of the positive experiences I had in this program with both my fellow students and mentors. I still look forward to reuniting with former REU students at various conferences and meetings and am certain that the novelty of these reunions will never grow old. I am proud that I am able to see so many from this program as emerging leaders within different aspects of the

atmospheric science landscape and greatly anticipate the opportunity for the collaborations and friendships generated from that program to continue into the future.

Eight years ago, I was placed into the Bradley Learning Community, a freshman dorm that immediately facilitated the growth of friendships and initiated the formation of my Madison family. The individuals that compose this group, including, but definitely not limited to, Reid Woolworth, Josh Braun, Nick Goeldner, Shawn Miller, Bryan Dow, Mary Erickson, Coral Graszer, Caitlin MacCoun, Lindsay Seibel, Shannon Miller, Jaime Goeldner, Meg Healy, Emily Powers, Clayton Stoffel, Lisa Lach, the Alpaca MUFA team, and the MKE family, have made my life that much brighter because of their presence in it. For me, Madison holds the place it does in my heart because of the moments I have shared with these individuals. There is nothing I would love more than to rewind the clock for another Wing Night at Brothers, a pitcher on the terrace, a football tailgate, a movie/game night, a HALO LAN party, a trip to the Farmer's market, a Mallards game, or a road trip to Pasadena with all of you. Yet, I will always look forward, with great anticipation, to the opportunities that will undoubtedly allow our paths to cross once again.

Finally, I am lucky to have the greatest and most supportive family in the world that has been with me every step of the way in my desire to study the weather. My grandfather, Wil Barbian has, and will continue to be, one of the greatest role models in my life. I will always hope to emulate the zeal with which he has lived his life and the compassion he has shown to so many around him. My brother, Nathan Winters, has been my best friend and the greatest ally I could ask for. I know that we haven't fulfilled our earliest dreams to co-anchor a newscast together, but I'm so proud to see us with careers that we both enjoy so deeply. Lastly, to my parents, Tim and Ellen Winters, there are no words to describe the gratitude that I have for the

encouragement you've shown as I've pursued my dreams. You are the brightest shining lights in my life and I love you both immensely.

In the end, the pages that follow mark both the end of an era and the beginning of a new one. I am deeply saddened to say goodbye to the people and places that have made the first 26 years of my life more fulfilling than I could ever dream of. At the same time, I'm thrilled to start a new professional journey that will hold new challenges and even greater rewards. When I began graduate school, my cousin Emily gave me a framed quote, which read,

'Life isn't about finding yourself, it's about creating yourself.'

Reflecting on these words, the truth of them is palpable. No one can wait for an opportunity to slap them in the face and nothing in life is ever guaranteed. There is always a reason behind the development of certain events and it is what one chooses to do with the challenges and opportunities that they are faced with that dictates who they are and what they become. Consequently, dreams must always be pursued with vigor, determination, and hard work. When we fall down and slip up, like we always do, one must always lean on the friends and family they have chosen to surround themselves with. After roughly 20 years of school, and strongly supported by the people listed above, this dissertation marks the end of a period of self-creation and self-development, both professionally and personally, and the accomplishment of my one overarching goal in life.

I always wanted to be a meteorologist. Now, I am.

Table of Contents

Dedication	i
Acknowledgments	ii
Table of Contents	viii
Figure Captions	x
Abstract	xix
1. Introduction	1
1.1. The “Discovery” of the Jet Stream	4
1.2. Cross-Stream Vertical Circulations within the Jet Environment	7
1.3. Two Distinct Jet Species: The Polar and Subtropical Jets	12
1.4. Vertical Jet Superpositions	15
2. Jet Identification Criteria and Case Overviews	29
2.1. Jet Identification	29
2.2. Synoptic Overviews of Selected Jet Superposition Cases	30
2.2.1. 18–20 December 2009 Mid-Atlantic Blizzard	31
2.2.2. 1–3 May 2010 Nashville Flood	33
3. The Role of a Polar/Subtropical Jet Superposition in the May 2010 Nashville Flood	41
3.1. Motivation	41
3.2. The Sawyer-Eliassen Circulation Equation	44
3.3. Synoptic Evolution of the Poleward Moisture Flux	47
3.4. Diagnosis of Sawyer-Eliassen Circulations	48
3.4.1. Role of the Superposed Jet in Facilitating Poleward Moisture Flux	49
3.4.2. Partition of Sawyer-Eliassen Forcing Terms	52
3.5. Discussion	56
4. The Development of Jet Superpositions from a Basic-State Variable Perspective	69
4.1. Motivation	69
4.2. Jet Evolution During the 18–20 December 2009 Mid-Atlantic Blizzard	72
4.3. Jet Evolution During the 1–3 May 2010 Nashville Flood	78
4.4. Discussion	81

5. Insights into Jet Superposition Gained from Employing Piecewise PV Inversion	94
5.1. Motivation	94
5.2. Methodology	97
5.2.1. PV Partition Scheme	98
5.2.2. PV Inversion Techniques	101
5.2.3. Piecewise Sawyer-Eliassen Circulations	105
5.3. Results from PV Inversions	106
5.3.1. 18–20 December 2009 Mid-Atlantic Blizzard	107
5.3.2. 1–3 May 2010 Nashville Flood	119
5.4. Discussion	128
6. Conclusions and Future Work	156
6.1. Lessons from the Case Studies	156
6.2. Avenues for Future Research	162
6.2.1. Environments Most Conducive for North American Jet Superpositions	162
6.2.2. Survey of Tropical Tropopause Anticyclones	166
6.2.3. Applicability of Diagnostic Tools to Other Atmospheric Structures	168
References	171

Figure Captions

Chapter 1	Page 19
------------------	-------------------

FIG. 1.1. 250 hPa wind speed shaded with the fill pattern every 10 ms^{-1} beginning at 30 ms^{-1} at 1200 UTC 22 April 2010.

FIG. 1.2. Cross section of temperature over Europe from the evening of 15 February 1935 that is constructed from the data acquired during the “swarm ascents” coordinated by Bjerknes and Palmén (1937). The region of baroclinicity centered near Hamburg is bounded by two black, bold lines and identify the location of the polar frontal zone. The tropopause is also identified by a single bold, black line that separates the nearly isothermal stratosphere from the troposphere.

FIG. 1.3. Vertical cross section of temperature and wind speed from Bismarck, ND to Brownsville, TX at 0300 UTC 29 January 1947. Isentropes are drawn with the thin dashed lines and isotachs are represented by the thin solid lines. The bold black lines identify the location of the tropopause or the boundaries of the frontal zone. The “J” identifies the location of the jet core (From University of Chicago 1947; Fig. 17).

FIG. 1.4. Conceptual diagram of the transverse vertical circulations, depicted by the arrows, upstream (left) and downstream (right) of an upper-level trough (From Palmén and Nagler 1949; Fig. 16).

FIG. 1.5. (a) A conceptual diagram depicting a region of confluence acting upon a meridional temperature gradient. (b) A cross section from A to B, as identified in (a), of the characteristic transverse vertical circulation that would respond to the confluent flow shown in (a). Both panels are taken from Namias and Clapp (1949).

FIG. 1.6. Cross section of a developing upper-level front in northwesterly flow over the Northern Plains at 0300 UTC 14 December 1953. Isentropes are identified with the dashed lines, isotachs with the thin solid lines, and the tropopause with the bold, black line (From Reed 1955; Fig. 12).

FIG. 1.7. 200 hPa temperatures at 0300 UTC 28 January 1947. Local maxima and minima in temperature are represented by a “W” and a “C”, respectively. The jet axis is identified by a thick black arrow (From Riehl 1948; Fig. 4a).

FIG. 1.8. A composite cross section constructed from 12 individual cross sections of the polar front during December 1946. Isotherms are drawn with the dashed lines and isotachs with the thin black lines. The bold black lines denote the frontal zone (From Palmén and Newton 1948; Fig. 1).

FIG. 1.9. The mean subtropical jet stream during the winter of 1955–1956. Isotachs are shown at 200 hPa in the thin black contours and the jet axis is identified by the bold black line (From Krishnamurti 1961; Fig. 3).

FIG. 1.10. Conceptual diagram illustrating the mean meridional circulation during the winter (From Palmén 1951; Fig. 11).

FIG. 1.11. Mean meridional cross section of potential temperature for 1 January 1956 with the polar, subtropical, and tropical tropopause steps and polar frontal zone labeled as indicated in the legend (Modified from DT57; Fig. 13).

FIG. 1.12. Northern Hemispheric map of tropopause height (hPa) at 0300 UTC 1 January 1956. Tropopause breaks that correspond to the subtropical (STJ) and polar jet (POLJ) are labeled accordingly. The area identified with a circle is a region characterized by a vertical superposition of the polar and subtropical jets. Green shading corresponds to the tropical tropopause, white shading to the subtropical tropopause, and red shading to the polar tropopause (Modified from DT57; Fig. 2).

FIG. 1.13. Northern Hemispheric map of tropopause temperature (Celsius) at 0300 UTC 1 January 1956. The axes of the polar (POLJ) and subtropical (STJ) jets are identified by the blue and red dashed lines, respectively. The location of jet superposition is highlighted by the yellow circle (Modified from DT57; Fig. 3).

FIG. 1.14. (a) Cross section of a jet over Japan in the West Pacific at 0300 UTC 9 December 1950. The polar and subtropical frontal layers are bounded by the blue and red lines, respectively, and the location of the jet core is identified with the yellow “J”. Isotachs are drawn with the thin solid lines and isotherms are shown by the dashed lines. (b) Cross section of the same jet 24 h later at 0300 UTC 10 December 1950. The yellow lines denote the frontal layer, which is now a consolidation of the polar and subtropical frontal layers identified in (a). Both panels are modified from Mohri (1953).

FIG. 1.15. Mean positions of the polar and subtropical jet streams during the winter (From Riehl 1962 with modifications by Palmén and Newton 1969).

Chapter 2

36

FIG. 2.1. (a) 300 hPa wind speeds (shaded every 10 m s^{-1} starting at 30 m s^{-1}) at 0000 UTC 27 April 2010 depicting separate polar and subtropical jets. (b) Cross section, A-A' in Fig. 2.1a, through separate polar and subtropical jet cores with the 1-, 2-, and 3-PVU contours (black); 4-, 5-, 6-, 7-, 8-, and 9-PVU contours (light blue); potential temperature every 5 K (dashed green); and wind speed every 10 m s^{-1} beginning at 30 m s^{-1} (red). The jet cores are shaded yellow and the 315-330- and 340-355-K isentropic layers, used to identify the locations of the jets, are shaded gray. The blue (red) column corresponds to a grid column with the black dot confirming a positive identification of a polar (subtropical) jet. (c) As in (a), but for a superposed jet at 0000 UTC 24 October 2010. (d) As in (b), but for the cross section B-B' shown in Fig. 2.1c, with two positive identifications (black dots) within a single grid column indicating a jet superposition (From Winters and Martin 2014).

FIG. 2.2. Accumulated snowfall during the period 18–20 December 2009 over the Mid-Atlantic and northeastern United States (Modified from NOAA HPC; National Weather Service 2014).

FIG. 2.3. [left column] 250 hPa wind speed is shaded with the gray fill pattern every 10 m s^{-1} beginning at 30 m s^{-1} , 250 hPa geopotential heights are contoured in red every 120 m, sea level pressure is contoured with the dashed black lines every 4 hPa below 1000 hPa, the location of the sea level pressure minimum is identified with the red “L”, and jet axes are identified as specified in the legend for (a) 0000 UTC 19 December 2009, (c) 1800 UTC 19 December 2009, and (e) 1200 UTC 20 December 2009. [right column] Cross sections, as identified in the plot immediately to its left, of wind speed shaded every 10 m s^{-1} beginning at 30 m s^{-1} (blue fill pattern), potential temperature contoured every 5 K (dashed green lines), and contours of 1-, 2-, 3-PVU (black) at (b) 0000 UTC 19 December 2009, (d) 1800 UTC 19 December 2009, (f) 1200 UTC 20 December 2009. The gray shaded isentropic layers are those used to identify the jet axes using the scheme outlined in the text and the 320-K and 325-K isentropes are highlighted with the dashed red lines in the cross sections for reasons discussed in the text.

FIG. 2.4. The 48 h precipitation estimates (shaded; mm; following the color bar) for 0000 UTC 1 May – 0000 UTC 3 May 2010 from the National Precipitation Verification Unit quantitative precipitation estimates product. The locations of Nashville (BNA), Memphis (MEM), and Jackson (MKL) are also identified (From Moore et al. 2012; their Fig. 2).

FIG. 2.5. Conventions are identical to Fig. 2.3 but for (a,b) 0000 UTC 1 May 2010, (c,d) 1200 UTC 1 May 2010, and (e,f) 0000 UTC 2 May 2010. The location of the precipitation shield at 1200 UTC 1 May 2010 in (c) is denoted by the green fill pattern and sea level pressure is now contoured every 4 hPa below 996 hPa within the panels shown in the left column.

Chapter 3

59

FIG. 3.1. The 4-day precipitable water anomalies (mm; fill pattern) during the period 30 April – 3 May 2010 across the eastern United States (Courtesy of Earth Systems Research Laboratory).

FIG. 3.2. Idealized configurations of jet circulations associated with a straight jet streak on an isobaric surface in the upper troposphere. Geopotential height (thick solid lines), potential temperature (dashed lines), geostrophic isotachs (fill pattern; with the jet speed maximum represented by the J), and Sawyer-Eliassen vertical motions indicated by “up” and “down” for a regime of (a) no geostrophic temperature advection, (b) upper-tropospheric geostrophic cold-air advection, and (c) upper-tropospheric geostrophic warm-air advection along the jet axis (From Fig. 3 in Lang and Martin 2012).

FIG. 3.3. Synoptic overview with sea level pressure every 4 hPa beginning at 996 hPa (thin black lines), the surface low pressure center (red “L”), surface frontal boundaries with the cold front denoted by the blue line, the warm front denoted by the red line, and the occluded front denoted by the purple line, the magnitude of the 925 hPa poleward moisture flux every 5 cm s^{-1} beginning at 10 cm s^{-1} (green fill pattern), the 250 hPa isotachs every 10 m s^{-1} beginning at 30 m s^{-1} (purple fill pattern), the locations of the polar (blue arrow), subtropical (red arrow), and superposed (purple line) jets, as identified using the scheme described in Section 2.1, and the axis of 925 hPa poleward moisture flux (red dashed line) at (a) 0000 UTC 1 May 2010 and (b) 0000 UTC 2 May 2010.

FIG. 3.4. Change in the magnitude of the 925 hPa (a) total, (b) geostrophic, and (c) ageostrophic poleward moisture fluxes over the southeast United States during the 24 h period from 0000 UTC 1 May to 0000 UTC 2 May. Changes in the moisture flux greater than (less than) 3 (-3) cm s^{-1} are shaded in the green (red/brown) fill pattern every 3 cm s^{-1} , with 0 cm s^{-1} contoured in black. The blue (red) dashed line represents the axis of maximum poleward moisture flux at 0000 UTC 1 May (2 May), as indicated in Fig. 3.3.

FIG. 3.5. (a) Cross section of the Sawyer-Eliassen streamfunction every 300 m hPa s^{-1} (black lines) along the cross section G-G', in Fig. 3.3a, at 0000 UTC 1 May, moisture flux associated with the Sawyer-Eliassen circulation every 3 cm s^{-1} beginning at 0 cm s^{-1} (0 cm s^{-1} is contoured in green with the green fill pattern used for values greater than 3 cm s^{-1}), and negative omega associated with the Sawyer-Eliassen circulation every 1 dPa s^{-1} (blue fill pattern, dashed contours). The sense of the circulation is depicted by the arrowheads plotted on the streamfunction contours, the location of the subtropical jet core is indicated by the "J", and GULF represents the Gulf coast. (b) The 925 hPa ageostrophic poleward moisture flux every 3 cm s^{-1} beginning at 0 cm s^{-1} (0 cm s^{-1} is contoured in black with the green fill pattern used for values greater than 3 cm s^{-1}) and the axis of maximum poleward moisture flux (red dashed line previously indicated in Fig. 3.3a) at 0000 UTC 1 May.

FIG. 3.6. Cross section of the Sawyer-Eliassen streamfunction (black contours, where dashed contours represent negative values) every 300 m hPa s^{-1} along the line H-H', in Fig. 3.3a, at 0000 UTC 1 May, moisture flux due to the Sawyer-Eliassen circulation every -3 cm s^{-1} beginning at 0 cm s^{-1} (0 cm s^{-1} is contoured in orange with the orange fill pattern used for values less than -3 cm s^{-1}), and negative omega associated with the Sawyer-Eliassen circulation every 1 dPa s^{-1} (blue fill pattern, dashed contours) beginning at 1 dPa s^{-1} . The sense of the circulation is denoted by the arrowheads plotted on the streamfunction contours and the location of the polar jet core is indicated by the "J".

FIG. 3.7. (a) Cross section of the Sawyer-Eliassen streamfunction along the line F-F', in Fig. 3.3b, at 0000 UTC 2 May. Labeling conventions are identical to those in Fig. 3.5a, with the "J" representing the superposed jet core. (b) As in Fig. 3.5b, but valid at 0000 UTC 2 May.

FIG. 3.8. Cross section along F-F', in Fig. 3.3b, at 0000 UTC 2 May showing (a) the Sawyer-Eliassen streamfunction, moisture flux, and negative omega (same conventions as in Fig. 3.5a) associated with the Q_g forcing; (b) the Sawyer-Eliassen streamfunction associated with the Q_{SH} forcing (same conventions as in Fig. 3.6), isotachs of the cross-section-normal geostrophic wind (gray fill pattern) every 10 m s^{-1} beginning at 30 m s^{-1} , and the cross-section-normal temperature gradient (negative, red dashed contours; positive, blue dashed contours) every $5 \times 10^{-6} \text{ K m}^{-1}$ (zero line omitted); and (c) the Sawyer-Eliassen streamfunction associated with the Q_{ST} forcing (same conventions as in Fig. 3.6), isotachs of the along-cross-section geostrophic wind with positive values oriented toward F (positive, thick red lines; negative, dashed red lines) every 5 m s^{-1} (zero line omitted), and magnitude of the along-cross-section potential temperature gradient every $10 \times 10^{-6} \text{ K m}^{-1}$ beginning at $10 \times 10^{-6} \text{ K m}^{-1}$ (fill pattern). The "J" represents the location of the superposed jet core in all panels.

FIG. 3.9. The 500 hPa GFS analysis at 0000 UTC 2 May with geopotential height contoured in black every 60 m, isotachs of the geostrophic wind (purple fill pattern) every 10 m s^{-1} beginning at 30 m s^{-1} , and horizontal geostrophic frontogenesis (warm-colored fill pattern) every $0.4 \text{ K (100 km)}^{-1} (3 \text{ h})^{-1}$ beginning at $0.4 \text{ K (100 km)}^{-1} (3 \text{ h})^{-1}$.

FIG. 3.10. The Sawyer-Eliassen streamfunction, moisture flux, and negative omega, labeled, contoured, and shaded as in Fig. 3.5a, associated with the diabatic forcing. Heating (K s^{-1}) contoured every $200 \times 10^{-6} \text{ K s}^{-1}$ beginning at $200 \times 10^{-6} \text{ K s}^{-1}$ (red contours). The “J” denotes the location of the superposed jet core. (b) The isotachs (red contours) every 10 m s^{-1} beginning at 30 m s^{-1} with the jet core shaded yellow, the 1-, 2-, 3-PVU surfaces (black contours), potential temperature every 5 K (dashed green contours), and negative omega every 2 dPa s^{-1} beginning at 0 dPa s^{-1} (0 dPa s^{-1} is contoured in blue with values greater than 2 dPa s^{-1} shaded with the blue fill pattern) from the GFS analysis at 0000 UTC 2 May 2010 along the cross section F-F’, in Fig. 3.3b.

Chapter 4

85

FIG. 4.1. [left column] 200 hPa geopotential height is contoured in red every 120 m, 200 hPa geostrophic isotachs are shaded with the gray fill pattern every 10 m s^{-1} beginning at 30 m s^{-1} , positive perturbation pressure depths within the 340-355-K isentropic layer are shaded in the green fill pattern every 10 hPa, 200 hPa irrotational wind vectors are denoted by the arrows, and the subtropical jet axis is identified with the thick, dashed red line at (a) 0000 UTC 19 December 2009, (c) 1800 UTC 19 December 2009, and (e) 1200 UTC 20 December 2009. [right column] Infrared satellite imagery from the University of Wisconsin – CIMSS for (b) 0000 UTC 19 December 2009, (d) 1800 UTC 19 December 2009, and (f) 1200 UTC 20 December 2009. The yellow box denotes the geographical source region for the trajectories shown in Fig. 4.2.

FIG. 4.2. 72 h forward trajectories initialized at 1200 UTC 18 December 2009 within the yellow box (5°N – 10°N ; 85°W – 90°W) shown in Fig. 4.1b over the eastern equatorial Pacific Ocean. Trajectories were initialized at 3 km above ground level within the NOAA HYSPLIT model and projected forward using archived GDAS data. The bottom panel depicts the potential temperature of the trajectories throughout the duration of the 72 h period.

FIG. 4.3. 250 hPa geostrophic isotachs are shaded with the gray fill pattern every 20 m s^{-1} beginning at 40 m s^{-1} , 300 hPa geostrophic cold (warm)-air advection is shaded in the blue (red) fill pattern every $4 \times 10^{-4} \text{ K s}^{-1}$, 500 hPa potential temperature is contoured in red every 3 K, and sea level pressure is contoured with the dashed black lines every 4 hPa below 1000 hPa at (a) 0000 UTC 19 December 2009, (b) 1800 UTC 19 December 2009, and (c) 1200 UTC 20 December 2009. The polar (subtropical) jet axis is indicated by the thick, dashed blue (red) line, the yellow circle highlights the region of jet superposition, and the red “L” marks the location of the sea level pressure minimum.

FIG. 4.4. Cross sections, as indicated in Fig. 4.3, of Sawyer-Eliassen streamfunction every 300 mPa s^{-1} with negative (positive) values contoured with the dashed (solid) black lines, potential temperature contoured in red every 5 K, positive omega associated with the Sawyer-Eliassen circulation shaded in the purple fill pattern every 1 dPa s^{-1} beginning at 1 dPa s^{-1} , geostrophic

isotachs shaded with the gray fill pattern every 10 m s^{-1} beginning at 30 m s^{-1} , and the 1.5–PVU contour identified by the bold blue line. The sense of the transverse circulation is depicted by the arrowheads plotted on the streamfunction contours and the 320-K and 325-K isentropes are bolded in (b) for reasons discussed in the text.

FIG. 4.5. Conceptual diagram summarizing the development of a superposed jet during the 18–20 December 2009 Mid-Atlantic Blizzard.

FIG. 4.6. 300 hPa geostrophic isotachs are shaded in the gray fill pattern every 20 m s^{-1} beginning at 40 m s^{-1} , 300 hPa geostrophic cold (warm)-air advection is shaded in the blue (red) fill pattern every $4 \times 10^{-4} \text{ K s}^{-1}$, and 400 hPa potential temperature is contoured in red every 3 K at (a) 0000 UTC 1 May 2010, (b) 1200 UTC 1 May 2010, and (c) 0000 UTC 2 May 2010. Polar jet axes are indicated by the thick, blue dashed line and the yellow circle highlights the region of jet superposition.

FIG. 4.7. Conventions are identical to those in Fig. 4.4, but for the cross section shown in Fig. 4.6a.

FIG. 4.8. 200 hPa velocity potential contoured every $3 \times 10^6 \text{ m}^2 \text{ s}^{-1}$ with positive (negative) values identified with solid (dashed) thick red lines, the 1–, 2–, and 3–PVU surfaces at 300 hPa (200 hPa) are identified with the thin blue (red) lines, and negative PV advection within the 1–3–PVU channel by the 200 hPa divergent wind (arrows) is shaded in the green fill pattern every $2 \times 10^{-5} \text{ PVU s}^{-1}$ at (a) 0000 UTC 1 May 2010, (b) 1200 UTC 1 May 2010, and (c) 0000 UTC 2 May 2010.

FIG. 4.9. Conceptual diagram summarizing the development of a superposed jet during the 1–3 May 2010 Nashville Flood.

Chapter 5

134

FIG. 5.1. Idealized circularly symmetric flows associated with an isolated (a) positive and (b) negative Ertel PV anomaly. The location of the positive (negative) PV anomaly is denoted by the + (–) symbol and the stippled pattern, while cold and warm temperature anomalies associated with each PV anomaly are labeled accordingly. The thick black line corresponds to the tropopause and the two sets of thin lines represent the potential temperature every 5 K and the wind velocity transverse to the cross section every 3 m s^{-1} . For more information on the methods used to compute these circulations, consult Thorpe (1985) (Adapted from Hoskins et al. 1985).

FIG. 5.2. The horizontal domains used for PV inversion during the 1–3 May 2010 Nashville Flood (outer green box) and the 18–20 December 2009 Mid-Atlantic Blizzard (inner blue box).

FIG. 5.3. (a) Schematic of the three-way perturbation PV partition applied to both cases. (b) Schematic of the partition used to isolate the perturbation PV associated with the individual polar (POL) and subtropical (STJ) jets during the 1–3 May 2010 Nashville Flood. The + and – symbols correspond to positive and negative PV anomalies, respectively. For more specific details on these schemes, refer to the discussion within the text.

FIG. 5.4. Flow chart describing the components of the flow that are (balanced) and are not recovered (unbalanced) via an inversion of the PV. For more information, refer to the discussion within the text.

FIG. 5.5. PV advection within the 1-3-PVU channel at 0000 UTC 19 December 2009 by the balanced non-divergent wind at (a) 300 hPa and (b) 200 hPa, with positive (negative) PV advection shaded every 5×10^{-5} PVU s^{-1} in the orange (blue) fill pattern and the streamfunction contoured every 120×10^5 $m^2 s^{-1}$ with the thin black lines. PV advection within the 1-3-PVU channel at 0000 UTC 19 December 2009 by the balanced divergent wind at (c) 300 hPa and (d) 200 hPa, with (positive) negative PV advection shaded every 2×10^{-5} PVU s^{-1} in the orange (blue) fill pattern and velocity potential contoured every 10×10^5 $m^2 s^{-1}$ with the thin black lines (negative values dashed). The blue “H” (red “L”) corresponds to a local maximum (minimum) in velocity potential. The 2-PVU surface at 300 hPa (200 hPa) is highlighted by the thick blue (red) line in all panels and represents the location of the polar (subtropical) tropopause break.

FIG. 5.6. Conventions are identical to those in Fig. 5.5, but for 1800 UTC 19 December 2009.

FIG. 5.7. PV advection within the 1-3-PVU channel at 1800 UTC 19 December 2009 by the non-divergent wind associated with (a,b) the mean PV, (c,d) the upper-tropospheric PV, and (e,f) the interior PV at 300 hPa and 200 hPa, respectively. Conventions are identical to those in Figs. 5.5a,b, except with the streamfunction now contoured with thin black lines (negative values dashed) every 120×10^5 $m^2 s^{-1}$ in (a) and (b) and every 60×10^5 $m^2 s^{-1}$ in (c-f). The blue “H” (red “L”) corresponds to a local maximum (minimum) in streamfunction.

FIG. 5.8. PV advection within the 1-3-PVU channel at 1800 UTC 19 December 2009 by the non-divergent wind associated with the (a,b) polar jet PV and (c,d) subtropical jet PV at 300 and 200 hPa, respectively. Conventions are identical to those in Figs. 5.5a,b, except with the streamfunction now contoured every 30×10^5 $m^2 s^{-1}$ in the thin black lines (negative values dashed) and PV advection now shaded every 2×10^{-5} PVU s^{-1} . The blue “H” and red “L” correspond to a local maximum or minimum in streamfunction, respectively.

FIG. 5.9. 200 hPa PV advection within the 1-3-PVU channel at 1800 UTC 19 December 2009 by the divergent wind associated with the (a) mean PV, (b) upper-tropospheric PV, and (c) interior PV. Conventions are identical to those in Figs. 5.5c,d, except that PV advection is now shaded every 1×10^{-5} PVU s^{-1} .

FIG. 5.10. 400 hPa balanced vertical motion field at 1800 UTC 19 December 2009 associated with the (a) full PV, (b) mean PV, (c) upper-tropospheric PV, (d) interior PV, and (e) surface PV. Ascent (descent) is shaded in the green (purple) fill pattern every 1 dPa s^{-1} in (a) and every 0.5 dPa s^{-1} in (b-e). The thick blue (red) line represents the 2-PVU surface and the polar (subtropical) tropopause breaks, as in previous figures.

FIG. 5.11. Cross section of Sawyer-Eliassen streamfunction along the line L-L’, as shown in Fig. 5.10a, associated with the (a) full PV, (c) mean PV, and (d) perturbation PV at 1800 UTC 19 December 2009. Streamfunction is contoured with black lines (negative values dashed) every 300 m hPa s^{-1} , potential temperature is contoured every 5 K in red, geostrophic isotachs are

shaded in the gray fill pattern every 10 ms^{-1} greater than 30 ms^{-1} , and the thick blue line denotes the 1.5–PVU surface. Descent associated with the Sawyer-Eliassen circulation is shaded with the purple fill pattern every 1 dPa s^{-1} and the arrowheads plotted on the streamfunction contours indicate the sense of the Sawyer-Eliassen circulation. (b) Subsidence recovered from the full prognostic PV inversion is shaded with the purple fill pattern every 1 dPa s^{-1} , isotachs of the full wind are shaded in the gray fill pattern every 10 ms^{-1} beginning at 30 ms^{-1} , potential temperature is contoured every 5 K in red, and the 1.5–PVU surface is identified by the bold blue line.

FIG. 5.12. Cross sections of Sawyer-Eliassen streamfunction along the line L-L', as shown in Fig. 5.10a, associated with the (a) upper-tropospheric PV, (b) interior PV, (c) surface PV, (d) polar jet PV, and (e) subtropical jet PV at 1800 UTC 19 December 2009. Conventions are identical to those in Fig. 5.11, except with streamfunction now contoured every 100 mhPa s^{-1} and descent now shaded every 0.5 dPa s^{-1} .

FIG. 5.13. Cross sections of Sawyer-Eliassen streamfunction along the line M-M', as shown in Fig. 5.10e, associated with the (a) full PV, (b) mean PV, (c) perturbation PV, (d) upper-tropospheric PV, (e) interior PV, and (f) surface PV at 0000 UTC 20 December 2009. Conventions in (a-c) are identical to those in Fig. 5.11, while conventions in (d-f) are identical to those in Fig. 5.12.

FIG. 5.14. Conventions are identical to those shown in Fig. 5.5, but for 1200 UTC 20 December 2009.

FIG. 5.15. Conventions are identical to those shown in Fig. 5.5, but for 0000 UTC 1 May 2010.

FIG. 5.16. Conventions are identical to those shown in Fig. 5.5, but for 1200 UTC 1 May 2010.

FIG. 5.17. Conventions are identical to those shown in Fig. 5.7, but for 1200 UTC 1 May 2010.

FIG. 5.18. Conventions are identical to those shown in Fig. 5.8, but for 1200 UTC 1 May 2010.

FIG. 5.19. 60 h backward trajectories initialized at 1200 UTC 1 May 2010 within the box, 27–32°N; 90–85°W, over the Gulf coast. Trajectories were initialized at 12 km above ground level within the NOAA HYSPLIT model and projected backwards using archived GDAS data. The bottom panel depicts the pressure (hPa) of the individual trajectories throughout the duration of the 60 h period.

FIG. 5.20. Conventions are identical to those shown in Fig. 5.9, but for 1200 UTC 1 May 2010.

FIG. 5.21. (a) 400 hPa balanced vertical motion field associated with the full PV at 1200 UTC 1 May 2010. Conventions are identical to those shown in Fig. 5.10. (b) Cross section along the line N-N' in (a) of balanced upward vertical motion (green fill pattern) shaded every 1 dPa s^{-1} , wind speed shaded in the gray fill pattern every 10 m s^{-1} above 30 m s^{-1} , and potential temperature contoured in red every 5 K. The thick blue line denotes the 1.5–PVU surface as a proxy for the tropopause.

FIG. 5.22. Conventions are identical to those shown in Fig. 5.5, but for 0000 UTC 2 May 2010.

Chapter 6

170

FIG. 6.1. Conceptual diagram summarizing the process of jet superposition. The orange arrows depict branches of a transverse vertical circulation, the + (–) symbol corresponds to the center of a cyclonic (anticyclonic) circulation anomaly with the blue (red) arrow indicating the movement of that particular anomaly. The purple fill pattern corresponds to isotachs with the darker shade of purple identifying faster wind speeds. For additional information refer to the discussion in the text.

Abstract

Careful observational work has demonstrated that the tropopause is typically characterized by a three-step pole-to-equator structure, with each break between steps in the tropopause height associated with a jet stream. While the two jet streams, the polar and subtropical jets, typically occupy different latitude bands, their separation can occasionally vanish, resulting in a vertical superposition of the two jets. A cursory examination of a number of historical and recent high-impact weather events over North America and the North Atlantic indicates that superposed jets can be an important component of their evolution. Consequently, this dissertation examines two recent jet superposition cases, the 18–20 December 2009 Mid-Atlantic Blizzard and the 1–3 May 2010 Nashville Flood, in an effort (1) to determine the specific influence that a superposed jet can have on the development of a high-impact weather event and (2) to illuminate the processes that facilitated the production of a superposition in each case.

An examination of these cases from a basic-state variable and PV inversion perspective demonstrates that elements of both the remote and local synoptic environment are important to consider while diagnosing the development of a jet superposition. Specifically, the process of jet superposition begins with the remote production of a cyclonic (anticyclonic) tropopause disturbance at high (low) latitudes. The cyclonic circulation typically originates at polar latitudes, while organized tropical convection can encourage the development of an anticyclonic circulation anomaly within the tropical upper-troposphere. The concurrent advection of both anomalies towards middle latitudes subsequently allows their individual circulations to laterally displace the location of the individual tropopause breaks. Once the two circulation anomalies position the polar and subtropical tropopause breaks in close proximity to one another, elements

within the local environment, such as proximate convection or transverse vertical circulations, can work to further deform the tropopause and to aid in the production of the two-step tropopause structure characteristic of a superposed jet. The analysis also demonstrates that the intensified transverse vertical circulation that accompanies a superposed jet serves as the primary mechanism through which it can influence the evolution of a high-impact weather event.

Chapter 1

Introduction

Narrow, rapidly flowing currents of air located near the tropopause are known as jet streams, or jets. These jets, often found nearly girdling the globe while exhibiting large meridional meanders, are among the most recognizable structures within the Earth's atmosphere and are known to play a significant role in the production of sensible weather. Locally, a typical jet stream, such as the one shown in Fig. 1.1 over the west Pacific, can extend on the order of thousands of kilometers and is associated with wind speeds that may occasionally exceed 100 m s^{-1} . The width of a jet stream, however, is on the order of hundreds of kilometers, roughly an order of magnitude smaller than its length. Given this narrow width, a jet stream is characterized by considerable lateral shear, with a maximum in cyclonic (anticyclonic) shear on the poleward (equatorward) side of the jet. These jets are also accompanied by large vertical shears both above and below the level of maximum wind speed in the upper troposphere. While identifying the exact position and characteristics of the jet stream are trivial tasks today, and a testament to the progress made in the field, the very existence of a jet stream eluded atmospheric scientists as recently as 75 years ago.

The seeds for the “discovery” of the jet stream were planted back in the 19th century amidst a growing interest to better understand the general circulation of the Earth's atmosphere. As part of that work, it quickly became apparent that the Earth's general circulation was closely tied to the existence of a pole-to-equator temperature gradient. Specifically, Ferrel indicated in 1878 that a direct proportionality exists between the magnitude of the column-averaged horizontal temperature gradient and the vertical shear of the geostrophic wind (Kutzbach 1979). This relationship, now commonly known as thermal wind balance, provides the theory that

underpins the existence of an upper-level wind speed maximum near the tropopause. Margules (1903) later demonstrated that the pole-to-equator temperature gradient also represented a reservoir of potential energy from which mid-latitude disturbances (e.g., cyclones) could draw their kinetic energy. Such a result indicated a theoretical link between the Earth's general circulation and the development of the types of disturbances that are responsible for the production of sensible weather at middle latitudes.

Given the connection of the pole-to-equator temperature gradient to the development of mid-latitude disturbances and the Earth's general circulation, the growing number of upper-air and surface observations following World War I accelerated a burgeoning interest to resolve the horizontal and vertical temperature structure of the mid-latitude atmosphere. Employing the most extensive use of upper-air observations to date, Dines (1925) suggested that cyclones (anticyclones) were characterized by cold (warm) column-averaged temperatures below ~ 9 km, while the opposite was true at higher altitudes. Together, these observations indirectly implied that a column-averaged horizontal temperature gradient existed between juxtaposed cyclonic and anticyclonic circulations below ~ 9 km, with the gradient reversing direction above that elevation. A valuable aspect of this result was the suggestion that the horizontal circulations associated with cyclones and anticyclones must be maximized in the upper troposphere (e.g., around 9 km), as would be expected from an application of the thermal wind relationship. Furthermore, Dines noted that there was a positive correlation between the tropopause height and the mean tropospheric temperature, which suggested that, on average, the tropopause sloped downward towards higher latitudes.

The analysis of a more spatially dense network of surface observations over western Europe around the same time also led to the development of "Polar Front Theory" (Bjerknes and

Solberg 1922). As part of that conceptual model, the polar front was believed to be a wavy and continuous boundary at middle latitudes that encircled the globe and separated dry air masses of polar origin from moist, tropical air masses found at low latitudes. Treated as a zero-order discontinuity in temperature, this boundary suggested that a large portion of the pole-to-equator baroclinicity was focused into a narrow meridional region within each hemisphere. Additionally, it was implied that this zone of baroclinicity extended from the surface through the troposphere, sloping upward in the direction of the colder air mass.

Several years later, Bjerknes and Palmén (1937) provided solid observational evidence of the vertical structure of the polar front by initiating a coordinated international effort to launch simultaneous balloon soundings at 18 different locations throughout Europe. These “swarm ascents” were performed at regular intervals during February 1935 in an effort to capture the horizontal and vertical temperature structure across the continent. Figure 1.2 shows an example of one characteristic cross section constructed through a frontal boundary as part of that study. From this analysis, it is evident that the polar front was characterized by a narrow *zone* of strong baroclinicity that occupied the entire depth of the troposphere and sloped back in the direction of the colder air mass with increasing elevation. A key difference from Polar Front Theory, however, is that the front in this case is not characterized as a zero-order discontinuity in temperature. Instead, Bjerknes and Palmén (1937) identify the front as a *transition zone* across which the temperature gradient, not the temperature itself, is discontinuous.

Another notable result from the Bjerknes and Palmén (1937) analysis concerns the structure of the tropopause. Similar to the conclusion implied by Dines’ (1925) correlations, the tropopause in Fig. 1.2 was identified a higher elevation on the equatorward side of the front than on the poleward side. However, instead of exhibiting a uniform slope from low to high latitudes,

the tropopause height abruptly lowered at the location where the polar frontal zone intersected the tropopause. This observation provided the first identification of what is known commonly today as a tropopause “break” – one of the leading structural characteristics of the tropopause at middle latitudes. Furthermore, locations directly above the tropopause break were characterized by a reversal in the sign of the meridional temperature gradient, lending additional evidence to support Dines’ (1925) analysis.

Observations from the “swarm ascents” also indicated that areas distinguished by a strong horizontal temperature contrast in the troposphere were, in fact, associated with a large vertical wind shear. However, no effort was made by Bjerknes and Palmén at the time to thoroughly examine the spatial relationship between wind speeds at upper-levels and the location of the mid-tropospheric baroclinic zone. While Bjerknes and Palmén (1937), and the other studies presented prior to World War II, provided a strong theoretical and observational foundation that would support the existence of a localized wind speed maximum in the upper troposphere, it was not until during and after the war that the growth of technology, and the accompanying influx of new observational data, would facilitate the “discovery” of the jet stream and an appreciation for its hemispheric continuity.

1.1 The “Discovery” of the Jet Stream

An important component of the Allies’ strategy in the Pacific Theater during World War II was the use of military aircraft for “high-altitude” bombing raids against Japan. The “high-altitude” nature of these missions was designed both to accommodate the maximum altitude that aircraft could fly at the time (~10 km) and to avoid the range of anti-aircraft guns scattered throughout the Japanese landscape. In an effort to support these missions, weather officers in the

United States Air Force were responsible for providing forecasts of upper-level winds up to 20 h in advance. However, the sparse availability of upper-level observations across the western Pacific made this task particularly difficult. While some observations were available from stations, ships, and reconnaissance aircraft throughout the region, oceanic locations were poorly sampled. Despite this complication, weather officers were still able to calculate a forecasted wind speed based off of the available observations by employing the thermal wind relationship.

Bryson (1994) provides an account of one particularly notable instance in which he and another weather officer, Bill Plumley, were tasked with providing an advance forecast of upper-level winds at 30,000-35,000 ft (~10km) prior to a large bombing raid in the fall of 1944. Upon assimilating the sparse data that was available to them, the two officers were able to determine that a cold front would be located over the Japanese Islands the following day. Provided with an estimate of the horizontal temperature gradient that characterized the frontal boundary, the officers used the thermal wind relationship to forecast a westerly wind speed of 168 knots (86.4 ms^{-1}) at 35,000 ft over Japan¹. Bryson and Plumley deduced that winds of this magnitude would pose a serious threat to the success of the raid, given that most aircraft did not fly much faster than the calculated wind speed.

The delivery of this forecast was met with much consternation from the general, who believed that the forecast must have been in error since winds of this magnitude had not been reported before by United States military aircraft over the west Pacific². Consequently, the raid continued on as planned, in spite of the forecast that had been provided. It soon became apparent, however, that the mission would indeed become a failure, as planes were essentially standing

¹ Using a height of 10 km (~250 hPa), and assuming no zonal wind at the surface (1000 hPa) at 35°N, this wind speed corresponds to a column-averaged, meridional temperature gradient of $-1.8 \text{ K (100 km)}^{-1}$.

² Large climatological zonal wind speeds within the upper troposphere over Japan had been observed and documented by Ooishi (1926) well before the war, however.

still as they attempted to fly up-wind. Furthermore, the strength of the winds severely decreased the ability of the pilots to accurately locate their bombing targets while flying at any other angle to the wind. Following the mission the general returned to apologize to Bryson and Plumley and noted that the aircraft had observed a wind speed of 170 knots (87.5 ms^{-1}) – remarkably close to the forecasted value!

The result of the mission sparked some concern among top members in the military as to how to conduct bombing raids in the presence of such strong upper-level wind speeds. The United States Air Force subsequently reached out to Carl-Gustaf Rossby, one of the most prominent meteorologists in the United States at the time from the University of Chicago, who called the phenomenon the “jet stream” – in reference to some of his earlier work on similar currents present within the ocean (Rossby 1936). Around the same time, an identification of the jet stream occurred independently in other parts of the world as well. In 1939, for example, German researcher Heinrich Seilkopf termed the phenomenon “die Strahlströmung”, which translates loosely to “jet flow” (Reiter 1963). Ultimately, knowledge of the position and strength of the jet stream became an important component in determining the success of air campaigns for the remainder of the war.

At the conclusion of the war, the U. S. Weather Bureau distributed two volumes of 500 hPa charts over the Northern Hemisphere during October and November 1945. The availability of this data made it possible for Rossby and his colleagues at the University of Chicago to provide one of the first hemispheric examinations of the atmospheric general circulation at middle latitudes (University of Chicago 1947). Upon reviewing these charts, several key characteristics of a mid-latitude jet stream became immediately apparent. First, the jet stream was characterized by a nearly continuous and narrow zone of extremely strong wind speeds that

meandered meridionally as it encircled the hemisphere. Second, the jet was situated atop the strongly baroclinic, and occasionally tropospheric-deep, polar front. Finally, it was clear that the jet stream was nestled squarely within a break in the tropopause, as indicated by the cross section shown in Fig. 1.3.

1.2 Cross-Stream Vertical Circulations within the Jet Environment

The University of Chicago group's seminal work marked the beginning of a furious research effort in the middle of the 20th century centered on understanding the formation and structure of the jet stream. An initial theory for the existence of a localized westerly wind maximum at middle latitudes, offered by Rossby and his colleagues, was based upon the hypothesis that large-scale horizontal mixing at high latitudes acted to create a uniform distribution of absolute vorticity poleward of the jet axis (University of Chicago 1947). The jet stream was then believed to exist within a critical zone of latitudes where this mixing was interrupted. While this theory provided by the University of Chicago group provided good agreement with the wind observations at the time, it did not propose a mechanism that acted to maintain the strength and structure of the jet stream and no supporting evidence was found to justify the existence of such critical mixing latitudes within the mid-latitude atmosphere in later analyses.

Subsequent studies, many of which were spearheaded by Finnish researcher Erik Palmén, quickly focused attention on cross-stream vertical circulations as a dynamical mechanism that could support the characteristic distribution of temperature and relative vorticity found in the vicinity of the jet. Initial support for the presence of a cross-stream vertical circulation was offered by Palmén and Newton (1948), who implied that horizontal divergence and convergence,

operating alone at the level of maximum wind, was not sufficient to generate relative vorticity that was of the same magnitude as that observed straddling the jet core. Consequently, it was believed that some sort of transverse vertical circulation must be superimposed on the flow. Palmén (1948) further suggested that such a vertical circulation would have the greatest impact within the lower stratosphere, where the presence of vertical motions could restructure the baroclinicity via vertical advection more effectively due to the greater stability in that location compared to the troposphere.

Less than a year later, Palmén and Nagler (1949) analyzed the movement of air parcels through a mid-latitude trough and established a conceptual model for the structure of transverse vertical circulations in the vicinity of a jet. In contrast to Palmén's (1948) initial hypothesis, which emphasized the importance of vertical motions in the lower stratosphere, Fig. 1.4 depicts a conceptual model that consisted of vertical circulations both above and below the level of maximum wind. On the upstream side of the trough axis in this particular case, Palmén and Nagler noted that air parcel trajectories were accelerating as they entered the base of the trough. Consequently, they suggested that both the troposphere and lower stratosphere were each characterized by thermally indirect circulations that acted to support an increase in baroclinicity both above and below the jet core via tilting. Alternatively, as parcels decelerated downstream of the trough axis, it was suggested that thermally direct circulations in the troposphere and lower stratosphere worked to decrease the horizontal baroclinicity in those locations. While this distribution of cross-stream vertical circulations was not found to be widely applicable, the success of Palmén and Nagler's model was the notion that cross-stream vertical circulations provided a dynamical link between the upper-tropospheric/lower-stratospheric baroclinicity and the jet itself.

Around the same time, Namias and Clapp (1949) attempted to provide an explanation for a process that could facilitate the development of cross-stream vertical circulations in the near-jet environment. They hypothesized that the jet stream was driven by the confluence of two air streams of separate origin, such as from the tropics or polar latitudes, which coincidentally acted to strengthen the horizontal temperature gradient in both the upper troposphere and lower stratosphere (Fig. 1.5a). Concurrent with the strengthened temperature gradient was an increased horizontal pressure gradient, as cold and warm columns of air became more closely juxtaposed. The associated vertical circulation, then, was believed to be a dynamical response to the imbalance between the strengthening pressure gradient and the flow itself.

A conceptual diagram of the circulation forced by the large-scale confluence is shown in Fig. 1.5b, which depicts a thermally direct circulation that extended through the full depth of the troposphere and into the lower stratosphere. As in Palmén and Nagler (1949), Namias and Clapp viewed the circulation as a dynamical mechanism that intricately connected the baroclinicity to the jet. Specifically, it was suggested that the circulation acted both in response to the confluent frontogenesis present within the flow and as a mechanism for conversion of the potential energy associated with the horizontal temperature gradient into the kinetic energy of the jet stream. It was also argued that the ascending and descending branches of the circulation were responsible for the development of the characteristic tropopause break found in the vicinity of the jet, producing higher (lower) tropopause heights equatorward (poleward) of the wind speed maximum. This idea, that the transverse vertical circulations could restructure *both* the tropopause and baroclinicity in the near jet environment, became a topic of considerable research attention in the decades that followed.

An increase in observational capabilities during the 1950's, including the expansion of the North American radiosonde network, provided additional opportunities to acquire observations that had the potential to validate the aforementioned conceptual models of transverse vertical circulations in the vicinity of the jet stream. One particularly novel result from the analysis of this data was that the development of intense baroclinicity beneath the jet core was, in contrast to Namias and Clapp's (1949) confluence model, predominantly accomplished by vertical motions. For example, Reed and Sanders (1953) calculated the magnitude of the terms in the Miller (1948) frontogenesis function and determined that the tilting term far outweighed the effects of confluence in strengthening the magnitude of the horizontal temperature gradient beneath the jet core. Furthermore, it was found that the tilting frontogenesis was driven by a maximum in subsidence positioned directly below the jet core and on the warm side of the developing baroclinic zone. Similar results were found in a later case study by Reed (1955), who demonstrated that the development of strong upper-level baroclinicity could be the by-product of a thermally indirect circulation with its subsiding branch located on the warm side of the mid-tropospheric front.

Another notable product of Reed's (1955) case study was the use of the potential vorticity (PV; Rossby 1940; Ertel 1942) to illuminate a key characteristic of the tropopause in the vicinity of a jet. The PV on an isentropic surface³ is defined as:

$$PV = -g(\zeta_{\theta} + f) \frac{\partial \theta}{\partial p} \quad (1.1)$$

where g is the gravitational constant, f is the Coriolis parameter ($f = 2\Omega \sin \phi$, with ϕ the latitude and Ω the Earth's rotation rate [$7.292 \times 10^{-5} \text{ s}^{-1}$]), θ is the potential temperature, ζ_{θ} is

³ An examination of PV on an isentropic surface is particularly optimal, as both the PV and potential temperature of an air parcel are conserved for adiabatic and inviscid motion. In subsequent instances, PV will refer to the Ertel (1942) form of the potential vorticity shown in (1.1).

the relative vorticity on an isentropic surface, and p is the pressure. From (1.1), it is clear that the PV can serve as a particularly useful tracer for stratospheric air, as the enhanced stability of the stratosphere typically results in substantially larger values of PV in those locations compared to the troposphere. The dynamical tropopause (defined as the 2-PVU surface⁴), then, is considered as the spatially continuous boundary that marks the transition between relatively uniform, low values of PV found in the troposphere and the higher values residing within the stratosphere (e.g., Danielsen and Hippskind 1980; Morgan and Nielsen-Gammon 1998). This definition for the tropopause stands in contrast to that used by the World Meteorological Society (WMO), in which the tropopause marks the transition to a neutral lapse rate in temperature (WMO 1992).

Upon examining the distribution of PV, Reed (1955) noted that coincident with the development of a strong mid-tropospheric front was a downward protrusion of stratospheric, high PV air into the upper troposphere beneath the jet core, creating what was termed a “folded” tropopause (Fig. 1.6). Consequently, Reed’s case study provided observational evidence that suggested a cross-stream vertical circulation could, indeed, act to restructure the tropopause to produce the characteristic tropopause break found in the vicinity of a jet. Subsequent studies over the course of the second half of the 20th century, which leveraged the growing capabilities of computing technology and the use of high-resolution data from airborne field campaigns, provided additional evidence that continued to confirm the relationship between cross-stream vertical circulations and the evolution of the tropopause and temperature structure that strongly characterizes the jet environment at middle latitudes (e.g., Sawyer 1956; Eliassen 1962; Danielsen et al. 1970; Bosart 1970; Shapiro 1981; Keyser and Pecnick 1985; Keyser and Shapiro

⁴ 1-PVU = $1 \times 10^{-6} \text{ K m}^2 \text{ kg}^{-1} \text{ s}^{-1}$

1986). Additional details from a sample of these studies are reserved for more extensive discussion in later chapters.

1.3 Two Distinct Jet Species: The Polar and Subtropical Jets

The wider availability of observations following World War II facilitated a more extensive examination of the horizontal distribution of temperature and wind speed in the upper troposphere, as well. Emerging from an analysis of this data was a growing body of evidence that supported the existence of two distinct jet streams within each hemisphere. One such piece of evidence, included within a study by Riehl (1948), was that the meridional temperature gradient in the upper troposphere exhibited a rather non-linear character. In particular, Fig. 1.7 indicates that in Riehl's selected case, the temperature distribution at 200 hPa was characterized by a ring of cold air that stretched zonally across the continental United States with warmer temperatures straddling the cold ring to its north and south. While Riehl accurately identified a jet stream on the poleward flank of the cold ring, it is apparent that the presence of an equatorward directed horizontal temperature gradient over Florida and the Caribbean would support the existence of a second zonal wind speed maximum above 200 hPa in that location. Figure 1.3, constructed 24 h following the analysis shown in Fig. 1.7, clearly identifies this secondary wind speed maximum over Brownsville, TX on the right-hand side of the plot.

Additional evidence for a second, distinct wind speed maximum at upper levels is also provided by Palmén and Newton (1948) and is shown in Fig. 1.8. Within this particular cross section, it is clear that the primary wind speed maximum is found around 45°N and sits directly atop the polar front, in agreement with many of the aforementioned observational studies. Further equatorward, however, a secondary wind speed maximum is analyzed between 35°–40°N

at a higher altitude. In comparison to its poleward counterpart, this particular wind speed maximum was associated with considerably weaker baroclinicity in the upper troposphere and lower stratosphere. The meridional location of this secondary wind speed maximum also coincided particularly well with the analyzed position of the climatological jet stream in January over North America by Namias and Clapp (1949). Referencing both of these studies, Palmén (1951) acknowledged the growing evidence supporting the existence of two separate westerly air streams within each hemisphere. The first of which, now known as the polar jet, is closely tied to the location of the polar front and is characterized by considerable meridional meanders as it circumnavigates the hemisphere at middle latitudes. The second, known as the subtropical jet, is characterized by a rather continuous band of zonal wind speeds at subtropical latitudes, which allow it to emerge from climatological studies such as the one performed by Namias and Clapp (1949).

During the early 1950's, several different studies examined the structure of the subtropical jet in different parts of the globe. For instance, Loewe and Radok (1950) examined the subtropical jet in the southern Pacific Ocean, Yeh (1950) and Mohri (1953) investigated it over eastern Asia, Koteswaram (1953) and Koteswaram and Parthasarathy (1954) surveyed the jet over India, and Sutcliffe and Bannon (1954) considered the subtropical jet over Africa. While each of these individual studies provided substantial insight into the structure of the subtropical jet in specific regions, these studies were limited in the sense that they were restricted to small geographical domains and primarily sampled only the strongest of jets.

In the early 1960's, Krishnamurti (1961) provided a detailed and comprehensive examination of the subtropical jet throughout the entire Northern Hemisphere. As part of that study, Krishnamurti confirmed that the subtropical jet during winter is characterized by a

continuous belt of zonal winds that encircle the hemisphere with speeds that, on occasion, could exceed 75 to 100 m s^{-1} (Fig. 1.9). Furthermore, the mean subtropical jet exhibits a standing, three-wave pattern, with ridges located over North America, the western Pacific, and Africa. Wind speeds were observed to be the strongest, on average, in the vicinity of the ridges and weakest in the troughs. Finally, the meridional position of the subtropical jet remains fixed to $\sim 30^\circ\text{N}$ throughout the winter, though occasional meridional shifts in its specific location at any given time were possible.

It also became apparent that, similar to the polar jet, the subtropical jet is closely associated with a transverse vertical circulation. In contrast to the polar jet, where transverse circulations work to transform the available potential energy associated with the meridional temperature gradient into the kinetic energy of the jet, the subtropical jet is tied to a meridional overturning circulation in the tropics known as the Hadley Cell (e.g., Palmén 1951; Krishnamurti 1961). A sample schematic of the Hadley Cell is taken from Palmén (1951) and reproduced in Fig. 1.10. The Hadley Cell develops in an attempt to resolve the imbalance in solar insolation that exists between low and high latitudes. The circulation itself is characterized by an ascending branch near the equator, which is associated with the development of tropical convection, and a poleward-directed branch in the upper troposphere. The mean subtropical jet is situated at the poleward edge of the Hadley Cell ($\sim 30^\circ$) and develops in response to the transport of angular momentum from the tropics to high latitudes by the poleward-directed branch of the circulation. Directly beneath the jet is a region of subsidence, which is responsible for the production of subtropical surface anticyclones as well as the weak horizontal baroclinicity that exists beneath the jet.

1.4 Vertical Jet Superpositions

Careful observational work by Defant and Taba (1957, hereafter DT57) was one of the first to demonstrate that the spatial location of the polar and subtropical jets is also intricately related to the hemispheric tropopause structure. Specifically, DT57 found that the atmosphere is typically characterized by the three-step pole-to-equator tropopause structure⁵ shown in Fig. 1.11 (modified from DT57, Fig. 13), wherein each step is separated from its neighbors by the presence of a westerly wind maximum. In particular, the subtropical jet is found within the break between the tropical (~ 90 hPa) and subtropical tropopause (~ 250 hPa) while the polar jet is located farther poleward in the break between the subtropical tropopause and the even lower polar tropopause (~ 300 hPa).

A particularly insightful element of the DT57 analysis was their construction of hemispheric maps of tropopause height (in hPa). On these maps, one of which is shown in Fig. 1.12 (modified from DT57, Fig. 2), breaks in the tropopause, and thus the location of the respective jets at any particular time, are characterized by sharp, isolated, and easily identifiable gradients in tropopause height. While such an analysis clearly demonstrates that both the polar and subtropical jets occupy different latitude bands, substantial meanders in their locations are common. Occasionally, the characteristic meridional separation between the two structures can disappear, as it does in Fig. 1.12 in the area bounded by the black circle over the North Atlantic, where the polar and subtropical jets vertically superpose⁶. One consequence of such a vertical superposition of the two jets is the development of a two-step tropopause structure from the

⁵ Several studies have also identified a less ubiquitous arctic jet, which is often located around 500 hPa and is situated in a third tropopause break between the polar tropopause and an even lower arctic tropopause (Shapiro et al. 1984; Shapiro 1985; Shapiro et al. 1987).

⁶ More recently, maps of tropopause height, pressure, and potential temperature along the dynamical tropopause have also been beneficial for identifying the location of tropopause breaks and the occasional vertical superposition of the polar and subtropical jets (e.g., Hoskins and Berrisford 1988; Davis and Emanuel 1991; Hakim et al. 1995; Bosart et al. 1996; Morgan and Nielsen-Gammon 1998; Shapiro et al. 1999).

tropics to high latitudes, rather than the more common three-step structure represented in Fig. 1.11.

Employing companion maps of tropopause temperature (Fig. 1.13), DT57 further demonstrated that in the vicinity of a superposition the upper-tropospheric and lower-stratospheric baroclinicity associated with each jet individually is combined into a substantially narrower zone of contrast. Consequently, the associated superposed jet structure possesses an anomalous fraction of the pole-to-equator baroclinicity. An example of this process is illustrated by Mohri (1953) in his study of an intense, and likely superposed, jet over the west Pacific in December 1950. Figure 1.14a shows that at 0300 UTC 9 December 1950 two distinct areas of horizontal baroclinicity were found in the vicinity of the jet: a polar front which extended down to the surface and a “subtropical front”, as Mohri defined it, which was confined to the upper troposphere. 24 h later, it is evident that the two areas of baroclinicity have consolidated into one single zone of intense temperature contrast (Fig. 1.14b). Coincident with, and directly above, this intensified mid-tropospheric baroclinicity were stronger jet wind speeds that now exceeded 100 m s^{-1} . The development of intensified baroclinicity associated with a superposed jet is also frequently attended by a strengthening of its associated transverse vertical circulation. These circulations, in addition to their aforementioned ability to restructure the tropopause and temperature structure, are the primary dynamical mechanism by which superposed jets can be involved the production of sensible weather.

Both Krishnamurti (1961) and Riehl (1962) indicated that there are three primary regions within the Northern Hemisphere where the axes of the mean polar and subtropical jet are out-of-phase with one another and, consequently, dwell in close proximity: the west Pacific, North America, and northern Africa (Fig. 1.15). Christenson and Martin (2014) independently

demonstrated that these same three regions climatologically experience the greatest frequency of jet superposition events. Over North America and the Atlantic Ocean, in particular, superposed jets have been linked, either directly or indirectly, to a number of historical and recent high-impact weather events. For instance, Defant (1959) discussed the impact of a dramatic jet superposition on an explosive cyclogenesis event south of Iceland on 8 January 1956, in which the sea level pressure dropped 61 hPa in 24 h. Furthermore, the 25–26 January 1978 Cleveland Superbomb (Hakim et al. 1995; Hakim et al. 1996), the 15–16 October 1987 Great October Storm (Hoskins and Berrisford 1988), the 4–5 January 1989 ERICA-IOP4 storm (Shapiro and Keyser 1990), the 12–14 March 1993 Storm of the Century (Bosart et al. 1996), the 18–20 December 2009 Mid-Atlantic Blizzard (National Weather Service 2014; Winters and Martin 2015), the 1–3 May 2010 Nashville Flood (Durkee et al. 2012; Moore et al. 2012; Winters and Martin 2014), and the 25–28 April 2011 severe weather outbreak (Christenson and Martin 2012; Knupp et al. 2014) are all examples of events that occurred within an environment characterized by a jet superposition⁷.

The association of jet superpositions with a class of high-impact weather events over North America and the north Atlantic warrants further consideration of (1) the role superposed jets can play in the evolution of high-impact events and (2) the mechanisms that can support the development of superposed jets in this part of the world. An effort to address to these two topics has remained absent from the refereed literature and is subsequently undertaken as the primary objective of this dissertation. Chapter 2 discusses the methodology used to objectively identify polar, subtropical, and superposed jets and details the two recent high-impact weather events over North America that were selected for examination in this study. Chapter 3 demonstrates one

⁷ All of the cases exhibited the two-step tropopause structure characteristic of a superposed jet at some point during their evolution.

pathway through which a superposed jet can impact the evolution of a high-impact weather event. Chapters 4 and 5 consider the processes that are most conducive for the development of a superposition in both cases from a basic-state variable perspective and a PV perspective, respectively. Chapter 6 finishes with a broad discussion and suggestions for future work.

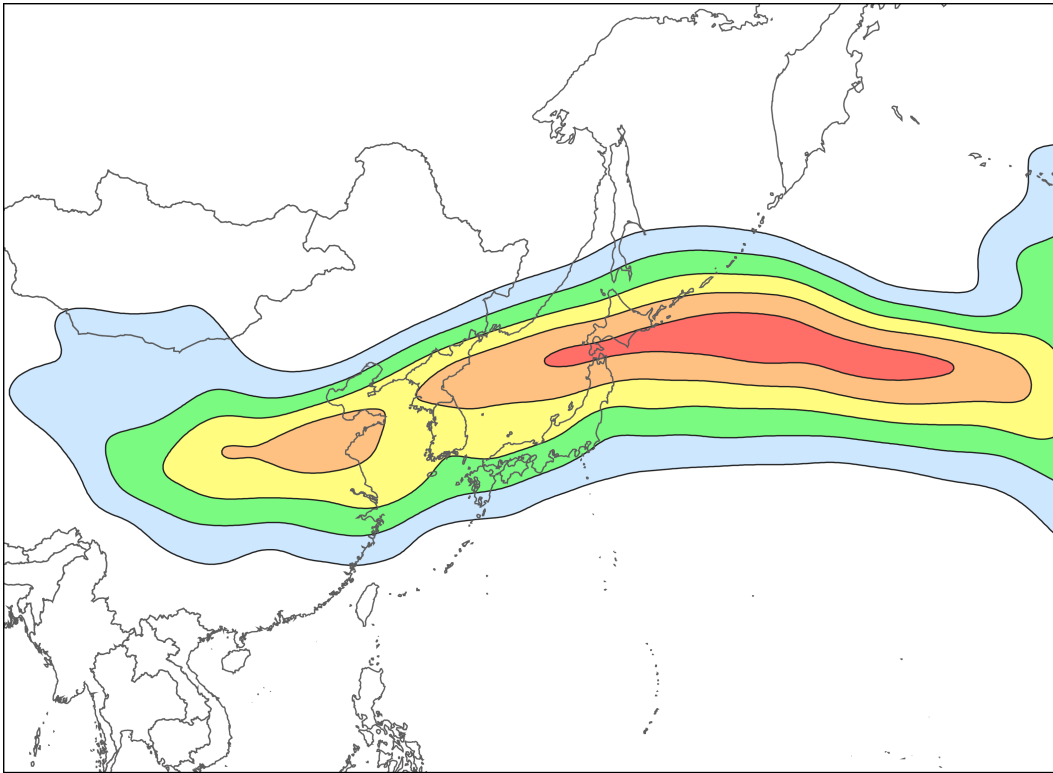


FIG. 1.1. 250 hPa wind speed shaded with the fill pattern every 10 ms^{-1} beginning at 30 ms^{-1} at 1200 UTC 22 April 2010.

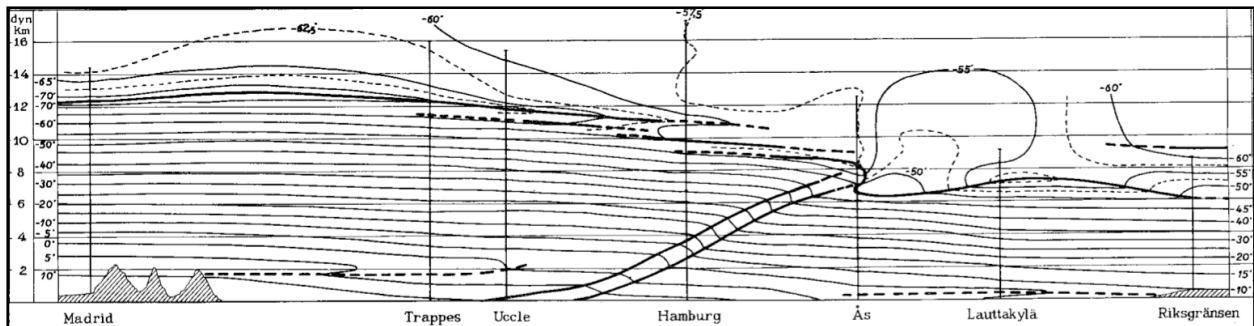


FIG. 1.2. Cross section of temperature over Europe from the evening of 15 February 1935 that is constructed from the data acquired during the “swarm ascents” coordinated by Bjerknes and Palmén (1937). The region of baroclinicity centered near Hamburg is bounded by two black, bold lines and identify the location of the polar frontal zone. The tropopause is also identified by a single bold, black line that separates the nearly isothermal stratosphere from the troposphere.

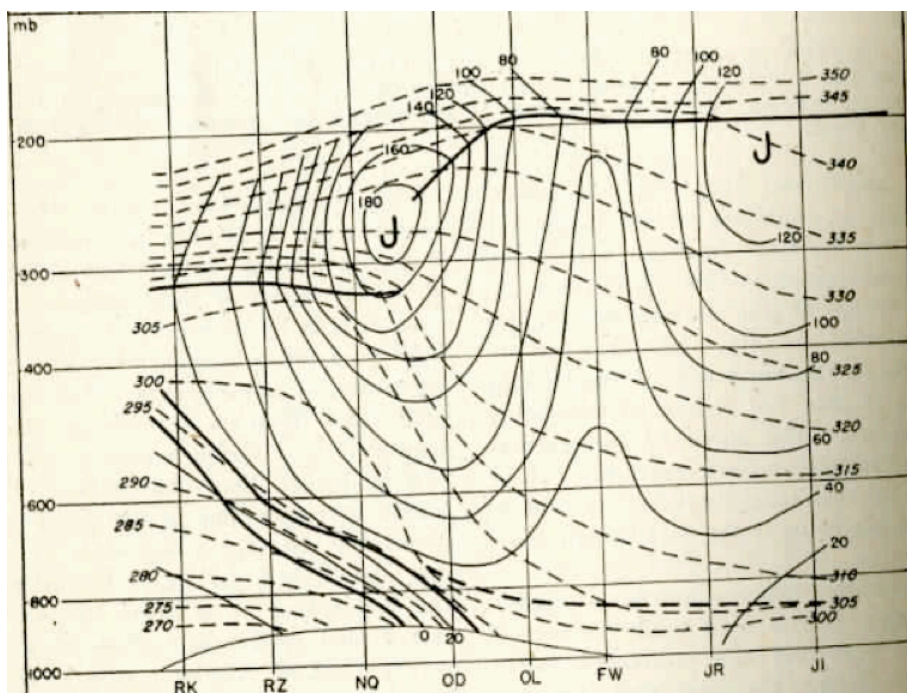


FIG. 1.3. Vertical cross section of temperature and wind speed from Bismarck, ND to Brownsville, TX at 0300 UTC 29 January 1947. Isentropes are drawn with the thin dashed lines and isotachs are represented by the thin solid lines. The bold black lines identify the location of the tropopause or the boundaries of the frontal zone. The “J” identifies the location of the jet core (From University of Chicago 1947; Fig. 17).

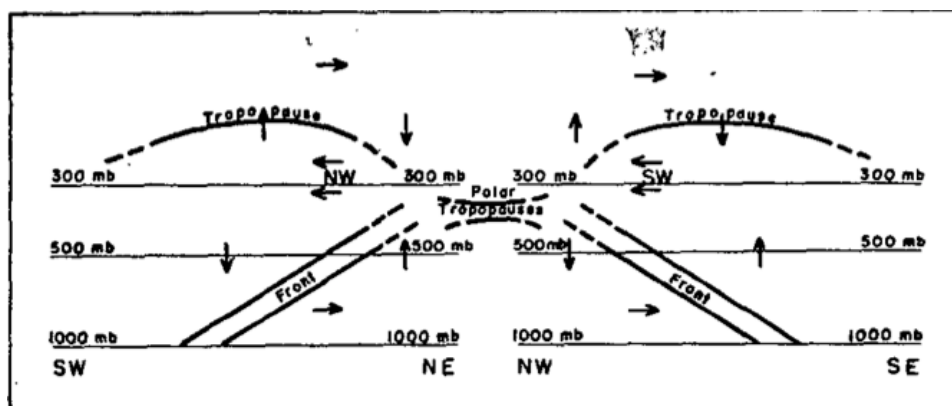


FIG. 1.4. Conceptual diagram of the transverse vertical circulations, depicted by the arrows, upstream (left) and downstream (right) of an upper-level trough (From Palmén and Nagler 1949; Fig. 16).

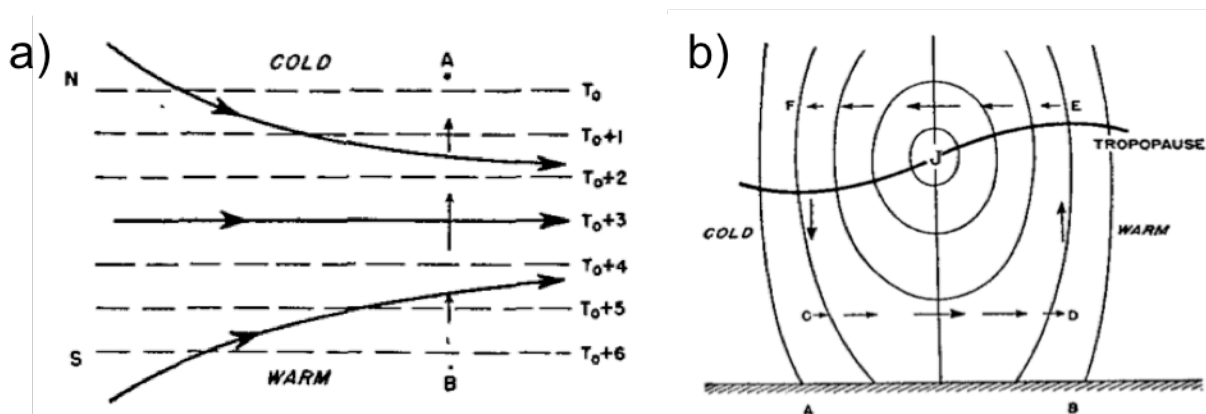


FIG. 1.5. (a) A conceptual diagram depicting a region of confluence acting upon a meridional temperature gradient. (b) A cross section from A to B, as identified in (a), of the characteristic transverse vertical circulation that would respond to the confluent flow shown in (a). Both panels are taken from Namias and Clapp (1949).

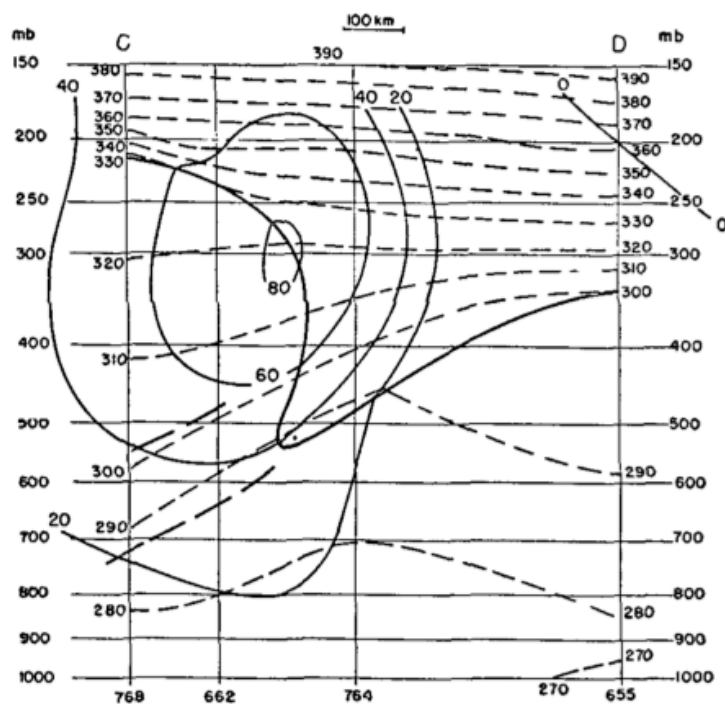


FIG. 1.6. Cross section of a developing upper-level front in northwesterly flow over the Northern Plains at 0300 UTC 14 December 1953. Isentropes are identified with the dashed lines, isotachs with the thin solid lines, and the tropopause with the bold, black line (From Reed 1955; Fig. 12).

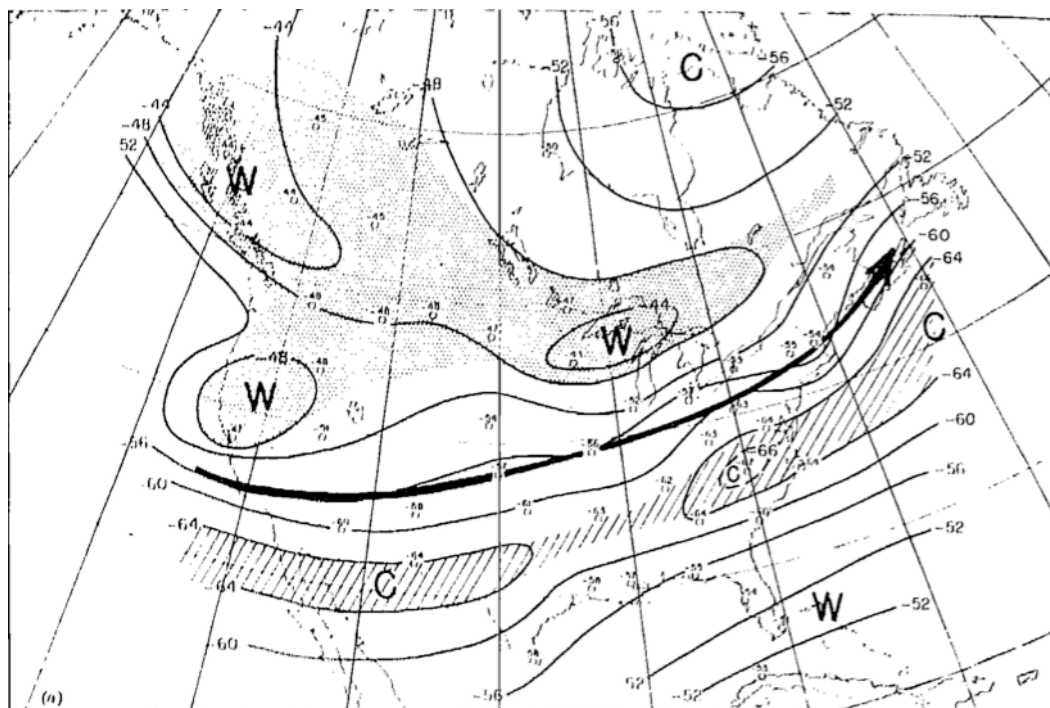


FIG. 1.7. 200 hPa temperatures at 0300 UTC 28 January 1947. Local maxima and minima in temperature are represented by a “W” and a “C”, respectively. The jet axis is identified by a thick black arrow (From Riehl 1948; Fig. 4a).

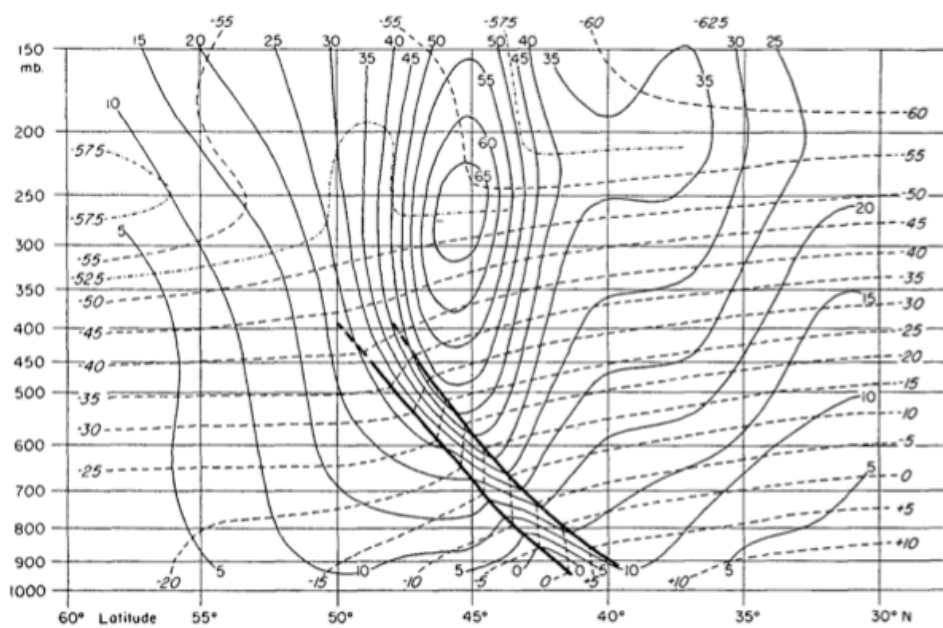


FIG. 1.8. A composite cross section constructed from 12 individual cross sections of the polar front during December 1946. Isotherms are drawn with the dashed lines and isotachs with the thin black lines. The bold black lines denote the frontal zone (From Palmén and Newton 1948; Fig. 1).

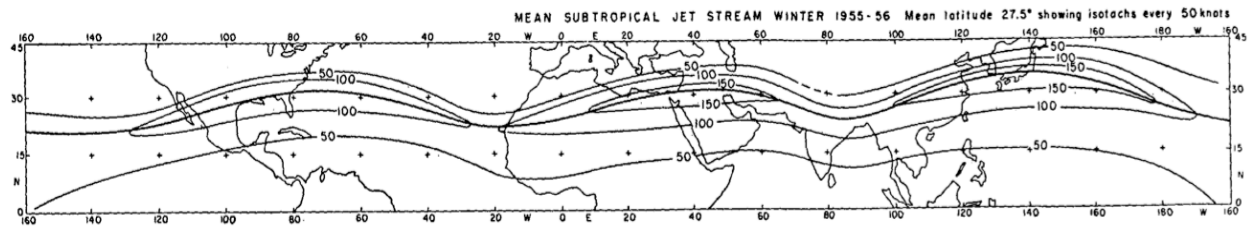


FIG. 1.9. The mean subtropical jet stream during the winter of 1955–1956. Isotachs are shown at 200 hPa in the thin black contours and the jet axis is identified by the bold black line (From Krishnamurti 1961; Fig. 3).

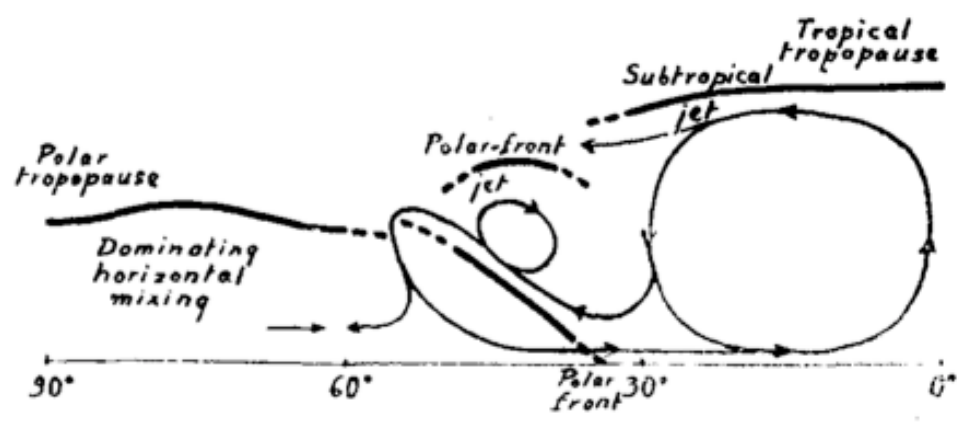


FIG. 1.10. Conceptual diagram illustrating the mean meridional circulation during the winter (From Palmén 1951; Fig. 11).

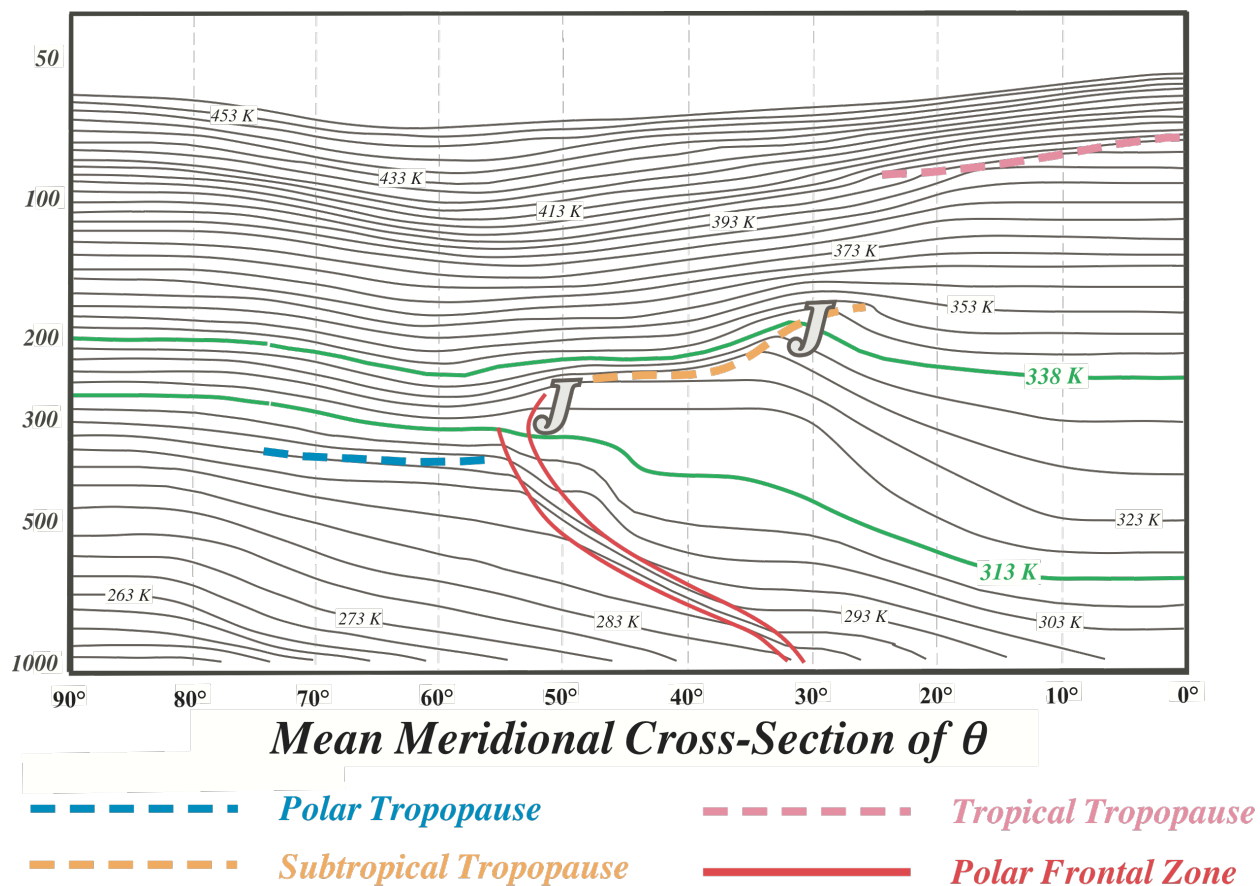


FIG. 1.11. Mean meridional cross section of potential temperature for 1 January 1956 with the polar, subtropical, and tropical tropopause steps and polar frontal zone labeled as indicated in the legend (Modified from DT57; Fig. 13).

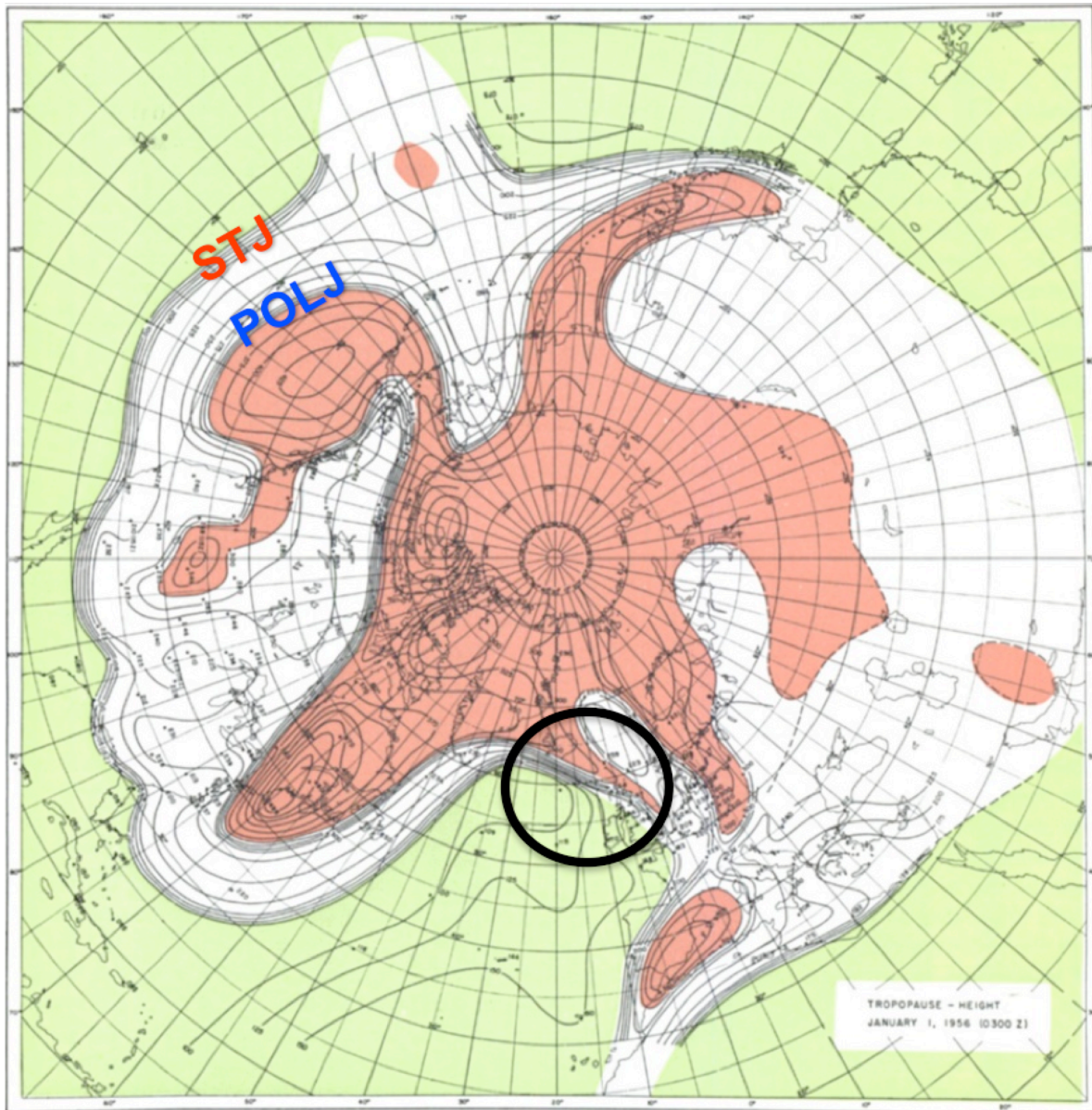


FIG. 1.12. Northern Hemispheric map of tropopause height (hPa) at 0300 UTC 1 January 1956. Tropopause breaks that correspond to the subtropical (STJ) and polar jet (POLJ) are labeled accordingly. The area identified with a circle is a region characterized by a vertical superposition of the polar and subtropical jets. Green shading corresponds to the tropical tropopause, white shading to the subtropical tropopause, and red shading to the polar tropopause (Modified from DT57; Fig. 2).

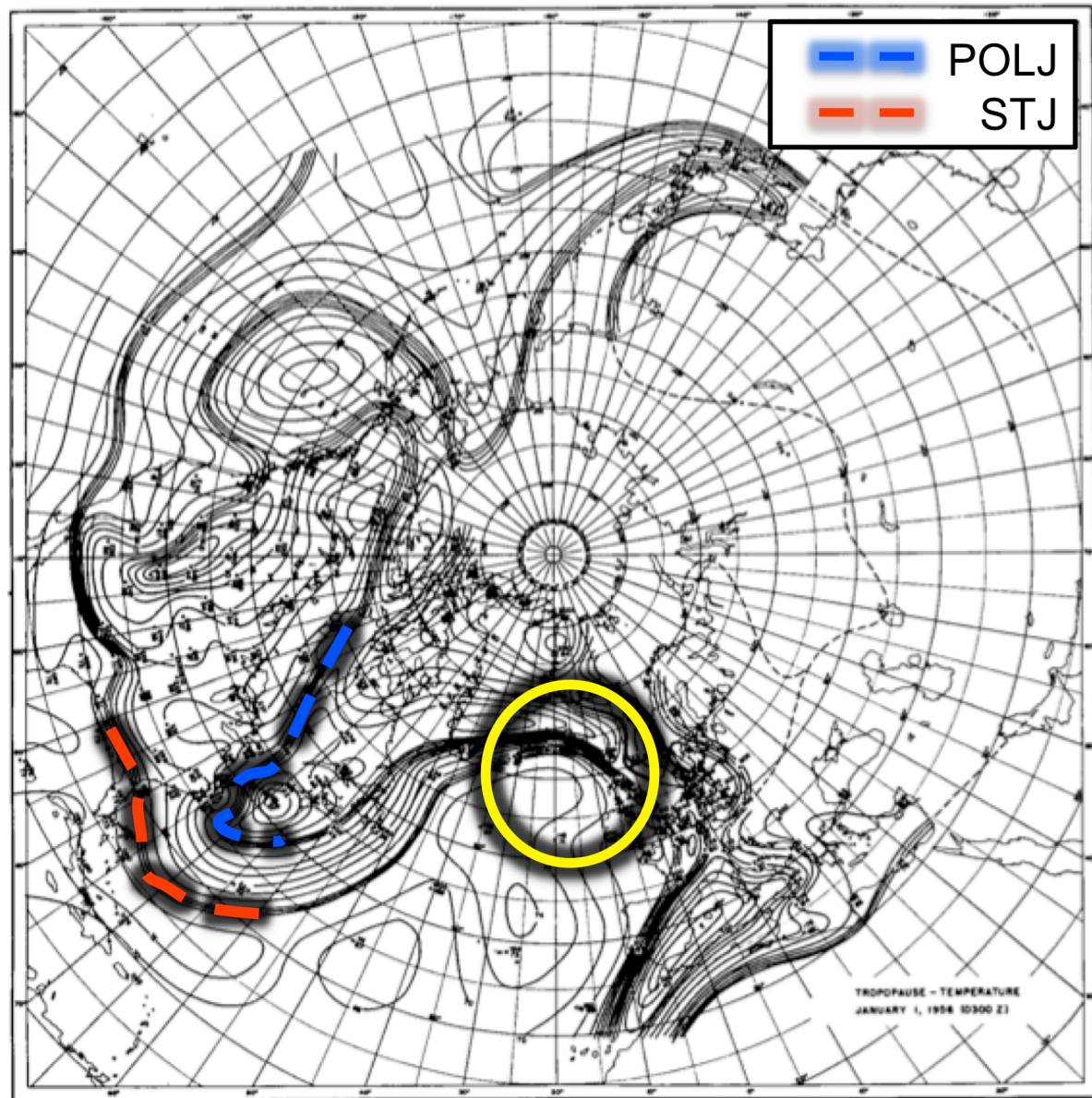


FIG. 1.13. Northern Hemispheric map of tropopause temperature (Celsius) at 0300 UTC 1 January 1956. The axes of the polar (POLJ) and subtropical (STJ) jets are identified by the blue and red dashed lines, respectively. The location of jet superposition is highlighted by the yellow circle (Modified from DT57; Fig. 3).

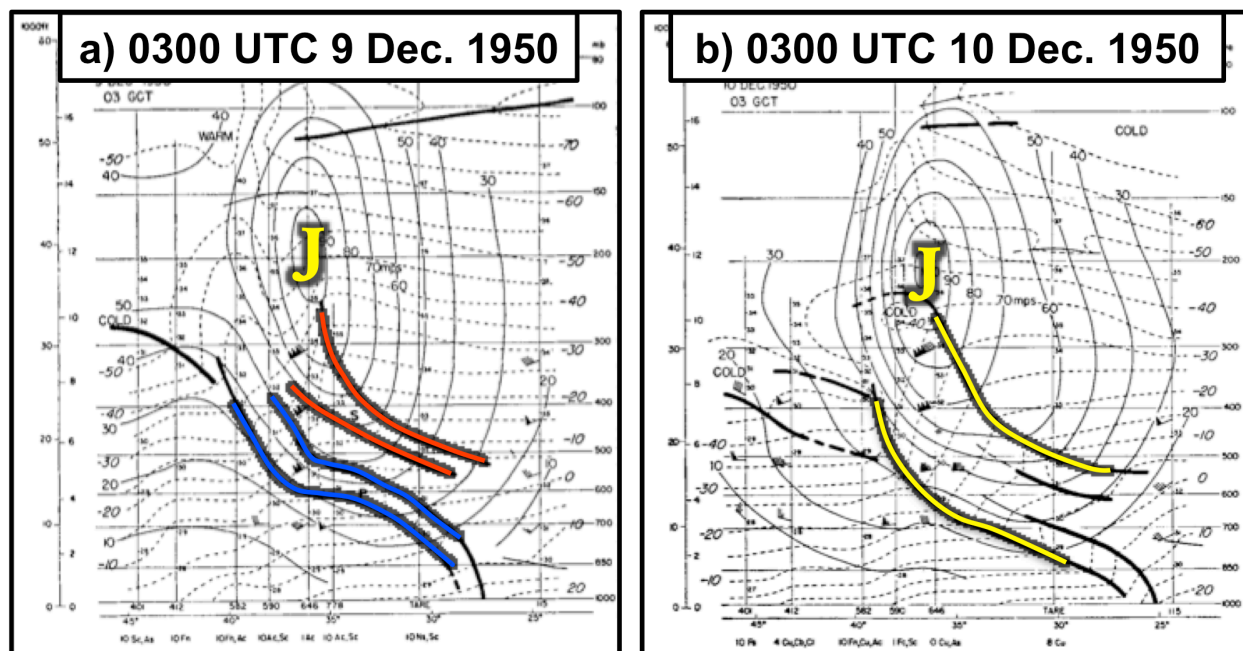


FIG. 1.14. (a) Cross section of a jet over Japan in the West Pacific at 0300 UTC 9 December 1950. The polar and subtropical frontal layers are bounded by the blue and red lines, respectively, and the location of the jet core is identified with the yellow “J”. Isotachs are drawn with the thin solid lines and isotherms are shown by the dashed lines. (b) Cross section of the same jet 24 h later at 0300 UTC 10 December 1950. The yellow lines denote the frontal layer, which is now a consolidation of the polar and subtropical frontal layers identified in (a). Both panels are modified from Mohri (1953).

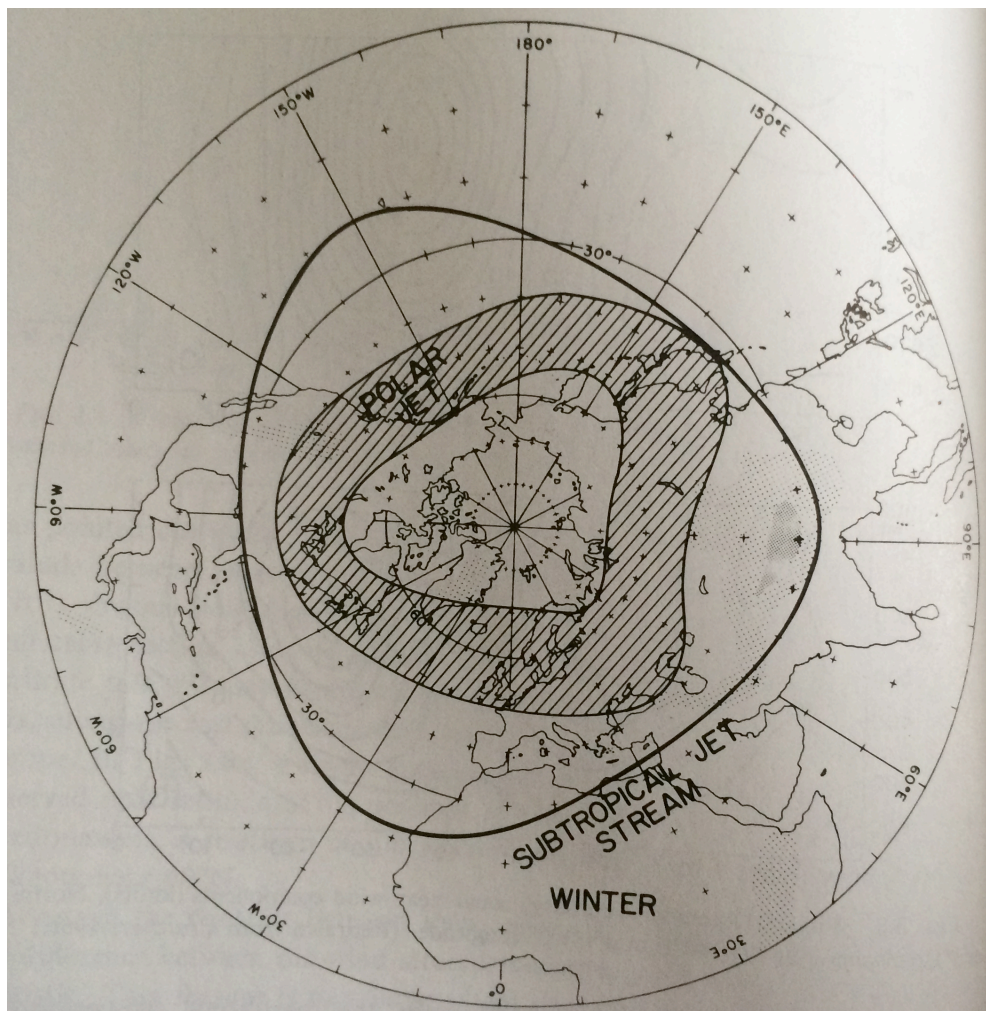


FIG. 1.15. Mean positions of the polar and subtropical jet streams during the winter (From Riehl 1962 with modifications by Palmén and Newton 1969).

Chapter 2

Jet Identification Criteria and Case Overviews

2.1 Jet Identification

The development of an identification scheme that accurately identifies the location of the polar and subtropical jets is an essential prerequisite for an objective analysis of a superposed jet's evolution¹. Recall from Chapter 1 that DT57 demonstrated that the atmosphere is typically characterized by a three-step pole-to-equator tropopause structure with each break in the tropopause associated with the presence of a westerly wind maximum (Fig. 1.11). This observation, in particular, forms the foundation for the jet identification scheme that follows.

The identification scheme for the polar, subtropical, and superposed jet streams matches that discussed in Winters and Martin (2014) and is described again here with reference to the features illustrated in Fig. 2.1. Figure 2.1a depicts an example of clearly separate polar and subtropical jet streaks in the eastern North Pacific. A vertical cross section through these distinct features unambiguously identifies the separate jet cores (Fig. 2.1b). From this cross section, it is clear that the core of the polar jet, located at approximately 300 hPa, is largely contained within the 315-330-K isentropic layer, while the subtropical jet core, located at approximately 200 hPa, occupies the 340-355-K layer. Additionally, both the polar and the subtropical jets lie at the low PV edge of the strong horizontal PV gradient that separates the upper troposphere from the lower stratosphere in their respective isentropic layers. With these specific attributes in mind, the identification scheme evaluates the characteristics of the PV and wind speed distributions within each grid column of analysis data. Within the 315-330-K (340-355-K) layer, whenever the magnitude of the PV gradient within the 1-3-PVU ($1\text{-PVU} = 1 \times 10^{-6} \text{ K m}^2 \text{ kg}^{-1} \text{ s}^{-1}$) channel

¹ For clarification, the terms “polar”, “subtropical”, and “superposed jets” will refer to the identification of individual jet *streaks*.

exceeds an empirically determined threshold value² and the integrated wind speed in the 400-100 hPa layer exceeds 30 m s^{-1} , a polar (subtropical) jet is identified in that grid column. The occurrence of both polar and subtropical jet characteristics in a single grid column, or in immediately neighboring grid columns, identifies a jet superposition event at that time in that grid column. An example of a jet superposition event is shown in a plan view in Fig. 2.1c. Not until a vertical slice through the jet core is examined can the superposition be identified, however (Fig. 2.1d). Notice that, rather than the three-step tropopause structure identified by DT57 and shown in Fig. 2.1b, a superposed jet is characterized by a two-step tropopause structure with a steep tropopause wall connecting the polar and tropical tropopause. This nearly vertical PV wall (from roughly 550 hPa to 150 hPa in this case) is the leading structural characteristic of a superposed jet.

2.2 Synoptic Overviews of Selected Jet Superposition Cases

To gain insight into the role that a superposed jet can play in the evolution of a high-impact weather event and the processes that can be conducive for the development of jet superpositions, the 18–20 December 2009 Mid-Atlantic Blizzard and the 1–3 May 2010 Nashville Flood were selected for study. These two events were chosen because they were jet superposition events that occurred at different times of the year and were associated with different types of high-impact weather (i.e., rapid cyclogenesis and an extreme precipitation event). For each case, model analyses were acquired from the National Centers for

² The threshold values are $1.4 \times 10^{-5} \text{ PVU m}^{-1}$ ($1.4 \times 10^{-11} \text{ K m kg}^{-1} \text{ s}^{-1}$) for the 315-330-K layer and $0.9 \times 10^{-5} \text{ PVU m}^{-1}$ for the 340-355-K layer.

Environmental Prediction (NCEP) Global Forecast System³ (GFS) at 6 h intervals with a horizontal grid spacing of $1.0^\circ \times 1.0^\circ$ and a vertical grid spacing of 50 hPa (25 hPa between 1000 and 900 hPa). In order to accommodate the aforementioned identification scheme, these data were then bilinearly interpolated onto isentropic surfaces at 5-K intervals from 300 to 370 K using programs within the General Meteorological Package (GEMPAK; desJardins et al. 1991).

2.2.1 18–20 December 2009 Mid-Atlantic Blizzard

Throughout the 72 h period of 18–20 December 2009, 30–60 cm (1–2 ft) of snow accumulated over large portions of the Mid-Atlantic and New England in conjunction with a rapidly deepening mid-latitude cyclone that formed over the northern Gulf of Mexico and tracked northeastward along the East Coast (Fig. 2.2; National Weather Service 2014). Specifically, locations in and around Washington, DC were the among the hardest hit, with Washington, DC measuring 45.7 cm (18 in.) of snow and Baltimore, MD tallying close to 51 cm (20 in.). Coincident with the cyclone’s most rapid period of intensification in this case was the development of a jet superposition over the southeastern United States. For brevity, the following overview will focus primarily on the jet evolution in the upper troposphere in the hours preceding superposition.

At 0000 UTC 19 December, 36 h prior to jet superposition, a subtropical jet with wind speeds in excess of 60 m s^{-1} extended from central Mexico northeastward across the Florida peninsula, while a weaker polar jet was identified upstream of a polar trough in northwesterly flow over the Central Plains (Fig. 2.3a). A cross section through the two separate jet structures at this time (Fig. 2.3b) indicates the presence of a three-step tropopause structure and demonstrates

³ There is strong confidence that other model analyses, such as the ECMWF, do not differ substantially when it comes to resolving the synoptic-scale features that are the focus of this study. Consequently, it is believed that employing those model analyses, as an alternative to the GFS, would not significantly change the results.

further that the jets were clearly distinct from one another. The developing mid-latitude cyclone responsible for producing blizzard conditions across much of the eastern United States was also firmly located in a favorable position for further deepening in the left exit region of the subtropical jet.

By 1800 UTC 19 December, the subtropical jet was displaced slightly poleward of its previous location and was noticeably stronger, with winds now in excess of 80 ms^{-1} (Fig. 2.3c). The surface cyclone, which had deepened by roughly 8 hPa, remained favorably located within the subtropical jet's left exit region off of the Mid-Atlantic coast, as well. Meanwhile, the polar jet, which was also characterized by increased wind speeds, had propagated around the base of the deepening polar trough and had assumed an orientation parallel to the subtropical jet over the southeastern United States. A cross section through the entrance regions of both of these jet structures (Fig. 2.3d) indicates the persistence of a three-step tropopause structure and that the two jets, while in closer proximity to one another by this time, were still not vertically superposed.

During the subsequent 18 h, the cyclone underwent its most rapid period of intensification, reaching a minimum central pressure below 980 hPa southeast of Cape Cod at 1200 UTC 20 December (Fig. 2.3e). Coincident with this period of most rapid intensification was a superposition of the polar and subtropical jets from central Georgia northeastward to off the North Carolina coast. This superposed jet was characterized by increased wind speeds, now well in excess of 90 ms^{-1} , and was positioned such that the cyclone was still firmly located in the jet's left exit region. An investigation of the movement of each individual jet from the previous time indicates that the subtropical jet was, once again, displaced only slightly poleward of its

prior location, while the polar jet was located farther southeast of its previous position, consistent with the continued propagation and deepening of the polar trough.

A cross section drawn through the superposed portion of this jet illustrates the two-step tropopause structure and vertical PV wall (extending from roughly 500 hPa to 150 hPa) characteristic of a superposed jet (Fig. 2.3f). Consistent with this structure, the cross section no longer depicts two separate wind speed maxima, but rather a single jet core with wind speeds in excess of 90 m s^{-1} . Particular attention is drawn to the 320-K and 325-K isentropes, highlighted in red, which are located at a significantly lower altitude beneath the jet core than at the prior times (Figs. 2.3b,d). This suggests that subsidence may have been responsible for the downward depression of these isentropes during the intervening 18 h and, therefore, potentially played a role in restructuring the tropopause into the characteristic superposed jet structure. The veracity of this inference is considered in greater detail as part of Chapters 4 and 5.

2.2.2 1–3 May 2010 Nashville Flood

During the first two days of May 2010, two consecutive mesoscale convective systems (MCSs) were responsible for historic rainfall accumulations in excess of 180 mm (7 in.) over a large portion of Tennessee, southern Kentucky, and northern Mississippi (Fig. 2.4). A few locations saw significantly higher rainfall totals, according to the National Weather Service office in Nashville, with Camden, Tennessee totaling 493 mm (19.41 in.) and Nashville recording 344 mm (13.54 in.) during that 2-day period. In addition to the heavy rainfall, both days were characterized by tornado outbreaks, as the environment was weakly stratified and favorable for severe convective development. The combination of sensible weather had enormous and wide-ranging impacts across the entire region, closing numerous roads, resulting

in 26 flood-related fatalities, causing around \$2 billion in property damage in the greater Nashville area, and swelling area rivers to record crests. Specifically, the Cumberland River at Nashville recorded a crest of 15.8 m (51.9 ft), which was 1.3 m (4.3 ft) higher than the previous record at the station in the post-flood control era (National Weather Service 2011).

Moore et al. (2012) and Durkee et al. (2012) provide excellent overviews of both the meso- and synoptic-scale processes responsible for the production of precipitation in this case and the reader is referred to those works for any additional information. As with the December 2009 case, here we present an abbreviated synoptic overview that focuses solely on the jet evolution in the upper troposphere during the 24 h period of 0000 UTC 1 May 2010 – 0000 UTC 2 May 2010 across the contiguous United States.

Figure 2.5a depicts a high amplitude flow pattern in place over a large portion of North America at 0000 UTC 1 May, with a deep, positively tilted trough over the western United States and a strong ridge over the east. A polar jet was identified downstream of the trough axis and extended from Baja California northeastward into the Central Plains, while a subtropical jet, which was of comparable strength to the polar jet, stretched from northern Mexico eastward along the Gulf coast. Note that at this time, even though the two jets are in close proximity to one another, they are not superposed. A cross section through the two separate jet cores (Fig. 2.5b) confirms this diagnosis and depicts a clear, three-step tropopause structure with each tropopause break associated with a distinct wind speed maximum.

At 1200 UTC 1 May, a broad area of precipitation situated over much of the Ohio River valley helped to further build the extensive ridge that was in place over a large portion of the eastern United States. Consequently, in response to the strengthened ridge, the axis of the subtropical jet shifted noticeably poleward and westward from its position at the prior time,

bringing it closer to the polar jet (Fig. 2.5c). A cross section through the two jet structures at this time illustrates that a three-step tropopause structure remained intact, while clearly showing the movement of the subtropical tropopause break towards the northwest as well as an accompanying wind speed increase in both jets (Fig. 2.5d).

At 0000 UTC 2 May, the polar and subtropical jets became superposed over portions of west Texas and southwestern Oklahoma, as the axis of the subtropical jet continued to migrate towards the northwest and the western trough shifted slowly eastward (Fig. 2.5e). A cross section through the superposed portion of the jet (Fig. 2.5f) shows both the appearance of a slight equatorward shift in the location of the polar tropopause break and the continued northwestward migration of the subtropical tropopause break within the plane of the cross section. The combination of these observations accounted for the production of the two-step tropopause structure and vertical PV wall characteristic of a superposition. Further note that the two wind speed maxima are now consolidated into a single jet core that featured wind speeds greater than 70 m s^{-1} , in response to the increased horizontal baroclinicity in the upper troposphere and lower stratosphere that accompanied the superposition. The processes that supported the development of a two-step tropopause structure and a superposed jet in this case are considered alongside an analysis of the 2009 Mid-Atlantic Blizzard in Chapters 4 and 5. An examination of the superposed jet in the 2010 Nashville Flood also demonstrated that it played an important role in the evolution of that particular heavy precipitation event. The details of this analysis immediately follow in Chapter 3.

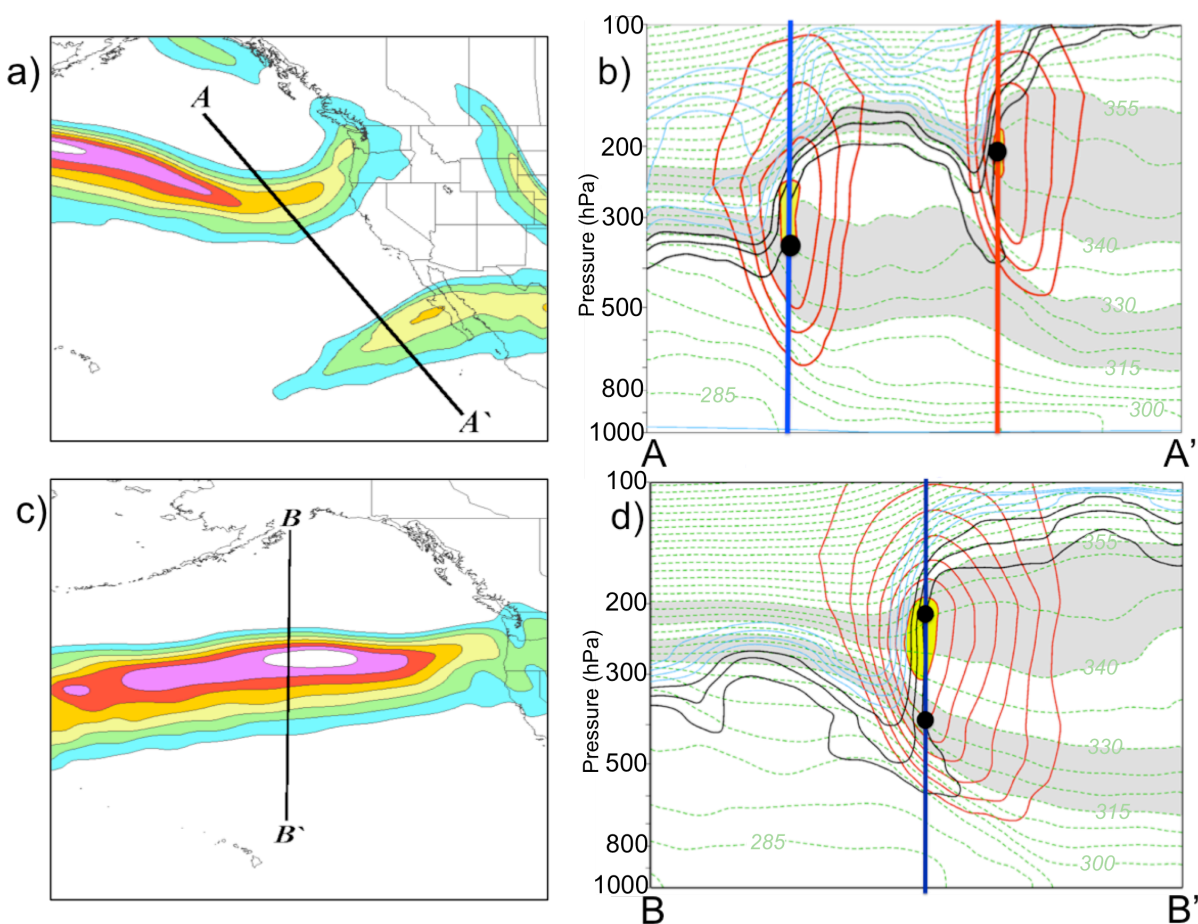


FIG. 2.1. (a) 300 hPa wind speeds (shaded every 10 m s^{-1} starting at 30 m s^{-1}) at 0000 UTC 27 April 2010 depicting separate polar and subtropical jets. (b) Cross section, A-A' in Fig. 2.1a, through separate polar and subtropical jet cores with the 1-, 2-, and 3-PVU contours (black); 4-, 5-, 6-, 7-, 8-, and 9-PVU contours (light blue); potential temperature every 5 K (dashed green); and wind speed every 10 m s^{-1} beginning at 30 m s^{-1} (red). The jet cores are shaded yellow and the 315-330- and 340-355-K isentropic layers, used to identify the locations of the jets, are shaded gray. The blue (red) column corresponds to a grid column with the black dot confirming a positive identification of a polar (subtropical) jet. (c) As in (a), but for a superposed jet at 0000 UTC 24 October 2010. (d) As in (b), but for the cross section B-B' shown in Fig. 2.1c, with two positive identifications (black dots) within a single grid column indicating a jet superposition (From Winters and Martin 2014).

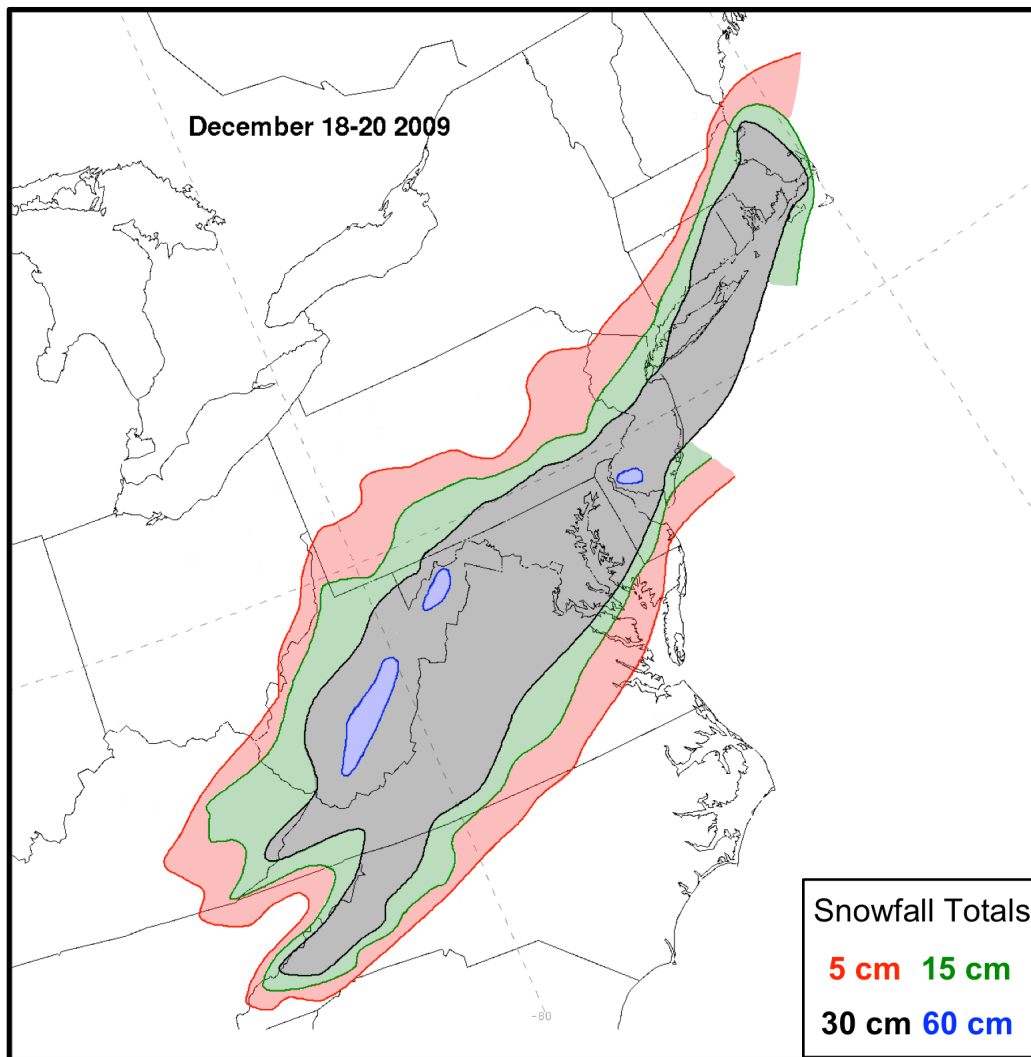
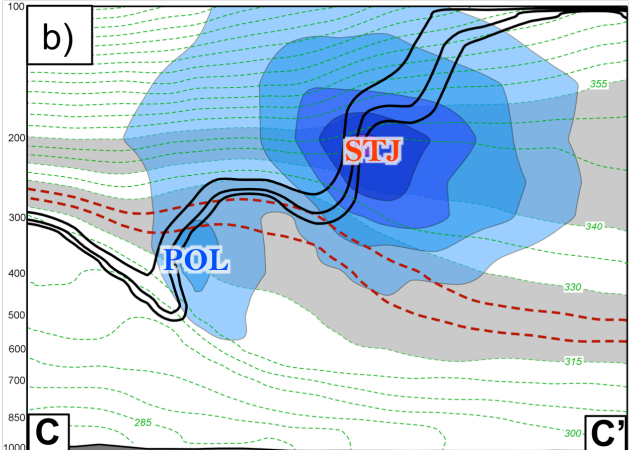
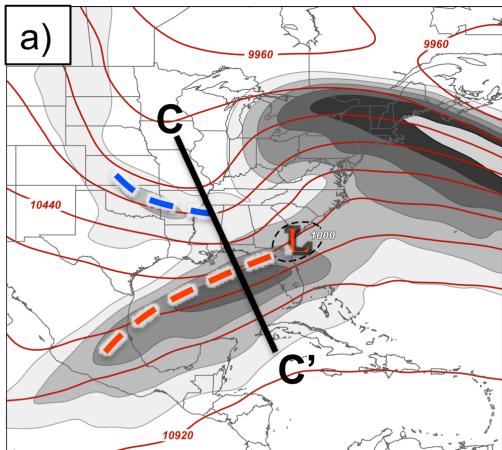
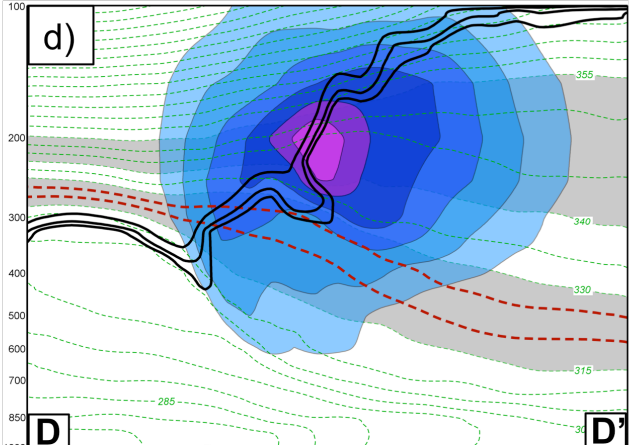
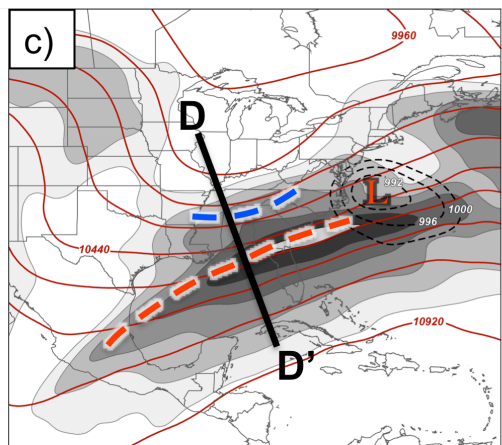


FIG. 2.2. Accumulated snowfall during the period 18–20 December 2009 over the Mid-Atlantic and northeastern United States (Modified from NOAA HPC; National Weather Service 2014).

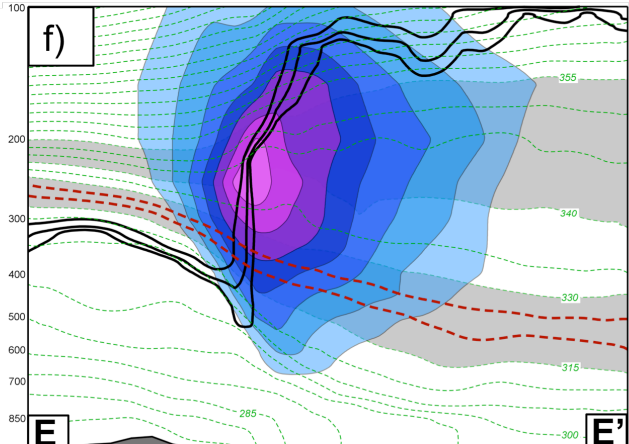
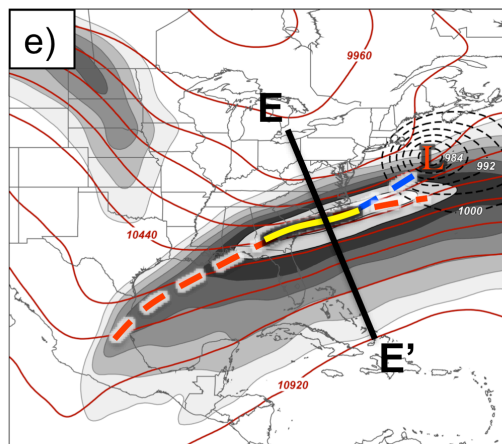
0000 UTC 19 Dec.



1800 UTC 19 Dec.



1200 UTC 20 Dec.



— — — POLJ
 — — — STJ
 — — — Superposed

FIG. 2.3. [left column] 250 hPa wind speed is shaded with the gray fill pattern every 10 m s^{-1} beginning at 30 m s^{-1} , 250 hPa geopotential heights are contoured in red every 120 m, sea level pressure is contoured with the dashed black lines every 4 hPa below 1000 hPa, the location of the sea level pressure minimum is identified with the red “L”, and jet axes are identified as specified in the legend for (a) 0000 UTC 19 December 2009, (c) 1800 UTC 19 December 2009, and (e) 1200 UTC 20 December 2009. [right column] Cross sections, as identified in the plot immediately to its left, of wind speed shaded every 10 m s^{-1} beginning at 30 m s^{-1} (blue fill pattern), potential temperature contoured every 5 K (dashed green lines), and contours of 1-, 2-, 3-PVU (black) at (b) 0000 UTC 19 December 2009, (d) 1800 UTC 19 December 2009, (f) 1200 UTC 20 December 2009. The gray shaded isentropic layers are those used to identify the jet axes using the scheme outlined in the text and the 320-K and 325-K isentropes are highlighted with the dashed red lines in the cross sections for reasons discussed in the text.

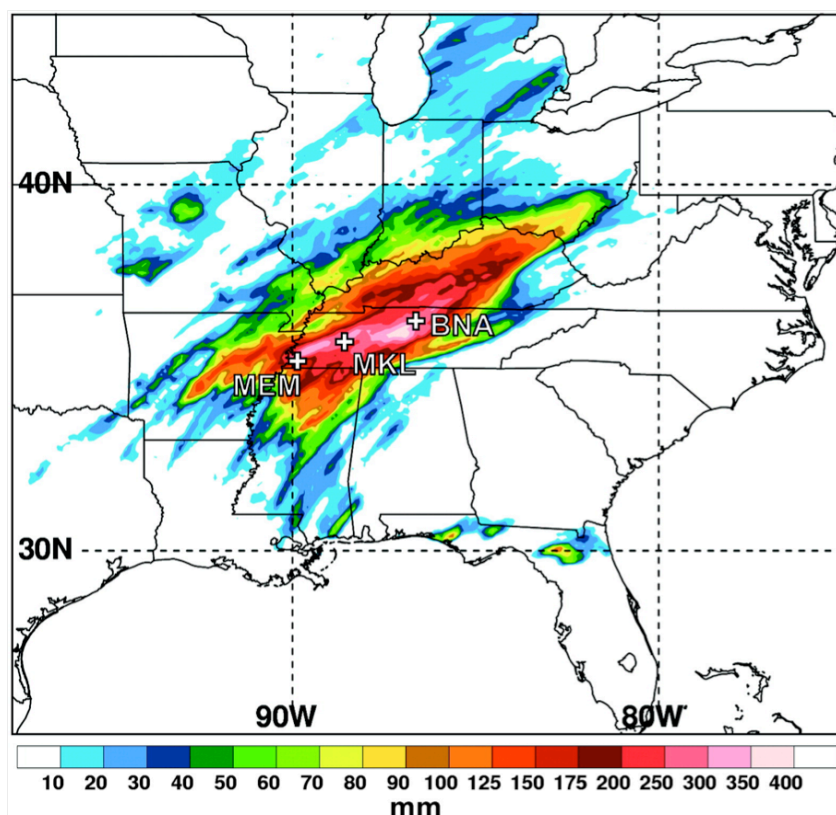


FIG. 2.4. The 48 h precipitation estimates (shaded; mm; following the color bar) for 0000 UTC 1 May – 0000 UTC 3 May 2010 from the National Precipitation Verification Unit quantitative precipitation estimates product. The locations of Nashville (BNA), Memphis (MEM), and Jackson (MKL) are also identified (From Moore et al. 2012; their Fig. 2).

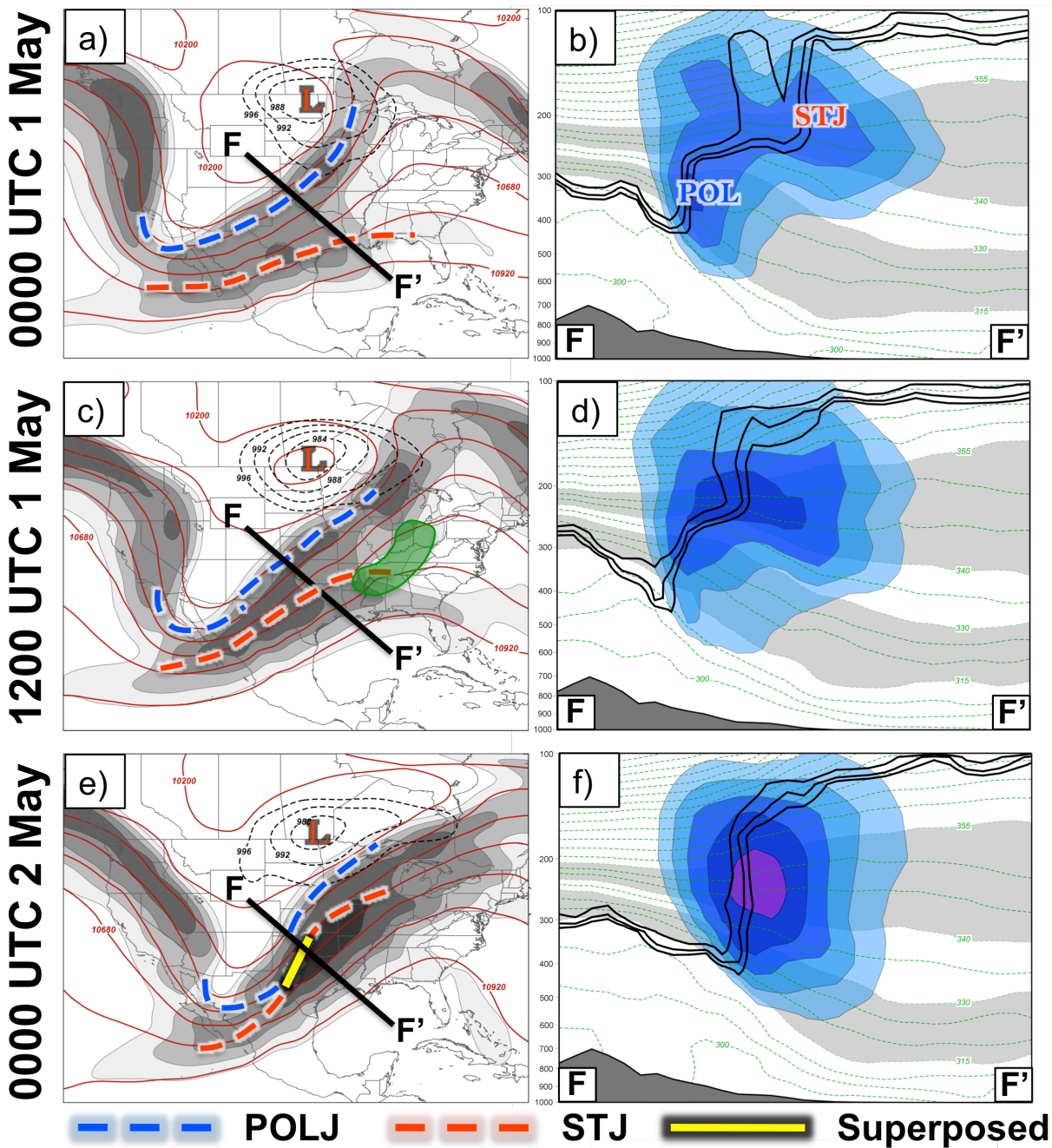


FIG. 2.5. Conventions are identical to Fig. 2.3 but for (a,b) 0000 UTC 1 May 2010, (c,d) 1200 UTC 1 May 2010, and (e,f) 0000 UTC 2 May 2010. The location of the precipitation shield at 1200 UTC 1 May 2010 in (c) is denoted by the green fill pattern and sea level pressure is now contoured every 4 hPa below 996 hPa within the panels shown in the left column.

Chapter 3

The Role of a Polar/Subtropical Jet Superposition in the May 2010 Nashville Flood*

3.1 Motivation

In addition to historic rainfall totals, one of the most notable aspects of the 1–3 May 2010 Nashville Flood was the presence of an anomalous and narrow plume of enhanced water vapor transport, or an atmospheric river (Newell et al. 1992; Zhu and Newell 1998), that extended from the Gulf of Mexico northward into the eastern United States. Figure 3.1 illustrates the anomalous nature of the moisture that was in place during the week of the event and shows that most areas east of the Mississippi River were characterized by precipitable water values that were at least 5 mm greater than normal for late April/early May. In association with the atmospheric river, Nashville, in particular, observed a precipitable water value of 51.3 mm (2.02 in.) at 0000 UTC 2 May, registering well above the 99th percentile for that time of year (45.7 mm) and indicating an almost unprecedented availability of moisture in the troposphere throughout the duration of the event (National Weather Service 2011). While several studies have investigated the impacts of atmospheric rivers on orographically forced precipitation events (e.g., Ralph et al. 2006; Stohl et al. 2008; Guan et al. 2010), the study by Moore et al. (2012) on the 2010 Nashville Flood demonstrated that atmospheric rivers can also play a considerable role in heavy rainfall events that are synoptically forced, such as those that occur over the central and eastern United States.

Specifically, Moore et al. (2012) found that a southerly low-level jet, driven by a strong geopotential height gradient between a lee trough along the east coast of Mexico and a strong subtropical ridge north of the Caribbean Sea, facilitated much of the anomalous moisture

* The analysis and discussion in this chapter are identical to that of Winters and Martin (2014) with only minor modifications. © American Meteorological Society. Used with permission.

transport out of Central America and into the southern Mississippi River valley. Furthermore, they noted that this moisture transport strengthened over the northern Gulf of Mexico and southern Mississippi River valley in the hours preceding the second day of the event (their Fig. 6). This finding was also noted in subsequent studies of the Nashville Flood (Durkee et al. 2012; Lackmann 2013; Lynch and Schumacher 2013). Together, these studies have demonstrated that this persistent and increased moisture transport into the region over the 2-day period, in conjunction with ascent along stationary, convectively generated outflow boundaries, aided in the production of heavy rainfall across portions of Tennessee, Kentucky, and northern Mississippi.

Coincident with the increase in moisture transport prior to the second day of heavy rainfall was a relatively rare vertical superposition of the normally distinct polar and subtropical jet streams and an attendant acceleration of jet wind speeds (Fig. 2.5). As noted in Chapter 1, a jet superposition is associated with an intensification of the upper-tropospheric and lower-stratospheric baroclinicity in the vicinity of the jet. Consequently, the superposed jet structure possesses an anomalous fraction of the pole-to-equator temperature gradient and is characterized by an anomalously deep layer of vertical shear, as required by the increased horizontal baroclinicity.

The development of intensified frontal structure associated with a superposed jet is often attended by a strengthening of its transverse, ageostrophic secondary circulation, as well, which is diagnosable using the Sawyer-Eliassen circulation equation (Sawyer 1956; Eliassen 1962). In addition to providing a dynamical link between the jet stream and its associated baroclinicity, as discussed in Chapter 1, such transverse circulations have been shown in numerous studies to play an important role in the production of sensible weather. For example, much attention has been

focused on upper-tropospheric fronts, which can form as a result of the differential vertical motions associated with Sawyer-Eliassen circulations and are important part of the extratropical cyclone life cycle (e.g., Uccellini et al. 1985; Whitaker et al. 1988; Barnes and Colman 1993; Lackmann et al. 1997). Additionally, the circulations associated with upper-tropospheric fronts have been shown to play an important role in the development of convective precipitation events, as first suggested by Omoto (1965) and further demonstrated by Hobbs et al. (1990) and Martin et al. (1993). While a number of studies have qualitatively considered the moisture flux accomplished by the lower-tropospheric horizontal branches of ageostrophic jet circulations (e.g., Uccellini and Johnson 1979; Uccellini et al. 1984; Uccellini and Kocin 1987), direct quantification of these effects has not received as much attention in the literature. Furthermore, if the static stability is low in a given region, as it was over the southern Mississippi River valley on 1–2 May 2010, a Sawyer-Eliassen circulation can occupy a considerable depth of the troposphere. In such a situation, the horizontal winds associated with the secondary circulation near the surface are capable of significant contributions to the moisture transport into the region.

While Moore et al. (2012) and Durkee et al. (2012) acknowledge a strengthening of both the jet and poleward moisture flux prior to the second day of heavy rainfall, they do not investigate the link between these processes. Consequently, the modulation of the structure and intensity of the Sawyer-Eliassen circulation by the diabatic residue of the heavy rainfall that characterized this event remains to be considered. To address these issues, this chapter aims to (1) quantify the contribution to the poleward moisture flux made by the superposed jet's ageostrophic circulation and (2) examine the impact that both geostrophic and diabatic forcing may have had in determining the strength and sense of the overall circulation.

The remainder of this chapter is organized as follows. Section 2 provides some background on the Sawyer-Eliassen circulation equation and the methodology used to solve for the transverse circulations. Section 3 dissects the evolution of the low-level poleward moisture flux across the southern Mississippi River valley. Section 4 discusses the impacts of the Sawyer-Eliassen circulations during each day of the event and further dissects the forcing responsible for the superposed jet's ageostrophic circulation. Section 5 presents a discussion and some brief conclusions.

3.2 The Sawyer-Eliassen Circulation Equation

A particularly useful way to interrogate the vertical circulations associated with jet-front structures, in nearly straight flow, is afforded by the Sawyer-Eliassen circulation equation (Sawyer 1956; Eliassen 1962):

$$\left(-\gamma \frac{\partial \theta}{\partial p}\right) \frac{\partial^2 \psi}{\partial y^2} + \left(2 \frac{\partial M}{\partial p}\right) \frac{\partial^2 \psi}{\partial p \partial y} + \left(-\frac{\partial M}{\partial y}\right) \frac{\partial^2 \psi}{\partial p^2} = Q_g - \gamma \frac{\partial}{\partial y} \left(\frac{d\theta}{dt}\right) \quad (3.1)$$

where γ is a constant on isobaric surfaces [$\gamma = (R/fp_0)(p_0/p)^{c_v/c_p}$], $p_0=1000$ hPa, $c_v=718$ Jkg⁻¹ K⁻¹, $c_p=1004$ Jkg⁻¹ K⁻¹, R is the gas constant for dry air, θ is the potential temperature, and f is the Coriolis parameter. In addition, M is the absolute geostrophic momentum ($M = U_g - fy$), where U_g and V_g are the along- and across-front geostrophic winds, respectively, and Q_g is the geostrophic forcing term, which is the sum of the shearing $\{Q_{SH} = 2\gamma[(\partial U_g / \partial y)(\partial \theta / \partial x)]\}$ and stretching deformation terms $\{Q_{ST} = 2\gamma[(\partial V_g / \partial y)(\partial \theta / \partial y)]\}$. The coefficients of the second-order terms on the left-hand side of (3.1) represent the static stability, baroclinicity, and inertial stability, respectively, and act to modulate the structure of the ageostrophic circulation. The ageostrophic circulation lies in a plane transverse to the frontal boundary (jet axis) and is

described by the distribution of the Sawyer-Eliassen streamfunction, ψ , such that $v_{ag} = -\partial\psi/\partial p$ and $\omega = dp/dt = \partial\psi/\partial y$. Given the second-order nature of this partial differential equation, positive (negative) values for the forcing function correspond to negative (positive) values for the streamfunction and thermally direct (indirect) circulations. For the full derivation and discussion of (3.1), the reader is referred to Eliassen (1962) or Keyser and Shapiro (1986).

From (3.1), it becomes evident that knowledge of the distribution of U_g, V_g, M, θ , and $d\theta/dt$, in a particular case, allows for the calculation of the coefficients on the left-hand side of (3.1) as well as the forcing function. Consequently, the absolute temperature and geostrophic wind are extracted from each grid point in the GFS analysis at 50-hPa vertical intervals from 1000 to 50 hPa. These variables are then interpolated onto the selected vertical cross section perpendicular to the jet axis. Subsequently, all of the coefficients and geostrophic forcing terms in (3.1) are calculated from these interpolated variables at each grid point within the interior of the cross section. Model vertical motion and relative humidity data are also extracted from the GFS analysis and interpolated onto the cross-sectional grid in order to determine $d\theta/dt$, or the rate of latent heating. Following the method of Emanuel et al. (1987), this term is calculated as:

$$\frac{d\theta}{dt} = \omega \left(\frac{\partial\theta}{\partial p} - \frac{\Gamma_m}{\Gamma_d} \frac{\theta}{\theta_e} \frac{\partial\theta_e}{\partial p} \right) \quad (3.2)$$

where ω is the model vertical motion, θ_e is the equivalent potential temperature, and Γ_m and Γ_d are the moist- and dry-adiabatic lapse rates, respectively. Using the Bolton (1980) approximation to the Clausius-Clapeyron relationship and the method of Bryan (2008), which contains assumptions that are particularly accurate in heavily precipitating situations, we determine θ_e .

Once all coefficients and forcings have been determined, successive over-relaxation (SOR) is used to converge on a solution for the Sawyer-Eliassen streamfunction. Since (3.1) is a

second-order differential equation, a unique solution is guaranteed only when the geostrophic Ertel PV is greater than zero at each grid point¹. Therefore, in order to facilitate convergence, if any grid point has PV less than zero, the SOR algorithm calculates a four-point average of the Sawyer-Eliassen streamfunction at the neighboring grid points and assigns the averaged value to the grid point of interest during each iteration. For the solutions presented here, the Sawyer-Eliassen streamfunction is set to zero on the boundaries of the cross section, as in the solutions presented by Todsén (1964) and Shapiro (1981).

Employing (3.1), Shapiro (1982) described a series of conceptual models detailing the characteristic transverse circulations associated with idealized upper-level jet-front systems. Specifically, he demonstrated that, in the absence of any along-jet geostrophic temperature advection, solutions for the ageostrophic circulations are driven purely by the geostrophic stretching deformation and resembled the traditional four-quadrant model, with a thermally direct (indirect) circulation in the jet-entrance (-exit) region (Fig. 3.2a). The introduction of along-jet geostrophic temperature advection mobilizes the geostrophic shearing deformation term, which acts to “shift” the thermally direct (indirect) circulation to the anticyclonic (cyclonic) shear side of the jet in cases of geostrophic cold-air advection, such that subsidence is present through the jet core (Fig. 3.2b). Conversely, geostrophic warm-air advection along the jet axis shifts the thermally direct (indirect) circulation to the cyclonic (anticyclonic) shear side of the jet, positioning ascent through the jet core (Fig. 3.2c)².

¹ This condition specifies that the discriminant is less than zero so that (3.1) is an elliptic second-order partial differential equation.

² These circulations are fortified by ascent and descent associated with positive and negative vorticity advection by the thermal wind (i.e., Sutcliffe 1947) as described by Martin (2014).

3.3 Synoptic Evolution of the Poleward Moisture Flux

Complementing the earlier discussion on the development of a superposed jet in Section 2.2.2, this section details the evolution of the low-level moisture flux throughout the flooding event from 0000 UTC 1 May to 0000 UTC 2 May. The large-scale pattern at 0000 UTC 1 May (Fig. 3.3a) depicted an occluding mid-latitude cyclone, with a sea level pressure minimum below 988 hPa, located along the North Dakota-Manitoba border. A warm front at the surface extended across the northern Great Lakes eastward toward New York, while a cold front stretched from northeastern Minnesota southward into eastern Texas. Immediately to the east of the cold front was a tongue of poleward moisture flux at 925 hPa, which flowed from the Gulf of Mexico into the Great Lakes. Maximum poleward moisture flux values³ over the northern Gulf of Mexico were greater than 30 cm s^{-1} at this time along the axis of maximum moisture flux⁴.

By 0000 UTC 2 May (Fig. 3.3b), the mid-latitude cyclone had remained stationary along the U.S.-Canadian border and had begun to decay. The cold front, while making slight progress to the east over the Great Lakes, was stationary over portions of the southern Mississippi River valley, helping to focus precipitation over the same areas for a second consecutive day. Notably, the poleward moisture flux at 925 hPa was substantially larger than at the earlier time, with maximum values over the northern Gulf of Mexico now exceeding 40 cm s^{-1} along the axis of maximum moisture flux. Coincident with this increase in moisture flux was the first indication of a jet superposition over portions of southwestern Oklahoma and western Texas, denoted in Fig. 3.3b by the purple line. The coincidence of the observed increase in poleward moisture flux with

³ Poleward moisture flux is computed as the product of the meridional velocity component, v (m s^{-1}), and the water vapor mixing ratio (kg kg^{-1}). Given typical values for the mixing ratio (5 g kg^{-1}) and wind speed (10 m s^{-1}), this calculation would yield a moisture flux of 0.05 m s^{-1} or 5 cm s^{-1} .

⁴ Defined as the axis of maximum convergence of the moisture flux gradient vector, it is included as a common reference point for determining the impact of the forthcoming Sawyer-Eliassen circulations on the poleward moisture flux.

a proximate jet superposition event suggests that the ageostrophic circulation associated with the superposed jet may have played a role in the increased poleward moisture flux observed over the southern Mississippi River valley.

To investigate this possibility, Fig. 3.4a depicts the total change in the 925 hPa poleward moisture flux across the southern Mississippi River valley during the 24 h period from 0000 UTC 1 May to 0000 UTC 2 May. Results demonstrate that the poleward moisture flux increases by roughly 9 cm s^{-1} south of the Gulf coast in the vicinity of the axis of maximum moisture flux at both times. This is in general agreement with the qualitative assessment made from Fig. 3.3. However, an examination of the difference in the geostrophic poleward moisture flux over the same period (Fig. 3.4b) shows little to no change along the axes of maximum moisture flux. Instead, increased geostrophic moisture fluxes are displaced to the north and east, consistent with a shift of the strongest southerly geostrophic winds in that direction. So, while Moore et al. (2012) and Durkee et al. (2012) note that the largest fraction of the moisture flux was accomplished by geostrophic processes during this event, the majority of the observed increase in moisture flux south of New Orleans is accounted for by changes in the ageostrophic poleward moisture flux (which includes the effects of the jet circulation, as well as curvature and friction). Figure 3.4c confirms this notion, depicting an increase on the order of 9 cm s^{-1} along the Gulf coast and centered squarely on the axes of maximum moisture flux. Given this conclusion, the analysis that follows aims to determine the specific impact of the superposed jet's transverse circulation on the ageostrophic poleward moisture flux over the northern Gulf of Mexico.

3.4 Diagnosis of Sawyer-Eliassen Circulations

The analysis begins with an investigation of the role the ageostrophic circulation

associated with the superposed jet played in facilitating poleward moisture flux into the southern Mississippi River valley. The individual forcing terms for the superposed jet circulation are then examined to better understand their impacts on the resultant circulation.

3.4.1 Role of the Superposed Jet in Facilitating Poleward Moisture Flux

At 0000 UTC 1 May, an area of convection was beginning to form over portions of central Arkansas. These thunderstorms would later move off to the east and form the first MCS that dropped considerable rainfall across portions of the Tennessee River valley on the first day of the event. Additionally, the polar and subtropical jets split over northern Texas, with the polar jet extending to the northeast over the Central Plains and the subtropical jet stretching eastward along the Gulf coast (Fig. 3.3). As such, a diagnosis at this time must consider the separate ageostrophic circulations associated with each jet and its respective overall contribution to the poleward moisture flux across the southern Mississippi River valley.

Figure 3.5a shows the Sawyer-Eliassen circulation along the cross section from G-G' in Fig. 3.3a, which is cut through the subtropical jet's exit region and is nearly parallel to the axis of maximum moisture flux near the Gulf coast. The solution depicts a rather weak thermally indirect circulation with the strongest upward vertical motions and streamfunction maximum centered close to Little Rock, Arkansas (LZK), largely attributable to the diabatic effects of the ongoing convection (not shown). Over the northern Gulf of Mexico, where the poleward moisture flux was maximized at this time, the role of the Sawyer-Eliassen circulation is rather unimpressive, with a maximum contribution on the order of 5 cm s^{-1} around 925 hPa. A comparison with the total observed ageostrophic poleward moisture flux at this time (Fig. 3.5b) shows that the magnitude of the poleward moisture flux associated with the Sawyer-Eliassen

circulation is on par with observed ageostrophic flux values over the northern Gulf of Mexico. As a result, it is reasonable to conclude that this calculation accurately captures the maximum contribution to the overall moisture flux made by the subtropical jet's ageostrophic circulation in that region.

As previously indicated, the polar jet was located further to the north and west over the Central Plains. Figure 3.6 demonstrates that the Sawyer-Eliassen circulation associated with the polar jet, along the cross section H-H' in Fig. 3.3a, is a stronger, thermally direct circulation, such that the low-level, horizontal branch of this circulation actually opposes the poleward moisture flux promoted by the subtropical jet. However, the juxtaposition of these two circulations is favorable for promoting upward vertical motions directly over Little Rock, where the ascending branches of both circulations are collocated. Therefore, while the separate jet circulations likely played a symbiotic role in aiding the initial formation of convection that occurred over central Arkansas at 0000 UTC 1 May, the subtropical jet's circulation was the only one capable of facilitating a poleward moisture flux into the southern Mississippi River valley at that time.

At 0000 UTC 2 May, an area of convection was ongoing over portions of southern Arkansas and northern Louisiana. As mentioned previously (and illustrated in Fig. 3.3), the poleward moisture flux increased considerably over the intervening 24 h to a maximum value greater than 40 cm s^{-1} , coincident with the jet superposition event. It is important to note that mixing ratios across the southern Mississippi River valley and northern Gulf of Mexico were largely unchanged between the two days (not shown). As a result, the increase in poleward moisture flux was a direct consequence of an increase in wind speed. To investigate the impact of the superposed jet on the poleward moisture flux, we return to the cross section labeled F-F' in

Figs. 2.5 and 3.3b, drawn perpendicular to the superposed jet axis and through the axis of maximum poleward moisture flux at 0000 UTC 2 May. The solution for the circulation within this cross section, shown in Fig. 3.7a, depicts a robust thermally indirect circulation, much stronger than the circulation associated solely with the subtropical jet at the previous time (Fig. 3.5a), which is shifted toward the anticyclonic shear side of the jet. The superposed jet circulation is characterized by (1) a plume of ascent that extends from the surface through the jet core with local maxima found in both the middle and lower troposphere and (2) much stronger moisture fluxes over the northern Gulf of Mexico, maximized around 15 cm s^{-1} near 925 hPa.

The cross section F-F' is oriented at an angle to the axis of maximum moisture flux at this time. Consequently, in order to facilitate a direct comparison between the poleward moisture fluxes associated with both the subtropical jet on 1 May and the superposed jet on 2 May, the component of the moisture flux associated with the superposed jet in the direction of the axis of maximum moisture flux at 0000 UTC 2 May was calculated and determined to be 11 cm s^{-1} at 925 hPa. This is an increase of about 6 cm s^{-1} (a 120% increase) from that associated solely with the subtropical jet at the earlier time. Figure 3.7b shows that this value is on par with, but slightly larger than, observed ageostrophic poleward moisture fluxes just south of New Orleans. This overestimate is at least partially a result of the fact that this analysis neglects the effects of friction and flow curvature on the ageostrophic circulation when solving the Sawyer-Eliassen circulation equation. Recalling that total ageostrophic moisture flux values increased by as much as 9 cm s^{-1} over the 24 h period (Fig. 3.4c), it is concluded that the ageostrophic circulation associated with the superposed jet accounts for the vast majority of the increased poleward moisture flux. As demonstrated by Moore et al. (2012), this moisture flux was crucial in the production of precipitation farther to the north during the flooding event. Thus, the analysis

presented here illustrates the role the intensified Sawyer-Eliassen circulation associated with the superposed jet played in magnifying the severity of the event.

3.4.2 Partition of Sawyer-Eliassen Forcing Terms

The diagnostic power of the Sawyer-Eliassen circulation equation (3.1) lies in the fact that the forcing can be broken down into the separate geostrophic forcing terms (shearing and stretching deformation) and a diabatic term. Consequently, the circulation associated with the superposed jet can be further dissected in order to gauge the significance of the respective forcing terms in shaping its sense and strength. The portion of the Sawyer-Eliassen circulation associated with the total geostrophic forcing (Q_g) is shown in Fig. 3.8a and depicts a circulation that, similar to the full circulation (Fig. 3.7a), is thermally indirect and shifted toward the anticyclonic shear side of the jet, positioning ascent directly beneath the jet core.

Intriguing differences, however, are found when comparing the distribution of the vertical motion and moisture flux to that shown in Fig. 3.7a. In contrast to the full circulation (Fig. 3.7a), which has a plume of ascent from the surface through the jet core, the Q_g circulation (Fig. 3.8a) has its strongest vertical motions primarily confined to the middle and upper troposphere. In addition, the low-level, horizontal branch of the Q_g circulation near the surface at the Gulf coast is far weaker, with low-level moisture flux values only around 3 cm s^{-1} , much smaller than those forced by the full circulation.

The Q_g circulation, in Fig. 3.8a, can be partitioned into the individual circulations associated with the geostrophic shearing (Q_{SH}) and stretching (Q_{ST}) deformation terms, respectively. The Q_{SH} circulation is shown in Fig. 3.8b and depicts a thermally indirect circulation that is positioned primarily on the cyclonic shear side of the jet. This places the most

intense part of the descending branch of the circulation directly beneath the jet core, opposite to the ascent observed in that region in the Q_g circulation. Examination of both the temperature gradient and geostrophic wind normal to the cross section suggests that areas between roughly 400 and 800 hPa were characterized by geostrophic cold-air advection in cyclonic shear ($Q_{SH} < 0$), consistent with the thermally indirect characteristics of the circulation observed in Fig. 3.8b.

Figure 3.8c shows that Q_{ST} acts to drive a thermally direct circulation about the strong upper-tropospheric front centered on the cyclonic shear side of the jet, but offset slightly poleward of the center of the Q_{SH} circulation (Fig. 3.8b). Consequently, Q_{ST} promotes ascent directly beneath the jet core, slightly poleward of, and thus counteracting, the subsidence associated with Q_{SH} . Investigation of the along-cross-section geostrophic wind shows a region of geostrophic confluence centered squarely on the upper-tropospheric front ($Q_{ST} > 0$), which would act to enhance the horizontal temperature gradient around 500 hPa and drive a thermally direct circulation.

Interestingly, this cross section is drawn through a geostrophic jet-exit region at 500 hPa, as shown in Fig. 3.9. Typically, such regions are characterized by diffluent flow and associated horizontal frontolysis in the vicinity of any regions of baroclinicity, resulting in a thermally indirect circulation. Figure 3.9 shows that in this case, an embedded short-wave trough over the panhandles of Oklahoma and Texas actually produces a region of geostrophic confluence in the vicinity of the geostrophic jet-exit region. This confluence is responsible for an area of horizontal geostrophic frontogenesis precisely at the location where a thermally direct circulation is observed in Fig. 3.8c.

Comparison of the intensities and areal extents of the Q_{SH} and Q_{ST} circulations demonstrates that the Q_{SH} circulation is the dominant component. Consequently, the sum of the

two circulations indicates that the Q_{ST} circulation acts to erode the updraft associated with the Q_{SH} circulation on the cyclonic shear side of the jet, while preserving the downdraft on the anticyclonic shear side. The net result remains a thermally indirect circulation, but one that is shifted toward the anticyclonic shear side of the jet with ascent directly beneath the jet core. This total Q_g circulation is displaced farther equatorward than might be expected under a regime of geostrophic cold-air advection in cyclonic shear within a geostrophic jet-exit region (Fig. 3.2b) due to the effects of the geostrophic confluence associated with the short-wave trough.

The final contribution to the full Sawyer-Eliassen circulation comes from the diabatic forcing. Figure 3.10a shows that the circulation associated with the diabatic forcing is focused entirely below 400 hPa, where latent heating acts to produce a dipole centered slightly north of the Gulf coast, with a thermally direct circulation farther to the north and a stronger thermally indirect circulation to the south. Upward vertical motions associated with this diabatically induced circulation pattern are also focused in the lower troposphere and coincide well with the area of most intense latent heat release from the initial convective activity. Most notably, the poleward moisture flux associated with the thermally indirect diabatic circulation (Fig. 3.10a) is much stronger than that associated with the Q_g circulation (Fig. 3.8a), with values greater than 9 cm s^{-1} over the northern Gulf of Mexico. Consequently, the majority of the poleward moisture flux produced by the full ageostrophic circulation is driven by the diabatic component.

The preceding discussion indicates that the Q_g forcing largely determines the mid-tropospheric portion of the full Sawyer-Eliassen circulation (Fig. 3.7a). The diabatic portion, then, provides a means by which the full tropospheric-deep circulation communicates directly with the surface, as it was responsible for the majority of the increase in low-level poleward

moisture flux into the southeast United States and also coupled surface-based vertical motions to those in the middle troposphere.

The analysis also suggests a crucial positive feedback mechanism that, on its own, may act to further strengthen and promote the longevity of the entire Sawyer-Eliassen circulation. Strong moisture flux and the subsequent ascent promote latent heat release through condensation. The latent heat release is associated with a lower-tropospheric ageostrophic circulation pattern that can further strengthen the poleward moisture flux into a region and, subsequently, increase the potential for additional latent heat release. The addition of mid- and upper-tropospheric ascent provided by the Q_g circulation to that induced by the diabatically forced circulation promotes the vigorous and tropospheric-deep vertical motions necessary for the production of heavy precipitation and intense latent heat release. In addition, the strong latent heat release beneath the jet core can act to erode upper-level PV, helping to fortify the vertical PV wall associated with the superposed jet structure and thereby acting to maintain or even strengthen, the strong wind speeds that are associated with it.

Support for the veracity of the superposed jet's diagnostic Sawyer-Eliassen circulation is also evident in the cross section of vertical motion from the GFS analysis, shown in Fig. 3.10b. Similar to the tropospheric-deep plume of ascent observed with the full superposed jet circulation in Fig. 3.7a, the GFS shows a continuous plume of ascent that runs roughly parallel to the leading edge of the upper-tropospheric front and through the jet core. In addition, the distribution of the vertical motion depicts two local maxima: one near the Gulf coast in the vicinity of the maximum latent heat release (Fig. 3.10a) and another in the middle to upper troposphere that is nearly collocated with the maximum in ascent associated with the Q_g portion of the superposed jet circulation (Fig. 3.8a).

A similar positive feedback mechanism, envisioned from a PV perspective, was proposed by Lackmann (2002) in his study of a warm conveyor belt during a February 1997 cyclogenesis event and serves as an analog to the mechanism discussed above. In that case, it was found that the circulation associated with a linear, diabatically generated positive PV anomaly along a low-level frontal boundary made a non-negligible contribution to the strength of the southerly low-level jet. The strengthened low-level jet then accomplished additional poleward moisture transport into the region, further conditioning the atmosphere for additional latent heat release. Indeed, Lackmann (2013) found similar conditions at work during the Nashville Flood, where the low-level jet was characterized by a linear positive PV anomaly to its west, along the stationary cold frontal boundary. While the study indicated that topographic effects along the Mexican Plateau were the primary mechanism behind the initial generation of low-level cyclonic PV present along the frontal boundary during the flooding event, diabatic effects acted to enhance the magnitude of these anomalies as they drifted eastward into the southern United States.

3.5 Discussion

The analysis presented here demonstrates that the lower-tropospheric horizontal branch of the Sawyer-Eliassen circulation pattern associated with a superposed jet helped to enhance the poleward moisture flux prior to the second day of the 2010 Nashville Flood. This explanation accounts for the analyses by Moore et al. (2012) and Durkee et al. (2012) and their particular observations of increased poleward moisture transport during the second day of the event. Mixing ratios on these two days were largely unchanged across the southern Mississippi River valley. Given this fact, an increased wind speed underlies the increased poleward moisture flux

that was observed on the second day. The analysis presented here shows that this increased wind speed is primarily attributable to the ageostrophic circulation associated with the superposed jet and illuminates one mechanism by which superposed jet structures may have an influence on the evolution of a high-impact weather event. Such a dynamical influence is undoubtedly magnified by the fact that the superposed jet circulation, by virtue of its association with the subtropical jet, is able to draw upon the moist and weakly stratified air mass characteristic of the lower troposphere equatorward of the subtropical jet.

Additionally, a partition of the forcings driving the superposed jet circulation provides insights into its internal dynamics. In the case presented here, the Q_{SH} term was more dominant than the Q_{ST} term. As a result, the entire Q_g circulation took on the thermally indirect characteristics of the Q_{SH} circulation. The thermally direct circulation associated with the Q_{ST} forcing, however, acted to significantly counteract a portion of the Q_{SH} circulation on the cyclonic shear side of the jet, shifting the locus of the entire Q_g circulation toward the anticyclonic shear side of the jet. Such an orientation can dynamically assist convection, as upward vertical motions on the anticyclonic shear side of the jet are exhausted in an area with much lower inertial stability. In comparison to the cases examined by Shapiro (1981, 1982), this observed circulation is atypical for an environment of geostrophic cold-air advection in a geostrophic jet-exit region. It is important to note, however, that throughout much of the evolution of a superposed jet structure, the environment is characterized by more than one jet core. Therefore, idealized models of transverse circulation patterns in environments characterized by single jet cores may not be expected to represent the patterns characterizing the more complex superposed jet environment.

Given that superposed jets are often characterized by anomalously strong wind speeds in the jet core, it is likely that the horizontal shear is also anomalously large in the vicinity of these features. Consequently, it is conceivable that the Q_{SH} term may consistently dominate the Q_g forcing for ageostrophic circulations associated with superposed jets, particularly away from geostrophic jet-entrance and -exit regions. A more comprehensive examination of other superposed jet streaks may illuminate the nature of the interaction between the two geostrophic forcing terms in the vicinity of these structures and how their circulations compare with established conceptual models (Section 6.2.1).

Moreover, this case illustrates that latent heat release can have a considerable impact on shaping and enhancing the entire ageostrophic circulation. If they couple favorably, the Q_g and diabatic circulations can drive a notable positive feedback mechanism, similar to that proposed by Lackmann (2002), which can act to both strengthen upward vertical motions and intensify the ageostrophic winds in the low-level horizontal branch of the circulation. Studies of jet circulations in other heavy precipitation events may help to further characterize this feedback mechanism.

The results from this particular case study demonstrate that superposed jets can, indeed, play a central role in the evolution of a high-impact weather event. Consequently, a greater understanding of the processes that conspire to form superposed jet structures, via consideration of the synoptic-dynamic environment from a basic-state variable or a PV perspective, is necessary. This particular topic is addressed in the two chapters that follow. Together, it is believed that information surrounding the development and influence of superposed jets can ultimately better inform forecasters regarding both the operation of such features as well as anticipation of their impacts.

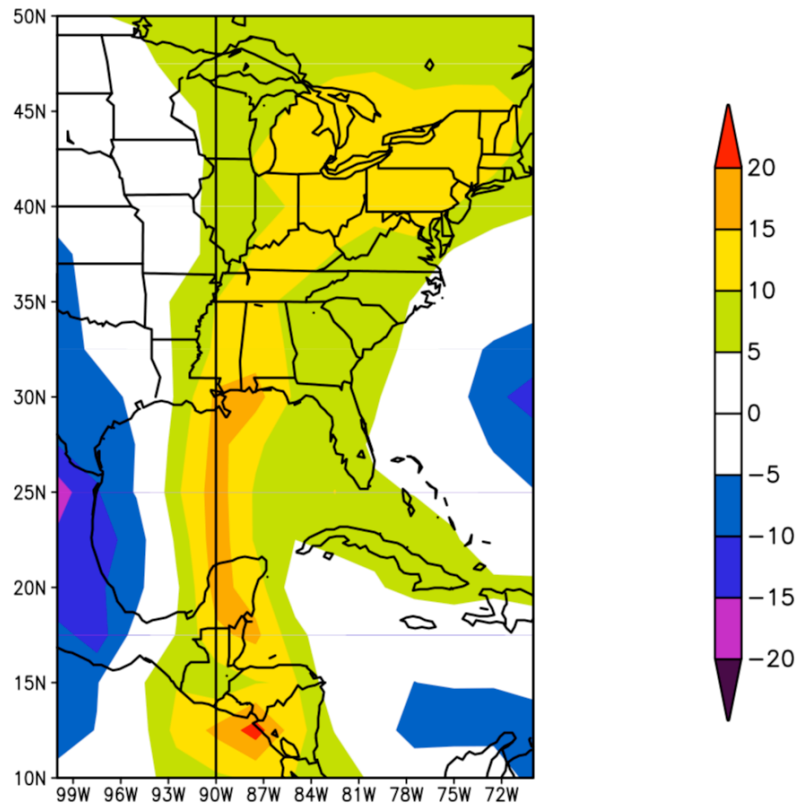


FIG. 3.1. The 4-day precipitable water anomalies (mm; fill pattern) during the period 30 April – 3 May 2010 across the eastern United States (Courtesy of Earth Systems Research Laboratory).

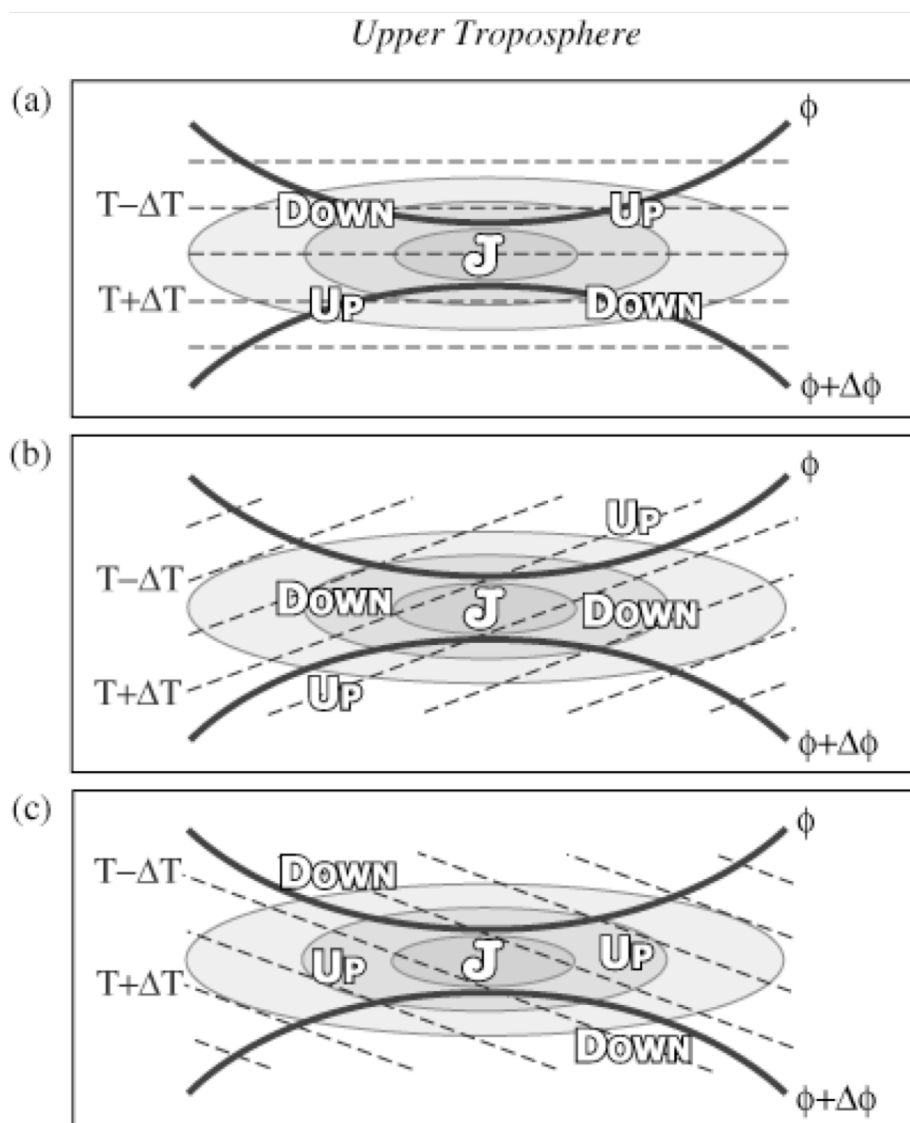


FIG. 3.2. Idealized configurations of jet circulations associated with a straight jet streak on an isobaric surface in the upper troposphere. Geopotential height (thick solid lines), potential temperature (dashed lines), geostrophic isotachs (fill pattern; with the jet speed maximum represented by the *J*), and Sawyer-Eliassen vertical motions indicated by “up” and “down” for a regime of (a) no geostrophic temperature advection, (b) upper-tropospheric geostrophic cold-air advection, and (c) upper-tropospheric geostrophic warm-air advection along the jet axis (From Fig. 3 in Lang and Martin 2012).

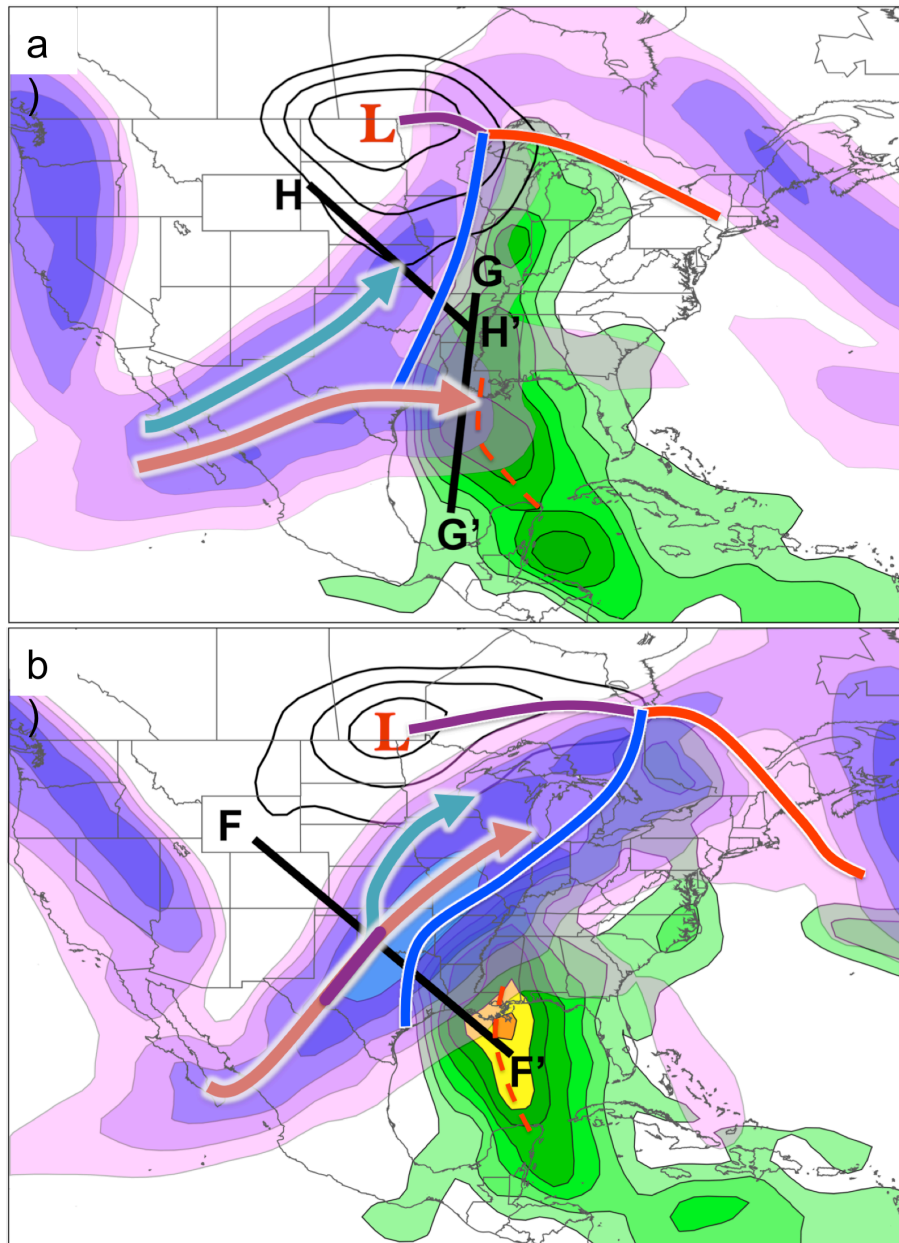


FIG. 3.3. Synoptic overview with sea level pressure every 4 hPa beginning at 996 hPa (thin black lines), the surface low pressure center (red “L”), surface frontal boundaries with the cold front denoted by the blue line, the warm front denoted by the red line, and the occluded front denoted by the purple line, the magnitude of the 925 hPa poleward moisture flux every 5 cm s^{-1} beginning at 10 cm s^{-1} (green fill pattern), the 250 hPa isotachs every 10 m s^{-1} beginning at 30 m s^{-1} (purple fill pattern), the locations of the polar (blue arrow), subtropical (red arrow), and superposed (purple line) jets, as identified using the scheme described in Section 2.1, and the axis of 925 hPa poleward moisture flux (red dashed line) at (a) 0000 UTC 1 May 2010 and (b) 0000 UTC 2 May 2010.

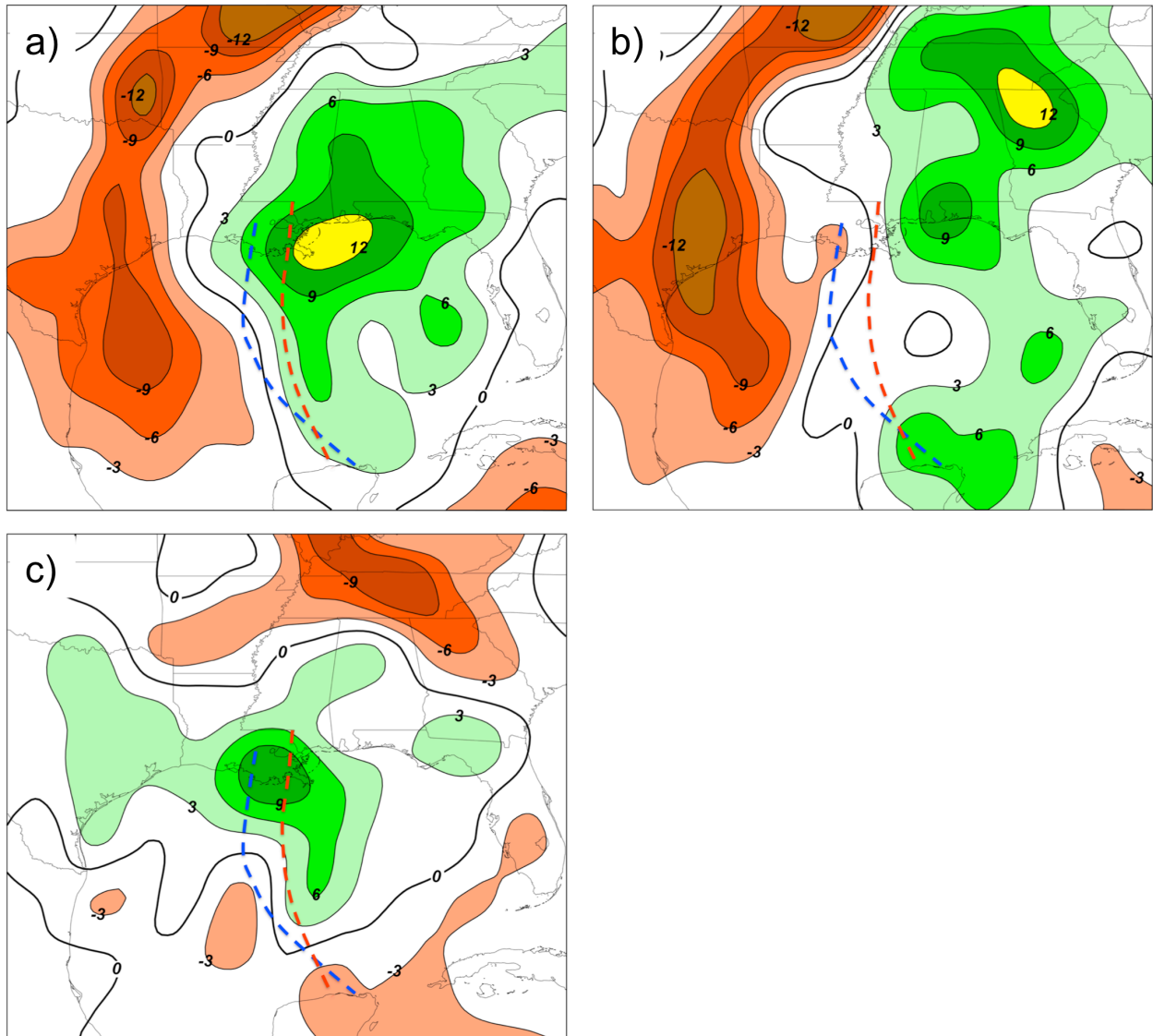


FIG. 3.4. Change in the magnitude of the 925 hPa (a) total, (b) geostrophic, and (c) ageostrophic poleward moisture fluxes over the southeast United States during the 24 h period from 0000 UTC 1 May to 0000 UTC 2 May. Changes in the moisture flux greater than (less than) 3 (-3) cm s^{-1} are shaded in the green (red/brown) fill pattern every 3 cm s^{-1} , with 0 cm s^{-1} contoured in black. The blue (red) dashed line represents the axis of maximum poleward moisture flux at 0000 UTC 1 May (2 May), as indicated in Fig. 3.3.

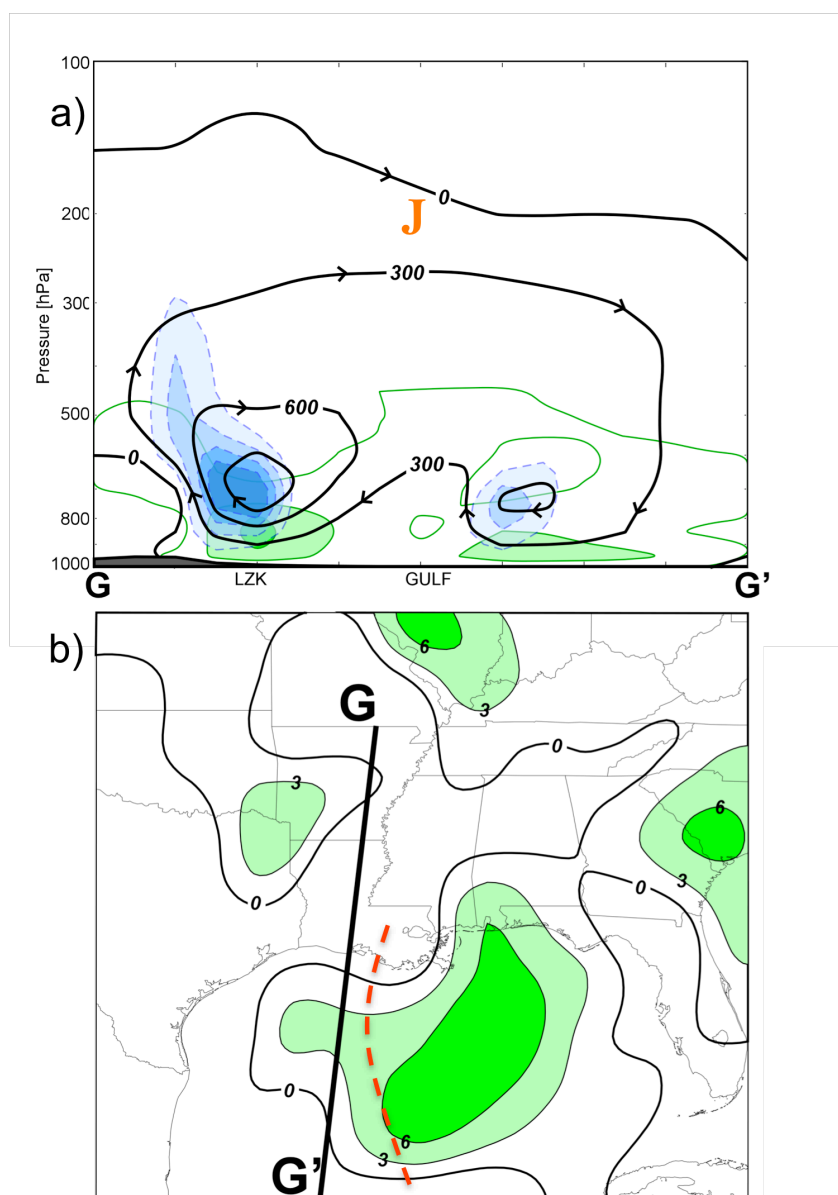


FIG. 3.5. (a) Cross section of the Sawyer-Eliassen streamfunction every 300 m hPa s^{-1} (black lines) along the cross section G-G', in Fig. 3.3a, at 0000 UTC 1 May, moisture flux associated with the Sawyer-Eliassen circulation every 3 cm s^{-1} beginning at 0 cm s^{-1} (0 cm s^{-1} is contoured in green with the green fill pattern used for values greater than 3 cm s^{-1}), and negative omega associated with the Sawyer-Eliassen circulation every 1 dPa s^{-1} beginning at 1 dPa s^{-1} (blue fill pattern, dashed contours). The sense of the circulation is depicted by the arrowheads plotted on the streamfunction contours, the location of the subtropical jet core is indicated by the "J", and GULF represents the Gulf coast. (b) The 925 hPa ageostrophic poleward moisture flux every 3 cm s^{-1} beginning at 0 cm s^{-1} (0 cm s^{-1} is contoured in black with the green fill pattern used for values greater than 3 cm s^{-1}) and the axis of maximum poleward moisture flux (red dashed line previously indicated in Fig. 3.3a) at 0000 UTC 1 May.

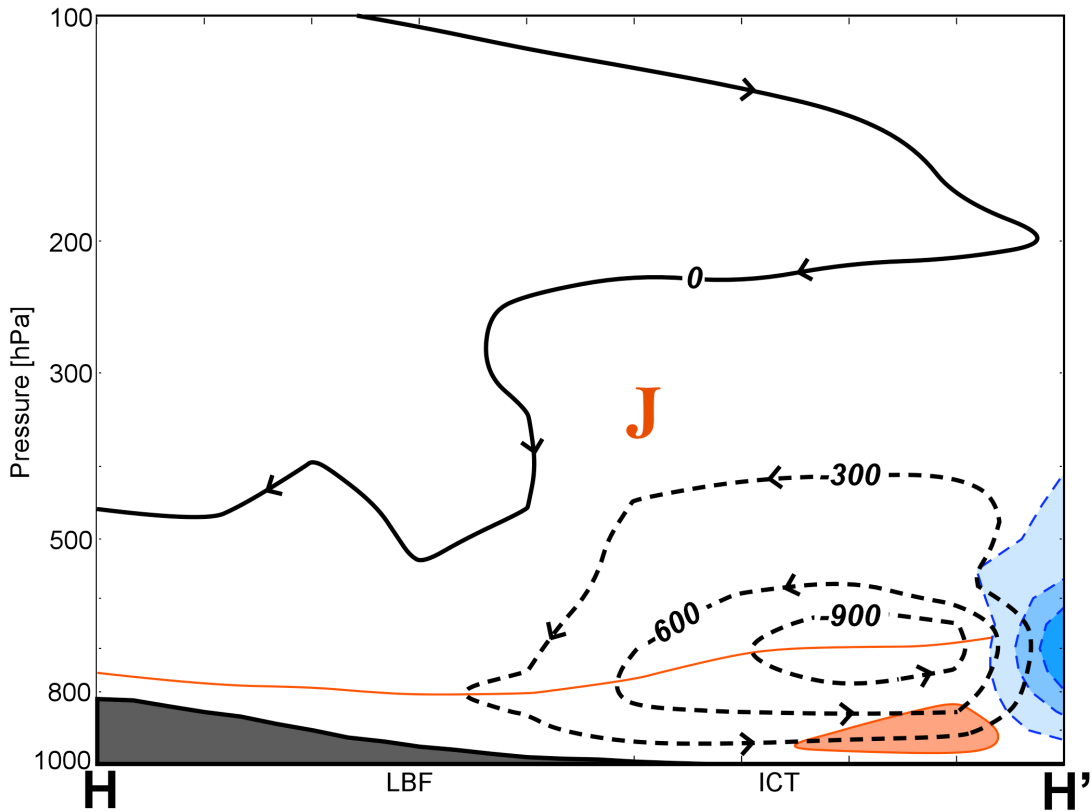


FIG. 3.6. Cross section of the Sawyer-Eliassen streamfunction (black contours, where dashed contours represent negative values) every 300 m hPa s^{-1} along the line H-H', in Fig. 3.3a, at 0000 UTC 1 May, moisture flux due to the Sawyer-Eliassen circulation every -3 cm s^{-1} beginning at 0 cm s^{-1} (0 cm s^{-1} is contoured in orange with the orange fill pattern used for values less than -3 cm s^{-1}), and negative omega associated with the Sawyer-Eliassen circulation every 1 dPa s^{-1} (blue fill pattern, dashed contours) beginning at 1 dPa s^{-1} . The sense of the circulation is denoted by the arrowheads plotted on the streamfunction contours and the location of the polar jet core is indicated by the "J".

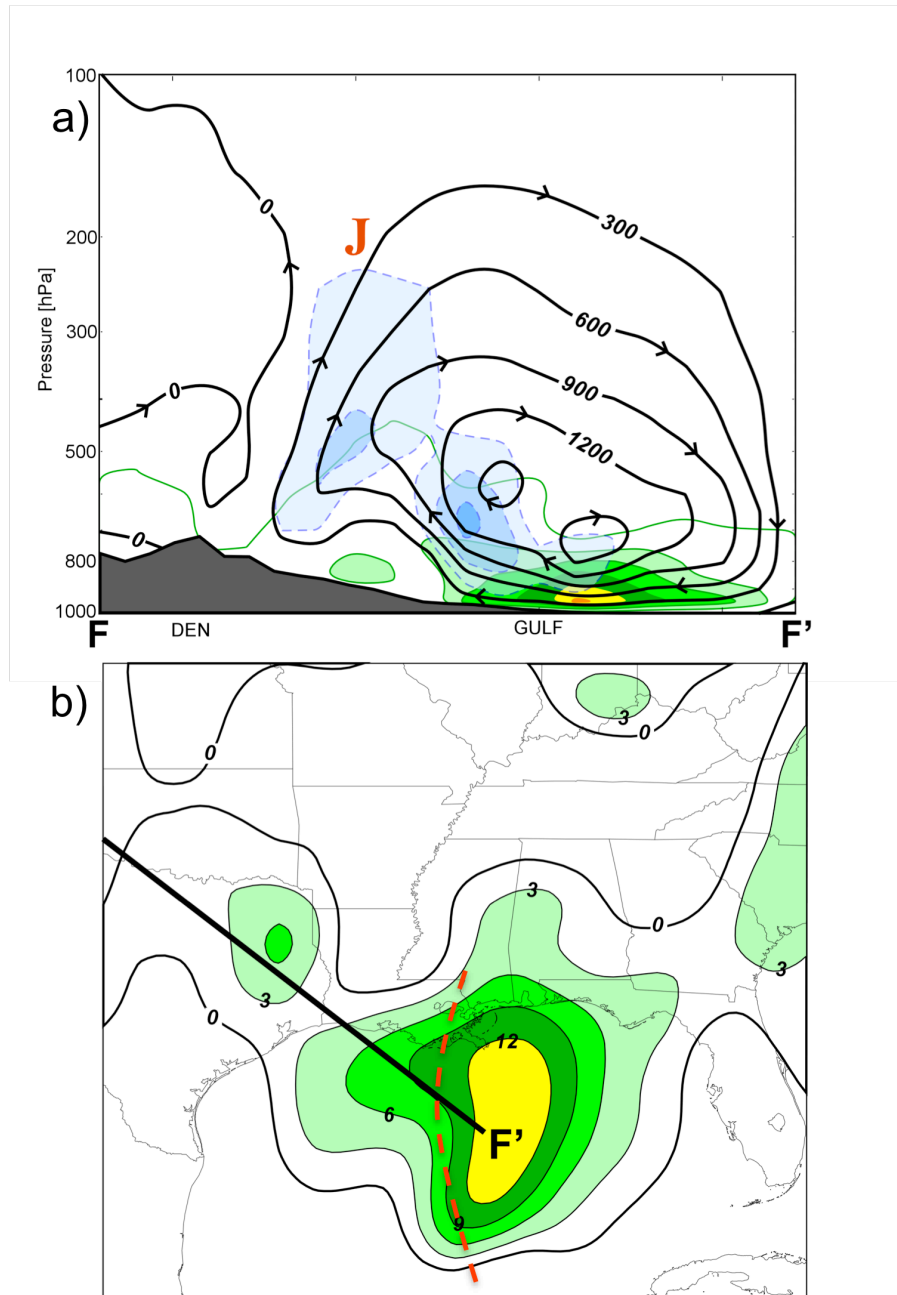


FIG. 3.7. (a) Cross section of the Sawyer-Eliassen streamfunction along the line F-F', in Fig. 3.3b, at 0000 UTC 2 May. Labeling conventions are identical to those in Fig. 3.5a, with the “J” representing the superposed jet core. (b) As in Fig. 3.5b, but valid at 0000 UTC 2 May.

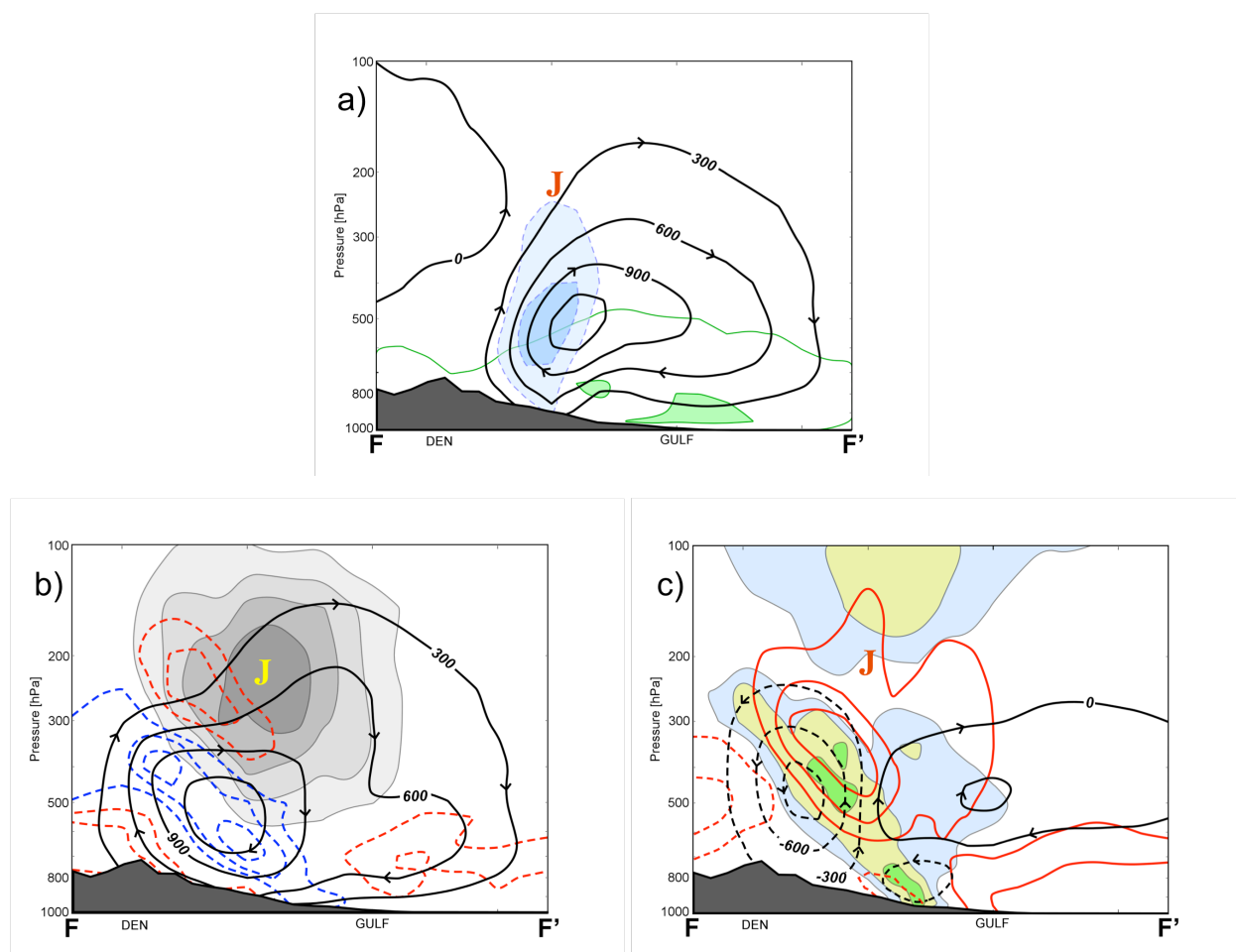


FIG. 3.8. Cross section along F-F', in Fig. 3.3b, at 0000 UTC 2 May showing (a) the Sawyer-Eliassen streamfunction, moisture flux, and negative omega (same conventions as in Fig. 3.5a) associated with the Q_g forcing; (b) the Sawyer-Eliassen streamfunction associated with the Q_{SH} forcing (same conventions as in Fig. 3.6), isotachs of the cross-section-normal geostrophic wind (gray fill pattern) every 10 m s^{-1} beginning at 30 m s^{-1} , and the cross-section-normal temperature gradient (negative, red dashed contours; positive, blue dashed contours) every $5 \times 10^{-6} \text{ K m}^{-1}$ (zero line omitted); and (c) the Sawyer-Eliassen streamfunction associated with the Q_{ST} forcing (same conventions as in Fig. 3.6), isotachs of the along-cross-section geostrophic wind with positive values oriented toward F (positive, thick red lines; negative, dashed red lines) every 5 m s^{-1} (zero line omitted), and magnitude of the along-cross-section potential temperature gradient every $10 \times 10^{-6} \text{ K m}^{-1}$ beginning at $10 \times 10^{-6} \text{ K m}^{-1}$ (fill pattern). The "J" represents the location of the superposed jet core in all panels.

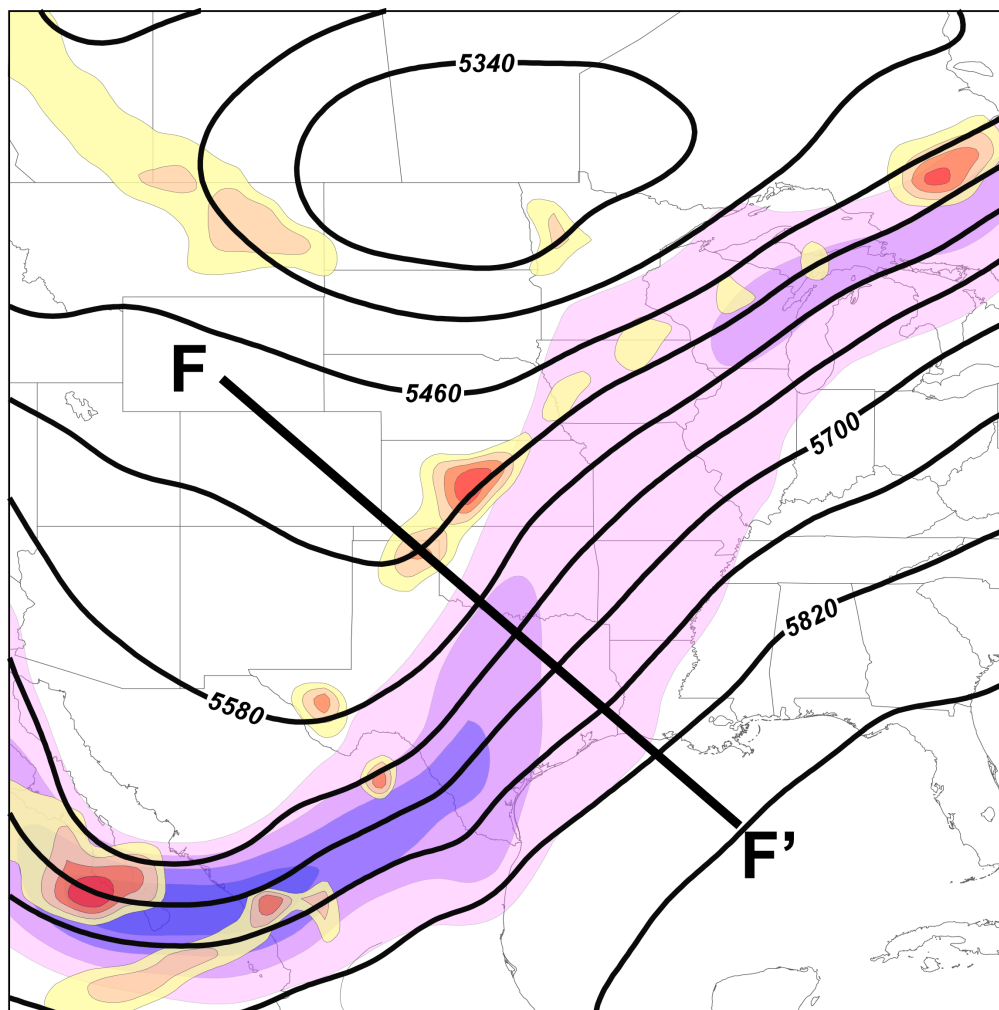


FIG. 3.9. The 500 hPa GFS analysis at 0000 UTC 2 May with geopotential height contoured in black every 60 m, isotachs of the geostrophic wind (purple fill pattern) every 10 m s^{-1} beginning at 30 m s^{-1} , and horizontal geostrophic frontogenesis (warm-colored fill pattern) every $0.4 \text{ K (100 km)}^{-1} (3 \text{ h})^{-1}$ beginning at $0.4 \text{ K (100 km)}^{-1} (3 \text{ h})^{-1}$.

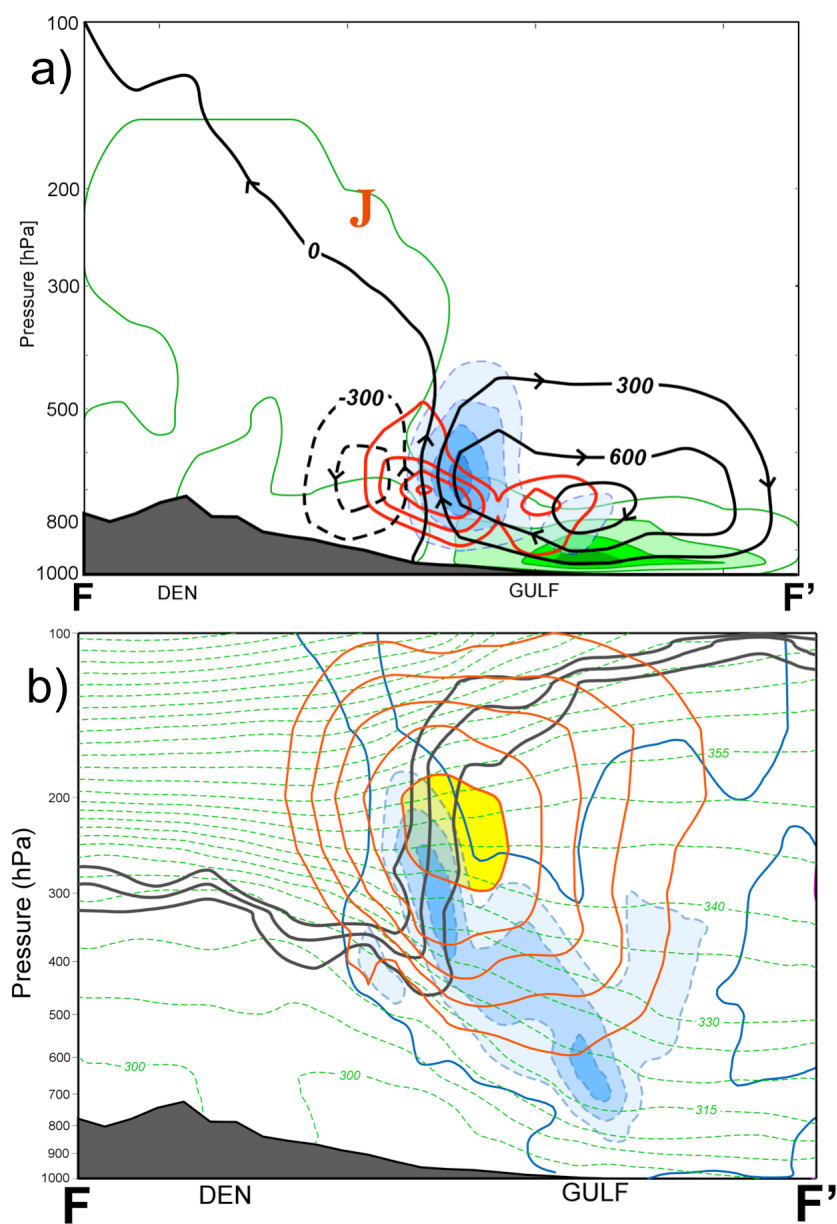


FIG. 3.10. The Sawyer-Eliassen streamfunction, moisture flux, and negative omega, labeled, contoured, and shaded as in Fig. 3.5a, associated with the diabatic forcing. Heating (K s^{-1}) contoured every $200 \times 10^{-6} \text{ K s}^{-1}$ beginning at $200 \times 10^{-6} \text{ K s}^{-1}$ (red contours). The “J” denotes the location of the superposed jet core. (b) The isotachs (red contours) every 10 m s^{-1} beginning at 30 m s^{-1} with the jet core shaded yellow, the 1-, 2-, 3-PVU surfaces (black contours), potential temperature every 5 K (dashed green contours), and negative omega every 2 dPas^{-1} beginning at 0 dPas^{-1} (0 dPas^{-1} is contoured in blue with values greater than 2 dPas^{-1} shaded with the blue fill pattern) from the GFS analysis at 0000 UTC 2 May 2010 along the cross section F-F’, in Fig. 3.3b.

Chapter 4

The Development of Jet Superpositions from a Basic-State Variable Perspective*

4.1 Motivation

In the last chapter, the analysis demonstrated that the transverse ageostrophic circulation associated with a superposed jet acted to intensify the poleward moisture flux over the southeastern United States prior to the second day of heavy rainfall that characterized the 1–3 May 2010 Nashville Flood. Moore et al. (2012) indicated that this increase in moisture flux was essential for the continued production of persistent heavy rainfall during the latter half of the event. More broadly, however, this analysis highlights one specific pathway through which a superposed jet can affect the evolution of a high-impact weather event.

In addition to the May 2010 Nashville Flood, recall that superposed jets have been linked, either directly or indirectly, to a number of other memorable high-impact weather events at middle latitudes, including an explosive cyclogenesis event south of Iceland in early-January 1956 (Defant 1959), the 25–26 January 1978 Cleveland Superbomb (Hakim et al. 1995; Hakim et al. 1996), the 12–14 March 1993 Storm of the Century (Bosart et al. 1996), and the 25–28 April 2011 severe weather outbreak (Christenson and Martin 2012; Knupp et al. 2014). The association of jet superpositions with a class of high-impact weather events motivates further investigation into the mechanisms that support the process of superposition and, specifically, the development of the two-step pole-to-equator tropopause structure that characterizes these events.

In the past, work that has addressed the related topic of jet “mergers” has been focused on either interannual or climate time scales (e.g., Harnik et al. 2014), has been strongly based on

* The analysis and discussion in this chapter is identical to that which has recently been submitted for publication in the *Quarterly Journal of the Royal Meteorological Society* (Winters and Martin 2015).

wave-wave interaction (e.g., Lee and Kim 2003; Son and Lee 2005; Martius et al. 2010; O'Rourke and Vallis 2013), and/or has been conducted within an idealized model environment (e.g., Lee and Kim 2003; Son and Lee 2005; O'Rourke and Vallis 2013). This circumstance, coupled with only limited analysis of these features using observations, has resulted in incomplete insight into the mechanisms that foster the development of jet superpositions from a synoptic-dynamic framework.

The concept of mid-latitude trough mergers (e.g., Lai and Bosart 1988; Gaza and Bosart 1990; Hakim et al. 1995; Hakim et al. 1996; Dean and Bosart 1996; Strahl and Smith 2001), in which two mid-tropospheric vorticity maxima with origins in distinctly different westerly air streams amalgamate into a single maximum, offers the closest physical analog to jet superpositions in the synoptic-dynamic literature. These studies emphasize that trough merger often results in explosive cyclogenesis – also a frequent by-product of jet superposition. While it appears that certain trough merger cases may be simultaneously characterized by jet superpositions, the aforementioned studies do not identify the merging air streams as distinctly related to separate polar and subtropical jets and do not specifically investigate the impact of trough merger on the evolution of the upper-tropospheric jet and tropopause structure. Instead, the focus of these studies is largely placed on the effects merger can have on the development of surface cyclones.

Numerous observationally based studies have addressed the different mechanisms that can be responsible for altering the structure of an *individual* jet stream, however. For instance, the presence of ageostrophic transverse circulations, and particularly the differential vertical motions associated with them, in the vicinity of an upper-level jet-front system can act not only to aid in the production of sensible weather, but also to significantly restructure the baroclinicity

and tropopause both above and below the jet. Specifically, Shapiro (1981,1982) indicated that the presence of geostrophic cold-air advection along the jet axis acted to produce subsidence directly beneath the jet core on the warm side of the developing baroclinic zone. This created an environment that was particularly favorable for the development of an upper-tropospheric front, as the subsidence increased the horizontal baroclinicity below the jet by tilting the isentropes into a more vertical orientation. Results from modeling and observational studies that followed lent further support to the notion that an environment characterized by geostrophic cold-air advection along the jet axis was favorable for upper-tropospheric frontogenesis (e.g., Keyser and Pecnick 1985; Lang and Martin 2012; Martin 2014). Many of the historical contributions to this problem are well summarized by Keyser and Shapiro (1986), while Lang and Martin (2012) provide a recent extension of these studies to the process of lower-stratospheric frontogenesis.

The influence of convection in altering the structure of the tropopause on the anticyclonic shear side of a jet has also been well-documented. In particular, Lang and Martin (2013) investigated four cases of upper-frontal evolution in southwesterly flow. They noted that latent heat release offers separate but simultaneous physical mechanisms that can alter the tropopause structure. First, direct diabatic erosion of PV above the heating maximum can increase the tropopause height in a given column. Second, the associated reduction in upper-tropospheric static stability intensifies the strength of an existing ageostrophic transverse circulation, which can then act to further tilt the tropopause. Convection (occurring at both middle and tropical latitudes) and cyclones have also been shown to exert a considerable influence on the location and strength of the subtropical jet via their associated tropopause-level irrotational outflow (e.g., Archambault et al. 2013; Grams et al. 2013; Griffin and Bosart 2014).

Despite extensive research on a variety of aspects of upper-level jet-front systems, no prior study has examined the role of the above dynamical mechanisms in supporting specifically the interaction and subsequent vertical superposition of the two, initially distinct, jet species. Consequently, this chapter will consider the specific roles that ageostrophic transverse circulations, convection, and the interaction of the two may play in reshaping the tropopause into the two-step structure that characterizes jet superposition events.

These topics will be addressed in the context of the two recent high-impact weather events outlined in Section 2.2: the 18–20 December 2009 Mid-Atlantic Blizzard and the aforementioned 1–3 May 2010 Nashville Flood. These events were selected because they occur at different times of the year and were associated with different types of high-impact weather events (i.e., rapid cyclogenesis and an extreme precipitation event). Synoptic overviews of these two cases were provided in Section 2.2 and the analysis will make reference to that discussion often in the current chapter. Sections 2 and 3 of this chapter focus on the development of a superposed jet during each of these individual cases and Section 4 finishes with a discussion of the results.

4.2 Jet Evolution During the 18–20 December 2009 Mid-Atlantic Blizzard

Given that polar and subtropical jets are each associated with unique tropopause breaks, insight into the formation of a superposed jet can be garnered through a diagnosis of the movement of each individual tropopause break as they eventually become vertically aligned¹. In this case, the existence of a subtropical jet was closely tied to the presence of remote tropical convection over portions of Central America and the eastern equatorial Pacific Ocean. One

¹ For our purposes the tropopause refers to the dynamical tropopause, which corresponds to the 2–PVU surface.

particularly insightful way to examine the effect that tropical convection can have on the subsequent evolution of the subtropical jet is through consideration of the anomalous pressure depth of the isentropic layer that contains the subtropical jet. Particularly telling is the depth of that layer on the anticyclonic shear side of the jet, where positive perturbation pressure depths correspond to excess mass, relative to a long term mean, residing in the layer. The perturbation pressure depths of various isentropic layers are calculated as the difference between instantaneous pressure depths and a 31-yr (1979–2009) average depth at each grid point and analysis time, determined using NCEP’s Climate Forecast System Reanalysis (CFSR) dataset (Saha et al. 2010). For the subtropical jet, we consider the pressure depth of the 340-355-K isentropic layer, the same layer used in the jet identification scheme (Section 2.1).

The outflow from tropical convection serves as one mechanism through which an isentropic layer can become anomalously inflated. Specifically, tropical convection often ingests boundary layer air with relatively high equivalent potential temperature (θ_e). Parcels embedded within convective updrafts are then exhausted at an isentropic layer that roughly corresponds to this boundary layer θ_e . Often, such air is within the range of 340-355-K, coinciding with the isentropic layer within which the subtropical jet resides. Furthermore, regions characterized by a strong horizontal gradient in perturbation pressure depth (p') are associated with a perturbation geostrophic vertical shear, in accordance with the isentropic thermal wind relationship:

$$\frac{\partial \vec{V}_g'}{\partial \theta} = -\frac{1}{\rho f \theta} \hat{k} \times \nabla p' \quad (4.1)$$

Consequently, a subtropical jet is typically positioned on the poleward edge of an area characterized by positive perturbation pressure depths in the 340-355-K isentropic layer.

Figure 4.1a demonstrates that, at 0000 UTC 19 December, positive perturbation pressure depths in the 340-355-K isentropic layer were found over much of the Gulf of Mexico and

Caribbean Sea on the anticyclonic shear side of the subtropical jet. Immediately upstream of the inflated isentropic layer were active areas of organized tropical convection over portions of the eastern equatorial Pacific Ocean and Central America (Fig. 4.1b), suggesting that convective outflow was a source of the excess mass found within the isentropic layer. Furthermore, the presence of a weak, poleward-directed divergent wind (calculated directly from the GFS analyses) along the subtropical tropopause break at 200 hPa² (red dashed line) encouraged a slight poleward shift in the location of the subtropical jet, consistent with the observations made from Figs. 2.3a,c.

At 1800 UTC 19 December, perturbation pressure depths increased in both magnitude and areal coverage over a large portion of the central Caribbean and off the southeastern United States coast and maintained an association with convection in the tropics (Figs. 4.1c,d). Figure 4.1c also identifies that weak, poleward-directed divergent winds persisted in the vicinity of the subtropical tropopause break, which continued to support a slight poleward shift of the subtropical jet's axis. Figure 4.1e demonstrates that this subtle poleward shift in the location of the subtropical jet continued up until 1200 UTC 20 December when the polar and subtropical jets superposed. Furthermore, coincident with the jet's increased wind speed is a strengthened gradient in perturbation pressure depth immediately equatorward of the jet axis from the eastern Gulf of Mexico northeastward towards Bermuda.

The upper-tropospheric evolution in the hours preceding superposition strongly suggests that persistent remote tropical convection over the eastern equatorial Pacific Ocean and Central America was responsible for an inflation of the 340-355-K isentropic layer. Trajectory analysis, using the NOAA/ARL HYSPLIT model (Draxler and Hess 1997; Draxler and Hess 1998;

² 200 hPa in this case, as well as the 2010 Nashville Flood, corresponds well to the level of maximum wind for the subtropical jet and cuts perpendicularly through the subtropical tropopause break, allowing it to be a suitable level to assess the horizontal advection of the tropopause break by the divergent wind.

Draxler 1999; Draxler and Rolph 2015; Rolph 2015), of parcels originating in the vicinity of the tropical convection at 1200 UTC 18 December (Fig. 4.2) confirms this assertion, with near a quarter of the trajectories characterized by rapid ascent in the 12-24 h following their initiation and warming to potential temperatures of 340-350-K. Upper-tropospheric southwesterly flow downstream of the low-latitude trough west of Mexico then acted to transport the convective outflow towards the Caribbean Sea in the 24-36 h prior to superposition, resulting in the positive perturbation pressure depths observed in that location. Consequently, there is strong evidence that the combination of both persistent tropical convection and the approach of a low-latitude trough contributed to the existence of the subtropical jet. First, by facilitating an inflation of the 340-355-K isentropic layer in the tropics and, secondly, by encouraging the subsequent advection of mass within that isentropic layer towards higher latitudes.

Focusing attention on the evolution of the polar jet, and its interaction with the subtropical jet, Fig. 4.3a shows that the polar jet sat atop a region of enhanced baroclinicity that extended from northwestern Kansas southeastward into northern Mississippi at 0000 UTC 19 December. Furthermore, the geostrophic jet exit region was characterized by weak geostrophic cold-air advection over southern Missouri and northern Arkansas. This suggests, based on Shapiro's (1982) conceptual model, that the transverse ageostrophic circulation associated with the polar jet's exit region was shifted relative to the jet axis such as to position descent through the jet core (Fig. 3.2b). The solution for the Sawyer-Eliassen circulation within the cross section identified in Fig. 4.3a confirms this notion, depicting a region of subsidence centered beneath the polar jet core (Fig. 4.4a). The subsidence was driven by the presence of dipole circulations, which consisted of a thermally direct (indirect) circulation to the south (north) of the jet core. Specifically, this subsidence was not only responsible for strengthening the mid-tropospheric

temperature gradient via tilting, but also for supporting a concomitant downward protrusion of high PV air characteristic of the development of a polar tropopause fold.

By 1800 UTC 19 December, the polar jet had propagated around the base of the polar trough and had assumed an orientation parallel to the axis of the subtropical jet over the southeastern United States (Fig. 4.3b). Furthermore, geostrophic wind speeds associated with the polar jet increased to greater than 60 m s^{-1} , in response to the intensified horizontal baroclinicity situated beneath the jet. The magnitude of the geostrophic cold-air advection also strengthened further from the prior time in the vicinity of both jets' entrance regions over northern Alabama, suggesting continued subsidence in the vicinity of the jet cores.

The Sawyer-Eliassen circulation within the cross section J-J', drawn through the entrance region of both the polar and subtropical jets at this time (Fig. 4.3b), is characterized by a strong thermally direct circulation with subsidence confirmed directly on and beneath the subtropical tropopause step³ (Fig. 4.4b). Consequently, this subsidence was favorably positioned to advect high PV air downward and to lower the altitude of the subtropical tropopause step with time. From another perspective, it is apparent that the 320-K and 325-K isentropes were situated within the horizontal baroclinicity that sat beneath the subtropical jet. The presence of a mid-tropospheric maximum in subsidence through the polar jet core, as indicated in Fig. 4.4b, implies that the 320-K isentrope was advected downward on the poleward side of the subtropical jet at a more rapid rate than the 325-K isentrope, reducing the horizontal baroclinicity beneath the subtropical jet. At the same time, the subsidence acted to incorporate these same isentropes into a strengthening region of baroclinicity beneath the polar jet core (Figs. 2.3d,f). Consequently, the subsidence associated with the Sawyer-Eliassen circulation promoted an intensification of the

³ Cross sections along the entire length of the polar and subtropical jets are consistent with the result shown in Fig. 4.4b and the diagnosed vertical motions strongly agree qualitatively with GFS vertical motions.

baroclinicity directly beneath the polar jet core at the expense of the subtropical jet's baroclinicity and, subsequently, the production of one consolidated region of intense horizontal temperature contrast that is characteristic of a superposed jet.

By 1200 UTC 20 December, the polar tropopause break became vertically aligned with the subtropical tropopause break, producing the vertical PV wall shown in Fig. 2.3f and a superposed jet from central Georgia northeastward to eastern North Carolina (Fig. 4.3c). Wind speeds in the core of the superposed jet increased as well, consistent with the consolidation of baroclinicity beneath the superposed jet. Notably, locations upstream of the superposed jet remained characterized by strong geostrophic cold-air advection, indicating continued forcing for subsidence on and beneath the subtropical tropopause step and supporting the development of the two-step tropopause structure observed downstream.

The preceding analysis of this case is summarized in the conceptual diagram shown in Fig. 4.5, which highlights the importance of internal jet dynamics in facilitating a vertical superposition of the polar and subtropical jets. While the convection over Central America and the equatorial Pacific Ocean was essential for strengthening and establishing the subtropical jet, it only promoted a slight poleward shift in the location of the jet axis. Transverse ageostrophic circulations, on the other hand, were crucial, not only in the production of a polar tropopause fold, but also in driving a downward protrusion of high PV air centered squarely on the subtropical tropopause step. It appears that these vertical motions, which were present along the entire length of the subtropical tropopause step between the polar and subtropical jet axes 18 h prior to superposition, were primarily responsible for reshaping the tropopause into the characteristic two-step structure associated with a superposed jet.

4.3 Jet Evolution During the 1-3 May 2010 Nashville Flood

This section considers the evolution of the tropopause and jet structure throughout the 1–3 May 2010 Nashville Flood. At 0000 UTC 1 May, the polar jet sat atop a rather extensive and continuous area of mid-tropospheric baroclinicity that stretched from just off the coast of southern California into northern Minnesota (Fig. 4.6a). Furthermore, the jet entrance region of the polar jet was characterized by an area of geostrophic cold-air advection centered squarely in the base of the western trough. As in the December 2009 case, Shapiro's (1982) conceptual model implies that this forcing will act to promote subsidence beneath the jet core, this time by shifting the thermally direct circulation in the jet entrance region towards the anticyclonic shear side of the jet (Fig. 3.2b).

The Sawyer-Eliassen circulation within the cross section K-K', identified in Fig. 4.6a, conforms to this idealized model, placing subsidence directly beneath the polar jet core and in the vicinity of the polar tropopause fold (Fig. 4.7). This subsidence, once again, acts both to facilitate a downward protrusion of high PV air into the middle troposphere and to increase the horizontal baroclinicity beneath the jet via tilting. Subsequently, regions of strong mid-tropospheric baroclinicity in Fig. 4.6 correspond roughly to the location of the polar tropopause fold. It is also likely that curvature effects associated with the western trough further enhanced the total subsidence observed in the jet entrance region beyond that estimated by the transverse circulation (not shown). Consequently, it is conceivable that flow curvature, in addition to the diagnosed transverse circulation, acted to accentuate the development of the polar tropopause fold in this location and to strengthen the polar jet.

At 1200 UTC 1 May, the axis of the polar jet became fractured near the United States/Mexico border (Fig. 4.6b), presumably under the influence of ongoing convection over the

southern Mississippi River valley. Additionally, the environment in the vicinity of the jet fracture was favorable for large-scale ascent, given the close proximity of the upstream trough, which acted to decrease the horizontal temperature gradient in the middle troposphere via tilting downstream of the Rio Grande (not shown). Further upstream, in the base of the trough, geostrophic jet wind speeds increased from the previous time in response to the strengthened baroclinicity beneath the jet. Geostrophic cold-air advection remained strong in the base of the trough at this time as well, suggestive of continued subsidence in the vicinity of the polar jet core and the subsequent maintenance of the polar tropopause fold.

At 0000 UTC 2 May, the polar jet streak in the base of the trough was positioned slightly downstream of its previous location, such that its most downstream edge overlapped with the region of superposition identified in Fig. 2.5e over southwestern Oklahoma and west Texas (Fig. 4.6c). Furthermore, rather intense baroclinicity, which extended from the Southern Plains upstream to Baja California, continued to characterize the polar jet streak. Recalling that this area of baroclinicity was also associated with the development of a polar tropopause fold, it becomes clear that the noted appearance of an equatorward displacement of the polar tropopause break within the cross sections shown in Figs. 2.5d,f was simply the downstream propagation of an intense polar tropopause fold into the area of superposition as the deep, polar trough slowly migrated eastward.

As suggested, the evolution of the subtropical jet is closely tied to the proximate convection present over portions of the southern Mississippi River valley throughout the duration of the flooding event. Recall that at 0000 UTC 1 May the subtropical jet was characterized by a rather zonal orientation and was distinct from the polar jet (Fig. 2.5a). Furthermore, Fig. 4.8a depicts a minimum in velocity potential at 200 hPa (approximately the level of maximum

irrotational outflow) centered along the Mississippi River valley, consistent with the presence of large-scale ascent in that location, and a maximum in velocity potential immediately upstream of the trough over the western United States. The juxtaposition of these two features indicated an easterly divergent wind over the spine of the Rocky Mountains and northern Mexico. At this time, this divergent wind field was responsible for only a weak region of negative PV advection over northern Mexico along the subtropical tropopause break, given the rather zonal orientation of the tropopause break.

By 1200 UTC 1 May, it is apparent that latent heating from the ongoing convection over the southern Mississippi River valley had acted to significantly erode upper-tropospheric PV in that location, as demonstrated by the poleward retreat of the 1- and 2-PVU contours at 200 hPa (Fig. 4.8b). Consequently, the subtropical jet became characterized predominantly by southwesterly flow and took on an orientation that was roughly parallel to the polar jet. The divergent wind across northern Mexico also strengthened considerably over the previous 12 h, largely due to the enhanced outflow from convection over portions of Tennessee and southern Kentucky. The combination of these two factors resulted in a significantly more favorable situation for the divergent wind to displace the subtropical tropopause break towards the northwest, as indicated by the increase in negative PV advection along the subtropical tropopause break. This northwestward shift in the position of the subtropical jet axis, aided by the convective outflow, continued up until 0000 UTC 2 May, when it vertically superposed with the polar jet axis over portions of west Texas and southwestern Oklahoma (Fig. 4.8c).

In contrast to the December 2009 case, jet superposition in the May 2010 case was more strongly driven by the presence of convection over the southeastern United States. The analysis, which is summarized in Fig. 4.9, illustrates that convection acted to substantially restructure the

tropopause via (1) the diabatic erosion of upper-tropospheric PV and, (2) advection of the subtropical jet axis westward towards the polar jet via its associated divergent outflow. This result aligns particularly well with existing evidence illustrating the role that tropopause-level divergent outflow can play in influencing the strength and location of a particular jet stream (e.g., Archambault et al. 2013, Grams et al. 2013; Griffin and Bosart 2014; Rowe and Hitchman 2015). However, much like the December 2009 case, persistent geostrophic cold-air advection in the base of the western trough was responsible for forcing an area of subsidence in the vicinity of the polar jet core and facilitated the development of a polar tropopause fold. This fold subsequently propagated downstream into west Texas and southwestern Oklahoma by 0000 UTC 2 May where it undercut the retreating subtropical tropopause break, thereby facilitating the development of the superposed jet structure.

4.4 Discussion

Motivated by the identification of jet superpositions in several historic and recent high-impact weather events, this study examines the dynamical processes responsible for the formation of a superposition during the 18–20 December 2009 Mid-Atlantic Blizzard and the 1–3 May 2010 Nashville Flood. The two cases selected highlight the fact that jet superpositions can be associated with different types of sensible weather events and can develop at different times of the year. Given that ageostrophic transverse jet circulations and convection both influence the tropopause structure within single jet environments, the analysis considers the role these same mechanisms play in reshaping the tropopause within the more complex double jet environment.

Both cases were characterized by mid-tropospheric geostrophic cold-air advection in cyclonic shear along a portion of the cyclonic shear side of the polar jet at some point prior to

superposition, indicating that subsidence was positioned directly through and beneath the polar jet core. Consequently, the descending motions were favorably positioned to facilitate a downward advection of high PV air from the stratosphere and to contribute to the requisite restructuring of the tropopause that characterizes a jet superposition. In the December 2009 case, this subsidence was specifically positioned directly on and beneath the subtropical tropopause step and in the immediate vicinity of both the polar and subtropical jets. Consequently, the subsidence was instrumental in lowering the tropopause height in the region between the two individual jets and for consolidating the baroclinicity associated with each jet into one single zone of contrast. For comparison, only the polar jet's entrance region was associated with subsidence during the May 2010 Nashville Flood. As a result, the subsidence associated with transverse ageostrophic circulations in that case only contributed to the development of a polar tropopause fold, instead of working to directly assimilate the two jets into a single structure.

The two cases examined as part of this study also demonstrate the different roles that convection can play in facilitating a superposition. For instance, during the May 2010 Nashville Flood, convection occurred primarily in the immediate vicinity of the subtropical jet. This convection subsequently acted to restructure the tropopause via material displacement and diabatic erosion of upper-tropospheric PV. Conversely, the December 2009 case was most strongly influenced by remote tropical convection. This tropical convection was primarily responsible for substantially enhancing the subtropical jet by inflating the anticyclonic shear side of the isentropic layer containing the jet. Together, these two cases demonstrate that the proximity of convection relative to the jet may determine the nature of its influence on the jet. For example, proximate convection can have a rapid local, yet transient impact on the jet structure through its divergent outflow and latent heat release. Alternatively, remote convection

can drive a slower acting, but more persistent impact via the development of what might be termed tropical tropopause anticyclones – the balanced response to upper-tropospheric mass deposition on the anticyclonic shear side of the subtropical jet.

While both cases illustrate that internal jet dynamics and convection can play important separate roles in the development of a superposition, it is clear that the relative importance of each component is case dependent. For instance, it appears that transverse ageostrophic circulations played a more prominent role during the December 2009 case, while convection was the dominant component during the May 2010 Nashville Flood. A broader survey of jet superposition events over North America may help (1) to pinpoint the environmental characteristics that are most conducive for the development of superpositions and (2) to determine whether or not that preferred environment varies seasonally or geographically. Furthermore, persistent observation of these jet superpositions by the author over the course of this study has made it clear that significant weather events are not tied to every superposed jet. Consequently, greater knowledge regarding the environmental differences that exist between null cases and those associated with significant sensible weather over North America remains an unanswered research question. This cornucopia of research questions is addressed in further detail as proposed future work in Section 6.2.1.

Finally, another particularly useful way to investigate the physical processes involved in jet superpositions is found by employing piecewise PV inversion techniques (e.g., Hoskins et al. 1985; Davis and Emanuel 1991). The following chapter details a scheme that isolates the individual PV anomalies associated with each jet structure by considering the distribution of PV within isentropic layers characteristic to each jet. A prominent outcome that emerges from an inversion of these PV anomalies, as well as those generated diabatically from convection, is the

ability to diagnose both the lateral and vertical interactions between separate PV anomalies within a dual jet environment and to assess the specific individual role that each anomaly plays in restructuring the tropopause during the process of superposition.

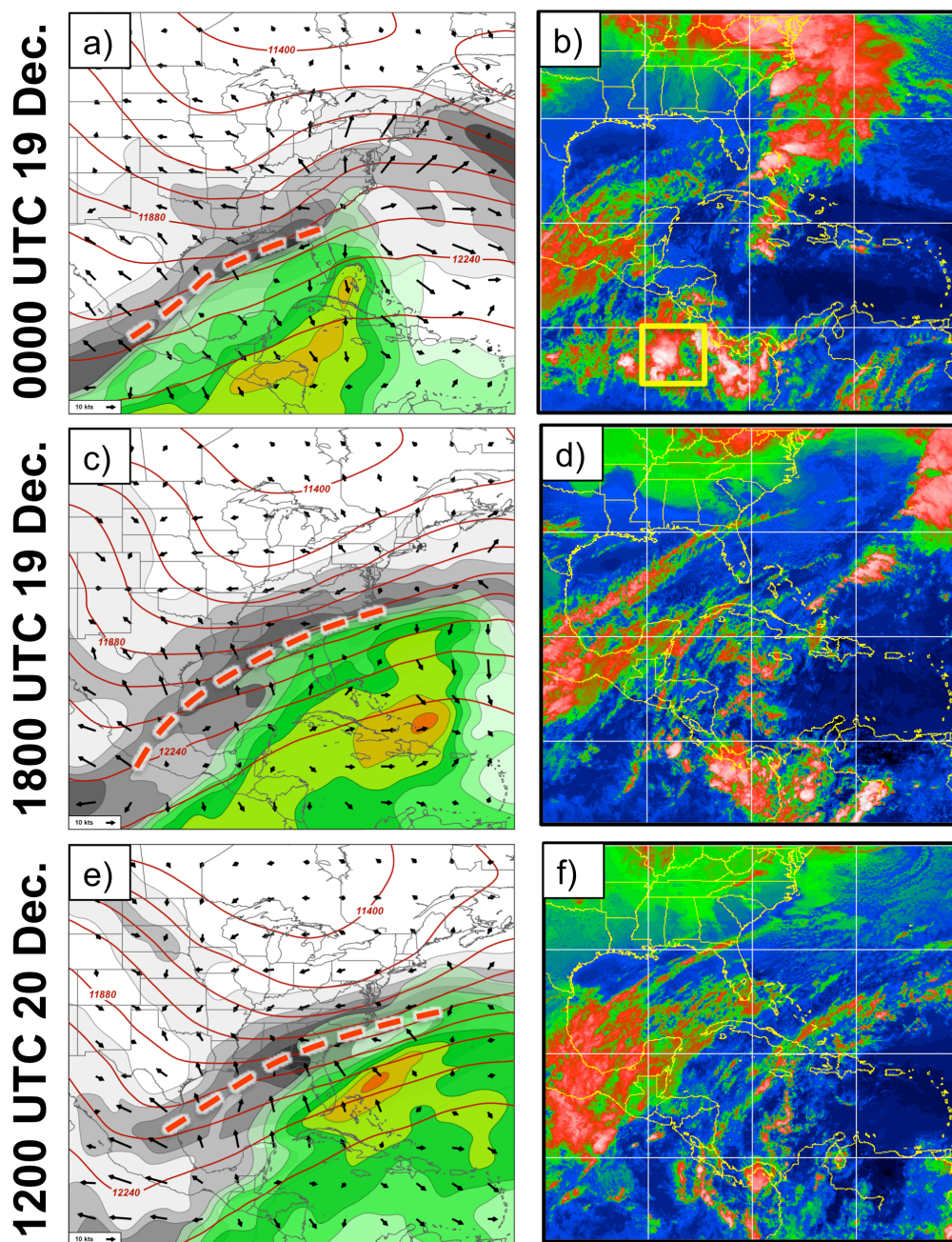


FIG. 4.1. [left column] 200 hPa geopotential height is contoured in red every 120 m, 200 hPa geostrophic isotachs are shaded with the gray fill pattern every 10 m s^{-1} beginning at 30 m s^{-1} , positive perturbation pressure depths within the 340-355-K isentropic layer are shaded in the green fill pattern every 10 hPa, 200 hPa irrotational wind vectors are denoted by the arrows, and the subtropical jet axis is identified with the thick, dashed red line at (a) 0000 UTC 19 December 2009, (c) 1800 UTC 19 December 2009, and (e) 1200 UTC 20 December 2009. [right column] Infrared satellite imagery from the University of Wisconsin – CIMSS for (b) 0000 UTC 19 December 2009, (d) 1800 UTC 19 December 2009, and (f) 1200 UTC 20 December 2009. The yellow box denotes the geographical source region for the trajectories shown in Fig. 4.2.

NOAA HYSPLIT MODEL
Forward trajectories starting at 1200 UTC 18 Dec 09
GDAS Meteorological Data

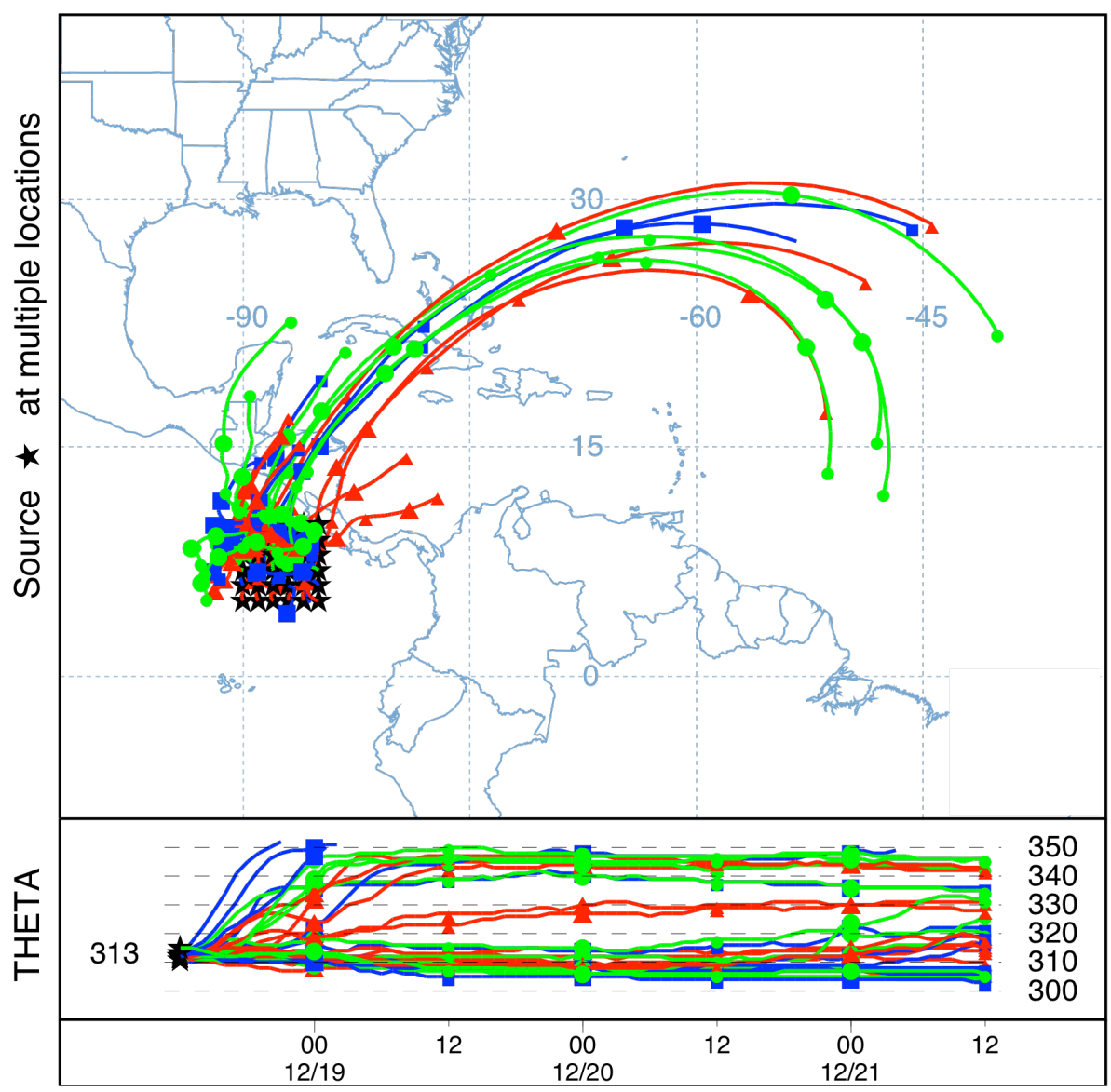


FIG. 4.2. 72 h forward trajectories initialized at 1200 UTC 18 December 2009 within the yellow box (5°N – 10°N ; 85°W – 90°W) shown in Fig. 4.1b over the eastern equatorial Pacific Ocean. Trajectories were initialized at 3 km above ground level within the NOAA HYSPLIT model and projected forward using archived GDAS data. The bottom panel depicts the potential temperature of the trajectories throughout the duration of the 72 h period.

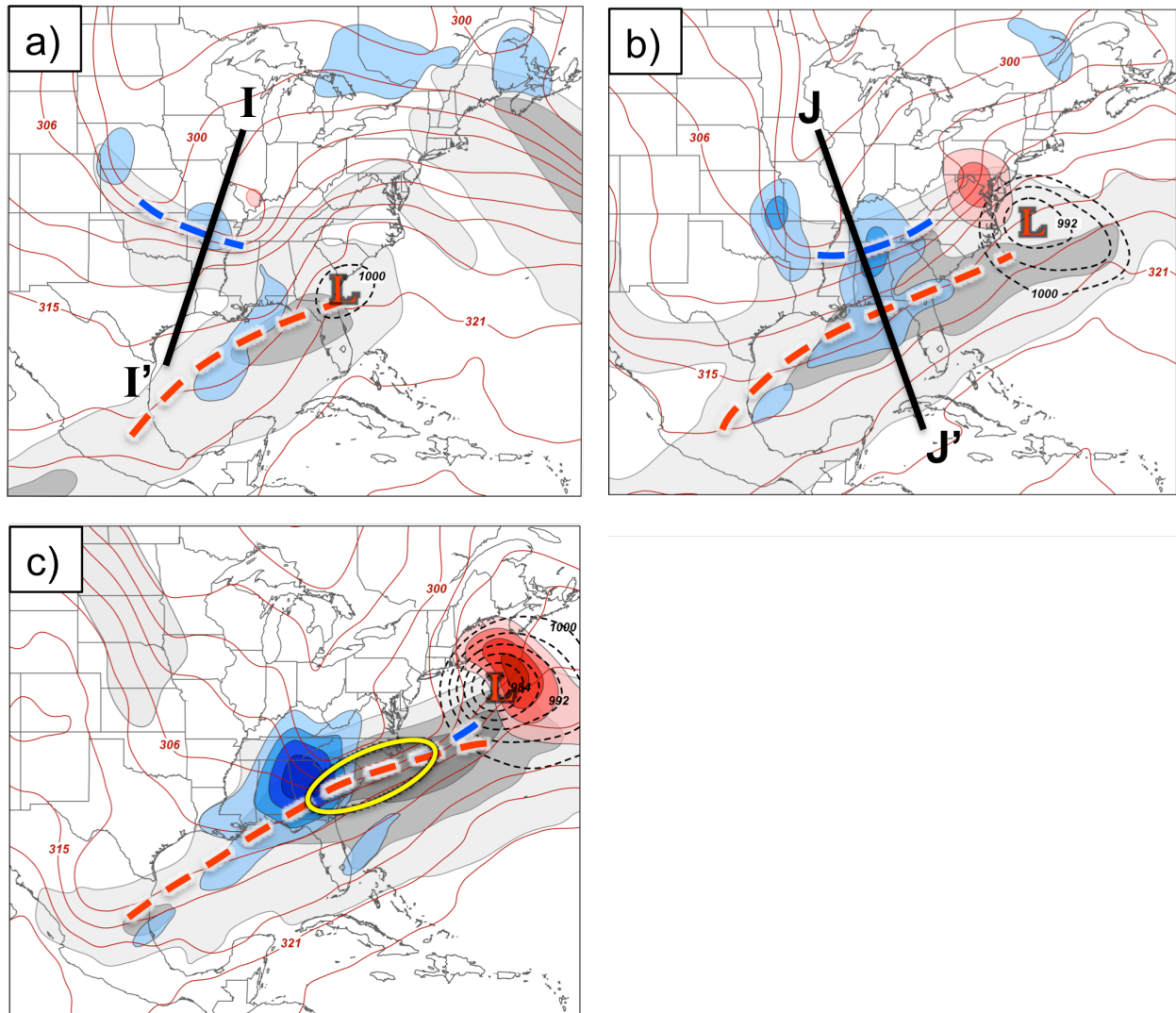


FIG. 4.3. 250 hPa geostrophic isotachs are shaded with the gray fill pattern every 20 m s^{-1} beginning at 40 m s^{-1} , 300 hPa geostrophic cold (warm)-air advection is shaded in the blue (red) fill pattern every $4 \times 10^{-4} \text{ K s}^{-1}$, 500 hPa potential temperature is contoured in red every 3 K, and sea level pressure is contoured with the dashed black lines every 4 hPa below 1000 hPa at (a) 0000 UTC 19 December 2009, (b) 1800 UTC 19 December 2009, and (c) 1200 UTC 20 December 2009. The polar (subtropical) jet axis is indicated by the thick, dashed blue (red) line, the yellow circle highlights the region of jet superposition, and the red “L” marks the location of the sea level pressure minimum.

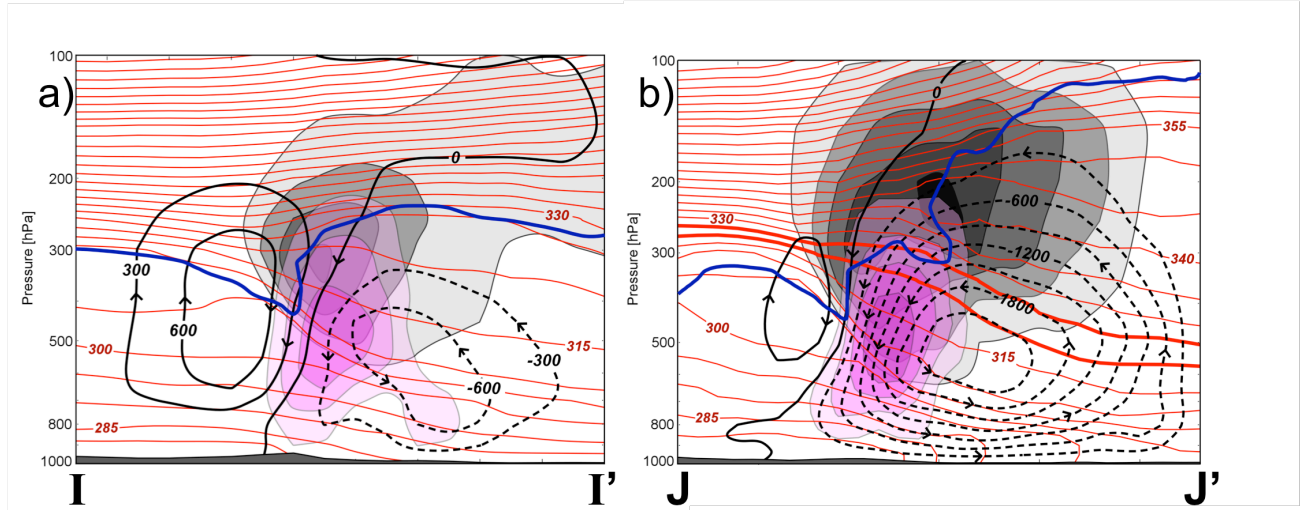


FIG. 4.4. Cross sections, as indicated in Fig. 4.3, of Sawyer-Eliassen streamfunction every 300 m hPa s^{-1} with negative (positive) values contoured with the dashed (solid) black lines, potential temperature contoured in red every 5 K, positive omega associated with the Sawyer-Eliassen circulation shaded in the purple fill pattern every 1 dPa s^{-1} beginning at 1 dPa s^{-1} , geostrophic isotachs shaded with the gray fill pattern every 10 m s^{-1} beginning at 30 m s^{-1} , and the 1.5-PVU contour identified by the bold blue line. The sense of the transverse circulation is depicted by the arrowheads plotted on the streamfunction contours and the 320-K and 325-K isentropes are bolded in (b) for reasons discussed in the text.

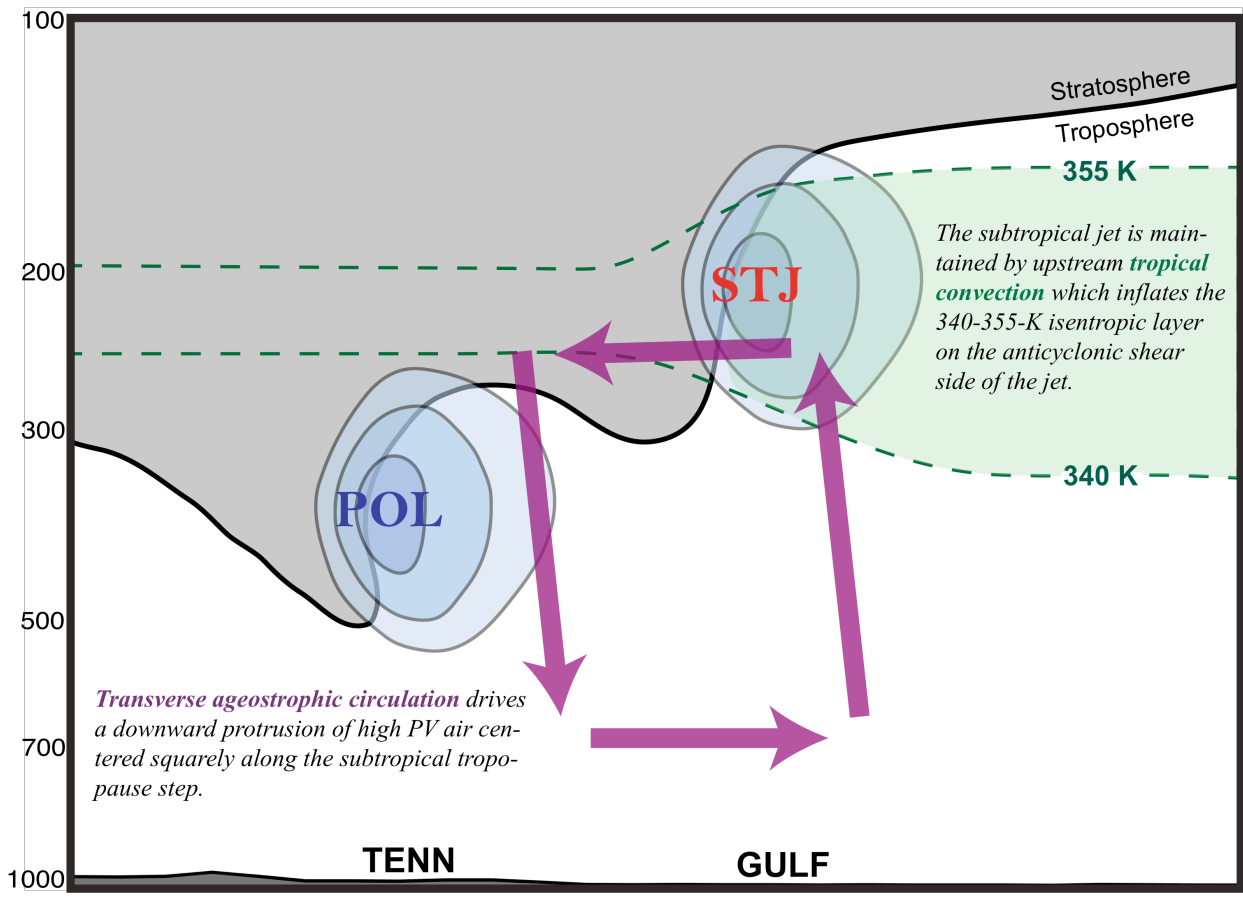


FIG. 4.5. Conceptual diagram summarizing the development of a superposed jet during the 18–20 December 2009 Mid-Atlantic Blizzard.

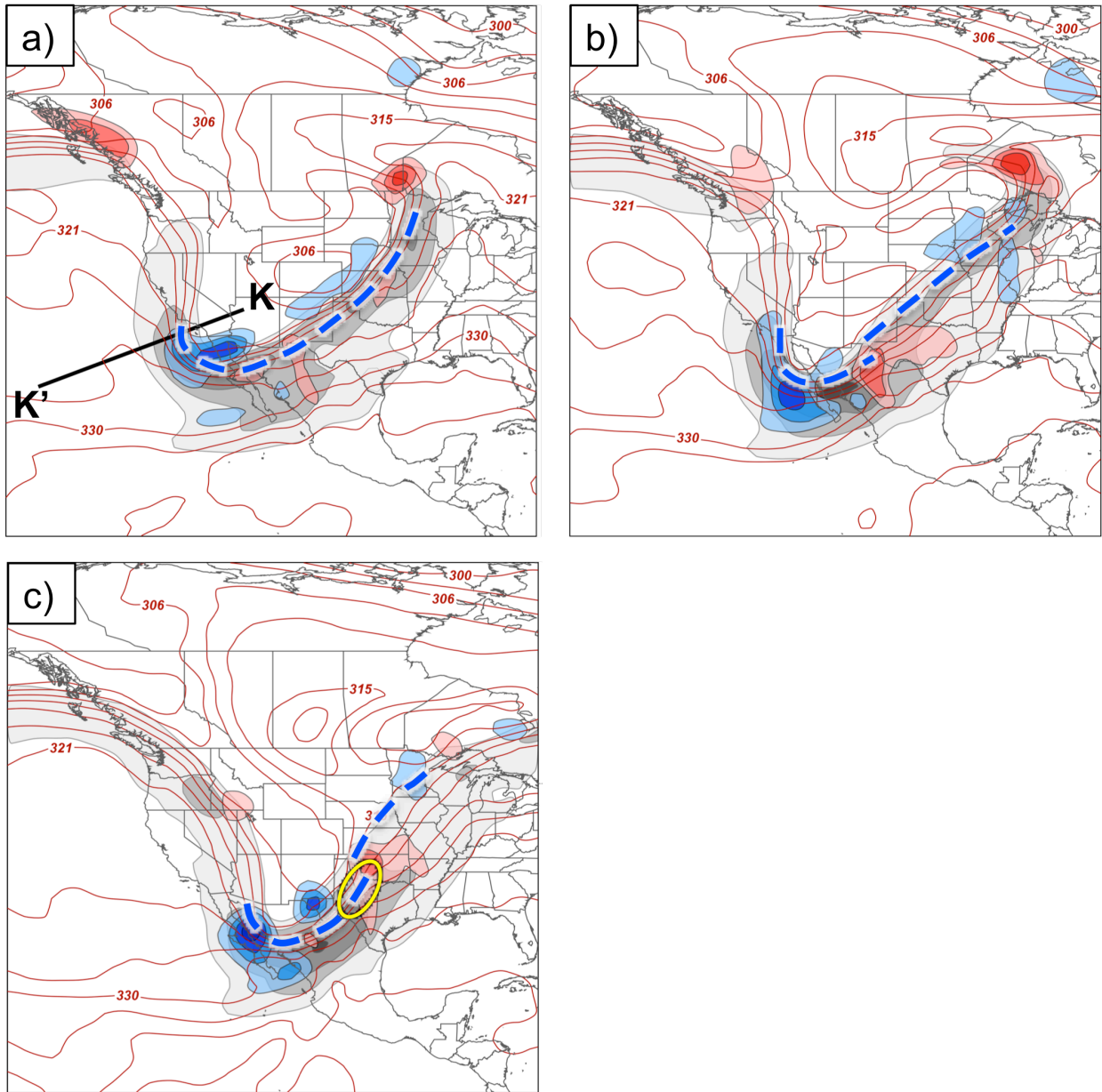


FIG. 4.6. 300 hPa geostrophic isotachs are shaded in the gray fill pattern every 20 m s^{-1} beginning at 40 m s^{-1} , 300 hPa geostrophic cold (warm)-air advection is shaded in the blue (red) fill pattern every $4 \times 10^{-4} \text{ K s}^{-1}$, and 400 hPa potential temperature is contoured in red every 3 K at (a) 0000 UTC 1 May 2010, (b) 1200 UTC 1 May 2010, and (c) 0000 UTC 2 May 2010. Polar jet axes are indicated by the thick, blue dashed line and the yellow circle highlights the region of jet superposition.

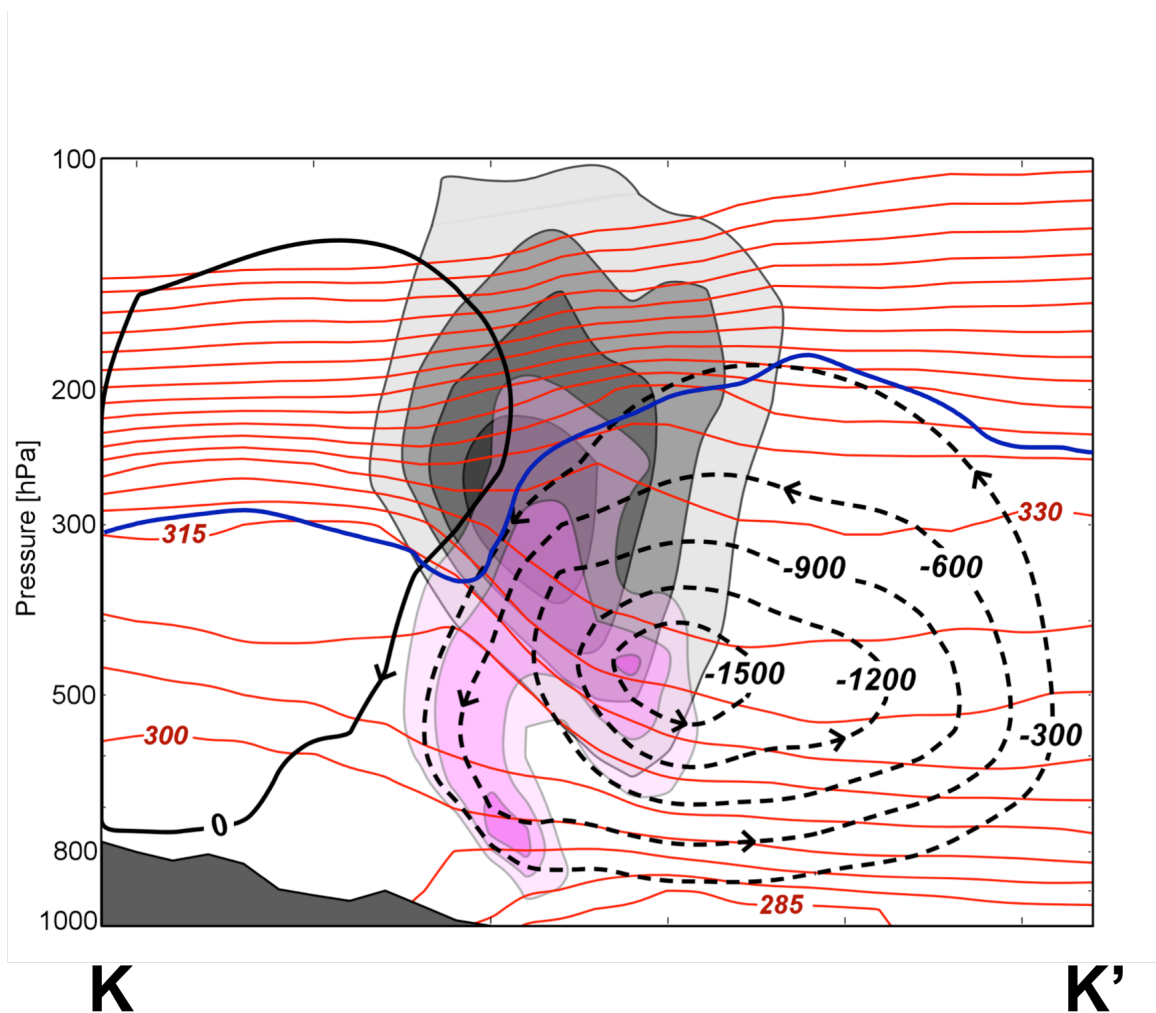


FIG. 4.7. Conventions are identical to those in Fig. 4.4, but for the cross section shown in Fig. 4.6a.

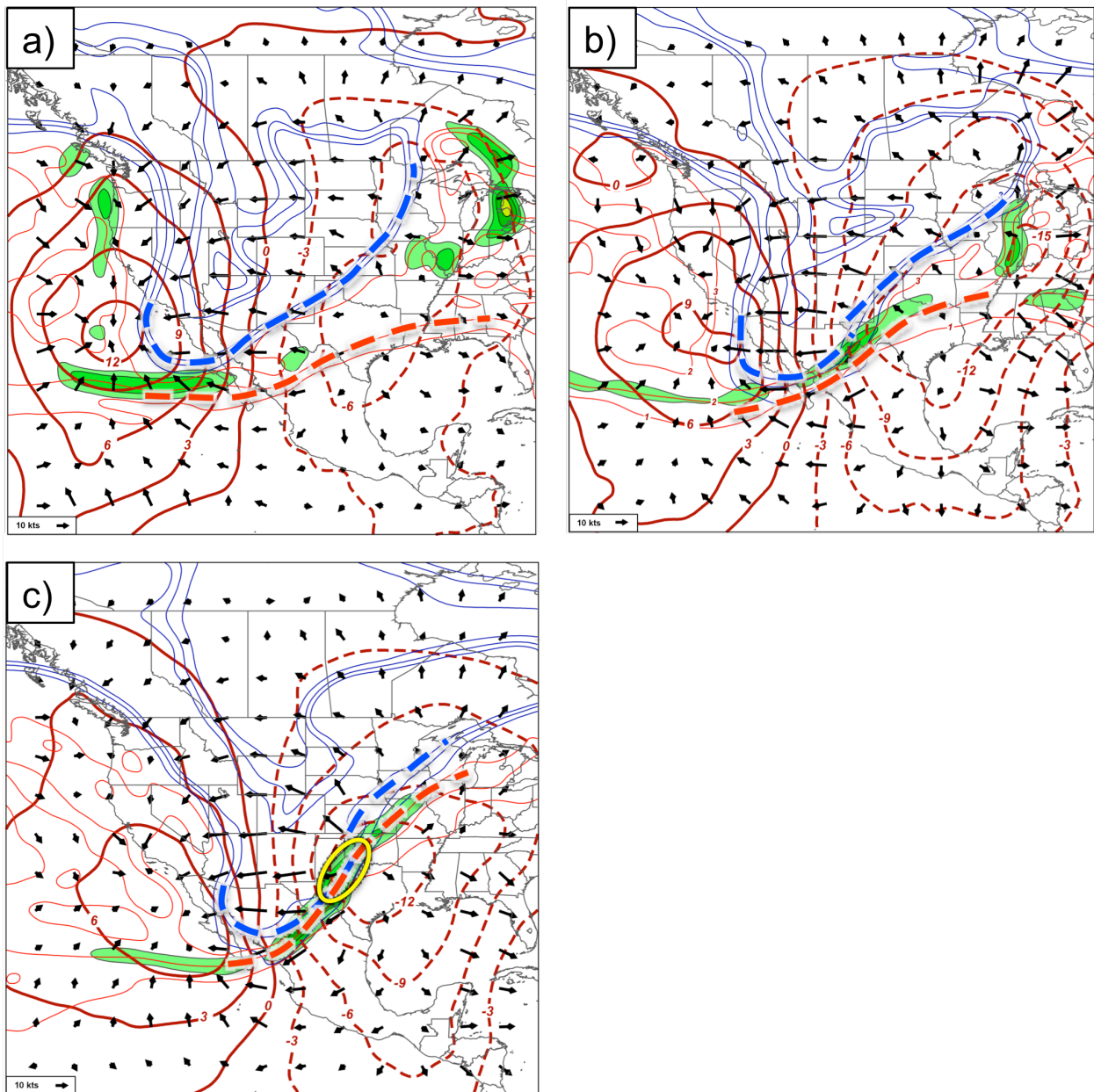


FIG. 4.8. 200 hPa velocity potential contoured every $3 \times 10^6 \text{ m}^2 \text{ s}^{-1}$ with positive (negative) values identified with solid (dashed) thick red lines, the 1-, 2-, and 3-PVU surfaces at 300 hPa (200 hPa) are identified with the thin blue (red) lines, and negative PV advection within the 1-3-PVU channel by the 200 hPa divergent wind (arrows) is shaded in the green fill pattern every $2 \times 10^{-5} \text{ PVU s}^{-1}$ at (a) 0000 UTC 1 May 2010, (b) 1200 UTC 1 May 2010, and (c) 0000 UTC 2 May 2010.

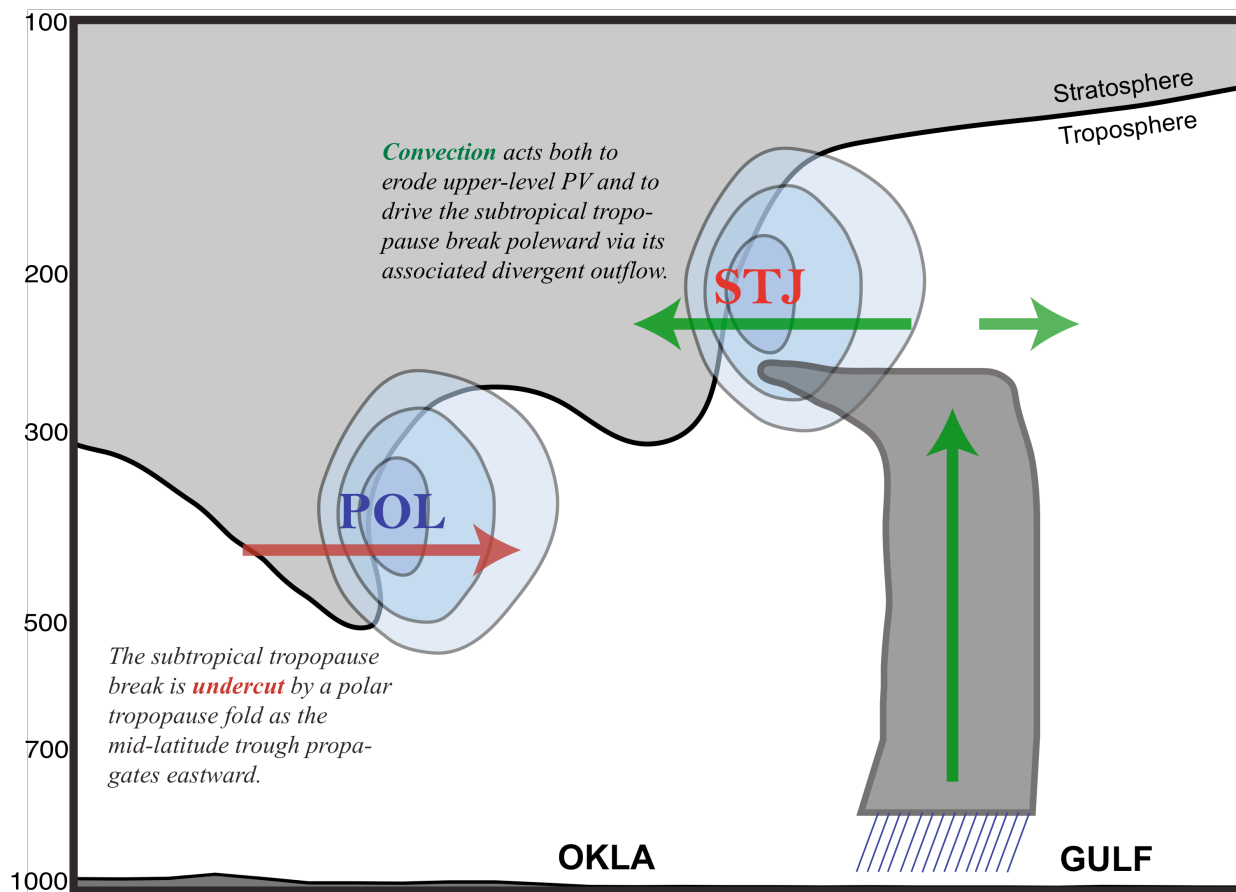


FIG. 4.9. Conceptual diagram summarizing the development of a superposed jet during the 1–3 May 2010 Nashville Flood.

Chapter 5

Insights into Jet Superposition Gained from Employing Piecewise PV Inversion

5.1 Motivation

The analysis presented in the previous chapter highlights the roles that convection and transverse vertical circulations played in the development of a superposed jet during the 18–20 December 2009 Mid-Atlantic Blizzard and the 1–3 May 2010 Nashville Flood. A drawback to the basic-state variable perspective employed in that analysis, however, is an inability to separate and quantify the specific influences that different atmospheric structures had in reshaping the dynamical tropopause during those respective jet superposition events. One solution to combat this shortcoming is to employ a PV inversion perspective. An advantage of examining the distribution of PV in a particular case is the ability to leverage the inherent principles of PV conservation and invertibility (Hoskins et al. 1985). Specifically, these principles imply that (1) the PV serves as a particularly good tracer for atmospheric motion under the assumption of adiabatic and inviscid flow and (2) that knowledge of a PV distribution at a given time, constrained by some balance condition, permits the recovery of its associated mass, momentum, and thermal fields.

“PV thinking”, which focuses on examining the PV distribution to gain insight into various atmospheric structures, dates back to the mid-20th century when PV was employed as a diagnostic tool to study mid-latitude weather systems, such as upper-tropospheric fronts and mid-latitude cyclones (e.g., Reed and Sanders 1953; Reed 1955; Kleinschmidt 1957; Danielsen 1968; Danielsen et al. 1970). As part of those studies, the downward protrusion of high PV, stratospheric air that characterizes a folded tropopause was examined extensively, in addition to the emerging relationship between tropopause folds and cyclogenesis at the surface. Hoskins et

al. (1985), however, are credited with summarizing the theoretical foundation for “PV thinking”, and has served as the basis for subsequent examinations of mid-latitude weather systems from a PV perspective.

A primary component of Hoskins et al. (1985), which references the work by Thorpe (1985), addresses the notion that a PV distribution can be split into a theoretically infinite number of pieces. As for the full PV field, an inversion of any piece of the PV allows for the recovery of the individual mass and thermal fields associated with that particular piece, subject to the particular assumptions made concerning the partition. An example of the mass and thermal fields accompanying an idealized positive and negative PV anomaly in the upper troposphere are taken from Thorpe (1985) and illustrated in Fig. 5.1. An examination of this conceptual model indicates that a positive (negative) PV anomaly is associated with a cyclonic (anticyclonic) circulation that is maximized at the level of the anomaly and decays with altitude both above and below the anomaly. In accordance with this vertical shear, the thermal wind relationship dictates that the positive (negative) PV anomaly must be associated with a relatively cold (warm) column of air below the anomaly and a warm (cold) column of air above the anomaly. This temperature distribution further necessitates the existence of a positive (negative) static stability anomaly that is coincident with the PV anomaly.

In the wake of Hoskins et al. (1985), the use of PV inversion began to take root as computational methodologies for performing the inversion were developed. For instance, Robinson (1988, 1989) and Holopainen and Kaurola (1991) developed techniques to partition and invert the quasi-geostrophic potential vorticity (QGPV), which approximates the conservation relationship for the full Ertel PV in flows with small curvature and Rossby number. The strength of QGPV inversion is that the inversion operator is linear in the geopotential. This

stands in contrast to an inversion of the Ertel PV, which requires navigating several non-linear terms in its system of balance equations (Section 5.2.2). Consequently, a partition and numerical inversion of the QGPV is more appealing computationally, but it is limited to situations in which the assumptions used in deriving it are valid. Davis and Emanuel (1991) were the first to propose a methodology that permitted a piecewise inversion of the Ertel PV and to apply it in an observed case of cyclogenesis. This development made it possible to examine the influence that individual pieces of the Ertel PV distribution had within a flow that could be characterized by considerable curvature and a much larger Rossby number.

Davis and Emanuel (1991) marked the beginning of a research effort to employ piecewise PV inversion in the examination of a myriad of structures within the mid-latitude atmosphere. The greatest attention thus far has been paid to the process of mid-latitude cyclogenesis and the individual roles that diabatic heating and structures in the lower and upper troposphere play in strengthening a surface cyclone (e.g., Davis 1992b; Davis et al. 1993; Davis et al. 1996; Hakim et al. 1996; Nielsen-Gammon and Lefevre 1996; Morgan and Nielsen-Gammon 1998). Emerging from these studies was confirmation that the process of cyclogenesis was characterized by a two-way, mutual interaction between the lower- and upper-tropospheric circulations and that latent heat release acted to further intensify both circulations and their interactions. Piecewise PV inversion has also been applied to investigate the influence of these same atmospheric structures in promoting tropospheric frontogenesis (e.g., Morgan 1999; Korner and Martin 2000), in facilitating the development of individual tropopause folds (e.g., Ramos 1997; Wandishin et al., 2000), and in the development and movement of tropical cyclones (e.g., Wu and Emanuel 1995a,b; Shapiro 1996; Shapiro and Franklin 1999; McTaggart-Cowan et al. 2001; Shapiro and Möller 2003).

Despite the versatility that piecewise PV inversion has shown in its ability to provide insight into a number of diverse atmospheric structures, no study has utilized piecewise PV inversion to investigate the process of jet superposition, and more broadly, the interaction between two proximate jet streams. The nearest approximation to such a study was provided by Hakim et al. (1996) in their consideration of a mid-latitude trough merger that occurred prior to the 25–26 January 1978 Cleveland Superbomb. While that particular study demonstrated that QGPV inversion was a useful tool in diagnosing the interaction between two mid-tropospheric vorticity maxima, the focus was placed primarily on the explosive cyclogenesis that took place at the surface. As a result, little attention was paid to the specific role those individual upper-level PV anomalies played in restructuring the tropopause during that event.

Consequently, the present chapter supplements the analysis presented in Chapter 4 by employing piecewise PV inversion to examine the processes and mechanisms responsible for the creation of a two-step tropopause structure and a jet superposition during both the 18–20 December 2009 Mid-Atlantic Blizzard and 1–3 May 2010 Nashville Flood. The remainder of this chapter is structured as follows. Section 2 discusses the piecewise PV inversion techniques that will be used to investigate the three-dimensional flow accompanying each PV anomaly in the two cases. Section 3 presents the results from the PV inversions and Section 4 finishes with a discussion and some conclusions.

5.2 Methodology

Insight into how the tropopause can be restructured from a PV perspective can be found by consulting Wandishin et al. (2000). In that particular study, the authors indicated that vertical motions could help to vertically tilt the tropopause if it was initially flat. Once the tropopause

exhibited a vertical tilt, the presence of a vertical shear could act more substantially to further tilt the tropopause into the vertical and to foster the development of a tropopause break. In the context of a jet superposition, which necessitates a vertical superposition of the two distinct tropopause breaks, vertical shear and vertical motions are also likely to play an important role. For instance, the presence of a vertical shear can result in the differential horizontal advection of the individual tropopause breaks, which may or may not result in a superposition. Furthermore, the presence of vertical motions on a flat portion of the tropopause can act to vertically displace or tilt the tropopause locally as well. Given that knowledge of the full three-dimensional flow is required to interrogate jet superpositions, the following PV inversion techniques outline the methods used to recover the balanced non-divergent and divergent wind fields associated with each piece of the PV distribution.

5.2.1 PV Partition Scheme

The degree to which insight is gained from a PV inversion is highly dependent on the effectiveness of the PV partition employed. Consequently, care must be taken to partition the flow into a finite number of pieces, such that each piece captures PV with a similar history or origin. In each case, the perturbation PV is defined against a 6 d mean that encompasses the jet superposition event. Specifically, PV perturbations in the December 2009 Blizzard are defined against a 6 d mean calculated from 0000 UTC 17 December 2009 – 0000 UTC 23 December 2009, while perturbations during the May 2010 Nashville Flood are calculated against a 6 d mean of 0000 UTC 27 April 2010 – 0000 UTC 3 May 2010. For each case, the PV was partitioned and inverted every 6 h within its corresponding $1^\circ \times 1^\circ$ horizontal domain (Fig. 5.2) and at 50 hPa intervals between 1000 hPa and 50 hPa. Observed wind, temperature, geopotential

height, and relative humidity data from GFS analyses were used as input to the PV inversion software.

PV perturbations from the 6 d mean at each time were isolated following a modified implementation of the standard three-way partition described by Korner and Martin (2000). A conceptual diagram illustrating this partition is shown in Fig. 5.3a. The surface PV encompasses the perturbation PV at grid points in the 950-850 hPa layer with a relative humidity less than 70%, as well as all temperature perturbations specified near the bottom boundary of the domain. Together, this particular piece of PV captures the effects of near-surface temperature anomalies, which themselves behave in a similar manner as PV anomalies (Bretherton 1966). The interior PV isolates perturbation PV at grid points within the 950-150 hPa layer with a relative humidity greater than or equal to 70%. This piece of the PV is designed to isolate the diabatic creation and erosion of PV that results from latent heat release. Finally, the upper-tropospheric PV captures the perturbation PV at grid points within the 650-100 hPa layer that have a relative humidity below 70%, as well as all temperature perturbations specified near the top boundary of the domain. This piece of the PV isolates dry air of either stratospheric or upper-tropospheric origin and captures the PV tied to dynamical structures in the middle and upper troposphere, including the jet streams. Together, these three pieces of the PV account for nearly all of the perturbation PV within the domain except for dry air ($RH < 70\%$) between 800-700 hPa and nearly saturated air ($RH \geq 70\%$) above 150 hPa. An examination of both of cases considered in this dissertation demonstrates that the omitted perturbation PV does not impact the analysis.

While this three-way partition of the perturbation PV can provide beneficial insight into the roles the lower troposphere, the upper troposphere, and convection can have in the development of a jet superposition, it does not separate the individual influence of the polar and

subtropical waveguides. Consequently, an additional PV partition is employed that isolates the perturbation PV associated with the individual polar and subtropical jets and is described with reference to the cross section shown in Fig. 5.3b. In the upper troposphere, an individual tropopause break can be conceptualized as the horizontal juxtaposition of a positive (negative) PV anomaly on the poleward (equatorward) side of the tropopause break (e.g., Davies and Rossa 1998; Morgan and Nielsen-Gammon 1998; Pyle et al. 2004). The horizontal circulations accompanying these PV anomalies subsequently combine to drive a jet stream that is situated parallel to its respective tropopause break. To capture these PV anomalies, the partition scheme, much like the jet identification scheme described in Section 2.1, isolates the PV associated with each jet by considering the characteristic isentropic layers that encompass the polar and subtropical tropopause breaks.

The isentropic layers used for the jet PV partition were subjective and found to be dependent on the individual case considered. For the December 2009 Blizzard, the polar jet PV (subtropical jet PV) captured the perturbation PV at grid points in the 305-325-K (325-355-K) isentropic layer and with relative humidity less than 70%. In the 2010 Nashville Flood, the polar jet PV (subtropical jet PV) isolated the perturbation PV at grid points in the 305-335-K (335-370-K) isentropic layer and with relative humidity less than 70%. The implementation of relative humidity criteria in this partition was designed to remove the influence of proximate convection when determining the balanced flow associated with each jet species. An examination of the polar and subtropical jet PV demonstrates that their sum closely approximates the distribution and magnitude of the upper-tropospheric PV, despite not being a strict division of that piece of the PV. Consequently, an examination of the individual three-dimensional circulations tied to the

polar and subtropical jets provides detailed insight into the flow associated with the full upper-tropospheric PV.

5.2.2 PV Inversion Techniques

The technique used to invert the full and piecewise Ertel PV is identical to that described by Davis and Emanuel (1991) and is summarized here. The reader is encouraged to consult Davis and Emanuel (1991) for any additional details. In contrast to QGPV inversion, which employs geostrophy as its balance condition, an inversion of the Ertel PV utilizes the Charney (1955) non-linear balance equation. This particular balance condition is less restrictive than that imposed by geostrophy because it provides high accuracy within environments exhibiting considerable curvature. Specifically, the Charney balance equation results from taking the horizontal divergence of the equations of motion and by assuming that the non-divergent component of the flow is much larger in magnitude than the divergent component. The resultant equation in spherical coordinates is defined as:

$$\nabla^2 \Phi = \nabla \cdot (f \nabla \psi) + \frac{2}{a^4 \cos^2 \phi} \left[\frac{\partial^2 \psi}{\partial \lambda^2} \frac{\partial^2 \psi}{\partial \phi^2} - \left(\frac{\partial^2 \psi}{\partial \lambda \partial \phi} \right)^2 \right] \quad (5.1)$$

where f is the Coriolis parameter, Φ is the geopotential, ψ is the non-divergent streamfunction, λ is the longitude, ϕ is the latitude, and a is the radius of the Earth. Given that (5.1) has two unknowns, Φ and ψ , another diagnostic equation is needed to close the system of equations.

This relationship is provided by an approximation for the Ertel PV in spherical coordinates:

$$q = \frac{g \kappa \pi}{p} \left[(f + \nabla^2 \psi) \frac{\partial^2 \Phi}{\partial \pi^2} - \frac{1}{a^2 \cos^2 \phi} \frac{\partial^2 \psi}{\partial \lambda \partial \pi} \frac{\partial^2 \Phi}{\partial \lambda \partial \pi} - \frac{1}{a^2} \frac{\partial^2 \psi}{\partial \phi \partial \pi} \frac{\partial^2 \Phi}{\partial \phi \partial \pi} \right] \quad (5.2)$$

where q is the Ertel PV, g is the gravitational constant, p is the pressure, $\kappa = R_d / c_p$, and π is the Exner function $[c_p (p / p_o)^\kappa]$, which serves as the vertical coordinate.

On the lateral edges of the domain, the observed geopotential within the GFS analysis is used to prescribe Φ , while ψ is specified such that the observed component of the wind normal to the boundary is consistent with the gradient of ψ along the boundary, and by ensuring that there is no net divergence in the domain. On the top and bottom boundaries of the domain (50 hPa and 1000 hPa), hydrostatic balance and the potential temperature at 75 hPa and 975 hPa, respectively, ($\partial\Phi/\partial\pi = f(\partial\psi/\partial\pi) = -\theta$) are used to determine Φ and ψ . Successive over-relaxation (SOR) is then applied to the system of equations, (5.1-5.2), at each time in an effort to solve for Φ and ψ within the interior of the domain. Convergence on a solution to this system of equations required changing negative values of Ertel PV within the domain to a small positive constant (0.01 PVU) and by maintaining that the stability never exceeded a profile that was super-adiabatic.

The system of equations used to invert the mean PV is identical to (5.1-5.2), except with Φ and ψ on the lateral boundaries and q replaced by their 6 d time-averaged values. The potential temperature near the top and bottom boundaries is also time-averaged to aid in the determination of the mean Φ and ψ on the top and bottom boundaries using the hydrostatic equation. An inversion of the mean q for its corresponding Φ and ψ within the domain subsequently permits a determination of the perturbation fields. Given the inherent non-linearity of the terms in (5.1) and (5.2), however, an inversion of the perturbation PV subsequently requires linearizing those equations. The methodology used for this linearization is discussed at length by Davis and Emanuel (1991) and was demonstrated by Davis (1992a) and Davis et al. (1996) to be particularly effective. Following the linearization, (5.1) and (5.2) become:

$$\nabla^2\Phi_n = \nabla \cdot (f\nabla\psi_n) + \frac{2}{a^4 \cos^2\phi} \left(\frac{\partial^2\psi^*}{\partial\lambda^2} \frac{\partial^2\psi_n}{\partial\phi^2} + \frac{\partial^2\psi^*}{\partial\phi^2} \frac{\partial^2\psi_n}{\partial\lambda^2} - 2 \frac{\partial^2\psi^*}{\partial\lambda\partial\phi} \frac{\partial^2\psi_n}{\partial\lambda\partial\phi} \right) \quad (5.3)$$

$$q_n = \frac{g\kappa\pi}{p} [(f + \nabla^2\psi^*) \frac{\partial^2\Phi_n}{\partial\pi^2} + \frac{\partial^2\Phi^*}{\partial\pi^2} \nabla^2\psi_n] - \frac{1}{a^2 \cos^2\phi} \left(\frac{\partial^2\psi^*}{\partial\lambda\partial\pi} \frac{\partial^2\Phi_n}{\partial\lambda\partial\pi} + \frac{\partial^2\Phi^*}{\partial\lambda\partial\pi} \frac{\partial^2\psi_n}{\partial\lambda\partial\pi} \right) - \frac{1}{a^2} \left(\frac{\partial^2\psi^*}{\partial\phi\partial\pi} \frac{\partial^2\Phi_n}{\partial\phi\partial\pi} + \frac{\partial^2\Phi^*}{\partial\phi\partial\pi} \frac{\partial^2\psi_n}{\partial\phi\partial\pi} \right) \quad (5.4)$$

where $[]^* = [] + 1/2 \sum_{n=1}^N []_n$. Equations (5.3) and (5.4) form a linear system of equations that can then be solved using SOR to determine the Φ_n and ψ_n associated with any piece of the perturbation PV, q_n . For each piece of the perturbation PV, Φ_n and ψ_n are set to zero along the lateral boundaries and the perturbation potential temperature attributed to each piece of the PV (specified in Section 5.2.1) is used to determine Φ_n and ψ_n on the top and bottom boundaries using the hydrostatic equation.

An inversion of the full or perturbation PV using either one of the systems of equations listed above only returns the balanced non-divergent flow associated with each piece of the PV. Given the indication that vertical motions appear to play an important role in the production of a jet superposition, recovery of the balanced divergent flow associated with each piece of the PV is also required. This particular task is accomplished by solving the system of prognostic balance equations outlined in Davis and Emanuel (1991):

$$\nabla^2\Phi^t = \nabla \cdot (f\nabla\psi^t) + \frac{2}{a^4 \cos^2\phi} \left(\frac{\partial^2\psi^t}{\partial\lambda^2} \frac{\partial^2\psi}{\partial\phi^2} + \frac{\partial^2\psi}{\partial\lambda^2} \frac{\partial^2\psi^t}{\partial\phi^2} - 2 \frac{\partial^2\psi}{\partial\lambda\partial\phi} \frac{\partial^2\psi^t}{\partial\lambda\partial\phi} \right) \quad (5.5)$$

$$q^t = \frac{g\kappa\pi}{p} [(f + \nabla^2\psi) \frac{\partial^2\Phi^t}{\partial\pi^2} + \frac{\partial^2\Phi}{\partial\pi^2} \nabla^2\psi^t] - \frac{1}{a^2 \cos^2\phi} \left(\frac{\partial^2\psi}{\partial\lambda\partial\pi} \frac{\partial^2\Phi^t}{\partial\lambda\partial\pi} + \frac{\partial^2\Phi}{\partial\lambda\partial\pi} \frac{\partial^2\psi^t}{\partial\lambda\partial\pi} \right) - \frac{1}{a^2} \left(\frac{\partial^2\psi}{\partial\phi\partial\pi} \frac{\partial^2\Phi^t}{\partial\phi\partial\pi} + \frac{\partial^2\Phi}{\partial\phi\partial\pi} \frac{\partial^2\psi^t}{\partial\phi\partial\pi} \right) \quad (5.6)$$

$$\begin{aligned}
& f\eta \frac{\partial}{\partial \pi} [\pi^{1-1/\kappa} \frac{\partial}{\partial \pi} (\pi^{1/\kappa-1} \omega^*)] + \nabla^2 (\frac{\partial^2 \Phi}{\partial \pi^2} \omega^*) - \frac{f}{a^2} \frac{\partial}{\partial \pi} (\frac{\partial^2 \psi}{\partial \phi \partial \pi} \frac{\partial \omega^*}{\partial \phi} + \frac{1}{\cos^2 \phi} \frac{\partial^2 \psi}{\partial \lambda \partial \pi} \frac{\partial \omega^*}{\partial \lambda}) \\
& + (f \frac{\partial \eta}{\partial \pi} \frac{1/\kappa - 1}{\pi} - f \frac{\partial^2 \eta}{\partial \pi^2}) \omega^* = \nabla^2 (\vec{v}_h \cdot \nabla \theta) + f \frac{\partial}{\partial \pi} (\vec{v}_h \cdot \nabla \eta) - \nabla f \cdot \nabla (\frac{\partial \psi^t}{\partial \pi}) \\
& - \frac{2}{a^4 \cos^2 \phi} \frac{\partial}{\partial \pi} (\frac{\partial^2 \psi^t}{\partial \lambda^2} \frac{\partial^2 \psi}{\partial \phi^2} + \frac{\partial^2 \psi}{\partial \lambda^2} \frac{\partial^2 \psi^t}{\partial \phi^2} - 2 \frac{\partial^2 \psi}{\partial \lambda \partial \phi} \frac{\partial^2 \psi^t}{\partial \lambda \partial \phi}) - \nabla^2 \frac{d\theta}{dt}
\end{aligned} \tag{5.7}$$

$$q^t = -\vec{v}_h \cdot \nabla q - \omega^* \frac{\partial q}{\partial \pi} + \frac{g\kappa\pi}{p} \vec{\eta} \cdot \nabla \frac{d\theta}{dt} \tag{5.8}$$

$$\nabla^2 \chi + \pi^{1-1/\kappa} \frac{\partial}{\partial \pi} (\pi^{1/\kappa-1} \omega^*) = 0 \tag{5.9}$$

where the superscript, t , indicates the time tendency of a particular variable, η is the absolute vorticity, and $\vec{v}_h = \vec{v}_\psi + \vec{v}_\chi$. The five equations above provide a solution for the time tendencies of Φ , ψ , and q , in addition to the velocity potential, χ , and vertical motion field ($\omega^* = \partial \pi / \partial t = (\kappa \pi / p) \omega$)¹. To solve this system, the lateral boundaries for Φ^t , ψ^t , q^t , χ , and ω^* are set to zero, with ω^* also set to zero on the top and bottom boundaries of the domain. Φ^t and ψ^t on the top and bottom boundaries were determined using the hydrostatic relationship, $\partial \Phi^t / \partial \pi = f(\partial \psi^t / \partial \pi) = -\theta^t$, where $\theta^t = -(\vec{v}_h \cdot \nabla \theta) - \omega^*(\partial \theta / \partial \pi) + d\theta / dt$, and all diabatic heating terms ($d\theta / dt$) were calculated using (3.2) (Emanuel et al. 1987).

In an effort to isolate the values of Φ^t , ψ^t , q^t , χ , and ω^* associated with each piece of the perturbation PV, the corresponding values of Φ_n , ψ_n , and q_n associated with each piece of the PV were subtracted from the full field of Φ , ψ , and q . A solution was then found by solving (5.5-5.9) using SOR with the artificially reduced values of Φ , ψ , and q . The difference between the solution of (5.5-5.9) associated with the full fields of Φ , ψ , and q and the reduced fields of Φ , ψ , and q subsequently produced the tendencies and vertical motion field associated with each

¹ In order to converge consistently on a solution to (5.5-5.9), smoothing of the individual forcing terms in the omega equation (5.7) was required.

piece of the PV. For additional details on the process used to solve this system of equations, the reader is again referred to Davis and Emanuel (1991).

The combination of the static and prognostic PV inversions recover the balanced three-dimensional flow associated with each piece of the PV distribution (Fig. 5.4). The unbalanced portion of the flow cannot be returned via these methods and falls under a residual term, which is primarily composed of motions that correspond to the non-divergent component of the ageostrophic wind (Davis et al. 1996). In the cases considered for this study, the residual also contains a part of the observed divergent wind field, given that the vertical motions appear to be underestimated by the balanced winds in the vicinity of any organized convection that is supported by weak synoptic forcing. This is likely due to the specification that the stability must always be positive when performing the PV inversion. In the two cases examined, while the unbalanced flow can exceed 20 m s^{-1} in the immediate vicinity of the developing superposed jet, it is aligned antiparallel to and is much weaker than the balanced non-divergent flow ($\sim 80\text{-}90 \text{ m s}^{-1}$) in these locations (not shown)². Consequently, the horizontal advection of the tropopause breaks accomplished by the unbalanced flow is outweighed by the influence of the balanced flow at all times considered and the process of jet superposition, in so far as it depends on rearrangement of the tropopause, is well explained by the balanced portion of the flow.

5.2.3 Piecewise Sawyer-Eliassen Circulations

Given that transverse vertical circulations were shown to play a substantial role in the process of jet superposition from a basic-state variable perspective, it is a worthy exercise to investigate which portions of the balanced flow are responsible for the production of these

² Davis et al. (1996) also noted that the unbalanced winds were maximized on the anticyclonic shear side of the upper-level jet stream in their analysis of the ERICA-IOP-4 storm.

transverse vertical circulations. The piecewise Sawyer-Eliassen circulation equation (Sawyer 1956; Eliassen 1962), which was proposed by Morgan (1999), is shown below with the diabatic forcing term omitted:

$$\left(-\gamma \frac{\partial \theta}{\partial p}\right) \frac{\partial^2 \psi_{se}}{\partial y^2} + \left(2 \frac{\partial M}{\partial p}\right) \frac{\partial^2 \psi_{se}}{\partial y \partial p} + \left(-\frac{\partial M}{\partial y}\right) \frac{\partial^2 \psi_{se}}{\partial p^2} = 2\gamma \left(\frac{\partial U_g'}{\partial y} \frac{\partial \theta}{\partial x} + \frac{\partial V_g'}{\partial y} \frac{\partial \theta}{\partial y}\right) \quad (5.10).$$

While all variables in (5.10) are defined identically as they are in (3.1) and correspond to their unpartitioned values, U_g' and V_g' represent the perturbation geostrophic wind components associated with each piece of the PV distribution. Subsequently, the technique for partitioning a transverse vertical circulation consists of isolating the geostrophic wind distribution associated with each piece of the PV field and calculating its respective geostrophic forcing term in (5.10) within a shared cross sectional domain. Solution to (5.10) for each piece of the PV distribution then proceeds with an identical methodology for inversion as outlined in Section 3.2. Given that all operators in (5.10) are linear, the piecewise transverse vertical circulations associated with each piece of the PV field add together to produce the full geostrophic transverse vertical circulation.

5.3 Results from PV Inversions

As demonstrated in Chapter 4, an insightful way to examine the process of jet superposition is to consider the movement of the individual tropopause breaks and, specifically, to diagnose the development of the characteristic two-step tropopause structure that is associated with a superposed jet. Consequently, the following analysis utilizes the aforementioned PV partition described in Section 5.2.1 to identify the atmospheric structures whose three-dimensional circulations are responsible for reshaping the tropopause during both the 18–20

December 2009 Mid-Atlantic Blizzard and the 1–3 May 2010 Nashville Flood. Synoptic overviews of these particular superposition events were provided in Section 2.2.

5.3.1 18–20 December 2009 Mid-Atlantic Blizzard

Figure 5.5 highlights the PV advection within the 1–3–PVU channel accomplished by the balanced non-divergent and divergent winds at 300 and 200 hPa, following an inversion of the full PV at 0000 UTC 19 December. These particular isobaric levels are chosen to highlight the location of the polar and subtropical tropopause breaks³, respectively, such that diagnosed areas of positive or negative PV advection suggest a lateral movement of either tropopause break. Noting that the fill interval for PV advection by the divergent wind is smaller than that used for the non-divergent wind in this figure and in similar figures that follow, it is apparent that the non-divergent wind is responsible for a majority of the PV advection observed along each tropopause break. In particular, Fig. 5.5a indicates that the polar tropopause break outlined the boundary of a clef of high PV air that was situated over much of the central United States. At the easternmost edge of this PV clef, negative PV advection was located from Arkansas southeastward towards the Gulf of Mexico while a strip of positive PV advection stretched from the southern Great Lakes to northern Florida. Together, these observations suggest a translation of the easternmost portions of the PV clef towards the northeast.

Along the subtropical tropopause break, a region of negative PV advection by the non-divergent wind was situated south of New Orleans and eastward across the Florida peninsula, encouraging a poleward shift of the subtropical waveguide in those locations (Fig. 5.5b). While the 300 hPa divergent wind in Fig. 5.5c appears to do little to counteract the diagnosed

³ Given that these two levels correspond approximately to the level of maximum wind for each jet species, an analysis performed on isentropic surfaces produced similar results.

northeastward translation of the 300 hPa PV clef by the non-divergent wind, the 200 hPa divergent wind was responsible for a strip of negative PV advection along the subtropical tropopause break over Mexico and the western Gulf of Mexico (Fig. 5.5d). This strip of negative PV advection was comparable in magnitude to a local maximum in positive PV advection by the non-divergent flow in the same location (Fig. 5.5b). Consequently, little eastward translation of the subtropical tropopause break over portions of central Mexico and the western Gulf of Mexico is diagnosed at this time.

Consistent with the preceding analysis, Fig. 5.6 indicates that the subtropical tropopause break remained stationary over Mexico and the western Gulf of Mexico at 1800 UTC 19 December, but had migrated farther poleward over the Florida peninsula. At 300 hPa, the PV clef associated with the polar tropopause break pivoted cyclonically over the eastern United States, such that the southernmost portion of the polar tropopause break was now aligned parallel to its subtropical counterpart. At this time, the polar tropopause break was characterized by positive (negative) PV advection by the non-divergent wind along the downstream (upstream) portion of the 300 hPa PV clef, indicating a continued downstream propagation of that feature (Fig. 5.6a). In the section of the polar tropopause break that was aligned parallel to the subtropical tropopause break, however, the PV advection was noticeably weak and any influence by the 300 hPa divergent wind was not substantial (Fig. 5.6c).

The subtropical tropopause break at 1800 UTC 19 December remained characterized by positive PV advection by the non-divergent wind downstream of the low-latitude trough west of Mexico (Fig. 5.6b). Almost entirely counteracting this region of positive PV advection was a strengthened strip of negative PV advection by the 200 hPa divergent wind along the same stretch of the subtropical tropopause break, implying that the break would remain relatively

stationary in this location (Fig. 5.6d). These 200 hPa divergent winds were associated, in particular, with a minimum in velocity potential over the Yucatan peninsula that was likely tied to the ongoing tropical convection observed over the eastern equatorial Pacific (Fig. 4.1). Patches of negative PV advection by the non-divergent wind along the subtropical tropopause break are also noted to the east of South Carolina (Fig. 5.6b), which continued to suggest a poleward migration of this portion of the subtropical waveguide.

Further insight into the diagnosed lateral movements of the polar and subtropical tropopause breaks at 1800 UTC 19 December can be found by considering the individual non-divergent circulations recovered from the piecewise PV inversion described in Section 5.2. The PV advection along the polar and subtropical tropopause breaks accomplished by the piecewise non-divergent circulations at 1800 UTC 19 December is shown in Fig. 5.7. Note that contributions from the surface PV are not included in Fig. 5.7 as they were found to be negligible. Along the polar tropopause break, Fig. 5.7a indicates that the mean PV was associated with a confluent flow over much of the eastern United States that produced a region of negative PV advection along the western edge of the 300 hPa PV clef and a strip of positive PV advection from northern Georgia to eastern Massachusetts. Counteracting the positive PV advection by the mean non-divergent wind over the Mid-Atlantic was a strip of negative PV advection in the same location that was driven by a perturbation southerly wind associated with the upper-tropospheric PV (Fig. 5.7c). Given that the flow associated with the interior PV suggested no discernible advection of the polar tropopause break (Fig. 5.7e), it can be concluded that the lack of horizontal PV advection along the southernmost portion of the polar tropopause break in Fig. 5.6a is a direct result of the competing influences of the mean and upper-tropospheric non-divergent winds. The southerly wind associated with the upper-tropospheric

PV is responsible, however, for the majority of the positive PV advection observed in Fig. 5.6a along the New-York-Pennsylvania border and, consequently, contributes to the diagnosed downstream translation of the 300 hPa polar trough by the full non-divergent wind.

At 200 hPa, Fig. 5.7b indicates that the mean non-divergent wind was primarily responsible for the strip of positive PV advection in Fig. 5.6b that was observed downstream of the low-latitude trough along the subtropical tropopause break. Further east, the mean non-divergent wind acted to drive localized patches of positive and negative PV advection off the coast of South Carolina. In this same location, Fig. 5.7d shows that the upper-tropospheric non-divergent wind was responsible for a spatially continuous strip of negative PV advection along the subtropical tropopause break. The combination of these two advection patterns accounts for the resultant maxima in negative PV advection observed in Fig. 5.6b off the coast of South Carolina and, subsequently, for the subtropical tropopause break's diagnosed poleward migration in that location. While the non-divergent circulation associated with the interior PV at 200 hPa in Fig. 5.7f was rather weak, its associated anticyclonic circulation situated over the Gulf of Mexico did produce a small region of negative PV advection along the subtropical tropopause break over Mexico. This result suggests that the interior non-divergent wind only made a minor contribution at this time by slightly counteracting the eastward translation of the low-latitude trough encouraged by the mean wind.

Given that the upper-tropospheric non-divergent wind, in addition to the mean, made the most substantial contribution to the observed advection patterns at 1800 UTC 19 December, additional insight can be gained by examining the non-divergent circulations associated with the polar and subtropical jet PV. Recall that while these two pieces of the PV distribution are not a strict partition of the upper-tropospheric PV, the sum of the polar and subtropical jet PV closely

approximates the distribution of the upper-tropospheric PV at the isobaric levels considered. The individual circulations associated with the polar and subtropical jet PV at 300 and 200 hPa are shown in Fig. 5.8. Figures 5.8a,c indicate that the non-divergent circulations tied to both the polar and subtropical jet PV appear to contribute equally to the observed PV advection patterns along the polar tropopause break in Fig. 5.7c. Along the subtropical tropopause break, however, Fig. 5.8d shows that the non-divergent circulation associated with the subtropical jet PV accounts for a large fraction of the total negative PV advection that is observed along the subtropical tropopause break in Fig. 5.7d. Particularly notable is that the non-divergent zonal flow associated with the polar jet PV is rather weak at 200 hPa, which suggests that the strong static stability in the stratosphere above the polar jet limited the vertical penetration depth of its non-divergent circulation and, consequently, its ability to significantly advect the subtropical tropopause break (Fig. 5.8b). As a result, it can be concluded that the non-divergent circulation associated with the subtropical jet had a much greater influence on horizontally advecting *both* tropopause breaks.

Also of significance from Fig. 5.6 was the diagnosed region of negative PV advection by the 200 hPa divergent wind along the subtropical tropopause break that acted to slow the eastward translation of the low-latitude trough west of Mexico. A partition of the PV advection accomplished by the divergent wind at 200 hPa is shown in Fig. 5.9, which demonstrates that the mean, upper-tropospheric, and interior divergent wind all contributed to the production of negative PV advection along the subtropical tropopause break. A closer examination illuminates a few subtle differences, however. In particular, Fig. 5.9a indicates that the mean divergent wind accounted for most of the negative PV advection that was observed from south of New Orleans to off the coast of South Carolina. Meanwhile, the upper-tropospheric and interior divergent

wind primarily contributed to the negative PV advection that occurred immediately downstream of the low-latitude trough (Figs. 5.9b,c). Consequently, it is reasonable to conclude that the ongoing tropical convection in the eastern equatorial Pacific and the presence of the low-latitude trough combined constructively to produce a 200 hPa divergent wind that slowed the eastward translation of the low-latitude trough encouraged by the mean non-divergent wind. However, also of importance was the longevity and stagnant nature of the flow pattern at low-latitudes that permitted a portion of the divergent wind to be attributable to the mean PV. This mean divergent wind, in particular, helped to facilitate the poleward migration of the subtropical tropopause break in the vicinity of the Florida peninsula.

A synthesis of the preceding analysis at 1800 UTC 19 December suggests that the mean and upper-tropospheric non-divergent wind conspired to translate the 300 hPa PV clef northeastward with negligible PV advection observed along the polar tropopause break on the southernmost edge of the PV clef. Along the subtropical tropopause break, the mean and upper-tropospheric non-divergent wind, in conjunction with the mean divergent wind, promoted a poleward migration of the tropopause break east of the South Carolina coast. Further upstream, however, both the 200 hPa divergent wind and interior non-divergent wind were essential in stalling the eastward translation of the low-latitude trough west of Mexico encouraged by the mean non-divergent wind. Both the presence of the low-latitude trough and tropical convection over the eastern equatorial Pacific were presumed to be the source of these 200 hPa divergent winds. Despite the insights gained from this partition of the PV advection patterns in the vicinity of both tropopause breaks, little evidence exists to suggest that differential horizontal advection was responsible for the development of a two-step tropopause structure 18 h later over the southeastern United States.

With that in mind, recall from Chapter 4 that the subsiding branch of the transverse vertical circulation associated with the dual jet structure was favorably located to aid in the production of the superposed jet's two-step tropopause structure (Fig. 4.4b). Consequently, consideration of the superposition process in this case from a PV perspective must also account for the role of vertical motion. Figure 5.10a shows the total vertical motion field recovered from an inversion of the full prognostic balance equations at 1800 UTC 19 December, which is characterized by a strip of subsidence at 400 hPa that is centered squarely between the polar and subtropical tropopause breaks across the southeastern United States. This result lends further support to the notion that subsidence played an integral role in the production of a superposed jet in the absence of differential horizontal advection by lowering the height of the subtropical tropopause step along the entire length of the region where the two jets paralleled one another.

As for the non-divergent and divergent wind fields, additional insight can be gained through a partition of the vertical motion field. A careful examination of Fig. 5.10 suggests that the largest fraction of subsidence upstream of Georgia in the vicinity of the two tropopause breaks is forced by the flow associated with the upper-tropospheric PV (Fig. 5.10c). Further downstream into the Carolinas, however, more substantial contributions to the subsidence are provided by the flow associated with the interior and surface PV (Figs. 5.10d,e). So, while the non-divergent circulations associated with the surface and interior PV had, at most, minor impacts on laterally displacing the location of the tropopause breaks, this analysis indicates that they still played an important role by fostering the production of vertical motions conducive for restructuring the tropopause in the vicinity of the surface cyclone. Finally, it is apparent that a large portion of the vertical motion field is accounted for by the flow associated with the total

perturbation PV, as the mean flow only forces weak subsidence over the southern Mississippi River valley (Fig. 5.10b).

Given the role that transverse vertical circulations are believed to play in restructuring the tropopause in this particular event, it is also necessary to determine the fraction of subsidence in Fig. 5.10 that is attributable to these transverse circulations. Consequently, the balanced geostrophic wind recovered from an inversion of the full PV field is used to force the Sawyer-Eliassen circulation equation along the cross section L-L' identified in Fig. 5.10a⁴. As expected, the resultant transverse vertical circulation, shown in Fig. 5.11a, is similar to that in Fig. 4.4b. The two circulations are not exact, however, since the diabatic forcing term was not included in the inversion of the Sawyer-Eliassen circulation for this analysis. Nevertheless, Fig. 5.11a depicts a strong thermally direct circulation with subsidence situated directly on and beneath the subtropical tropopause step. The lateral extent of this circulation is also likely enhanced by the reduced inertial stability equatorward of the dual jet structure. For comparison, the magnitude of the subsidence at 400 hPa in Fig. 5.11a is about 4 dPa s^{-1} , or an overestimate of the total subsidence recovered from the full prognostic PV inversion shown in Fig. 5.11b by roughly 1 dPa s^{-1} . Despite this overestimate, it is evident that the transverse vertical circulation accounts for a majority of the total subsidence observed between the two jet cores and there is strong qualitative agreement on the placement of subsidence in Figs. 5.11a,b.

The total transverse vertical circulation shown in Fig. 5.11a can also be partitioned into components that are forced by the geostrophic wind associated with individual pieces of the PV distribution. For instance, Figs. 5.11c,d show the individual transverse vertical circulations that are forced by the mean and perturbation geostrophic wind, respectively, which suggest that the

⁴ The bounds of the cross section L-L' are taken to be identical to those in Figure 4.4b, for comparison.

perturbation geostrophic wind forces the largest fraction of the subsidence observed in the full transverse vertical circulation. Most illuminating, however, is the more granular partition of the perturbation transverse circulation shown in Fig. 5.12. Upon examination of the transverse vertical circulations shown in Figs. 5.12a,b,c, it is apparent that circulation forced by the upper-tropospheric geostrophic wind accounts for a majority of the full perturbation circulation shown in Fig. 5.11d. Specifically, Fig. 5.12a shows that the transverse vertical circulation associated with the upper-tropospheric PV consisted of dipole circulations, with a thermally direct (indirect) circulation to the south (north) of an area of focused descent on and beneath the subtropical tropopause step. While the contribution from the surface geostrophic wind appears to be negligible (Fig. 5.12c), a minor contribution to the observed subsidence in Fig. 5.11d was forced by the interior geostrophic wind. Specifically, Fig. 5.12b shows that the transverse vertical circulation associated with the interior geostrophic wind was characterized by a weak thermally direct circulation that was shifted towards the equatorward side of the polar tropopause break, such that weak descent was present beneath the polar tropopause fold.

Given that the large majority of the subsidence in Fig. 5.11d was accounted for by the transverse vertical circulation tied to the upper-tropospheric PV, Figs. 5.12d,e highlight the individual transverse circulations associated with the polar and subtropical jet PV, respectively. Upon consideration of these two panels, it appears that the geostrophic wind associated with the polar jet PV forces the majority of the upper-tropospheric transverse vertical circulation shown in Fig. 5.12a. This result may largely be a function of the proximity of the strongest mid-tropospheric baroclinicity to the polar jet's horizontal geostrophic circulation. Since the geostrophic forcing term in the Sawyer-Eliassen circulation equation (5.10) is characterized by products of first derivatives of the geostrophic wind and the temperature gradient, the strongest

forcing for a transverse vertical circulation within a dual jet environment is likely to reside in the location of the strongest mid-tropospheric baroclinicity, or beneath the polar jet. Subsequently, the horizontal geostrophic circulation associated with the subtropical jet must penetrate through a greater depth of the troposphere before it can interact with the polar jet's baroclinicity to force a transverse circulation. Therefore, while the non-divergent circulation associated with the subtropical jet appeared to exert a greater influence on the *lateral* displacement of the individual tropopause breaks, the horizontal geostrophic circulation associated with the polar jet more strongly controlled the production of subsidence from Kansas to Georgia that was essential to the development of a superposition in this case.

Recall from Fig. 5.10, however, that locations downstream of Alabama were characterized by much greater contributions to the vertical motion field from the flow associated with the interior and surface PV. Given that these locations were in closer proximity to the deepening surface cyclone and its associated precipitation shield, it is conceivable that the horizontal circulations associated with the interior and surface PV became more capable of forcing vertical motions in the 18 h prior to superposition. To investigate this possibility further, Fig. 5.13 shows the individual Sawyer-Eliassen circulations forced by a piecewise partition of the geostrophic wind at 0000 UTC 20 December along the cross section M-M' in Fig. 5.10e. The choice of a later time than that shown in Fig. 5.10 captures the nature of the transverse vertical circulations as the surface cyclone was in the midst of its most rapid period of intensification and helps to illustrate the persistence of subsidence in fostering a jet superposition.

Figure 5.13a demonstrates that the full geostrophic Sawyer-Eliassen circulation at 0000 UTC 20 December bore much similarity to the full transverse vertical circulation shown in Fig. 5.11a. Although the circulation was slightly weaker, it was still characterized by a thermally

direct circulation that was shifted towards the equatorward side of the dual jet structure, such that descent was positioned on and beneath an eroding subtropical tropopause step. Much like the upstream transverse vertical circulation, an initial partition of the mean and perturbation components of this circulation illustrated that a majority of the circulation, and resultant subsidence, is driven by the perturbation geostrophic wind (Figs. 5.13b,c). Further partitioning of the perturbation transverse circulation illustrates some notable differences from the vertical circulation that was dissected further upstream 6 h earlier, however.

Specifically, Fig. 5.13d indicates that the transverse vertical circulation forced by the upper-tropospheric geostrophic wind featured two thermally indirect circulation cells that straddled a minimum in streamfunction beneath the jet core. This configuration produced a narrow strip of subsidence that was positioned directly on and beneath the subtropical tropopause step and that accounted for roughly half of the total subsidence shown in Fig. 5.13c. In contrast to the upstream transverse circulation, however, the interior geostrophic wind in this location drove a more substantial thermally direct circulation that positioned stronger descent directly beneath the polar tropopause break (Fig. 5.13e). Furthermore, Fig. 5.13f indicates that while the surface-driven transverse vertical circulation did not contribute much to the total perturbation subsidence, it was noticeably stronger than in the transverse vertical circulation dissected further upstream. Consequently, while the upper-tropospheric geostrophic wind continued to be the dominant mechanism for producing subsidence beneath the subtropical tropopause step, it is worth noting that the interior and surface geostrophic wind contributed more significantly to the total transverse vertical circulation diagnosed near the developing surface cyclone.

A synthesis of the impact the partitioned three-dimensional flow had on the tropopause structure can be made in the context of Fig. 5.14, which depicts the horizontal PV advection by

the total non-divergent and divergent wind along each tropopause break at 1200 UTC 20 December. Consistent with the diagnosis from Fig. 5.6, it is clear that the non-divergent wind has translated the 300 hPa PV clef towards the northeast. At the same time, however, it is also evident that the polar tropopause break along the southernmost edge of the PV clef has migrated to lower latitudes, which is a direct consequence of the subsidence forced by transverse vertical circulations along the length of the dual jet structure. On the other hand, the subtropical tropopause break migrated slightly poleward over the southeastern United States, in response to the negative PV advection diagnosed in that location 18 h earlier by the non-divergent and divergent wind (Fig. 5.6). The subtropical tropopause break remained stationary over portions of the western Gulf of Mexico, as well, in response to the influence of the 200 hPa upper-tropospheric and interior divergent wind to stall the eastward translation of the low-latitude trough.

Ultimately, the distribution of PV advection at 1200 UTC 20 December along both tropopause breaks does little to refute the importance of vertical motions in fostering the development of the two-step tropopause structure over the southeastern United States. Specifically, Fig. 5.14 indicates that no substantial regime of horizontal PV advection developed along either tropopause break in the intervening 18 h that would have further encouraged jet superposition via differential horizontal advection of the two tropopause breaks. Consequently, it can be concluded that while the horizontal non-divergent circulations aided in positioning the polar and subtropical tropopause breaks in close proximity to one another, it was the presence of subsidence, and particularly the subsidence forced by transverse vertical circulations in the dual jet environment, that was essential for the production of a superposition.

5.3.2 1–3 May 2010 Nashville Flood

As in the previous case, this analysis of the 1–3 May 2010 Nashville Flood focuses on the development of the characteristic two-step tropopause structure associated with the superposed jet. At 0000 UTC 1 May 2010, Fig. 5.15 indicates that the polar tropopause break outlined a clef of high PV air situated over the western United States while the subtropical tropopause break was zonally oriented across Mexico and the southern United States. Figure 5.15a shows that the 300 hPa non-divergent wind was responsible a strip of positive PV advection along the polar tropopause break over Baja California and northern Mexico with rather negligible PV advection observed further downstream over the Central and Southern Plains. In the same locations, Fig. 5.15c demonstrates that an easterly 300 hPa divergent wind produced a continuous strip of negative PV advection along the polar tropopause break from Baja California northeastward into western Iowa. Together these two observations suggest that, while the divergent wind acted to slow an eastward motion of the mid-latitude trough over northern Mexico, it also clearly supported a slight westward propagation of the polar tropopause break over the Central and Southern Plains at this time. Along the subtropical tropopause break, the 200 hPa non-divergent wind is responsible for localized maxima in negative PV advection stretching from southern Baja California eastward to Alabama (Fig. 5.15b). Given that that the subtropical tropopause break was aligned approximately parallel to the 200 hPa divergent wind, Fig. 5.15d indicates no diagnosed PV advection by the divergent wind along the break. Consequently, it is clear that the non-divergent wind acted alone at this time to encourage a poleward shift in the location of the subtropical tropopause break over northern Mexico and the Southern Plains.

By 1200 UTC 1 May, the subtropical tropopause break had migrated substantially farther poleward in response to the negative PV advection diagnosed at the prior time by the non-

divergent wind over portions of Texas and the southern Mississippi River valley (Fig. 5.16). In addition, the presence of convection over the southeastern United States aided in the substantial erosion of upper-tropospheric PV over much of the eastern United States (Fig. 2.5), given the absence of any diagnosed PV advection at the prior time in this location. Further upstream, Fig. 5.16 shows that the base of the western U.S. trough migrated a bit further to the east, allowing the polar tropopause break to vertically superpose with the subtropical tropopause break over Baja California and northern Mexico⁵. Downstream of the trough axis over the Central Plains, however, the polar tropopause break was located a bit farther west of its previous location, consistent with the diagnosed negative PV advection by the 300 hPa divergent wind at 0000 UTC 1 May (Fig. 5.15c).

Figures 5.16a,c continue to show that the polar tropopause break was characterized by positive (negative) PV advection by the non-divergent (divergent) wind over northern Mexico and the Southern Plains 12 h prior to superposition. Given that the PV advection by the non-divergent wind remained larger in magnitude than that accomplished by the divergent wind, it is clear that the 300 hPa divergent wind largely slowed the eastward translation of the deep mid-latitude trough over the western United States. Meanwhile, the subtropical tropopause break remained associated with a strip of negative PV advection by the 200 hPa non-divergent wind from northern Texas into Arkansas, which continued to encourage a poleward translation of that tropopause break in those locations (Fig. 5.16b). In contrast to the prior time, however, Fig. 5.16d indicates that the subtropical tropopause break was no longer characterized by a zonal orientation and was subsequently more susceptible to PV advection by the 200 hPa easterly divergent wind. This is particularly evident by the development of a strip of negative PV

⁵ Note that this particular location was not characterized by a superposed jet (Fig. 2.5c), as the jet identification method also requires satisfying an integrated wind speed criterion.

advection in Fig. 5.16d over portions of northern Mexico and western Texas. Consequently, it appears that the 200 hPa non-divergent and divergent winds worked in concert at this time to facilitate a diagnosed poleward and westward translation of the subtropical tropopause break.

Taken together, the slow eastward propagation of the polar tropopause break over northern Mexico and eastern New Mexico and the continued poleward and westward translation of the subtropical tropopause break appears conducive for the vertical superposition of the two tropopause breaks over the Southern Plains by 0000 UTC 2 May. Consequently, greater insight into the production of the PV advection patterns in Fig. 5.16 can be found by partitioning the flow in line with the schemes discussed in Section 5.2. To this aim, Fig. 5.17 shows the piecewise PV advection accomplished by the mean, upper-tropospheric, and interior non-divergent wind. As in the December 2009 case, the contributions from the non-divergent wind associated with surface PV were negligible and are not shown in the subsequent analysis.

Figure 5.17a shows that the mean non-divergent wind produced negative (positive) PV advection along portions of the polar tropopause break that were upstream (downstream) of the western United States trough. Consequently, the predominantly zonal flow associated with the mean PV was responsible for encouraging the diagnosed eastward propagation of the deep trough over the western United States. Examination of Fig. 5.17c indicates that the upper-tropospheric non-divergent circulation was characterized by a cyclonic circulation centered over the Gulf of California and a broad anticyclone over the eastern United States. The juxtaposition of these circulation anomalies produced a perturbation southerly wind over the Central and Southern Plains that accounted for only weak negative PV advection along the polar tropopause break at this time, given that the streamlines paralleled the polar tropopause break. Figure 5.17e also indicates that, while the anticyclonic circulation over eastern Canada associated with the

interior PV promoted negative PV advection along the polar tropopause break in Iowa and Wisconsin, negligible PV advection is observed over the Southern Plains in the vicinity of where the two jets would later superpose. Consequently, the non-divergent circulations associated with the upper-tropospheric and interior PV appeared to only slightly mitigate the tendency for the mean non-divergent wind to translate the western trough and polar tropopause break eastward.

As previously mentioned, the subtropical tropopause break was characterized by a southwest-to-northeast orientation at 1200 UTC 1 May over portions of the Southern Plains. Consequently, this section of the tropopause break was now associated with a strip of positive PV advection by the rather zonal, mean non-divergent wind (Fig. 5.17b). In contrast to the polar tropopause break, however, Fig. 5.13d indicates that the subtropical tropopause break was positioned at a more perpendicular angle to the upper-tropospheric non-divergent wind over the Southern Plains. Consistent with this observation, Fig. 5.13d depicts a much stronger region of negative PV advection along the subtropical tropopause break from northern Mexico into Arkansas that was roughly the same magnitude, or greater than, the positive PV advection encouraged by the mean non-divergent wind. Figure 5.13f shows that the anticyclonic circulation associated with the interior PV over eastern Canada only contributed a band of negative PV advection at 200 hPa over the central Mississippi River valley, with no substantial PV advection diagnosed over the Southern Plains. Consequently, it appears that the horizontal non-divergent wind associated with the interior PV, and subsequently, the ongoing convection, did not contribute much to the lateral translation of the subtropical tropopause break over the Southern Plains. Instead, it appears that the upper-tropospheric non-divergent wind played a substantial role in fostering the development of a superposition by stalling the eastward translation of the subtropical tropopause break and by displacing it farther poleward over north Texas and

Oklahoma. As a result, the subtropical tropopause break was in a favorable position to be undercut by the advancing polar tropopause break associated with the eastward propagating trough over the western United States.

Given the significant role that the upper-tropospheric non-divergent wind appears to have played in facilitating the vertical superposition of the individual tropopause breaks via horizontal displacement, additional insight can be gathered by considering the non-divergent circulations associated with the polar and subtropical jet PV at 1200 UTC 1 May. Figure 5.18a demonstrates that the non-divergent circulation associated with the polar jet PV is only responsible for a compact region of negative PV advection along the polar tropopause break over portions of west Texas and southeastern New Mexico. Similar to the December 2009 Blizzard, the polar jet's non-divergent circulation is far weaker at 200 hPa, producing negligible PV advection along the subtropical tropopause break over the Southern Plains (Fig. 5.18b). Meanwhile, the non-divergent circulation associated with the subtropical jet PV also promoted a localized region of negative PV advection over western Mexico along the polar tropopause break (Fig. 5.18c). Consequently, it appears that the strip of negative PV advection observed in Fig. 5.17c along the polar tropopause break is a product of the non-divergent circulations associated with *both* the polar and subtropical jet PV. However, Fig. 5.18d indicates that the subtropical jet's non-divergent circulation accounted for the large majority of the negative PV advection observed along the subtropical tropopause break at 200 hPa. Therefore, as in the December 2009 case, the non-divergent circulation associated with the subtropical jet PV had a more substantial ability to influence the lateral displacement of both tropopause breaks.

A major component of the non-divergent circulation associated with the subtropical jet PV (and upper-tropospheric PV) in this case is the broad anticyclonic circulation that was

positioned directly over the Gulf coast. In an effort to gain additional insight into the development of this circulation feature, Fig. 5.19 depicts a series of backward trajectories initialized at 12 km above ground level at the center of the upper-tropospheric anticyclone centered over the Gulf coast in Fig. 5.18d. Trajectories were calculated using the NOAA/ARL HYSPLIT model (Draxler and Hess 1997; Draxler and Hess 1998; Draxler 1999; Draxler and Rolph 2015; Rolph 2015), which was initialized at 1200 UTC 1 May and run backwards 60 h to 0000 UTC 29 April. An examination of Fig. 5.19 indicates that all trajectories originated in the upper troposphere over the tropical Pacific ($\sim 10^{\circ}\text{N}$) between 150°W and 120°W . While roughly two-thirds of the trajectories exhibit some slight anticyclonic curvature as they leave the tropics, the remaining third are characterized by cyclonic curvature southeast of Hawaii. The latter trajectories, in particular, highlight the presence of a relatively stationary low-latitude trough that appears to have facilitated the transport of a poorly stratified, upper-tropospheric tropical air mass towards the Gulf coast.

From a PV perspective, the upper-tropospheric anticyclone shown in Fig. 5.18d must be associated with a negative PV anomaly and a localized reduction in the static stability. Consequently, the transport of a poorly stratified environment from the equatorial Pacific supports the existence of a negative PV anomaly in the vicinity of the Gulf coast. Further consideration of the trajectories in Fig. 5.19 also indicates that all air parcels were characterized by potential temperatures between 340-355-K (not shown) and by gentle subsidence and drying as they moved towards the Gulf coast. With this in mind, and recalling that the subtropical jet PV isolates grid points in the 340-355-K isentropic layer with low relative humidity, the presence of the perturbation anticyclone in Fig. 5.18d cannot correspond to saturated ascent from the proximate convection over the southeastern United States, but instead embodies a prolonged and

balanced atmospheric response to the export of a poorly stratified, upper-tropospheric tropical air mass into the subtropics.

An examination of Fig. 5.16, as well as the analysis in Chapter 4, suggests that the 200 hPa divergent wind also played a particularly important role in the poleward and westward displacement of the subtropical tropopause break during the May 2010 Nashville Flood. Consequently, Fig 5.20 considers the piecewise PV advection accomplished by mean, upper-tropospheric, and interior 200 hPa divergent wind. Given that the deep trough over the western United States was a particularly stationary feature throughout the week of the event (Fig. 2.5), Fig. 5.20a depicts a minimum (maximum) in the mean velocity potential immediately downstream (upstream) of the trough axis. This dipole acted to drive an easterly mean divergent wind that was responsible for a weak strip of negative PV advection over northern Mexico and west Texas. Figure 5.20b shows that the upper-tropospheric divergent wind, which was also tied to the presence of the mid-latitude trough, was responsible for a weak strip of negative PV advection in a similar location along the United States-Mexico border.

An examination of Fig. 5.20c suggests that the interior divergent wind did not contribute much to the total negative PV advection accomplished by the 200 hPa divergent wind (Fig. 5.16d). It is important to note, however, that the divergent wind and advection patterns shown in Fig. 5.16d and Fig. 5.20c underestimate the role of ongoing convection over portions of the southern Mississippi River valley at this time. Given that this area of convection was not associated with strong synoptic scale forcing (Moore et al. 2012), a solution for the vertical motion at this time, through an inversion of the PV tendency equations, does not capture the full extent of the ascent over the southern Mississippi River valley (Fig. 5.21a). Consequently, it is extremely likely that the interior divergent flow contributed more substantially to the negative

PV advection along the subtropical tropopause break at this time than what is indicated by Fig. 5.16d and Fig. 5.20c. Such a conclusion is supported by the analysis of the model-derived divergent wind field shown in Fig. 4.8 and upon consideration of the unbalanced wind field (not shown).

While the non-divergent and divergent wind associated with individual pieces of the PV appear to sufficiently account for the development of a jet superposition over portions of west Texas and Oklahoma by 0000 UTC 2 May via differential horizontal advection, it remains a worthy exercise to consider the role that vertical motions may have played in restructuring the tropopause. Figure 5.21a depicts the full 400 hPa vertical motion field at 1200 UTC 1 May recovered from an inversion of the prognostic balance equations. Upon examination of this panel, it is clear that the deep trough over the western United States was associated with a dipole in vertical motion, with ascent (descent) downstream (upstream) of the trough axis. The diagnosed linear strip of descent located upstream of the trough axis further supports the notion that transverse vertical circulations contributed to the development of a polar tropopause fold in that location, as discussed in the previous chapter (Fig. 4.7). In addition, Fig. 5.21a indicates that the band of ascent found downstream of the trough axis was positioned between the polar and subtropical tropopause breaks over much of west Texas.

A cross section of the balanced upward vertical motion along the line N-N' in Fig. 5.21a confirms this observation, depicting a focused area of ascent that was maximized around 500 hPa directly beneath the subtropical tropopause step (Fig. 5.21b). In contrast to the December 2009 Blizzard, where descent between the two jet cores was favorably positioned to foster a downward displacement of the subtropical tropopause step, the presence of ascent between the two jets in this case does not appear to be conducive for the vertical displacement of the

subtropical tropopause step. Specifically, the decreasing magnitude of the ascent above 500 hPa and the strong static stability of the stratosphere suggest that a rapid upward displacement of the subtropical tropopause step would be unlikely in the absence of strong diabatic heating⁶. This assertion is further bolstered by observations of the altitude of subtropical tropopause step throughout the duration of this 2010 Nashville Flood, which show little to no change in the height of the subtropical tropopause step over the Southern and Central Plains in the 24 h prior to superposition (not shown).

Upon jet superposition over the Southern Plains at 0000 UTC 2 May, Fig. 5.22 demonstrates that the polar tropopause break had indeed translated further to the east over central Texas and Oklahoma, consistent with the diagnosed eastward propagation of the western trough at the prior time. Meanwhile, the subtropical tropopause break remained stationary over portions of west Texas, where it became vertically superposed with the polar tropopause break, and was located considerably farther poleward over portions of Kansas and Missouri. Consequently, the 200 hPa divergent wind, the 200 hPa upper-tropospheric non-divergent wind, and the diabatic erosion of upper-level PV accompanying the convection clearly acted in concert to position the subtropical tropopause break in a location where it was undercut by the eastward advancing western United States trough.

A synthesis of the above analysis indicates that, in contrast to the December 2009 case, jet superposition during the May 2010 Nashville Flood is largely driven by the lateral displacement of the polar and subtropical tropopause breaks by the non-divergent and divergent wind. Specifically, an examination of the horizontal non-divergent wind field 12 h prior to superposition indicated that the upper-tropospheric non-divergent wind, and particularly that

⁶ Radar analysis at 1200 UTC 1 May only depicts scattered showers over portions of central and western Texas. Consequently, it is not believed that the diabatic heating associated with this activity was widespread or strong enough to substantially erode the upper-tropospheric PV between the two jet cores.

associated with the subtropical jet, was instrumental in facilitating the displacement of each individual tropopause break along with the mean flow over the Southern Plains. While a diagnosis of the balanced vertical motions indicated ascent beneath the subtropical tropopause step and between the two jet cores 12 h prior to superposition, it was concluded that the strong static stability of the lower stratosphere precluded any substantial upward displacement of the subtropical tropopause step in the absence of any notable diabatic heating.

5.4 Discussion

A benefit to employing a PV perspective to examine jet superpositions is the ability to partition the flow into dynamically significant pieces. Consequently, one is afforded a greater ability to examine the interactions between the three-dimensional circulations associated with different atmospheric structures throughout the development of a superposed jet. For this study, a standard three-way partition of the perturbation PV, similar to that employed by Korner and Martin (2000), is applied to both the 18–20 December 2009 Mid-Atlantic Blizzard and the 1–3 May 2010 Nashville Flood. This partition, which isolates the balanced flow associated with dynamical structures in the upper troposphere, near the surface, and tied to latent heating, was specifically applied to examine the development of a superposed jet's characteristic two-step tropopause structure.

In the upper troposphere, an individual tropopause break can be characterized by the horizontal juxtaposition of a cyclonic and anticyclonic PV anomaly. A jet streak is then positioned between the cyclonic and anticyclonic PV anomalies, as the horizontal circulations that accompany each anomaly constructively combine to drive a strong anomalous flow parallel to the proximate tropopause break. In the traditional three-way partition described above, the

individual PV anomalies attributable to each jet species are buried within the upper-tropospheric PV. Unfortunately, this fact precludes determination of which jet species has a stronger influence on reshaping the tropopause into its characteristic two-step structure during a superposition event. To address this complication, this study utilized an additional PV partition that determines the balanced circulations associated with each jet species by isolating the PV within isentropic layers characteristic to each jet. The sum of the PV associated with each jet species was found to be approximately equal to the upper-tropospheric PV in both cases considered.

An examination of these two cases from a PV perspective provides additional evidence supporting the mechanisms identified in Chapter 4 as important to the development of a superposition. During the December 2009 Mid-Atlantic Blizzard, the analysis indicated that the horizontal non-divergent and divergent wind fields were important in positioning the two tropopause breaks such that they were parallel to one another prior to superposition. However, no systematic patterns of horizontal PV advection were diagnosed along either tropopause break to suggest superposition through lateral displacement of the tropopause breaks. Consequently, transverse vertical circulations were diagnosed as essential to the process of superposition by positioning subsidence on and beneath the subtropical tropopause step along the entire channel where the two jets paralleled one another. This subsidence was responsible for a downward displacement of the subtropical tropopause step and the development of the superposed jet's two-step tropopause structure.

In contrast, the analysis of the May 2010 Nashville Flood diagnosed a strip of ascent beneath the subtropical tropopause step 12 h prior to superposition over the Southern Plains. Such a configuration, in the absence of substantial diabatic heating, was determined to not be conducive for the development of a two-step tropopause structure, given the strong static

stability residing in the lower stratosphere that would deter any substantial vertical advection of subtropical tropopause step. Despite the conclusion that vertical motions did not substantially restructure the tropopause during the May 2010 Nashville Flood, the analysis indicated that the divergent wind (though underestimated by the PV inversion) was important to the horizontal displacement of the two tropopause breaks. The presence of convection over the southern Mississippi River valley also played a significant role by diabatically eroding upper-tropospheric PV over much of the eastern United States.

In addition to the role of proximate convection, insights garnered from the PV inversion in this particular case suggest that the non-divergent wind also played a substantial role in the production of a superposition through its ability to laterally displace the location of the individual tropopause breaks. In particular, the non-divergent circulation associated with the upper-tropospheric PV was characterized by a perturbation cyclone (anticyclone) over the western (eastern) United States. The juxtaposition of these circulation anomalies accounted for a perturbation southerly wind over the Southern Plains that differentially advected the subtropical tropopause break poleward and into closer proximity with the polar tropopause break. Investigation into the origin of the perturbation anticyclone over the eastern United States demonstrated that it was not solely a product of proximate convection over the Mississippi River valley. Instead, a large fraction of this circulation was attributed to the transport of a poorly stratified, middle and upper-tropospheric tropical air mass from the equatorial Pacific. This result, in particular, suggests that the poleward transport of air masses associated with historical tropical convection is an important mode of tropical-extratropical interaction worthy of additional consideration. Further discussion of this idea, and its relevance to the production of sensible weather, is reserved for the following chapter.

A partition of the non-divergent wind in these two cases also provided broader insights into the general evolution of the tropopause structure at middle latitudes. For instance, the analysis demonstrated that the lateral displacement of the individual tropopause breaks is most strongly controlled by the mean and upper-tropospheric components of the non-divergent wind field. Specifically, the analysis indicated that the mean wind was primarily responsible for the zonal propagation of individual troughs and ridges. The upper-tropospheric non-divergent wind, then, acted to slow the zonal propagation of troughs and ridges by the mean wind and/or to translate the position of the individual tropopause breaks meridionally.

Additional consideration of the non-divergent circulations associated with the jet PV also implied that the subtropical jet was able to more substantially displace the lateral position of both tropopause breaks, compared to its polar counterpart. Specifically, an examination of the PV advection patterns along the polar tropopause break in both cases indicated that the polar and subtropical jet's non-divergent circulations contributed nearly equivalent amounts to the PV advection patterns produced by the total upper-tropospheric non-divergent wind. Conversely, the non-divergent circulation tied to the subtropical jet PV accounted for the large majority of the PV advection patterns observed along the subtropical tropopause break in both cases. Therefore, it is believed that the strong static stability of the lower stratosphere above the polar jet reduces the penetration depth of its non-divergent circulation and handicaps the polar jet's ability to horizontally displace the subtropical tropopause break. The subtropical jet, on the other hand, can more effectively interact with the polar tropopause break, as its horizontal non-divergent circulation is not dampened with altitude as rapidly by the comparatively reduced static stability that resides in the troposphere beneath the subtropical jet.

While the subtropical jet's non-divergent circulation appears to more substantially influence the lateral displacement of both tropopause breaks, the analysis of transverse vertical circulations within the dual jet environment during the December 2009 Blizzard demonstrated that the polar jet's geostrophic circulation forced a greater fraction of the total transverse vertical circulation compared to the subtropical jet. This result was believed to be a function of the observation that the strongest mid-tropospheric baroclinicity typically resides in closer proximity to the polar jet. Consequently, the geostrophic circulation associated with the polar jet may have a stronger hand in forcing the development of transverse vertical circulations that can vertically restructure the tropopause within a dual jet environment. Together, these results imply that the *horizontal* structure of the tropopause may be more strongly governed by the subtropical jet, while the polar jet largely controls the *vertical* restructuring of the tropopause.

Both of the cases considered were also associated with either widespread convection or a rapidly deepening surface cyclone and, consequently, significant diabatic heating in the vicinity of the two jet structures. Despite the erosion of upper-level PV that accompanied this diabatic heating, the balanced non-divergent circulations in the upper troposphere that responded to the proximate diabatic heating (i.e., those tied to the interior PV) had little impact on the lateral displacement of the individual tropopause breaks. While the non-divergent circulations associated with *proximate* convection did not play a significant role in restructuring the tropopause, the perturbation anticyclone that substantially aided in the displacement of the subtropical tropopause break during the May 2010 Nashville Flood did have an association with *remote* tropical convection. Specifically, this anticyclonic circulation was connected to a poorly stratified, tropical air mass that was transported poleward from the equatorial Pacific. Consequently, it is hypothesized that the non-divergent, upper-tropospheric response to

convection (i.e., a perturbation anticyclone) may only be capable of altering the position of the waveguides if its associated air mass originated outside of the mid-latitudes. In the immediate vicinity of proximate convection, both the diabatic erosion of upper-tropospheric PV and the divergent wind field appear to be the dominant mechanisms that most strongly influence the tropopause structure. However, given that this hypothesis is constructed based upon only two cases, a consideration of a greater number of events is required to refine this research question.

Finally, despite the meager role that the non-divergent circulations associated with the interior and surface PV played in the lateral displacement of the tropopause breaks, the geostrophic circulations associated with both the interior and surface PV did play a more substantial part in restructuring the tropopause immediately upstream of the surface cyclone by contributing to the development of transverse vertical circulations along the dual jet structure during the December 2009 Blizzard. Specifically, their individual geostrophic circulations were strong enough near the surface cyclone to interact with the mid-tropospheric baroclinicity and to subsequently aid in the development of a transverse vertical circulation that promoted subsidence on and beneath the subtropical tropopause step between the two jet cores. In line with this observation, and with previous studies (e.g., Ramos 1997; Morgan and Nielsen-Gammon 1998; Wandishin et al. 2000), it is clear upon examining these two cases that the evolution of the hemispheric tropopause structure not only necessitates a consideration of dynamical structures that originate both in and outside of the extratropics, but also those that reside throughout the full depth of the troposphere.

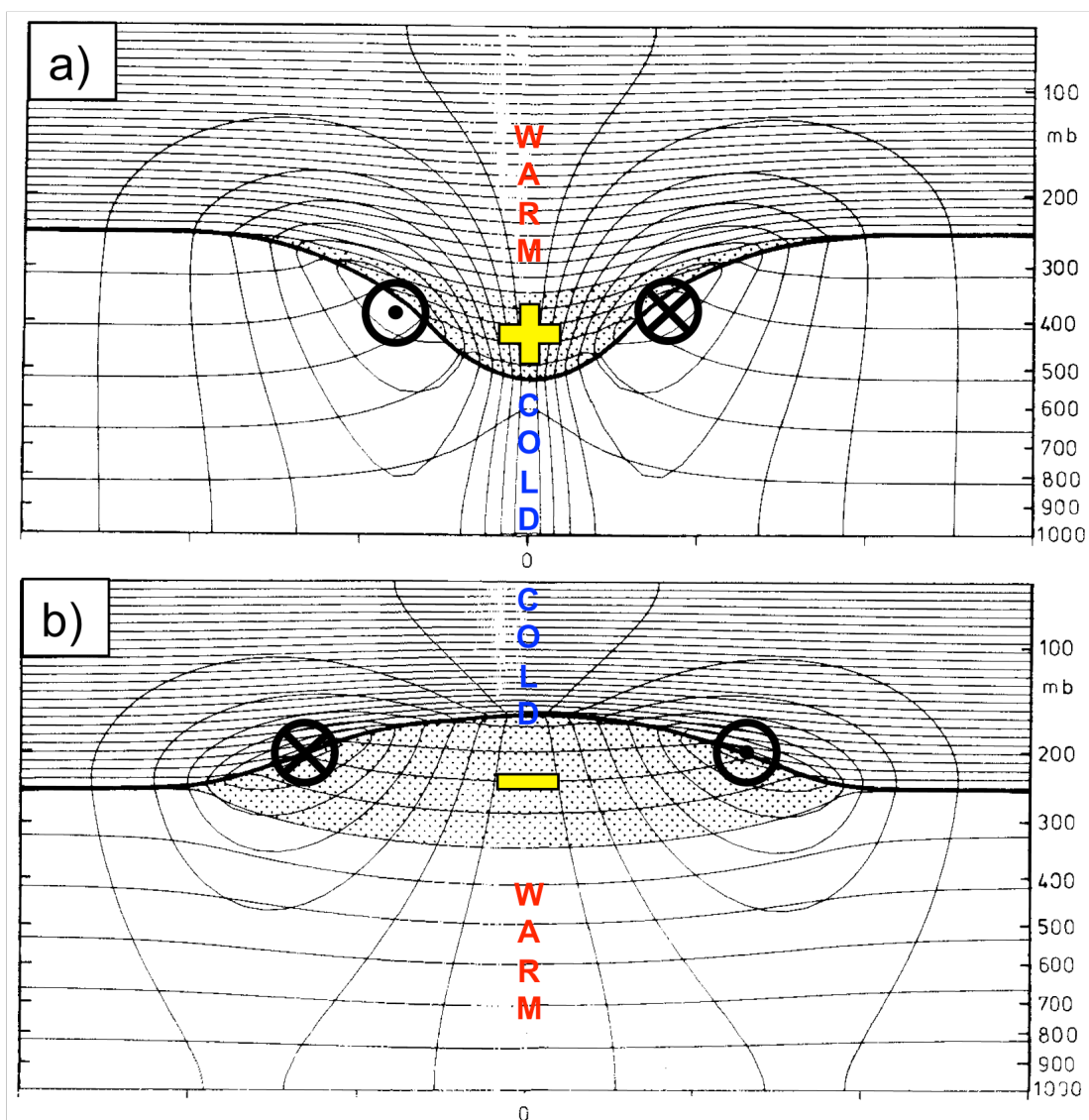


FIG. 5.1. Idealized circularly symmetric flows associated with an isolated (a) positive and (b) negative Ertel PV anomaly. The location of the positive (negative) PV anomaly is denoted by the + (−) symbol and the stippled pattern, while cold and warm temperature anomalies associated with each PV anomaly are labeled accordingly. The thick black line corresponds to the tropopause and the two sets of thin lines represent the potential temperature every 5 K and the wind velocity transverse to the cross section every 3 ms^{−1}. For more information on the methods used to compute these circulations, consult Thorpe (1985) (Adapted from Hoskins et al. 1985).

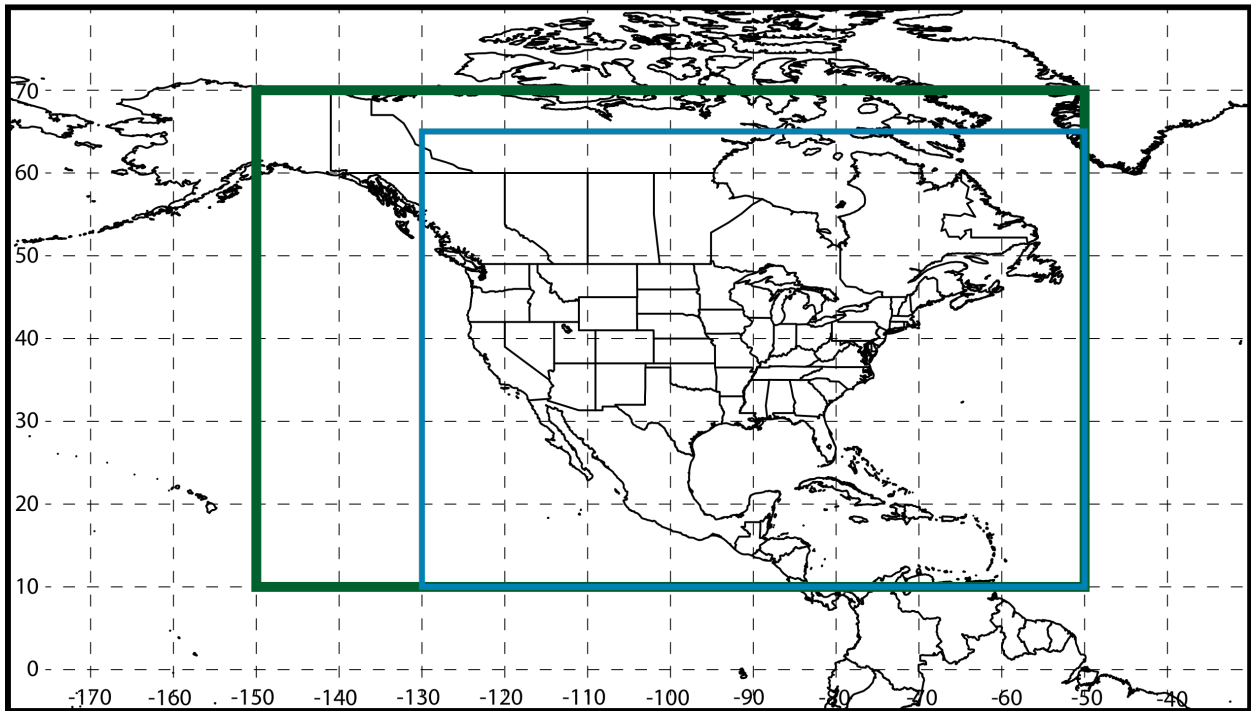


FIG. 5.2. The horizontal domains used for PV inversion during the 1–3 May 2010 Nashville Flood (outer green box) and the 18–20 December 2009 Mid-Atlantic Blizzard (inner blue box).

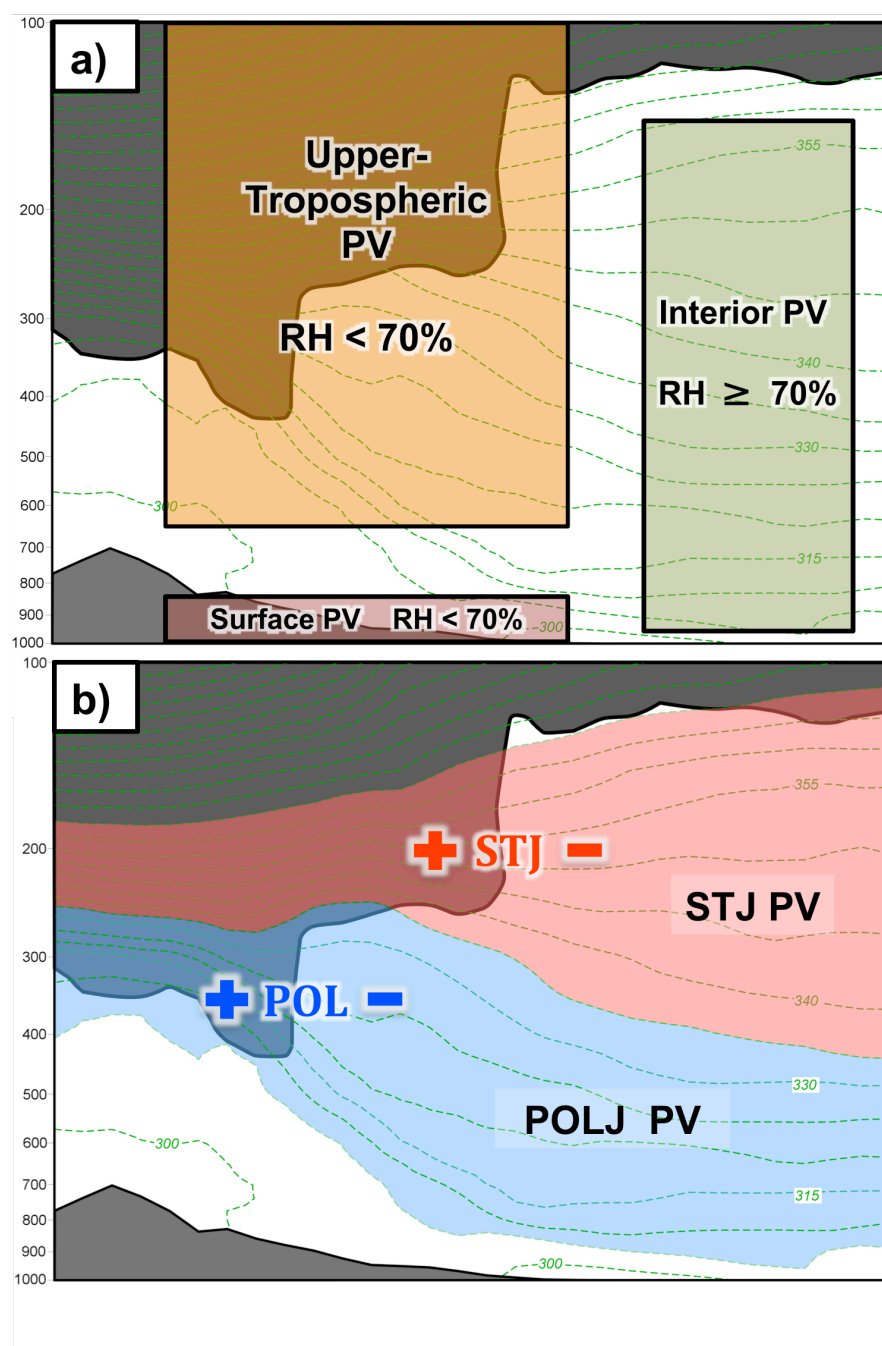
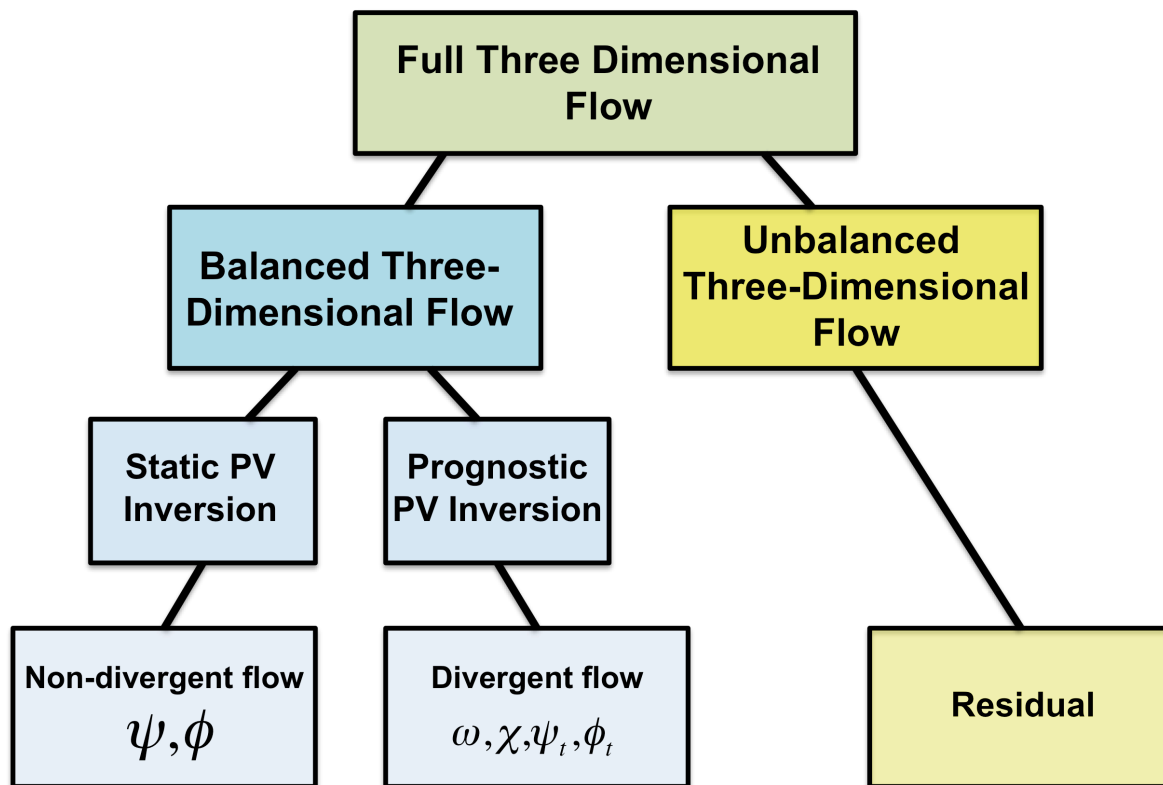


FIG. 5.3. (a) Schematic of the three-way perturbation PV partition applied to both cases. (b) Schematic of the partition used to isolate the perturbation PV associated with the individual polar (POL) and subtropical (STJ) jets during the 1–3 May 2010 Nashville Flood. The + and – symbols correspond to positive and negative PV anomalies, respectively. For more specific details on these schemes, refer to the discussion within the text.



Davis and Emanuel (1991)

FIG. 5.4. Flow chart describing the components of the flow that are (balanced) and are not recovered (unbalanced) via an inversion of the PV. For more information, refer to the discussion within the text.

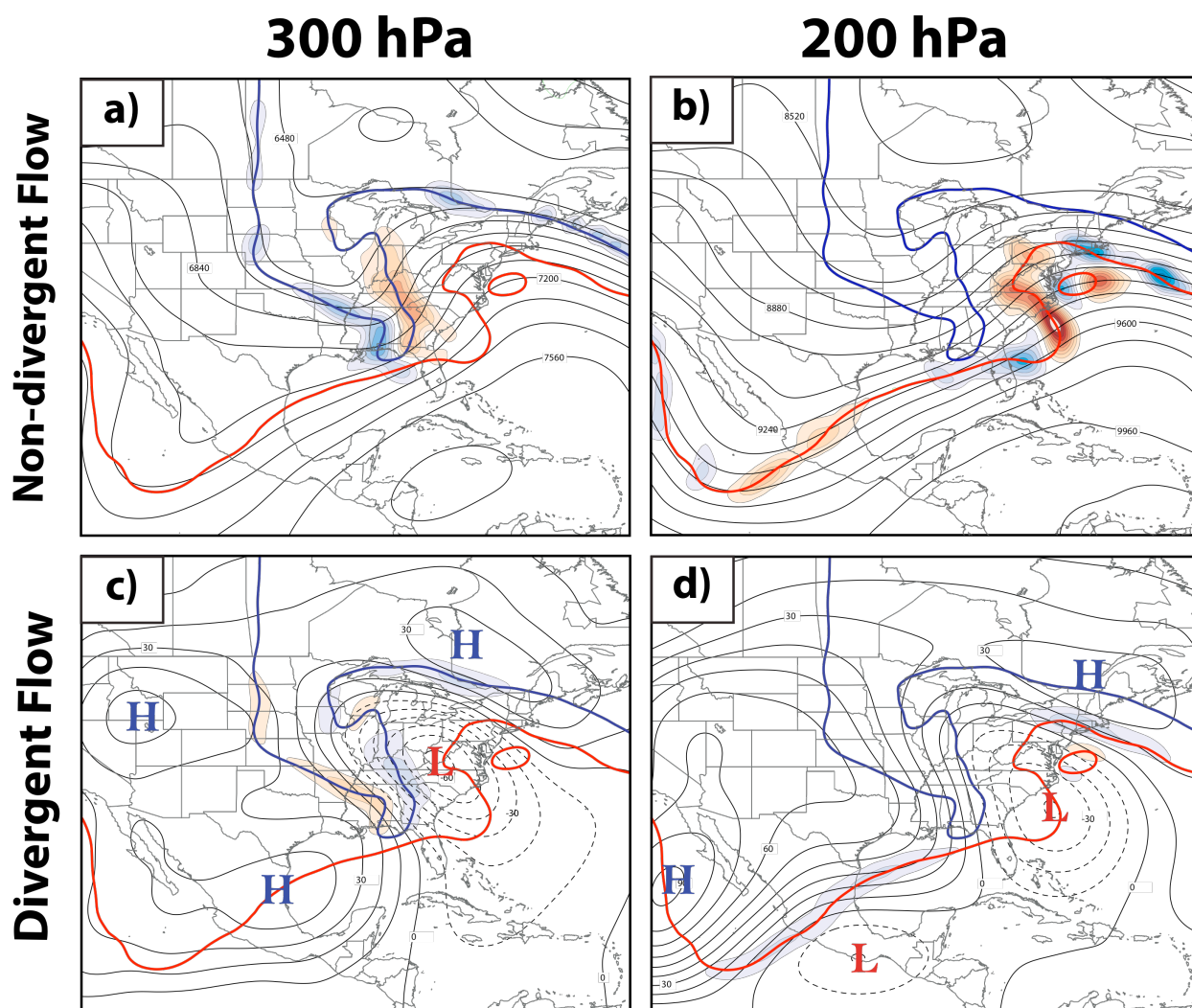


FIG. 5.5. PV advection within the 1-3-PVU channel at 0000 UTC 19 December 2009 by the balanced non-divergent wind at (a) 300 hPa and (b) 200 hPa, with positive (negative) PV advection shaded every 5×10^{-5} PVU s^{-1} in the orange (blue) fill pattern and the streamfunction contoured every 120×10^5 $m^2 s^{-1}$ with the thin black lines. PV advection within the 1-3-PVU channel at 0000 UTC 19 December 2009 by the balanced divergent wind at (c) 300 hPa and (d) 200 hPa, with (positive) negative PV advection shaded every 2×10^{-5} PVU s^{-1} in the orange (blue) fill pattern and velocity potential contoured every 10×10^5 $m^2 s^{-1}$ with the thin black lines (negative values dashed). The blue “H” (red “L”) corresponds to a local maximum (minimum) in velocity potential. The 2-PVU surface at 300 hPa (200 hPa) is highlighted by the thick blue (red) line in all panels and represents the location of the polar (subtropical) tropopause break.

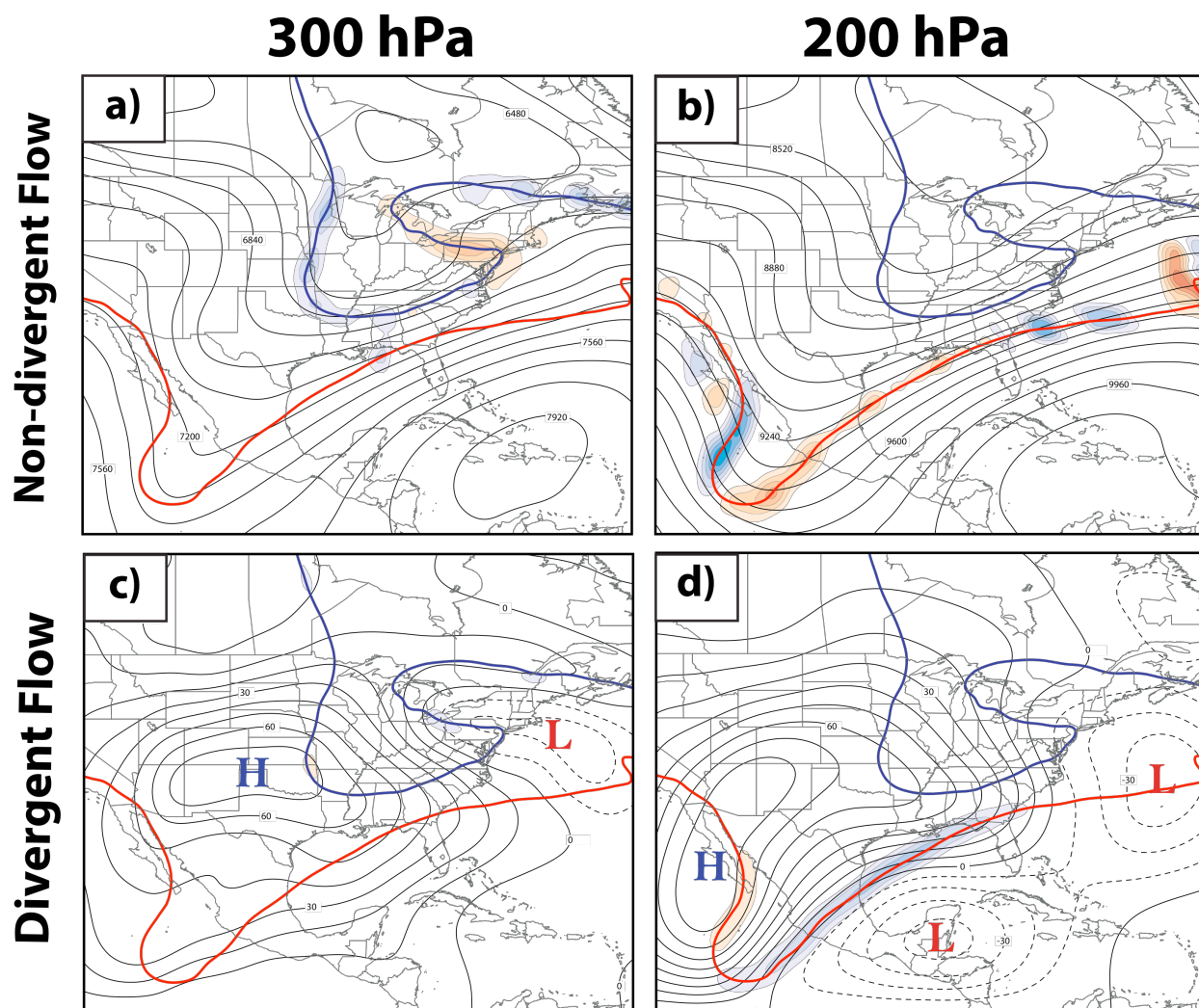


FIG. 5.6. Conventions are identical to those in Fig. 5.5, but for 1800 UTC 19 December 2009.

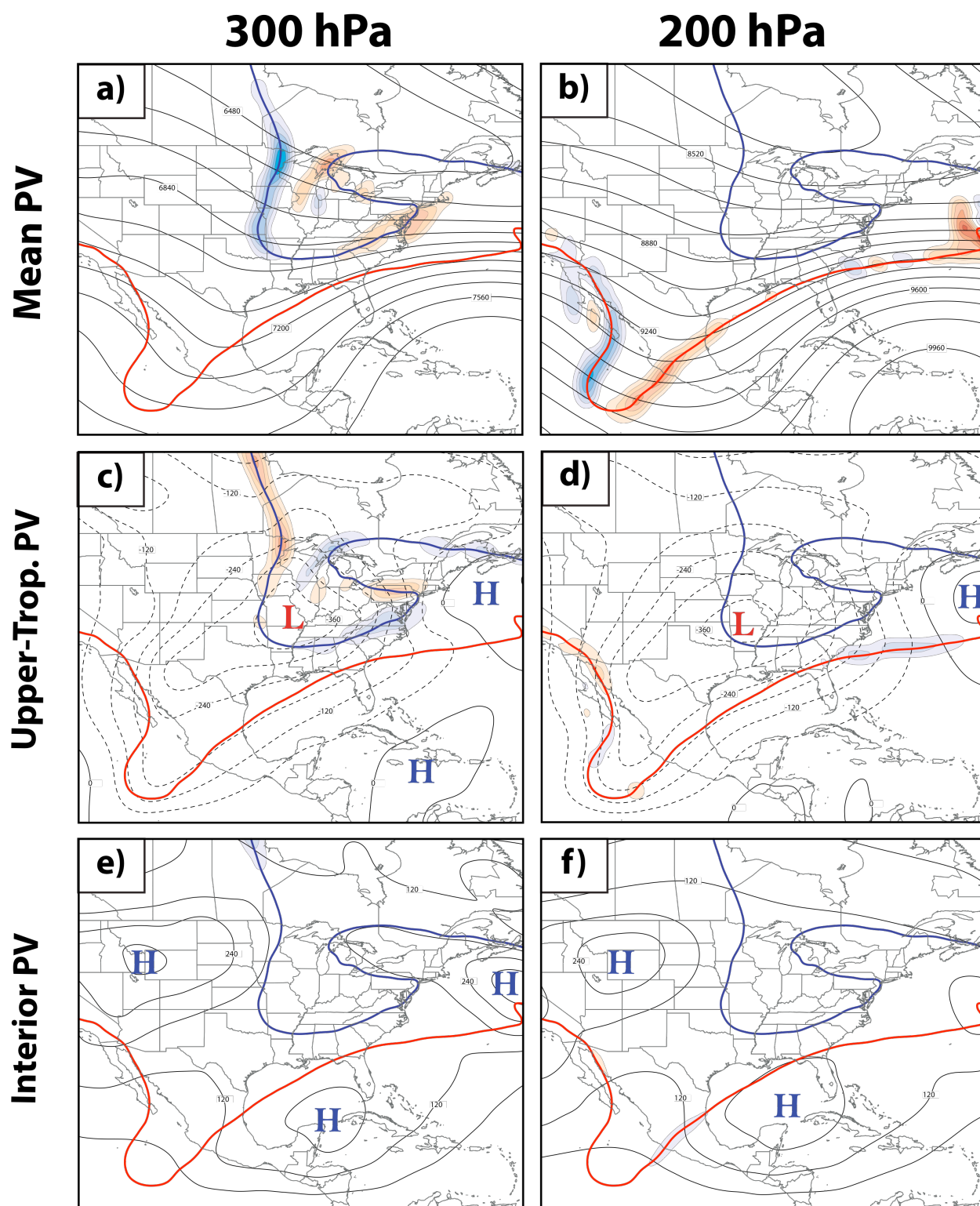


FIG. 5.7. PV advection within the 1-3-PVU channel at 1800 UTC 19 December 2009 by the non-divergent wind associated with (a,b) the mean PV, (c,d) the upper-tropospheric PV, and (e,f) the interior PV at 300 hPa and 200 hPa, respectively. Conventions are identical to those in Figs. 5.5a,b, except with the streamfunction now contoured with thin black lines (negative values dashed) every $120 \times 10^5 \text{ m}^2 \text{ s}^{-1}$ in (a) and (b) and every $60 \times 10^5 \text{ m}^2 \text{ s}^{-1}$ in (c-f). The blue “H” (red “L”) corresponds to a local maximum (minimum) in streamfunction.

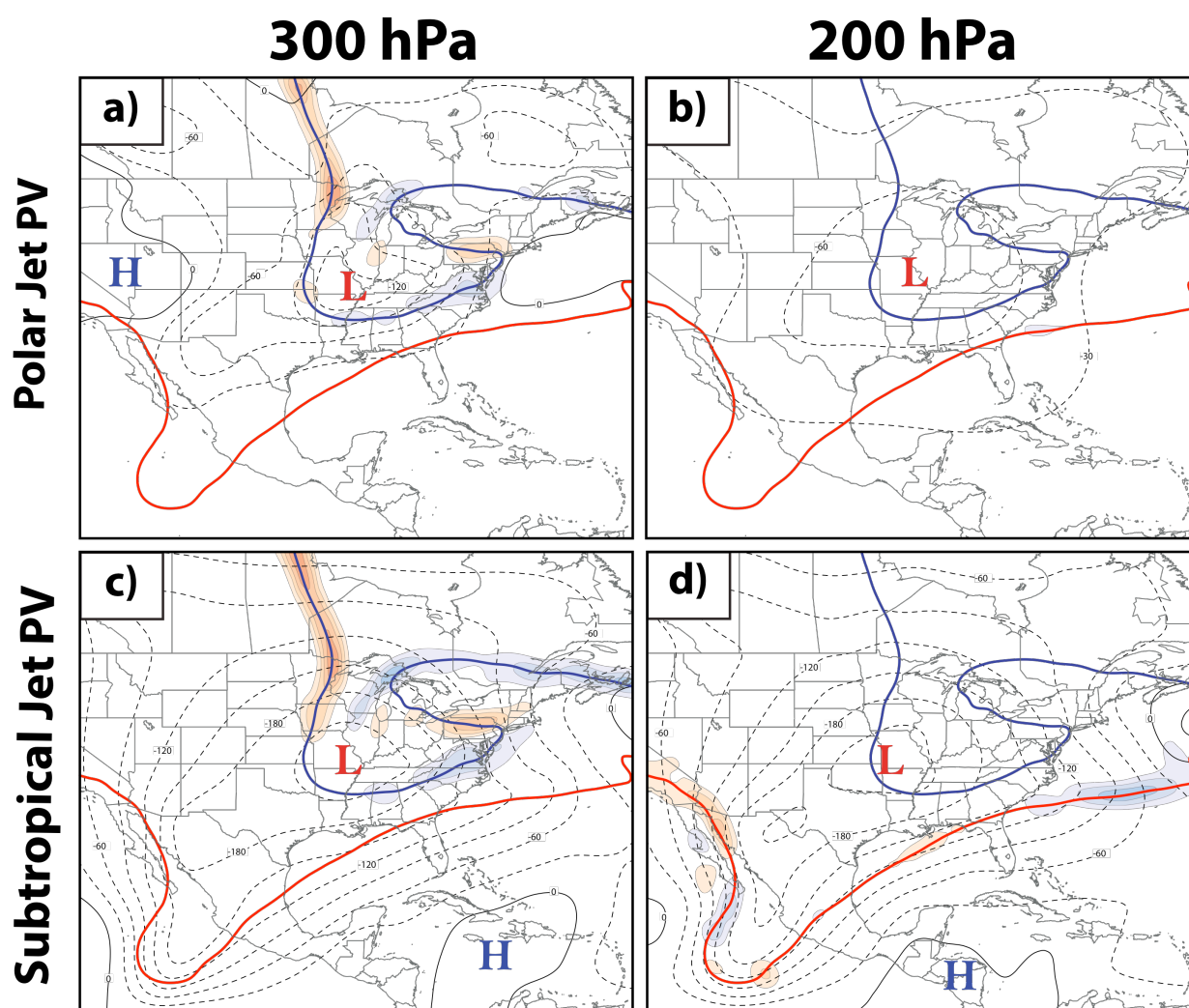


FIG. 5.8. PV advection within the 1-3-PVU channel at 1800 UTC 19 December 2009 by the non-divergent wind associated with the (a,b) polar jet PV and (c,d) subtropical jet PV at 300 and 200 hPa, respectively. Conventions are identical to those in Figs. 5.5a,b, except with the streamfunction now contoured every $30 \times 10^5 \text{ m}^2 \text{ s}^{-1}$ in the thin black lines (negative values dashed) and PV advection now shaded every $2 \times 10^{-5} \text{ PVU s}^{-1}$. The blue “H” and red “L” correspond to a local maximum or minimum in streamfunction, respectively.

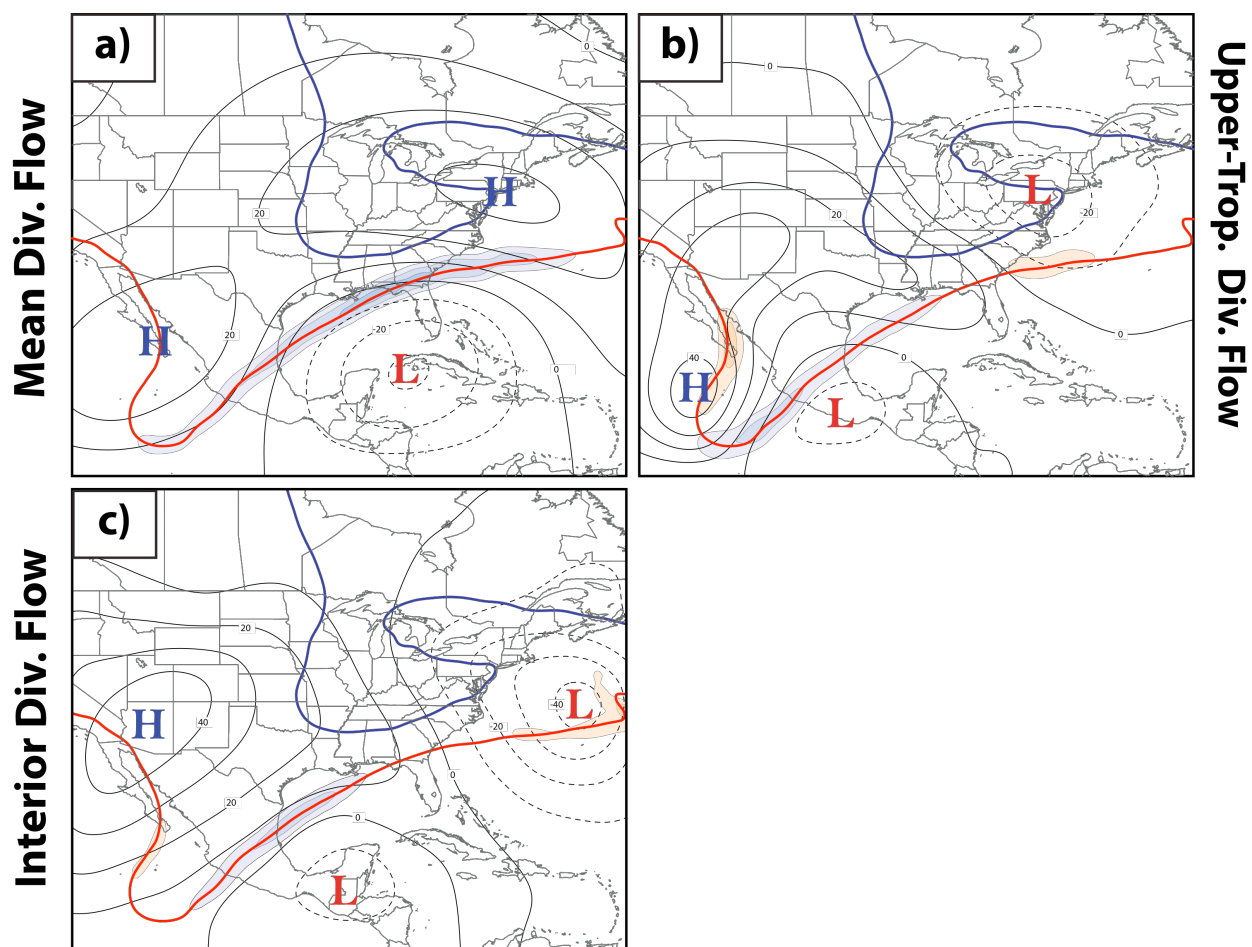


FIG. 5.9. 200 hPa PV advection within the 1-3-PVU channel at 1800 UTC 19 December 2009 by the divergent wind associated with the (a) mean PV, (b) upper-tropospheric PV, and (c) interior PV. Conventions are identical to those in Figs. 5.5c,d, except that PV advection is now shaded every $1 \times 10^{-5} \text{ PVUs}^{-1}$.

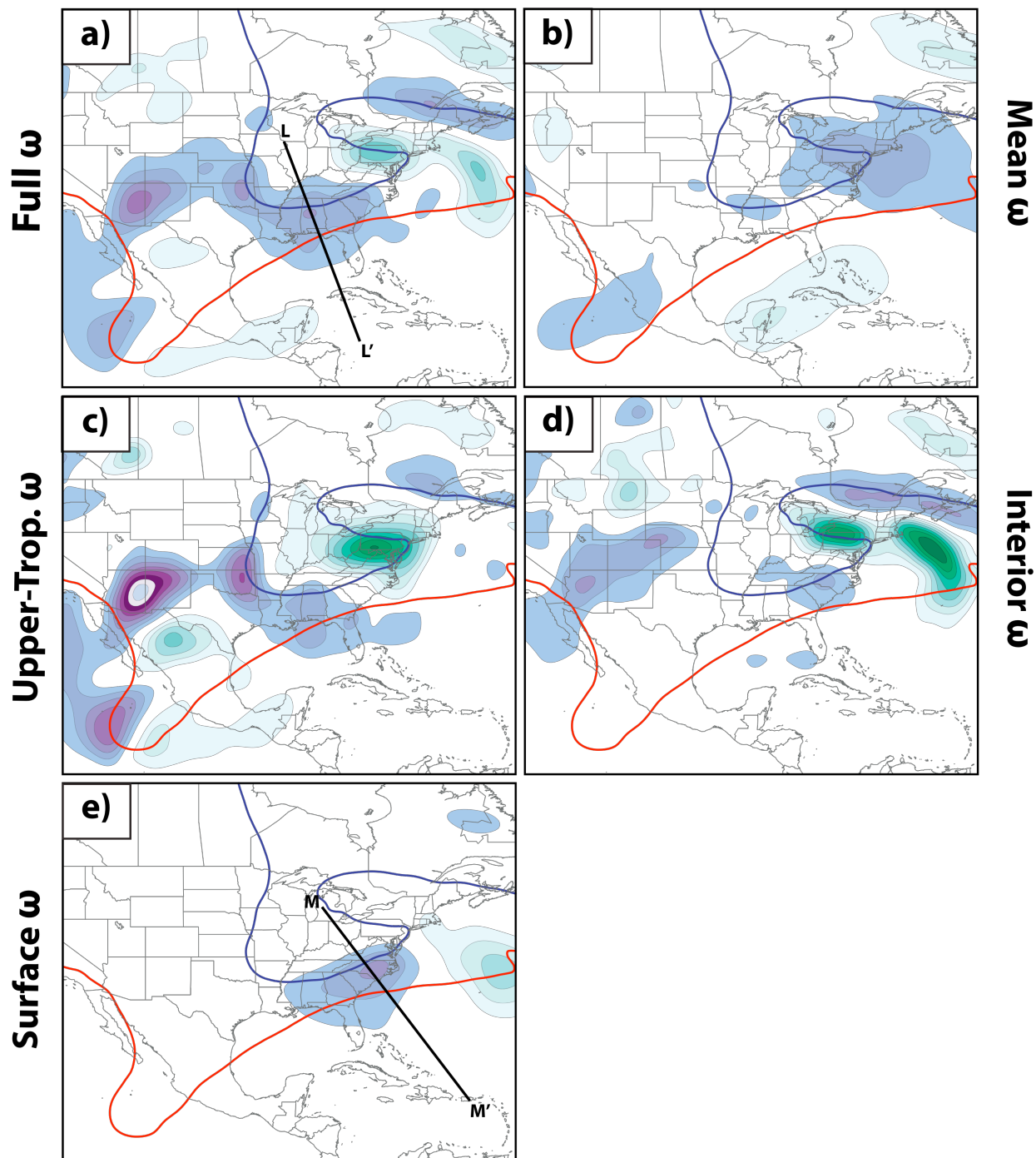


FIG. 5.10. 400 hPa balanced vertical motion field at 1800 UTC 19 December 2009 associated with the (a) full PV, (b) mean PV, (c) upper-tropospheric PV, (d) interior PV, and (e) surface PV. Ascent (descent) is shaded in the green (purple) fill pattern every 1 dPa s^{-1} in (a) and every 0.5 dPa s^{-1} in (b-e). The thick blue (red) line represents the 2-PVU surface and the polar (subtropical) tropopause breaks, as in previous figures.

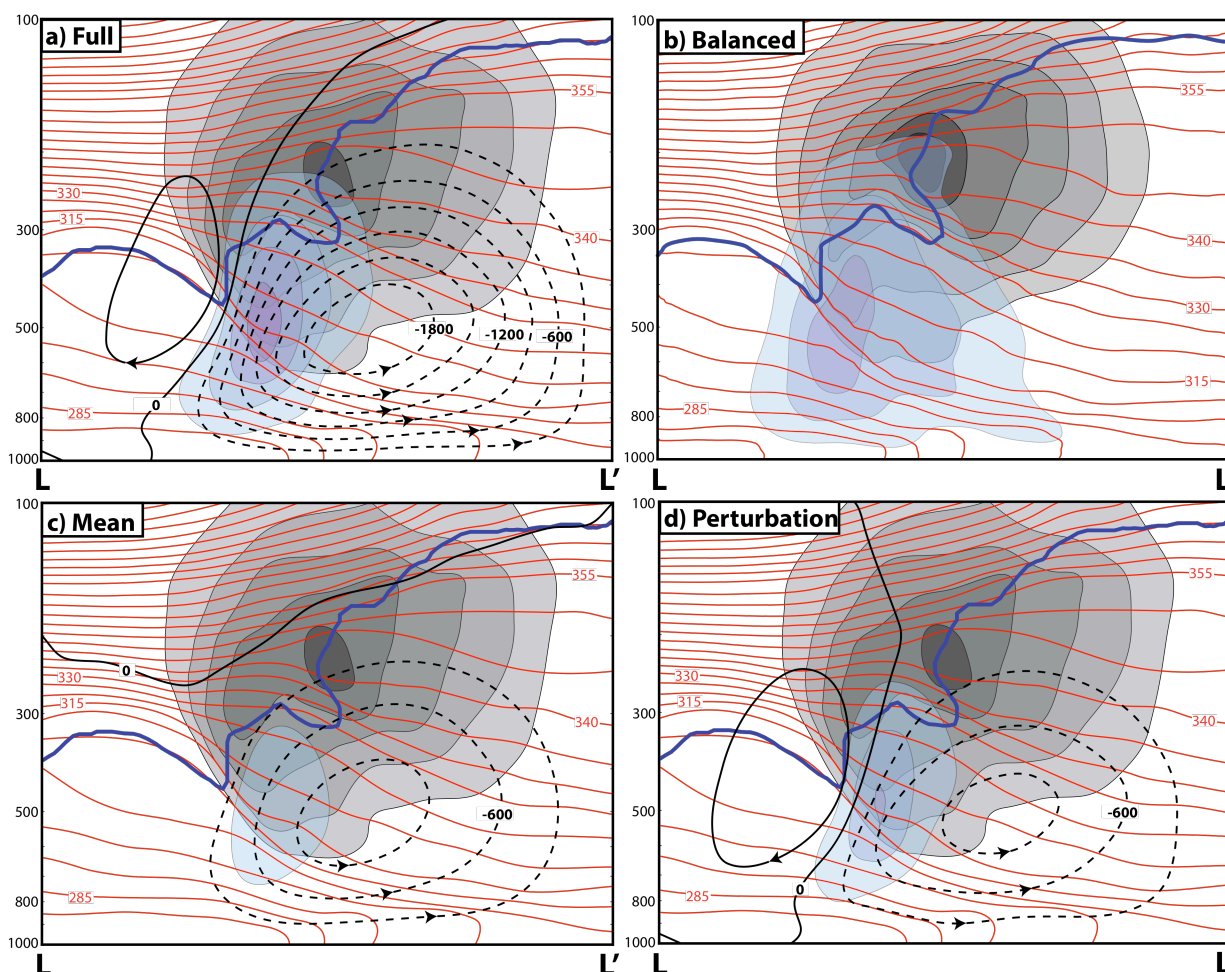


FIG. 5.11. Cross section of Sawyer-Eliassen streamfunction along the line L-L', as shown in Fig. 5.10a, associated with the (a) full PV, (c) mean PV, and (d) perturbation PV at 1800 UTC 19 December 2009. Streamfunction is contoured with black lines (negative values dashed) every 300 m hPa s^{-1} , potential temperature is contoured every 5 K in red, geostrophic isotachs are shaded in the gray fill pattern every 10 ms^{-1} greater than 30 ms^{-1} , and the thick blue line denotes the 1.5-PVU surface. Descent associated with the Sawyer-Eliassen circulation is shaded with the purple fill pattern every 1 dPa s^{-1} and the arrowheads plotted on the streamfunction contours indicate the sense of the Sawyer-Eliassen circulation. (b) Subsidence recovered from the full prognostic PV inversion is shaded with the purple fill pattern every 1 dPa s^{-1} , isotachs of the full wind are shaded in the gray fill pattern every 10 ms^{-1} beginning at 30 ms^{-1} , potential temperature is contoured every 5 K in red, and the 1.5-PVU surface is identified by the bold blue line.

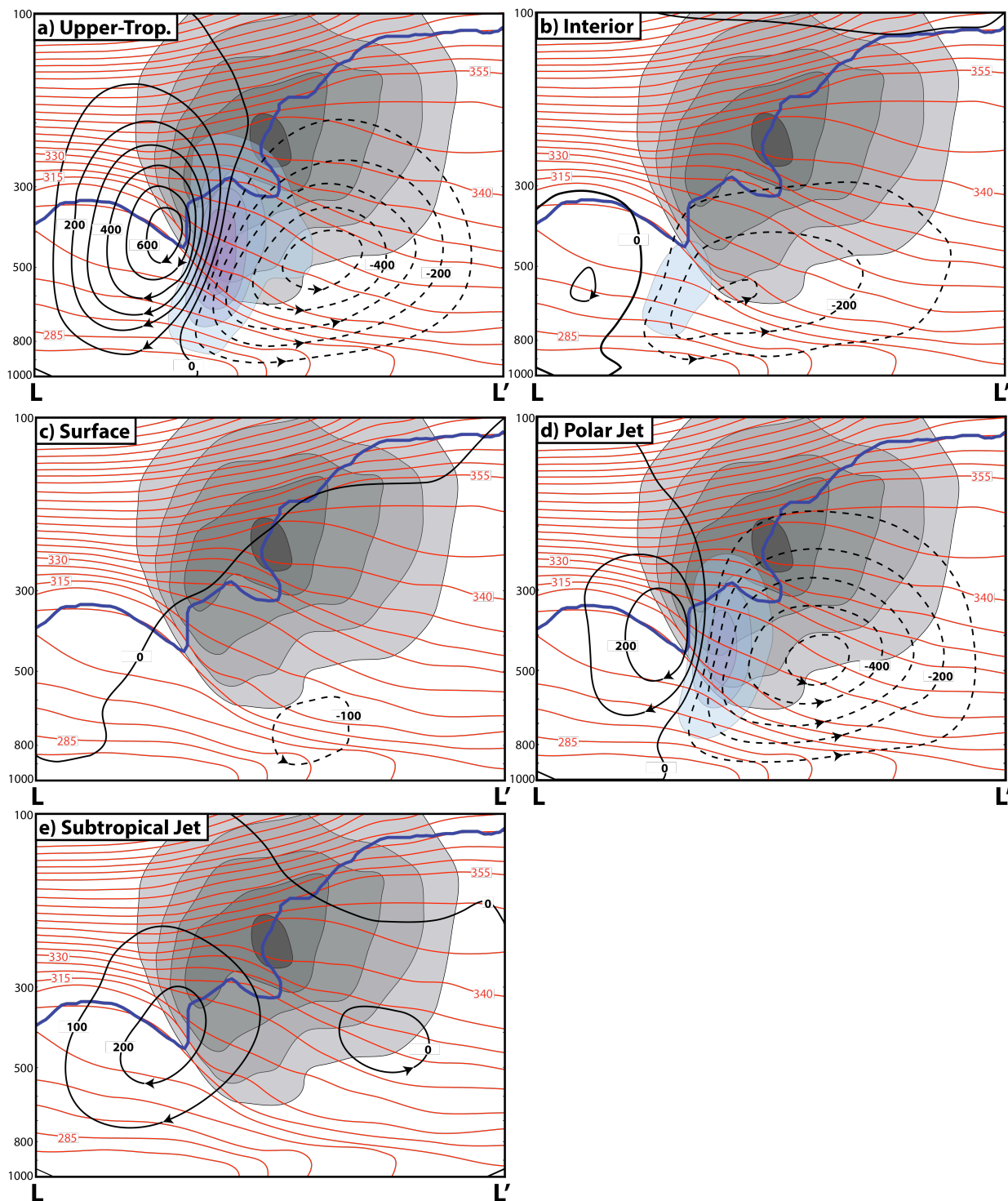


FIG. 5.12. Cross sections of Sawyer-Eliassen streamfunction along the line L-L', as shown in Fig. 5.10a, associated with the (a) upper-tropospheric PV, (b) interior PV, (c) surface PV, (d) polar jet PV, and (e) subtropical jet PV at 1800 UTC 19 December 2009. Conventions are identical to those in Fig. 5.11, except with streamfunction now contoured every 100 mhPa⁻¹ and descent now shaded every 0.5 dPa^s⁻¹.

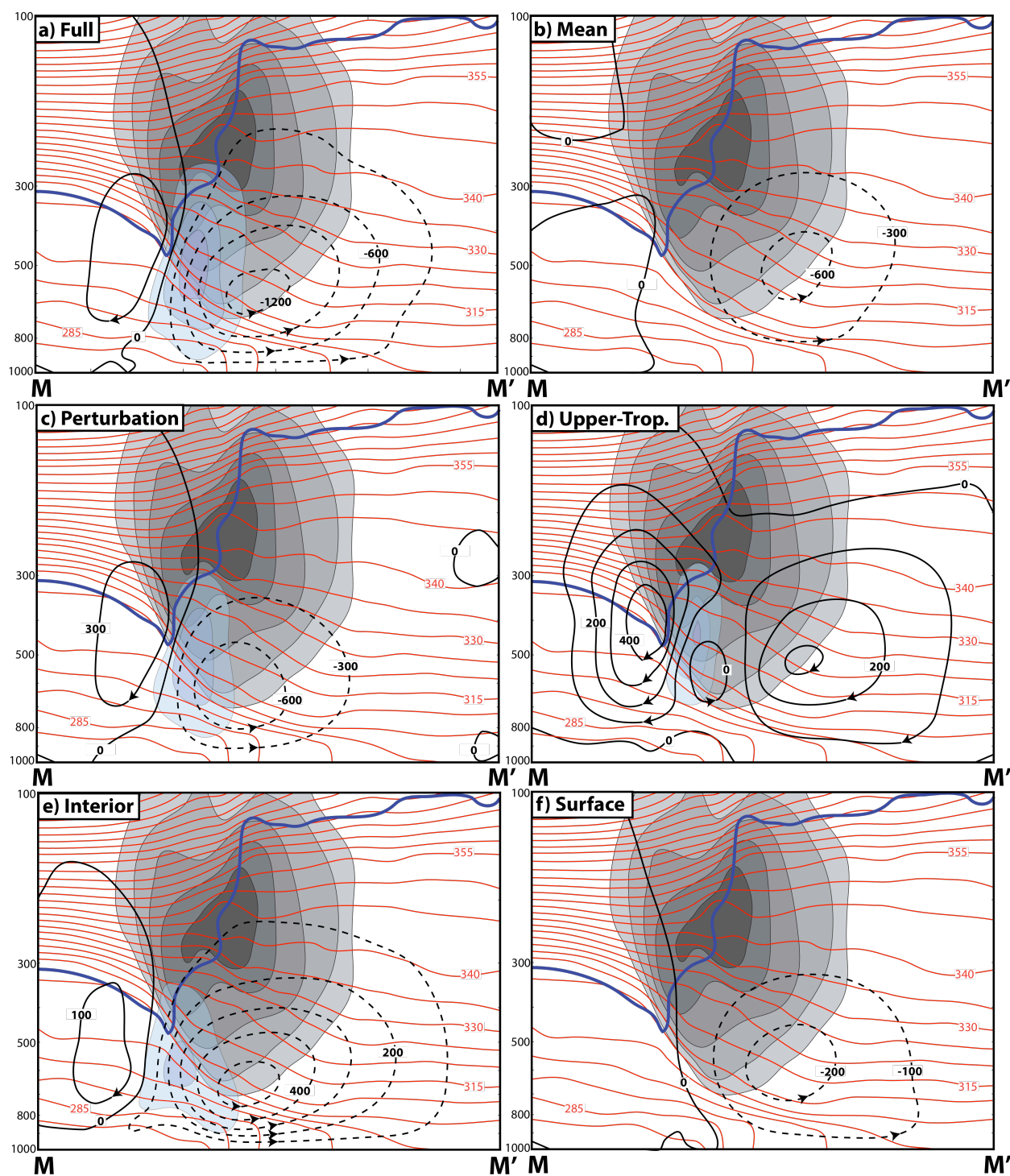


FIG. 5.13. Cross sections of Sawyer-Eliassen streamfunction along the line M-M', as shown in Fig. 5.10e, associated with the (a) full PV, (b) mean PV, (c) perturbation PV, (d) upper-tropospheric PV, (e) interior PV, and (f) surface PV at 0000 UTC 20 December 2009. Conventions in (a-c) are identical to those in Fig. 5.11, while conventions in (d-f) are identical to those in Fig. 5.12.

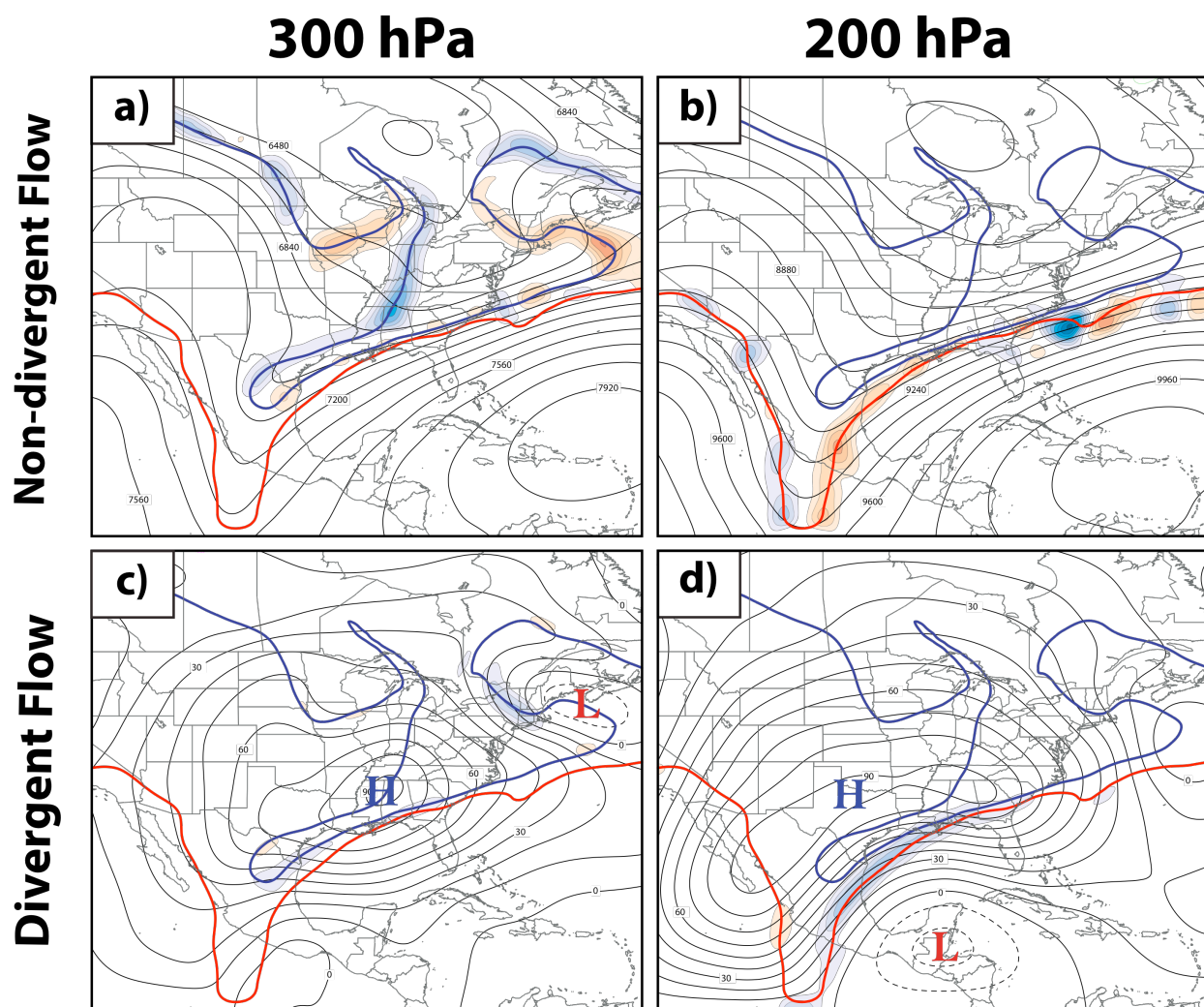


FIG. 5.14. Conventions are identical to those shown in Fig. 5.5, but for 1200 UTC 20 December 2009.

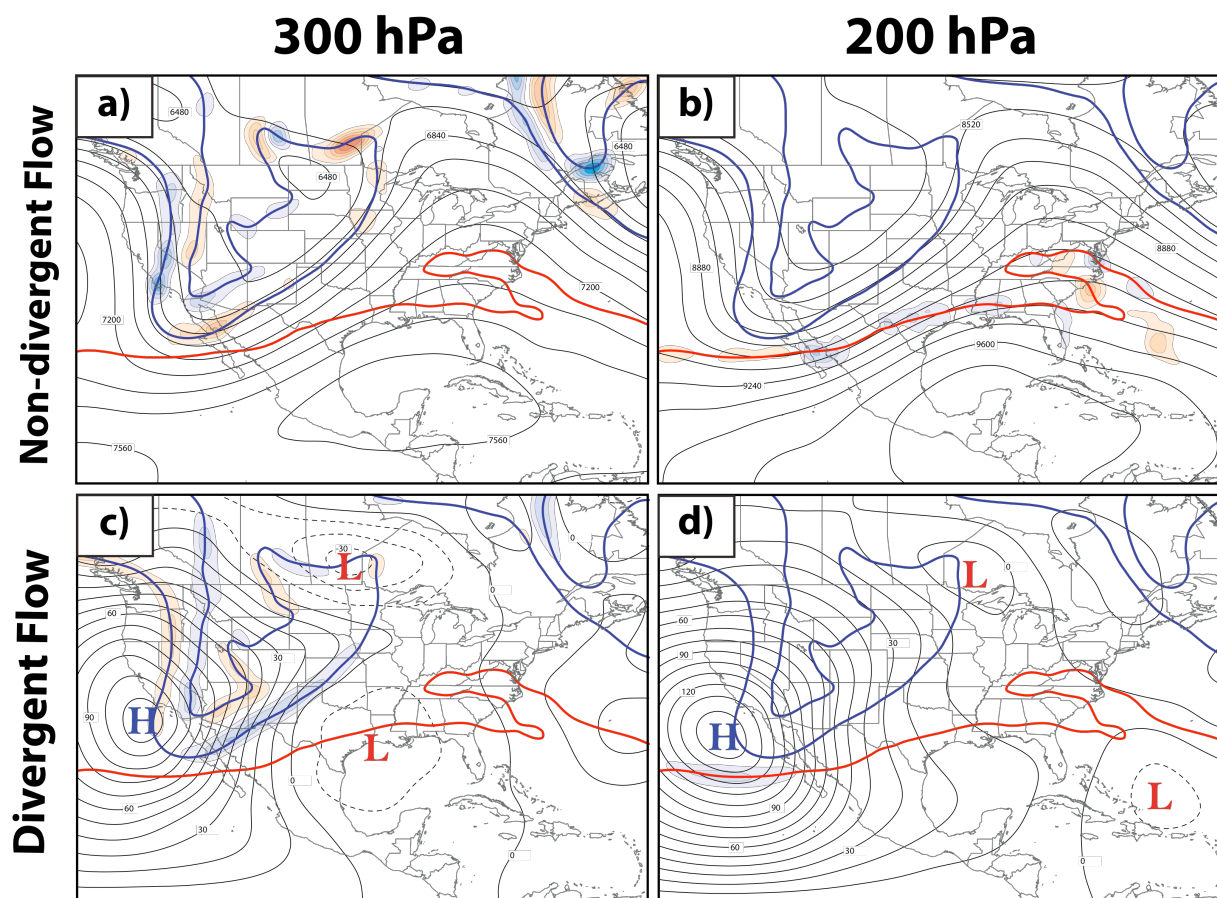


FIG. 5.15. Conventions are identical to those shown in Fig. 5.5, but for 0000 UTC 1 May 2010.

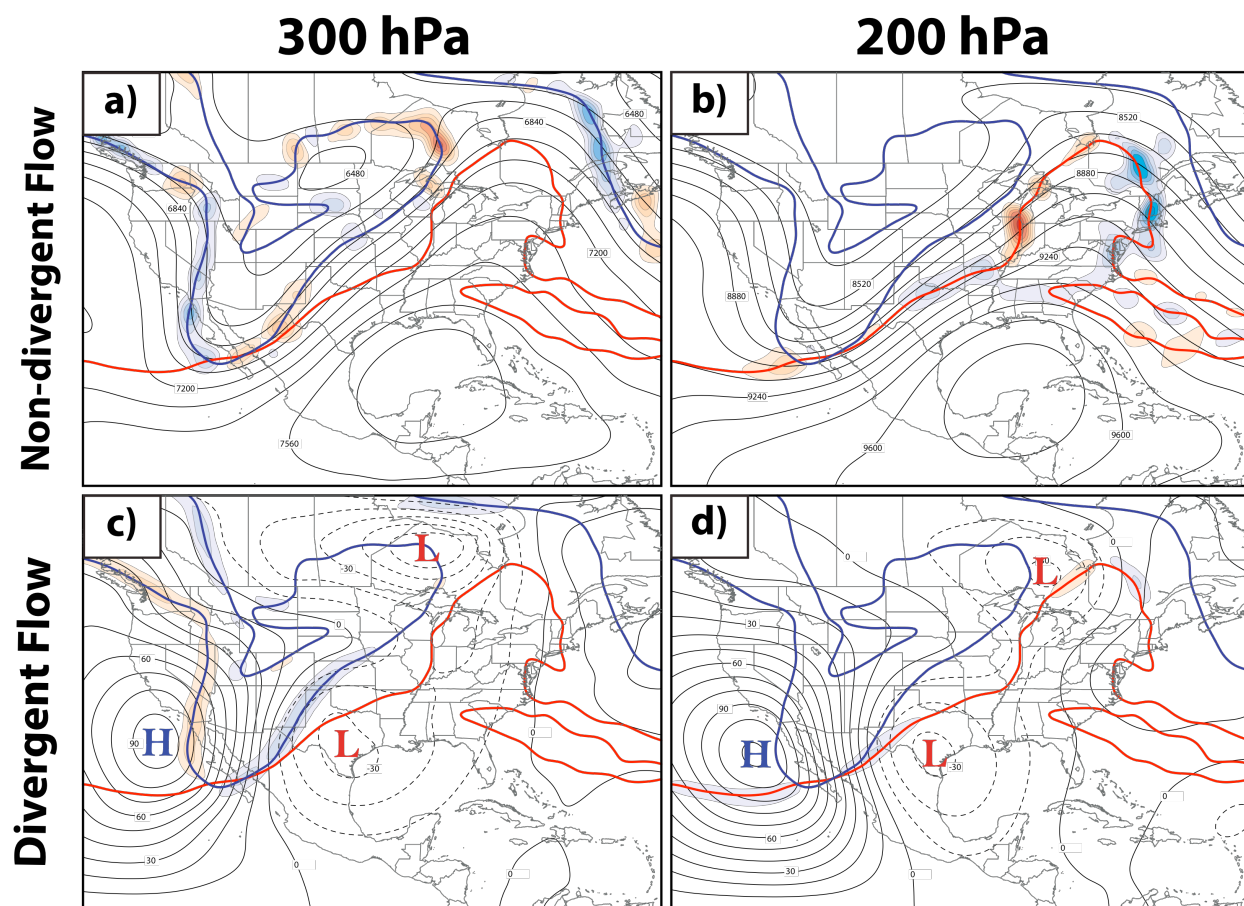


FIG. 5.16. Conventions are identical to those shown in Fig. 5.5, but for 1200 UTC 1 May 2010.

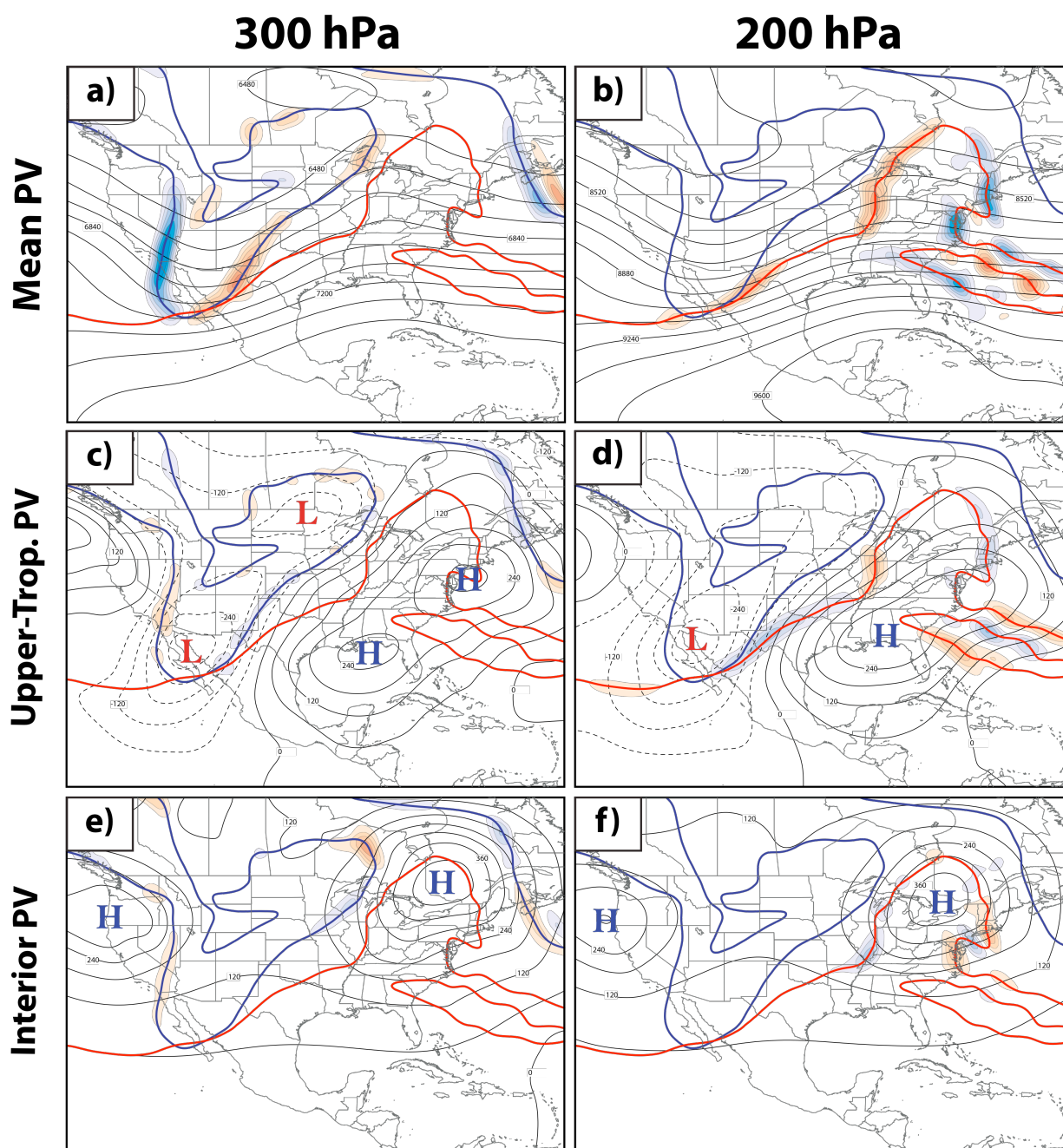


FIG. 5.17. Conventions are identical to those shown in Fig. 5.7, but for 1200 UTC 1 May 2010.

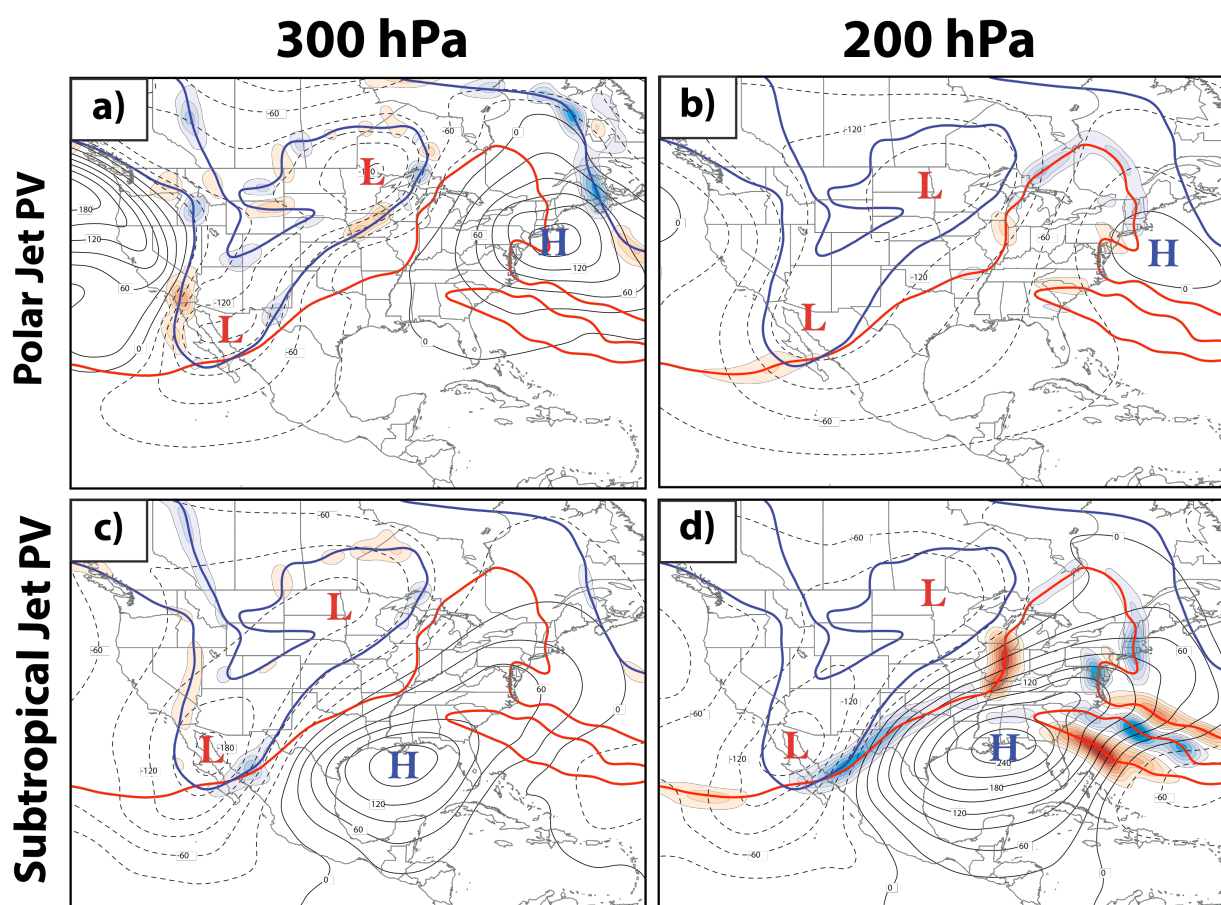


FIG. 5.18. Conventions are identical to those shown in Fig. 5.8, but for 1200 UTC 1 May 2010.

NOAA HYSPLIT MODEL
 Backward trajectories ending at 1200 UTC 01 May 10
 GDAS Meteorological Data

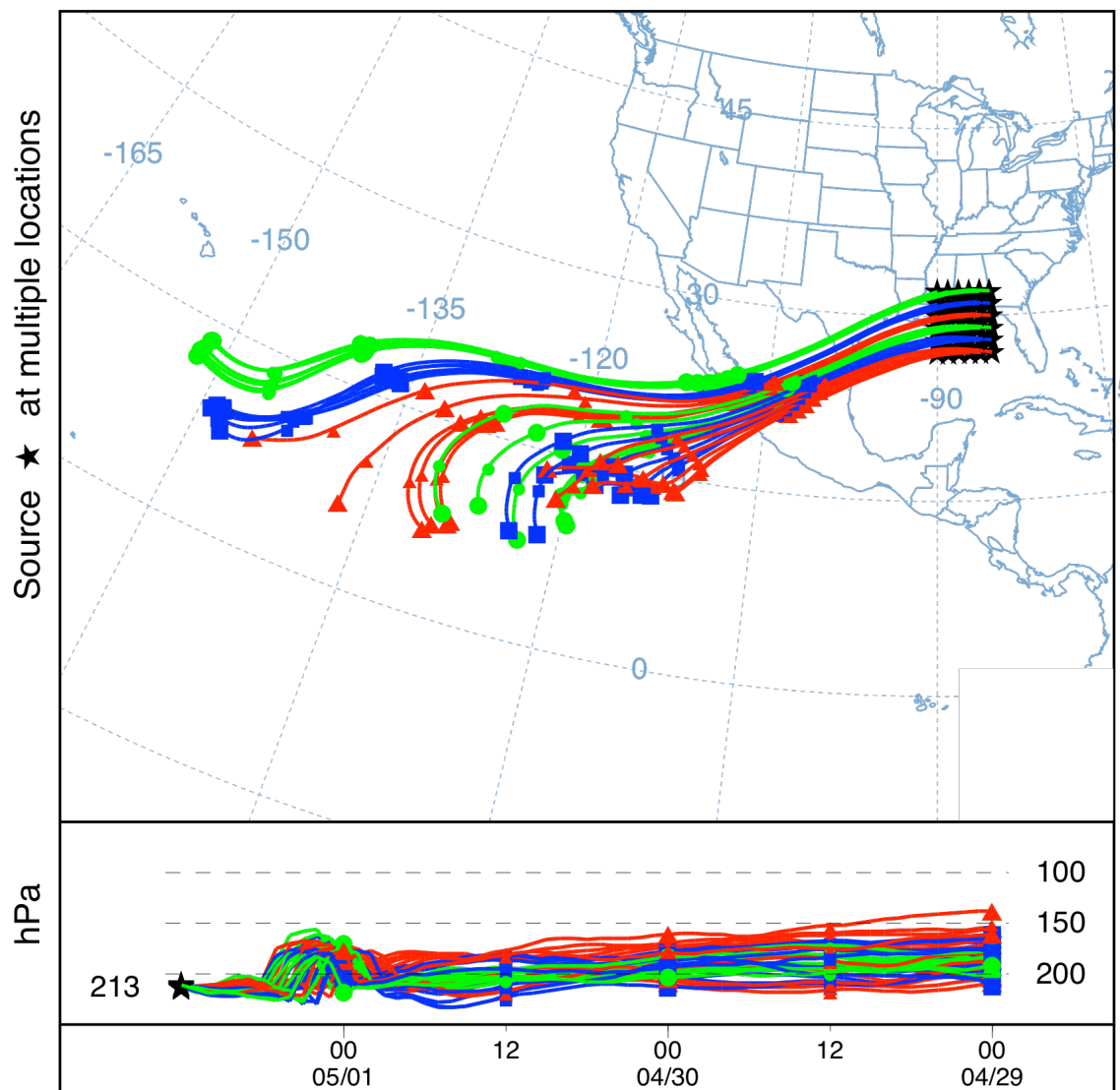


FIG. 5.19. 60 h backward trajectories initialized at 1200 UTC 1 May 2010 within the box, 27–32°N; 90–85°W, over the Gulf coast. Trajectories were initialized at 12 km above ground level within the NOAA HYSPLIT model and projected backwards using archived GDAS data. The bottom panel depicts the pressure (hPa) of the individual trajectories throughout the duration of the 60 h period.

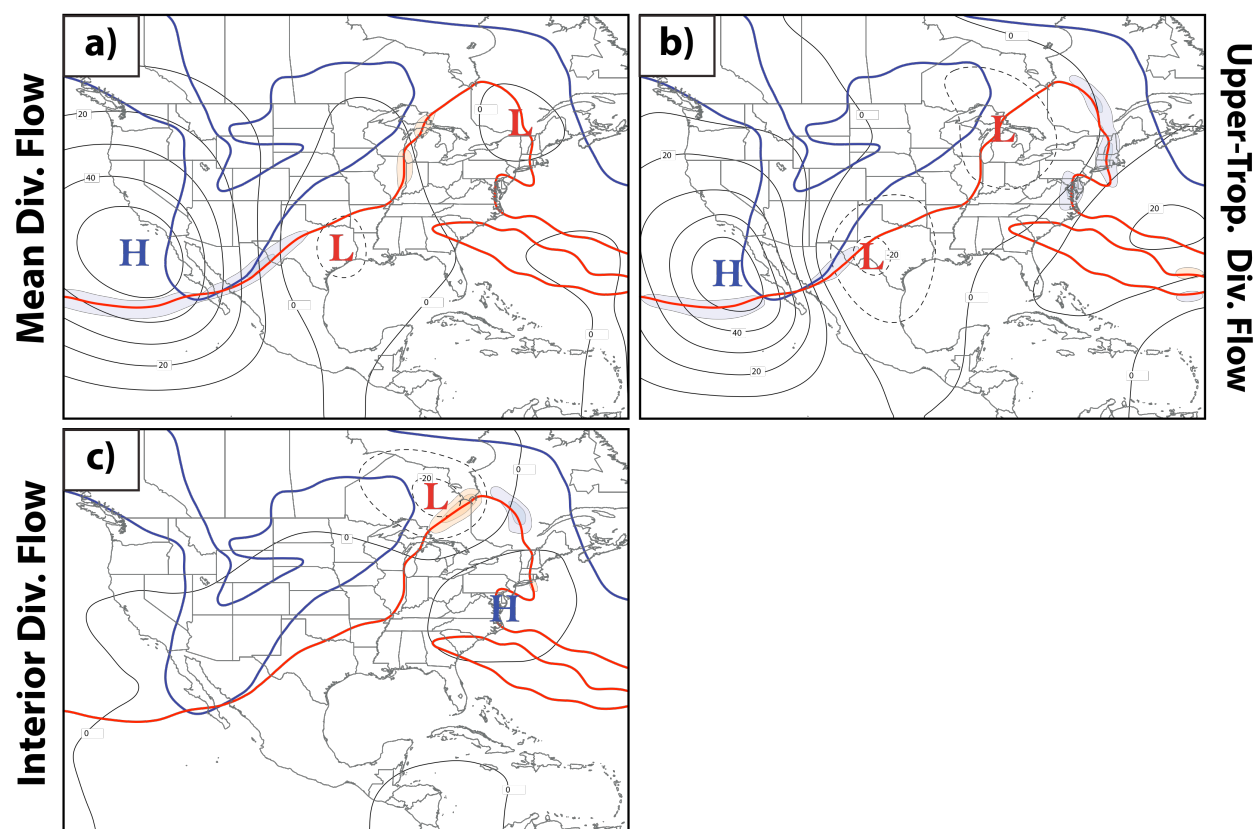


FIG. 5.20. Conventions are identical to those shown in Fig. 5.9, but for 1200 UTC 1 May 2010.

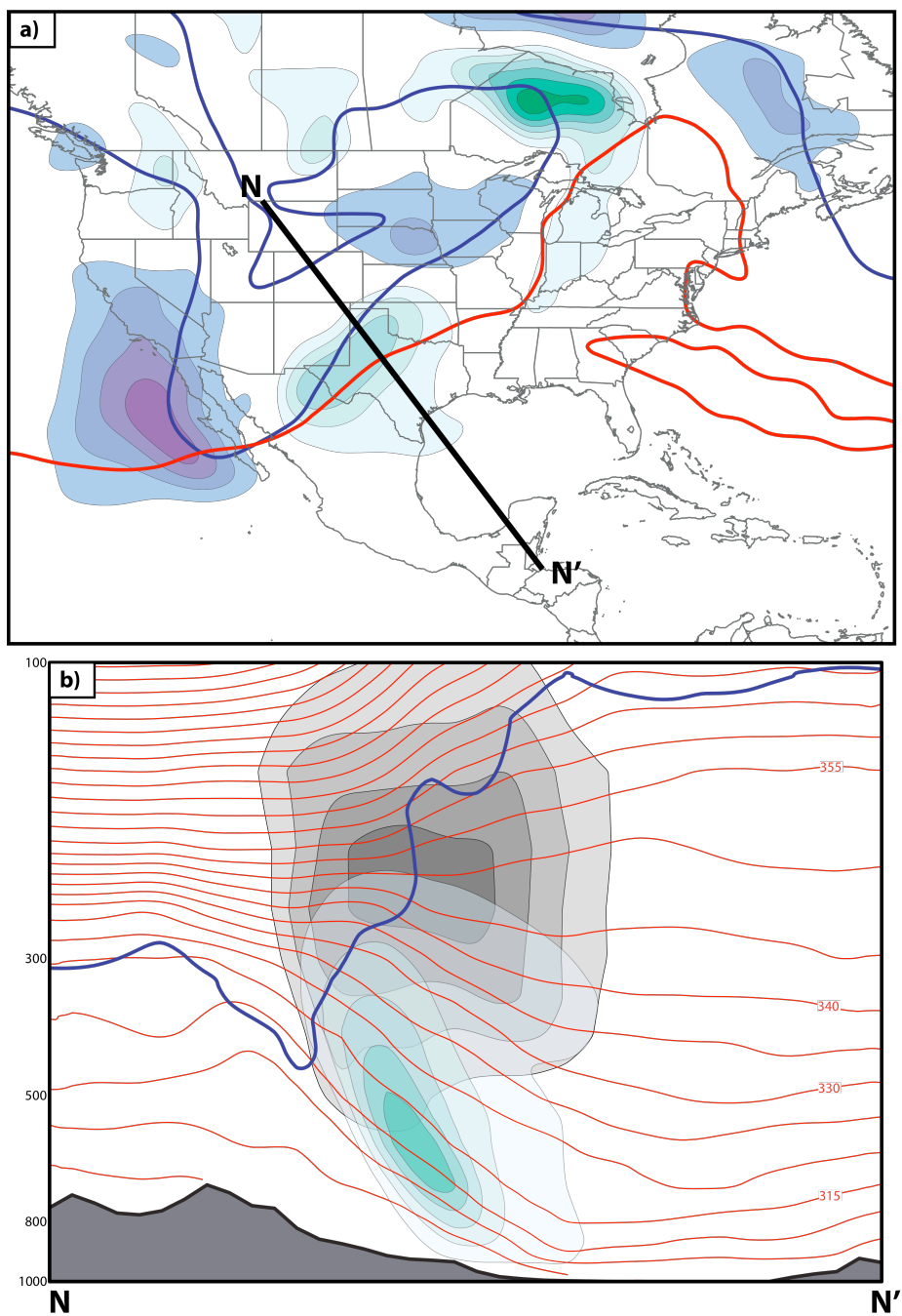


FIG. 5.21. (a) 400 hPa balanced vertical motion field associated with the full PV at 1200 UTC 1 May 2010. Conventions are identical to those shown in Fig. 5.10. (b) Cross section along the line N-N' in (a) of balanced upward vertical motion (green fill pattern) shaded every 1 dPa s^{-1} , wind speed shaded in the gray fill pattern every 10 m s^{-1} above 30 m s^{-1} , and potential temperature contoured in red every 5 K. The thick blue line denotes the 1.5-PVU surface as a proxy for the tropopause.

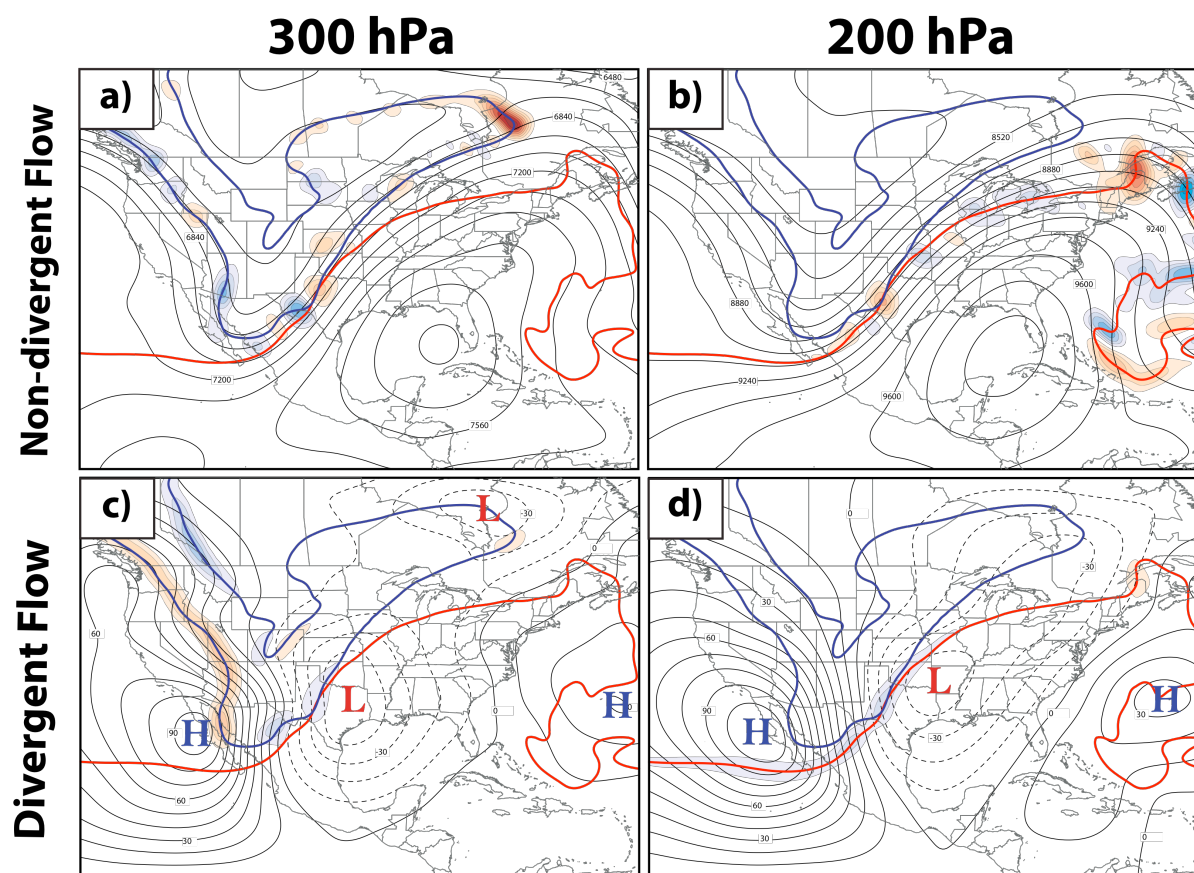


FIG. 5.22. Conventions are identical to those shown in Fig. 5.5, but for 0000 UTC 2 May 2010.

Chapter 6

Conclusions and Future Work

Strongly motivated by observations from military aircraft during World War II, considerable attention in the meteorological research community over the past 75 years has been dedicated to the examination of rapidly flowing currents of air located near the tropopause known as jet streams. While the two primary jet streams, the polar and the subtropical jets, typically reside in different latitude bands within each hemisphere, their meridional separation occasionally vanishes resulting in a vertical jet superposition. Accompanying a superposition is an acceleration of jet wind speeds, a consolidation of the pole-to-equator baroclinicity into a narrow zone of contrast, and the development of a two-step pole-to-equator tropopause structure. A cursory examination of a number of historical and recent high-impact weather events over North America and the North Atlantic has indicated that superposed jets are an important component of their evolution. Consequently, this dissertation isolates two recent jet superposition cases, the 18–20 December 2009 Mid-Atlantic Blizzard and the 1–3 May 2010 Nashville Flood, in an effort to (1) discern the influence that a superposed jet can have on the development of a high-impact weather event and (2) determine the processes that were conducive for the production of a superposition in each case. The following discussion highlights the primary conclusions and future research questions that have emerged from a consideration of these two cases.

6.1 Lessons from the Case Studies

The development of intensified baroclinicity both above and below a superposed jet is often attended by the strengthening of an associated ageostrophic transverse circulation, known

as a Sawyer (1956)-Eliassen (1962) circulation. In addition to providing the dynamical link between the baroclinicity and the jet itself, these transverse vertical circulations have been shown in numerous studies to play an integral role in the production of sensible weather at middle latitudes. Consequently, they also serve as a primary mechanism through which a superposed jet can affect the evolution of a high-impact weather event.

One specific pathway through which a superposed jet's transverse circulation can influence the development of a high-impact weather event was found through an examination of the 1–3 May 2010 Nashville Flood. In that case, it was clear that the development of a superposed jet was coincident with a marked increase in poleward moisture flux over the southern Mississippi River valley and northern Gulf of Mexico. This increase in poleward moisture flux was deemed essential for the continued production of heavy precipitation on the second day of the flooding event (Moore et al. 2012; Durkee et al. 2012). A subsequent diagnosis of the transverse vertical circulation that accompanied the superposed jet indicated that a strong thermally indirect circulation was positioned over the southern Mississippi River valley. Given that a jet superposition is characterized by the horizontal juxtaposition of polar and tropical air masses, the dynamical influence of the transverse vertical circulation in the May 2010 Nashville Flood was magnified as a result of its ability to draw from the poorly stratified, tropical air mass situated on the equatorward side of the jet. Consequently, it was determined that the poleward-directed, lower-tropospheric branch of the transverse circulation accounted for a majority of the observed increase in poleward moisture flux that was important in the evolution of the event.

This case illuminates the more general observation that the development of a superposed jet is accompanied by the creation of an environment that permits extratropical dynamics (e.g., transverse vertical circulations) to interact with a tropical thermodynamic environment. As a

result, the magnified dynamical response of the transverse vertical circulation in the May 2010 case is likely a common element that characterizes other superposition events. It is conceivable that this enhanced dynamical response can contribute in multiple ways to the development of significant weather beyond the specific pathway illustrated in this case, such as through strengthened vertical motions or through changes to the local thermodynamic environment that are facilitated by the lower-tropospheric branch of the transverse vertical circulation. Examinations of other superposed jet events can help to more confidently characterize the nature of transverse vertical circulations within a superposed jet environment and to realize the full spectrum of impacts that a superposed jet can have throughout the evolution of high-impact weather events.

The association of a superposed jet with the 1–3 May 2010 Nashville Flood, and to a number of other high-impact weather events, motivated further investigation into the processes that conspire to produce jet superpositions. In the wake of the investigations into the May 2010 Nashville Flood and the December 2009 Blizzard, it is clear that elements of both the local and remote synoptic environment are worthy of consideration when diagnosing the development of a superposed jet. Locally, transverse vertical circulations are not only limited to the role they can play in the production of sensible weather, but also in their ability to transform the tropopause structure and the mid-tropospheric baroclinicity. Specifically, the December 2009 Blizzard case study demonstrated that, if the two jets are in close proximity to one another, the descending branch of the transverse vertical circulation associated with the dual jet structure can be favorably positioned between the two tropopause breaks to facilitate the production of a two-step tropopause structure by lowering the height of the subtropical tropopause step and by consolidating the baroclinicity associated with each jet into a single zone of contrast. In that

particular case, the dual jet environment was characterized by mid-tropospheric, geostrophic cold-air advection, which served as a favorable environment to shift the location of the transverse vertical circulation so as to position descent through the polar jet core and beneath the subtropical tropopause step (Fig. 3.2b).

Conversely, the May 2010 Nashville Flood was characterized by ascent between the two tropopause breaks and beneath the subtropical tropopause step. Such a configuration of vertical motion was determined to inhibit the development of a two-step tropopause structure, as the strong static stability residing above the subtropical tropopause step prevented any substantial vertical advection of the tropopause in the absence of diabatic heating. While not explicitly shown in the analysis, the mid-tropospheric environment in the vicinity of the polar jet during the May 2010 Nashville Flood was characterized by geostrophic warm-air advection, which would favor ascent through the jet core (Fig. 3.2c). Subsequently, a comparison between these two cases suggests that the presence of mid-tropospheric, geostrophic cold-air advection may characterize a preferential environment within which transverse vertical circulations can contribute most effectively to the development of a superposition within a dual jet environment. This hypothesis can be evaluated as part of the proposed work discussed in Section 6.2.1.

Also essential to consider within a superposed jet's local environment is the presence of proximate convection. In particular, the analysis of the May 2010 Nashville Flood highlighted the importance of organized convection over the southeastern United States for diabatically eroding upper-tropospheric PV and for altering the position of the subtropical tropopause break via its associated divergent outflow. Such an interaction between convection and the tropopause structure has been well discussed within the literature (e.g., Ramos 1997; Morgan and Nielsen-Gammon 1998; Lang and Martin 2013; Archambault et al. 2013; Grams et al. 2013).

Consequently, it is not necessarily a surprise that proximate convection can be an essential component of the superposition process. There is reason to believe that the placement of convection is important to consider, however. In the May 2010 Nashville Flood, convection occurred primarily on the equatorward side of the subtropical jet, which aided in displacing the subtropical tropopause break westward and into closer proximity with the polar tropopause break. Convection that occurs between the two jet cores may not necessarily be favorable for the development of a superposed jet, as the erosion of upper-tropospheric PV that accompanies the convection may result in the creation of a PV trough between the two tropopause breaks that further isolates them from one another. Furthermore, the divergent outflow from convection that occurs between the two jets could act to differentially advect the polar tropopause break poleward and farther away from its subtropical counterpart.

The role of remote tropical convection outside of the dual jet environment was also important to consider during the evolution of both superposition cases. As discussed above, tropical convection can have a local, yet transient impact on the jet structure via its divergent outflow and latent heat release. On the other hand, tropical convection can also drive a slower acting, but more persistent impact via the development of what could be termed a tropical tropopause anticyclone. As mentioned, these particular circulation anomalies represent the balanced dynamical response to the upper-tropospheric mass deposition (i.e., the formation of a negative PV anomaly) that occurs in conjunction with convection. Not only can these tropical tropopause anticyclones either drive or sustain the presence of a jet stream on their poleward flank, as was found in the December 2009 case, they can also be advected out of the tropics and towards middle latitudes where they can restructure the tropopause via differential horizontal

advection of the individual tropopause breaks, as was the case during the May 2010 Nashville Flood.

Attention should be focused on the remote polar environment when considering the development of jet superpositions, as well. For instance, both cases considered were associated with cyclonic PV anomalies (e.g., polar geopotential troughs) that were present at middle latitudes. The origin of these cyclonic PV anomalies, which have been referred to in the literature as coherent tropopause disturbances (CTDs; Pyle et al. 2004), can often be traced to polar latitudes where radiational effects typically account for their formation (Cavallo and Hakim 2010). Once these circulation anomalies are advected towards middle latitudes, their balanced horizontal circulations can work in conjunction with tropical tropopause anticyclones to displace the individual tropopause breaks. Following the arrival of these cyclonic and anticyclonic circulation anomalies at middle latitudes, local environmental kinematics and dynamics (e.g., the effects of curvature, transverse vertical circulations, convection) can act to further accentuate their magnitude and strength.

A conceptual model that summarizes both the development of a jet superposition and its role in the production of high-impact weather is found by considering Fig. 6.1. Generally, the development of a superposition may begin with the remote production of a cyclonic (anticyclonic) tropopause disturbance at high (low) latitudes. The cyclonic disturbance most often has roots in polar latitudes, where radiational cooling, as an example, can lead to the development of a cyclonic vortex. At low latitudes, areas of organized tropical convection result in the deposition of mass into the upper troposphere and the subsequent development of an anticyclonic circulation anomaly. A confluent background flow can then advect both circulation anomalies towards the middle latitudes, where their individual horizontal circulations can work

to displace the location of the individual tropopause breaks. Once the two circulation anomalies are brought into close proximity with one another, local dynamical effects, such as transverse vertical circulations or convection, can act to further deform the tropopause and aid in the development of a superposition. The final result is a horizontal juxtaposition of the two primary circulation anomalies that constructively combine to drive a superposed jet between the two circulation centers. Coincident with the jet superposition, the transverse vertical circulations associated with the jet can contribute further to the production of sensible weather via their ability to leverage the poorly stratified, tropical air mass that resides equatorward of the superposed jet structure.

6.2 Avenues for Future Research

The results from the aforementioned case studies motivate additional research concerning the nature of jet superpositions over North America. Furthermore, the diagnostic methods used to examine superposed jets can also be applied to other atmospheric structures at middle latitudes in an effort to gain additional insight into their characteristics and development. The following discussion highlights some of these future research endeavors and some proposed methods for the subsequent analysis.

6.2.1 Environments Most Conducive for North American Jet Superpositions

While an examination of the two cases above provides insight into some of the diverse dynamical mechanisms that can be at play during the development of a jet superposition, the relative importance of each mechanism differs depending on the case considered. For instance, jet superposition during the May 2010 Nashville Flood was most strongly influenced by the

effects of remote and proximate convection in the days and hours preceding superposition, while the superposed jet that characterized the December 2009 Blizzard was mostly a product of transverse vertical circulations acting within the dual jet environment. The inherent dynamical differences between these two cases leaves lingering research questions surrounding the effort to determine the most conducive environment for the development of a jet superposition. Consequently, a more comprehensive investigation of additional jet superposition events over North America is a worthwhile endeavor.

In brief, this particular investigation can be conducted by constructing jet-centered composites of superposition events over North America from 1979–2010 using a database of superposed jets constructed by Christenson and Martin (2014) from the NCEP-NCAR Reanalysis dataset (Kalnay et al. 1996). Identified jet superposition events can then be classified by the time of year they occur, the type of weather systems with which they are associated (e.g., mid-latitude cyclones, severe convective events, no sensible weather), their geographical location, the flow regime within which they are embedded, and the longevity of the superposed jet structure. For the cases selected, the NCEP Climate Forecast System Reanalysis (CFSR) dataset (Saha et al. 2010) will be used to construct the composites of the superpositions. It is believed that the 0.5° resolution of the CFSR dataset will more accurately capture the details of the superposed jet environment in comparison to the coarser NCEP-NCAR Reanalysis (2.5° resolution). Within a particular classification of events, composite maps can also be calculated at several 6 h lags prior to and following superposition, in an effort to capture the general evolution of the synoptic environment. Overall, the use of these composites will aid in the identification of the environments that most strongly encourage the production of a superposition in a variety of different circumstances, which has important implications for short-term weather prediction.

Furthermore, this knowledge may lead, to the degree to which these structures can be identified within climate models, to an increased capability for interrogating the nature of the jet structure within a future climate.

Specifically, a delineation of the environments associated with the jet superposition composites can also provide additional insight into the influence and nature of transverse vertical circulations within a dual jet environment. Yet, while the transverse vertical circulations examined during the cases in this study agree well with the model vertical motion fields, it remains clear that the superposed jet environment is one that exhibits considerable flow curvature. Consequently, it may be most informative to calculate the distribution of psi vectors (Keyser et al. 1989; Keyser et al. 1992; Keyser 1999) within each composite, as they include the along-front component of the vertical circulation that is omitted within a Sawyer-Eliassen framework. Not only can this analysis serve as a validation metric for the general applicability of the Sawyer-Eliassen circulation equation within an observed dataset, but it also provides additional information on the nature of vertical motions that can restructure the tropopause within subsets of jet superposition cases.

The approach employed by Wandishin et al. (2000) to diagnose the formation of individual tropopause folds may also be useful to consider while examining the jet superposition composites. For instance, the individual three-dimensional circulations that are recovered from a piecewise PV inversion can be interpolated onto the dynamical tropopause. Such an approach would benefit from the underlining assumption of PV conservation and permit the diagnosis of jet superposition on a single horizontal surface. On the dynamical tropopause, the development of a superposition is manifest as a frontogenetical process that results in the consolidation of the baroclinicity associated with each tropopause break into a single zone of contrast. Consequently,

the piecewise PV perspective allows for quantification of the contributions from the individual circulation anomalies to frontogenesis on the tropopause (e.g., Ramos 1997).

An additional result that emerged from Chapter 5 was the notion that the non-divergent circulation associated with subtropical jet most strongly controlled the horizontal displacement of both tropopause breaks. On the other hand, the geostrophic circulation tied to the polar jet had the most substantial contribution towards the development of transverse vertical circulations that were also capable of restructuring the tropopause via vertical advection within the dual jet environment. In light of this analysis, it is apparent that the piecewise PV inversion technique outlined in Chapter 5, which isolates the PV in isentropic layers that encompass each jet, provides a novel perspective from which to study the interaction between the polar and subtropical waveguides within a traditional synoptic framework. As mentioned in Chapter 4, several recent studies have already investigated the nature of the interaction between the two waveguides, but the focus was primarily placed on wave-wave interaction and occurred within an idealized model environment (e.g., Lee and Kim 2003; Son and Lee 2005; Martius et al. 2010; O'Rourke and Vallis 2013). Consequently, the piecewise PV inversion techniques, and particularly the jet PV partition, utilized in this dissertation have the potential to provide a complementary perspective on the interaction between the two waveguides. This analysis may ultimately serve as a bridge to the results presented within many of the aforementioned investigations that are rooted in wave dynamics.

Once investigations into a preferred synoptic environment for observed jet superpositions have concluded, the use of idealized model simulations may contribute additional understanding. For instance, a study into the specific role of convection during a superposition event can follow an approach taken by Posselt and Martin (2004). In that particular study, the authors examined

the role of latent heat release on the occluded thermal structure of a mid-latitude cyclone by prohibiting latent heat release to occur within the model environment. In the context of jet superpositions, a similar experiment can be done with a case that was characterized by strong tropical convection, such as one similar to the May 2010 Nashville Flood, but with a focus on the resultant tropopause structure. The results from the simulations subsequently can provide useful information concerning the tropopause and jet structure in the absence of convection and, ultimately, whether the formation of superposed jet was truly dependent on the presence of latent heat release in the cases considered. Furthermore, knowledge of the preferred synoptic environments associated with jet superpositions may motivate the use of an idealized primitive equation model, such as a channel model, to investigate whether the identified environments are truly capable of fostering the development of a superposition when implemented as initial conditions.

6.2.2 Survey of Tropical Tropopause Anticyclones

An important component of both superposition cases was the role of remote tropical convection in the formation of tropical tropopause anticyclones. These circulation anomalies, which represent a long-lasting, balanced dynamical response to upper-tropospheric mass deposition from convection, were subsequently found to play a part in the development of a jet superposition following their advection into subtropical and middle latitudes. While much attention in the research community has been focused on the formation and advection of CTDs and tropopause polar vortices towards middle latitudes where they can impact the production of sensible weather (e.g., Pyle et al. 2004; Cavallo and Hakim 2010), limited attention has been paid to the complementary role of tropical tropopause anticyclones. Not only can the circulations

associated with these anticyclones modulate the position of the individual tropopause breaks, they also represent an environment characterized by reduced upper-tropospheric static and inertial stability. Consequently, their advection towards middle latitudes signifies the development of a thermodynamic environment supportive of deep convection and favorable for divergent outflow. The relative absence of literature concerning these transient tropical tropopause anticyclones, and their link to the production of sensible weather, motivates a study focused on the development of these circulation anomalies in the tropics and the synoptic patterns that facilitate their advection towards middle latitudes.

The following discussion highlights an approach to probe this particular research question. Utilizing the CFSR dataset, the perturbation PV (defined against a long term mean) can be calculated within a large domain straddling the equator and inverted at 6 h intervals during a multi-year period. Analysis can subsequently focus on identifying anomalously strong perturbation anticyclones in the upper troposphere with tropical origin and cataloging where they are located spatially throughout the domain. Specifically, a tracking scheme can be implemented that identifies the position of each individual anticyclone by considering the upper-tropospheric PV distribution (i.e., the identification of negative PV anomalies). The resultant knowledge of the frequency and preferred tracks of these tropical tropopause anticyclones will help to pinpoint the most favorable locations for their generation and where they subsequently translate. Tropical tropopause anticyclones that follow a similar track into the middle latitudes can also be grouped together and composited in an effort to determine the optimal synoptic environment that facilitates their advection out of the tropics, any seasonal differences that exist with respect to that environment, and how often tropical tropopause anticyclones are associated with the production of sensible weather at middle latitudes.

6.2.3 Applicability of Diagnostic Tools to Other Atmospheric Structures

The methods employed in this dissertation also have a general applicability to the investigation of a number of other atmospheric phenomena. For example, the jet PV partition employed in this study has the ability to provide new insight into episodes of cyclogenesis within a dual jet environment. Furthermore, both Bell and Keyser (1993) and Martin (2014) discuss the utility of partitioning the PV into its shear and curvature components and subsequently utilizing piecewise PV inversion to illuminate the three-dimensional circulations associated with those individual portions of the PV field and their impact on cyclogenesis or tropospheric frontogenesis. The software that has been developed as part of this dissertation enables such an analysis to occur with ease. Furthermore, the jet PV partition allows one to potentially isolate the individual shear and curvature PV anomalies that are attributable to each jet. While it is unclear whether this partition of the jet PV will have dynamical significance, it undoubtedly offers more versatility in the ability to investigate various atmospheric structures.

Finally, one of the primary characteristics of the May 2010 Nashville Flood was the superposed jet's connection to a band of increased poleward moisture flux over the southern Mississippi River valley, known as an atmospheric river (e.g., Newell et al. 1992; Zhu and Newell 1998). Given that the transverse vertical circulation in the May 2010 Nashville Flood was found to play an important role in magnifying the poleward moisture flux associated with that atmospheric river, it is worthwhile research endeavor to further investigate the role that transverse vertical circulations may have in other atmospheric river cases. The Sawyer-Eliassen software, as well as the psi vectors discussed in Section 6.2.1 (Keyser et al. 1989; Keyser et al. 1992; Keyser 1999), are diagnostic tools that can be easily applied to this particular analysis and

may better characterize the evolution of these particular structures that are vitally important to global moisture transport and the development of prolonged heavy precipitation events.

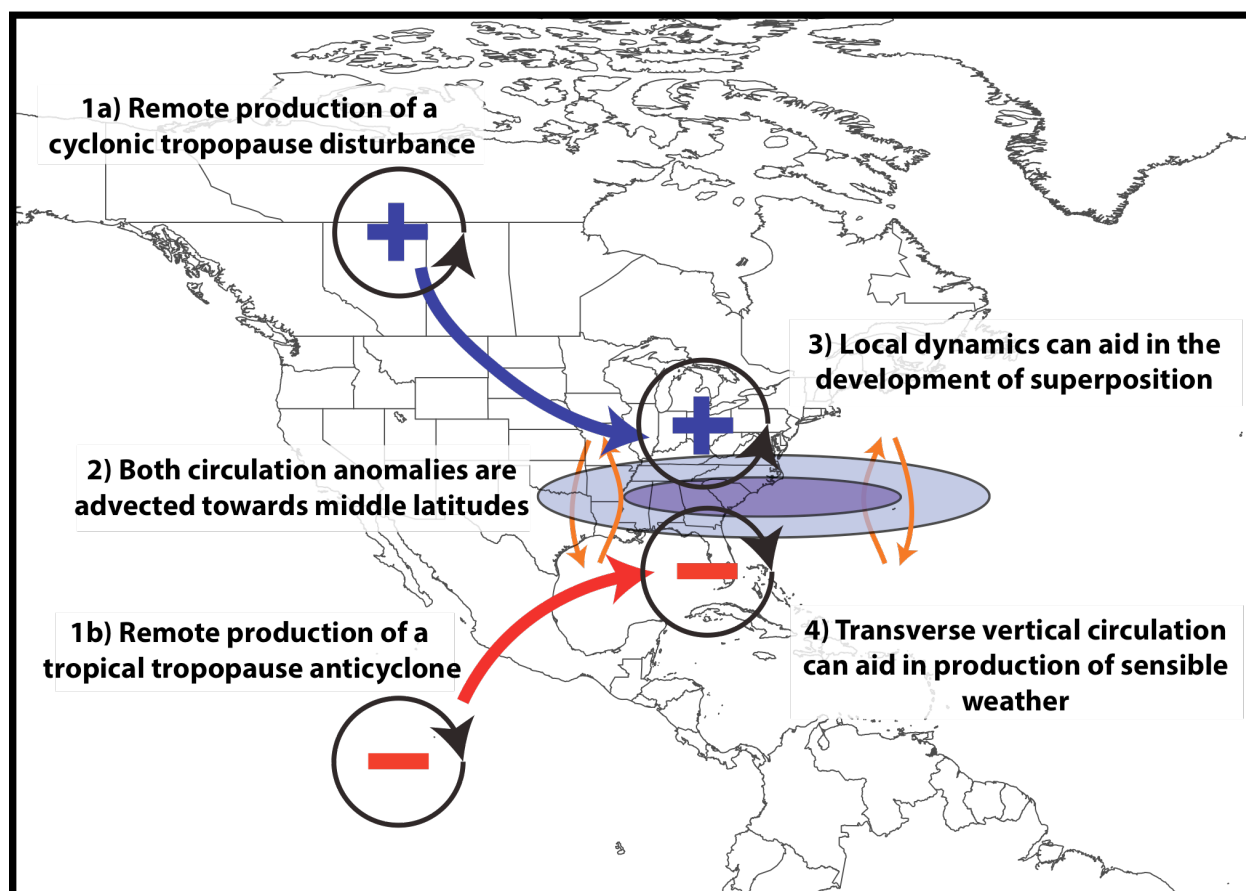


FIG. 6.1. Conceptual diagram summarizing the process of jet superposition. The orange arrows depict branches of a transverse vertical circulation, the + (-) symbol corresponds to the center of a cyclonic (anticyclonic) circulation anomaly with the blue (red) arrow indicating the movement of that particular anomaly. The purple fill pattern corresponds to isotachs with the darker shade of purple identifying faster wind speeds. For additional information refer to the discussion in the text.

References

- Archambault, H. M., L. F. Bosart, D. Keyser, and J. M. Cordeira, 2013: A climatological analysis of the extratropical flow response to recurving western North Pacific tropical cyclones. *Mon. Wea. Rev.*, **141**, 2325-2346.
- Barnes, S. L., and B. R. Colman, 1993: Quasigeostrophic diagnosis of cyclogenesis associated with a cutoff extratropical cyclone – The Christmas 1987 storm. *Mon. Wea. Rev.*, **121**, 1613-1634.
- Bell, G. D., and D. Keyser, 1993: Shear and curvature vorticity and potential-vorticity interchanges: Interpretation and application to a cutoff cyclone event. *Mon. Wea. Rev.*, **121**, 76-102.
- Bjerknes, J. and H. Solberg, 1922: Life cycle of cyclones and the polar front theory of atmospheric circulation. *Geofys. Publik.*, **3** (1), 1-18.
- , and E. Palmén, 1937: Investigations of selected European cyclones by means of serial ascents. *Geofys. Publik.*, **12** (2), 1-62.
- Bolton, D., 1980: The computation of equivalent potential temperature. *Mon. Wea. Rev.*, **108**, 1046-1053.
- Bosart, L. F., 1970: Mid-tropospheric frontogenesis. *Quart. J. Roy. Meteor. Soc.*, **96**, 442-471.
- , G. J. Hakim, K. R. Tyle, M. A. Bedrick, W. E. Bracken, M. J. Dickenson, and D. M. Schultz, 1996: Large-scale antecedent conditions associated with the 12-14 March 1993 cyclone (“Superstorm ‘93”) over eastern North America. *Mon. Wea. Rev.*, **124**, 1865-1891.
- Bretherton, F. P., 1966: Critical layer instability in baroclinic flows. *Quart. J. Roy. Meteor. Soc.*, **92**, 325-334.
- Bryan, G. H., 2008: On the computation of pseudoadiabatic entropy and equivalent potential temperature. *Mon. Wea. Rev.*, **136**, 5239-5245.
- Bryson, R., 1994: *Discovery of the Jet Stream*. Wisconsin Academy Review 40 (3) Madison, Wisconsin: Wisconsin Academy of Science, Arts, and Letters, Summer 1994.
- Cavallo, S. M., and G. J. Hakim, 2010: Composite structure of tropopause polar cyclones. *Mon. Wea. Rev.*, **138**, 3840-3857.
- Charney, J. G., 1955: The use of primitive equations of motion in numerical prediction. *Tellus*, **7**, 22-26.
- Christenson, C. E., and J. E. Martin, 2012: The large-scale environment associated with the 25-28 April 2011 severe weather outbreak. *16th NWA Severe Storms and Doppler Radar Conference*, Des Moines, IA, National Weather Association, 31 March 2012.

- , and ———, 2014: A synoptic-climatology of Northern Hemisphere polar and subtropical jet superposition events. *J. Climate*, **27**, (submitted).
- Danielsen, E., 1968: Stratospheric-tropospheric exchange based on radioactivity, ozone, and potential vorticity. *J. Atmos. Sci.*, **25**, 502-518.
- , R. Bleck, J. Shedlovsky, A. Wartburg, P. Haagenson, and W. Pollock, 1970: Observed distribution of radioactivity, ozone, and potential vorticity associated with tropopause folding. *J. Geophys. Res.*, **75** (12), 2353-2361.
- , and R. Hipskind, 1980: Stratospheric-tropospheric exchange at polar latitudes in summer. *J. Geophys. Res.*, **85**, 393-400.
- Davies, H. C., and A. M. Rossa, 1998: PV frontogenesis and upper-tropospheric fronts. *Mon. Wea. Rev.*, **126**, 1528-1539.
- Davis, C. A., and K. E. Emanuel, 1991: Potential vorticity diagnostics of cyclogenesis. *Mon. Wea. Rev.*, **119**, 1929-1953.
- , 1992a: Piecewise potential vorticity inversion. *J. Atmos. Sci.*, **49**, 1397-1411.
- , 1992b: A potential vorticity diagnosis of the importance of initial structure and condensational heating in observed cyclogenesis. *Mon. Wea. Rev.*, **120**, 2409-2428.
- , M. T. Stoelinga, and Y.-H. Kuo, 1993: The integrated effect of condensation in numerical simulations of extratropical cyclogenesis. *Mon. Wea. Rev.*, **121**, 2309-2330.
- , E. D. Grell, and M. A. Shapiro, 1996: The balanced dynamical nature of a rapidly intensifying oceanic cyclone. *Mon. Wea. Rev.*, **124**, 3-26.
- Dean, D. B., and L. F. Bosart, 1996: Northern Hemisphere 500-hPa trough merger and fracture: A climatology and case study. *Mon. Wea. Rev.*, **124**, 2644-2671.
- Defant, F., 1959: On hydrodynamic instability caused by an approach of subtropical and polarfront jet stream in northern latitudes before the onset of strong cyclogenesis. *The Atmosphere and Sea in Motion*, New York, Rockefeller and Oxford University Presses, 305-325.
- , and H. Taba, 1957: The threefold structure of the atmosphere and the characteristics of the tropopause. *Tellus*, **9**, 259-275.
- desJardins, M. L., K. F. Brill, and S. S. Schotz, 1991: Use of GEMPAK on UNIX workstations. Preprints, *Seventh Int. Conf. on Interactive Information and Processing Systems for Meteorology, Oceanography, and Hydrology*, New Orleans, LA, Amer. Meteor. Soc., 449-453.
- Dines, W. H., 1925: The correlation between pressure and temperature in the upper air with a suggested explanation. *Quart. J. Roy. Meteor. Soc.*, **51**, 31-38.
- Draxler, R. R., 1999: HYSPLIT4 user's guide. NOAA Tech. Memo. ERL ARL-230, NOAA Air Resources Laboratory, Silver Spring, MD.

- , and G. D. Hess, 1997: Description of the HYSPLIT_4 modeling system. NOAA Tech. Memo. ERL ARL-224, NOAA Air Resources Laboratory, Silver Spring, MD, 24 pp.
- , and ———, 1998: An overview of the HYSPLIT_4 modeling system of trajectories, dispersion, and deposition. *Aust. Meteor. Mag.*, **47**, 295-308.
- , and G. D. Rolph, 2015: HYSPLIT (Hybrid Single-Particle Lagrangian Integrated Trajectory) Model, access via NOAA ARL READY Website (<http://ready.arl.noaa.gov/HYSPLIT.php>). NOAA Air Resources Laboratory, Silver Spring, MD.
- Durkee, J. D., L. Campbell, K. Berry, D. Jordan, G. Goodrich, R. Mahmood, and S. Foster, 2012: A synoptic perspective of the record 1-2 May 2010 mid-South heavy precipitation event. *Bull. Amer. Meteor. Soc.*, **93**, 611-620.
- Eliassen, A., 1962: On the vertical circulation in frontal zones. *Geophys. Publ.*, **24**, 147-160.
- Emanuel, K. A., M. Fantini, and A. J. Thorpe, 1987: Baroclinic instability in an environment of small stability to slantwise moist convection. Part I: Two-dimensional models. *J. Atmos. Sci.*, **44**, 1559-1573.
- Ertel, H., 1942: Ein neuer hydrodynamischer wirbelsatz. *Meteor. Z.*, **59**, 271-281.
- Gaza, R. S., and L. F. Bosart, 1990: Trough merger characteristics over North America. *Wea. Forecasting*, **5**, 314-331.
- Grams, C. M., S. C. Jones, C. A. Davis, P. A. Harr, and M. Weissmann, 2013: The impact of Typhoon Jangmi (2008) on the midlatitude flow. Part I: Upper-level ridgebuilding and modification of the jet. *Quart. J. Roy. Meteor. Soc.*, **139**, 2148-2164.
- Griffin, K. S., and L. F. Bosart, 2014: The extratropical transition of Tropical Cyclone Edisoana (1990). *Mon. Wea. Rev.*, **142**, 2772-2793.
- Guan, B., N. P. Molotch, D. E. Waliser, E. J. Fetzer, and P. J. Neiman, 2010: Extreme snowfall events linked to atmospheric rivers and surface air temperature via satellite measurements. *Geophys. Res. Lett.*, **37**, L20401.
- Hakim, G. J., L. F. Bosart, and D. Keyser, 1995: The Ohio Valley wave merger cyclogenesis event of 25-26 January 1978. Part I: Multiscale case study. *Mon. Wea. Rev.*, **123**, 2663-2692.
- , D. Keyser, and L. F. Bosart, 1996: The Ohio Valley wave merger cyclogenesis event of 25-26 January 1978. Part II: Diagnosis using quasigeostrophic potential vorticity inversion. *Mon. Wea. Rev.*, **124**, 2176-2205.
- Harnik, N., E. Galanti, O. Martius, and O. Adam, 2014: The anomalous merging of the African and North Atlantic jet streams during Northern Hemisphere winter of 2010. *J. Climate*, **27**, 7319-7334.

- Hobbs, P. V., J. D. Locatelli, and J. E. Martin, 1990: Cold fronts aloft and forecasting of precipitation and severe weather east of the Rocky Mountains. *Wea. Forecasting*, **5**, 613-626.
- Holopainen, E. O., and J. Kaurola, 1991: Decomposing the atmospheric flow using potential vorticity framework. *J. Atmos. Sci.*, **48**, 2614-2625.
- Hoskins, B. J., M. E. McIntyre, and A. W. Robertson, 1985: On the use and significance of isentropic potential vorticity maps. *Quart. J. Roy. Meteor. Soc.*, **111**, 877-946.
- , and P. Berrisford, 1988: A potential vorticity perspective of the storm of 15-16 October 1987. *Weather*, **43**, 122-129.
- Kalnay, E., and co-authors, 1996: The NCEP/NCAR 40-year reanalysis project. *Bull. Amer. Meteor. Soc.*, **77**, 437-471.
- Keyser, D. A., 1999: On the representation and diagnosis of frontal circulations in two and three dimensions. *The Life Cycles of Extratropical Cyclones*, M. A. Shapiro and S. Grønås, Eds., Amer. Meteor. Soc., 239-264.
- , and M. J. Pecnick, 1985: A two-dimensional primitive equation model of frontogenesis forced by confluence and horizontal shear. *J. Atmos. Sci.*, **42**, 1259-1282.
- , and M. A. Shapiro, 1986: A review of the structure and dynamics of upper-level frontal zones. *Mon. Wea. Rev.*, **114**, 452-496.
- , B. D. Schmidt, and D. G. Duffy, 1989: A technique for representing three-dimensional vertical circulations in baroclinic disturbances. *Mon. Wea. Rev.*, **117**, 2463-2494.
- , ———, and ———, 1992: Quasigeostrophic diagnosis of three-dimensional ageostrophic circulations in an idealized baroclinic disturbance. *Mon. Wea. Rev.*, **120**, 698-730.
- Kleinschmidt, E., 1957: Cyclones and anticyclones. *Dynamic Meteorology. Handbuch der Physik*, **48**, S. Flugge, Ed., Springer-Verlag, 112-154.
- Knupp, K. R., T. A. Murphy, T. A. Coleman, R. A. Wade, S. A. Mullins, C. J. Schultz, E. V. Schultz, L. Carey, A. Sherrer, E. W. McCaul Jr., B. Carcione, S. Latimer, A. Kula, K. Laws, P. T. Marsh, and K. Klockow, 2014: Meteorological overview of the devastating 27 April 2011 Tornado Outbreak. *Bull. Amer. Meteor. Soc.*, **95**, 1041-1062.
- Korner, S. O., and J. E. Martin, 2000: Piecewise frontogenesis from a potential vorticity perspective: Methodology and a case study. *Mon. Wea. Rev.*, **128**, 1266-1288.
- Koteswaram, P., 1953: An analysis of the high tropospheric wind circulation over India in winter. *Indian J. Meteor. Geophys.*, **4**, 13-21.
- , and S. Parthasarathy, 1954: The mean jet stream over India in the pre-monsoon and post-monsoon seasons and vertical motions associated with subtropical jet streams. *Indian J. Meteor. Geophys.*, **5**, 138-156.

- Krishnamurti, T. N., 1961: The subtropical jet stream of winter. *J. Meteor.*, **18**, 172-191.
- Kutzbach, G., 1979: *The Thermal Theory of Cyclones: A History of Meteorological Thought in the Nineteenth Century*. Amer. Meteor. Soc., 255 pp.
- Lackmann, G. M., 2002: Potential vorticity redistribution, the low-level jet, and moisture transport in extratropical cyclones. *Mon. Wea. Rev.*, **130**, 59-74.
- , 2013: The south-central U.S. flood of May 2010: Present and future. *J. Climate*, **26**, 4688-4709.
- , D. Keyser, L. F. Bosart, 1997: A characteristic life cycle of upper-tropospheric cyclogenetic precursors during Experiment on Rapidly Intensifying Cyclones of the Atlantic (ERICA). *Mon. Wea. Rev.*, **125**, 2729-2758.
- Lai, C.-C, and L. F. Bosart, 1988: A case study of trough merger in split westerly flow. *Mon. Wea. Rev.*, **116**, 1838-1856.
- Lang, A. A., and J. E. Martin, 2012: The structure and evolution of lower stratospheric frontal zones. Part I: Examples in northwesterly and southwesterly flow. *Quart. J. Roy. Meteor. Soc.*, **138**, 1350-1365.
- , and ———, 2013: The structure and evolution of lower stratospheric frontal zones. Part II: The influence of tropospheric convection on lower stratospheric frontal development. *Quart. J. Roy. Meteor. Soc.*, **139**, 1798-1809.
- Lee, S., and H.-K. Kim, 2003: The dynamical relationship between subtropical and eddy-driven jets. *J. Atmos. Sci.*, **60**, 1490-1503.
- Loewe, F., and V. Radok, 1950: A meridional aerological cross section in the southwest Pacific. *J. Meteor.*, **7**, 58-65.
- Lynch, S. and R. Schumacher, 2013: Ensemble-based analysis of the May 2010 extreme rainfall in Tennessee and Kentucky. *Mon. Wea. Rev.*, **142**, 222-239.
- Margules, M., 1903: Über die energie der stürme. *Jahrb. Zentralanst. Meteorol. Wien.*, 1-26.
- Martin, J. E., 2014: Quasi-geostrophic diagnosis of the influence of vorticity advection on the development of upper level jet-front systems. *Quart. J. Roy. Meteor. Soc.*, **140**, 2658-2671.
- , J. D. Locatelli, and P. V. Hobbs, 1993: Organization and structure of clouds and precipitation on the mid-Atlantic coast of the United States. Part VI: The synoptic evolution of a deep tropospheric frontal circulation and attendant cyclogenesis. *Mon. Wea. Rev.*, **121**, 1299-1316.
- Martius, O., C. Schwiertz, and H. C. Davies, 2010: Tropopause-level waveguides. *J. Atmos. Sci.*, **67**, 866-879.

- McTaggart-Cowan, R., J. R. Gyakum, and M. K. Yau, 2001: Sensitivity testing of extratropical transition using potential vorticity inversion to modify initial conditions: Hurricane Earl case study. *Mon. Wea. Rev.*, **129**, 1617-1636.
- Miller, J. E., 1948: On the concept of frontogenesis. *J. Meteor.*, **5**, 169-171.
- Mohri, K., 1953: On the fields of wind and temperature over Japan and adjacent waters during winter of 1950-1951. *Tellus*, **5**, 340-358.
- Moore, B. J., P. J. Neiman, F. M. Ralph, and F. E. Barthold, 2012: Physical processes associated with heavy flooding rainfall in Nashville, Tennessee, and vicinity during 1-2 May 2010: The role of an atmospheric river and mesoscale convective systems. *Mon. Wea. Rev.*, **140**, 358-378.
- Morgan, M. C., 1999: Using piecewise potential vorticity inversion to diagnose frontogenesis. Part I: A partitioning of the Q vector applied to diagnosing surface frontogenesis and vertical motion. *Mon. Wea. Rev.*, **127**, 2796-2821.
- , and J. W. Nielsen-Gammon, 1998: Using tropopause maps to diagnose midlatitude weather systems. *Mon. Wea. Rev.*, **126**, 241-265.
- Namias, J., and P. F. Clapp, 1949: Confluence theory of the high tropospheric jet stream. *J. Meteor.*, **6**, 330-336.
- National Weather Service, 2011: Record floods of greater Nashville: Including flooding in middle Tennessee and western Kentucky, May 1-4, 2010. National Weather Service Assessment, 93 pp. [Available online at http://www.weather.gov/os/assessments/pdfs/Tenn_Flooding.pdf.]
- , cited 2014: December 18-19, 2009 winter storm. [Available online at <http://www4.ncsu.edu/~nwsfo/storage/cases/20091218/>.]
- Newell, R. E., N. E. Newell, Y. Zhu, and C. Scott, 1992: Tropospheric rivers? – A pilot study. *Geophys. Res. Lett.*, **19**, 2401-2404.
- Nielsen-Gammon, J. W., and R. J. Lefevre, 1996: Piecewise tendency diagnosis of dynamical processes governing the development of an upper-tropospheric mobile trough. *J. Atmos. Sci.*, **53**, 3120-3142.
- Omoto, Y., 1965: On pre-frontal precipitation zones in the United States. *J. Meteor. Soc. Japan*, **43**, 310-330.
- Ooishi, W., 1926: Raporto de la Aerologia Observatorio de Tateno (in Esperanto). Aerological Observatory Rep. 1, Central Meteorological Observatory, Japan, 213 pp.
- O'Rourke, A. K., and G. K. Vallis, 2013: Jet interaction and the influence of a minimum phase speed bound on the propagation of eddies. *J. Atmos. Sci.*, **70**, 2614-2628.
- Palmén, E., 1948: On the distribution of temperature and wind in the westerlies. *J. Meteor.*, **5**, 20-27.

- , 1951: The role of atmospheric disturbances in the general circulation. *Quart. J. Roy. Meteor. Soc.*, **77**, 337-354.
- , and C. W. Newton, 1948: A study of the mean wind and temperature distribution in the vicinity of the polar front in winter. *J. Meteor.*, **5**, 220-226.
- , and ———, 1969: *Atmospheric Circulation Systems: Their Structure and Physical Interpretation*. Academic Press, 603 pp.
- , and K. M. Nagler, 1949: Formation and structure of a large-scale disturbance in the westerlies. *J. Meteor.*, **6** (4), 227-242.
- Posselt, D. J., and J. E. Martin, 2004: The effect of latent heat release on the evolution of a warm occluded thermal structure. *Mon. Wea. Rev.*, **132**, 578-599.
- Pyle, M. E., D. Keyser, and L. F. Bosart, 2004: A diagnostic study of jet streaks: Kinematic signatures and relationship to coherent tropopause disturbances. *Mon. Wea. Rev.*, **132**, 297-319.
- Ralph, F. M., P. J. Neiman, G. A. Wick, S. I. Gutman, M. D. Dettinger, D. R. Cayan, A. B. White, 2006: Flooding on California's Russian River: Role of atmospheric rivers. *Geophys. Res. Lett.*, **33**, L13801.
- Ramos, R. A., 1997: The role of latent heat release on the formation of an upper tropospheric outflow jet. M.S. thesis, Department of Atmospheric and Oceanic Sciences, University of Wisconsin-Madison, 149 pp. [Available from University of Wisconsin-Madison, Dept. of Atmospheric and Oceanic Sciences, 1225 W. Dayton St., Madison, WI 53706.]
- Reed, R. J., 1955: A study of a characteristic type of upper-level frontogenesis. *J. Meteor.*, **12**, 226-237.
- , and F. Sanders, 1953: An investigation of the development of a mid-tropospheric frontal zone and its associated vorticity field. *J. Meteor.*, **10**, 338-349.
- Reiter, E., 1963: *Jet Stream Meteorology*. University of Chicago Press, 515 pp.
- Riehl, H., 1948: Jet stream in upper troposphere and cyclone formation. *Trans. Am. Geophys. Union*, **29**, 175-186.
- , 1962: Jet streams of the atmosphere. Dept. of Atmospheric Science Tech. Rep. 32, Colorado State University, Fort Collins, CO, 117 pp.
- Robinson, W. A., 1988: Analysis of LIMS data by potential vorticity inversion. *J. Atmos. Sci.*, **45**, 2319-2342.
- , 1989: On the structure of potential vorticity in baroclinic instability. *Tellus*, **41**, 275-284.
- Rolph, G. D., 2015: Real-time Environmental Applications and Display sYstem (READY) Website (<http://ready.arl.noaa.gov>). NOAA Air Resources Laboratory, Silver Spring, MD.

- Rossby, C.-G., 1936: Dynamics of steady ocean currents in the light of experimental fluid mechanics. *M.I.T. and Woods Hole Ocean. Inst., Papers in Phys. Ocean. And Met.*, **5** (1).
- , 1940: Planetary flow patterns in the atmosphere. *Quart. J. Roy. Meteor. Soc.*, **66**, 68-87.
- Rowe, S. M., and M. H. Hitchman, 2015: On the role of inertial instability in stratosphere-troposphere exchange near midlatitude cyclones. *J. Atmos. Sci.*, **72**, 2131-2151.
- Saha, S., and co-authors, 2010: The NCEP Climate Forecast System Reanalysis. *Bull. Amer. Meteor. Soc.*, **91**, 1015-1057.
- Sawyer, J. S., 1956: The vertical circulation at meteorological fronts and its relation to frontogenesis. *Proc. Roy. Soc. London*, **234A**, 346-362.
- Shapiro, L. J., 1996: The motion of Hurricane Gloria: A potential vorticity diagnosis. *Mon. Wea. Rev.*, **124**, 2497-2508.
- , and J. L. Franklin, 1999: Potential vorticity asymmetries and tropical cyclone motion. *Mon. Wea. Rev.*, **127**, 124-131.
- , and J. D. Möller, 2003: Influence of atmospheric asymmetries on the intensification of Hurricane Opal: Piecewise PV inversion diagnosis of a GFDL model forecast. *Mon. Wea. Rev.*, **131**, 1637-1649.
- Shapiro, M. A., 1981: Frontogenesis and geostrophically forced secondary circulations in the vicinity of the jet stream-frontal zone systems. *J. Atmos. Sci.*, **38**, 954-973.
- , 1982: Mesoscale weather systems of the central United States. CIRES, 78 pp.
- , 1985: Dropwindsonde observations of an Icelandic Low and a Greenland mountain-lee wave. *Mon. Wea. Rev.*, **113**, 680-683.
- , R. C. Schnell, F. P. Parungo, S. J. Oltmans, and B. A. Bodhaine, 1984: El Chichon volcanic debris in an arctic tropopause fold. *Geophys. Res. Lett.*, **11** (5), 421-424.
- , T. Hampel, and A. J. Krueger, 1987: The arctic tropopause fold. *Mon. Wea. Rev.*, **115**, 444-454.
- , and D. Keyser, 1990: Fronts, jet streams, and the tropopause. *Extratropical Cyclones: The Erik Palmén Memorial Volume*, C. Newton and E. O. Holopainen, Eds., Amer. Meteor. Soc., 167-191.
- , H. Wernli, J.-W. Bao, J. Methven, X. Zou, J. Doyle, T. Holt, E. Donall-Grell, and P. Neiman, 1999: A planetary-scale to mesoscale perspective of the life cycles of extratropical cyclones: The bridge between theory and observations. *The Life Cycles of Extratropical Cyclones*, M. Shapiro and S. Grønås, Eds., Amer. Meteor. Soc., 139-185.
- Son, S.-W., and S. Lee, 2005: The response of westerly jets to thermal driving in a primitive equation model. *J. Atmos. Sci.*, **62**, 3741-3757.

- Strahl, J. L. S., and P. J. Smith, 2001: A diagnostic case study of an explosively developing extratropical cyclone and an associated 500-hPa trough merger. *Mon. Wea. Rev.*, **129**, 2310-2328.
- Stohl, A., C. Forster, and H. Sodemann, 2008: Remote sources of water vapor forming precipitation on the Norwegian west coast at 60°N: A tale of hurricanes and an atmospheric river. *J. Geophys. Res.*, **113**, D05012.
- Sutcliffe, R. C., 1947: A contribution to the problem of development. *Quart. J. Roy. Meteor. Soc.*, **73**, 370-383.
- , and J. K. Bannon, 1954: Seasonal changes in the upper-air conditions in the Mediterranean Middle East area. *Proc. Int. Association of Meteorology*, Rome, Italy, Int. Union of Geodesy and Geophysics, 322-334.
- Thorpe, A. J., 1985: Diagnosis of balanced vortex structure using potential vorticity. *J. Atmos. Sci.*, **42**, 397-406.
- Todsen, M., 1964: A computation of the vertical circulation in a frontal zone from the quasi-geostrophic equations. Air Force Cambridge Laboratories Tech. Note 4, OAR Contribution AF 61(052)-525, 23 pp.
- Uccellini, L. W., and D. R. Johnson, 1979: The coupling of upper and lower tropospheric jet streaks and implications for the development of severe convective storms. *Mon. Wea. Rev.*, **107**, 682-703.
- , and P. J. Kocin, 1987: The interaction of jet streak circulations during heavy snow events along the East Coast of the United States. *Wea. Forecasting*, **2**, 289-308.
- , ———, R. A. Petersen, C. H. Wash, and K. F. Brill, 1984: The Presidents' Day cyclone of 18-19 February 1979; Synoptic overview and analysis of the subtropical jet streak influencing the pre-cyclogenetic period. *Mon. Wea. Rev.*, **112**, 31-55.
- , D. Keyser, K. F. Brill, and C. H. Wash, 1985: The Presidents' Day cyclone of 18-19 February 1979: Influence of upstream trough amplification and associated tropopause folding on rapid cyclogenesis. *Mon. Wea. Rev.*, **113**, 962-988.
- University of Chicago, Department of Meteorology, 1947: On the general circulation of the atmosphere in middle latitudes. *Bull. Amer. Meteor. Soc.*, **28**, 255-280.
- Wandishin, M. S., J. W. Nielsen-Gammon, and D. Keyser, 2000: A potential vorticity diagnostic approach to upper-level frontogenesis within a developing baroclinic wave. *J. Atmos. Sci.*, **57**, 3918-3938.
- Whitaker, J. S., L. W. Uccellini, and K. F. Brill, 1988: A model-based diagnostic study of the rapid development phase of the Presidents' Day cyclone. *Mon. Wea. Rev.*, **116**, 2337-2365.
- Winters, A. C., and J. E. Martin, 2014: The role of a polar/subtropical jet superposition in the May 2010 Nashville Flood. *Wea. Forecasting*, **29**, 954-974.

- , and ———, 2015: A two-case examination of the synoptic and mesoscale processes supporting vertical superposition of the polar and subtropical jets over North America. *Quart. J. Roy. Meteor. Soc.*, **141**, (in revision).
- World Meteorological Organization, 1992: *International Meteorological Vocabulary*. WMO, 784 pp.
- Wu, C.-C., and K. A. Emanuel, 1995a: Potential vorticity diagnosis of hurricane movement. Part I: A case study of Hurricane Bob (1991). *Mon. Wea. Rev.*, **123**, 69-92.
- ,———, 1995b: Potential vorticity diagnosis of hurricane movement. Part II: Tropical Storm Ana (1991) and Hurricane Andrew (1992). *Mon. Wea. Rev.*, **123**, 93-109.
- Yeh, T. C., 1950: The circulation of the high tropopause over China in the winter of 1945-46. *Tellus*, **2**, 173-183.
- Zhu, Y., and R. E. Newell, 1998: A proposed algorithm for moisture fluxes from atmospheric rivers. *Mon. Wea. Rev.*, **126**, 725-735.